University of Alberta
Department of Civil Engineering

Structural Engineering Report No. 171

Fatigue of Drill Pipe

by
G. Y. Grondin
and
G. L. Kulak

April, 1991

Fatigue of Drill Pipe

by

G. Y. Grondin

and

G.L. Kulak

Structural Engineering Report No. 171

Department of Civil Engineering

The University of Alberta

Edmonton, Alberta

April, 1991

Abstract

Field failures of drill pipe can have serious economic consequences, and the drilling industry reports that such failures are increasing in number. The basis of existing design guidelines for the fatigue strength of drill pipe is work that was presented in the early 1950's. Although the experimental data upon which the rules were based appear to be valid, the physical models used do not correspond to modern drilling conditions in a number of significant ways. Accordingly, an investigation of the fatigue strength of drill pipe manufactured in accordance with today's standards was conducted. The effects of stress range, mean stress, corrosion, and pipe geometry were investigated. Because of the number of parameters involved, it was not practical to conduct a full factorial experiment, however. Full-size drill pipe was tested in rotating bending under conditions of axial preload and with or without corrosion present. These test conditions correspond closely to the situation in the field. The program included 29 tests conducted in air and 21 tests conducted in a 3.5 percent NaCl solution.

The effects of both stress range and mean stress were found to be significant, and this was true in both non-corrosive and corrosive environments. The change in pipe geometry that exists in the upset region between the pipe body and the tool joint did not influence the fatigue strength for the cases examined. With one exception, the fatigue failures that occurred in the tests took place in the drill pipe body. The exception was a crack that occurred in the upset region and it started from a slag inclusion on the outer surface of the pipe.

It is required that all drill pipe be inspected before it is released for service. One result of the inspection procedure is light grinding on the surface of the pipe, done in order to remove small imperfections. The effect of this grinding was found to be detrimental to the fatigue life of the pipe. About 50 percent of the test specimens failed as the result of fatigue cracks that originated at grinding marks. The reason is twofold. The notch effect created by the grinding affects the fatigue strength; this phenomenon is well known. Furthermore, X-ray diffraction studies showed that beneficial compressive residual stresses on the surface of the pipe are removed by this grinding and replaced by high tensile residual stresses. The latter promote fatigue crack growth.

Fractographic examinations and a fracture mechanics analysis of the failed drill pipe both indicated that once a fatigue crack has grown through the wall thickness, the fatigue

crack will propagate rapidly. Thus, rupture of the drill pipe is likely to occur shortly after a fatigue crack has been detected in the field operation.

A critical evaluation of the current design guidelines of the American Petroleum Institute for drilling in a non-corrosive environment shows that those rules overestimate the fatigue life of drill pipe. They predict less fatigue damage than predicted by the results of the investigation reported herein. A similar examination shows that, when drilling in a corrosive environment, the existing guidelines are conservative under conditions of high axial load in the pipe and unconservative under conditions of low axial load.

Acknowledgements

The research described in this report was conducted with financial assistance received from the Natural Sciences and Engineering Research Council of Canada. Drill pipe for part of the test program were supplied *gratis* by National-Oilwell Canada Ltd., who also donated equipment used for the power drive of the rotating beam test series. Help in making up the connection in the specimens with a tool joint was provided by Lee Oilfield Service Ltd. All of these contributions are acknowledged with thanks.

The senior author acknowledges financial support received in the form of scholarships from the following organizations: the Natural Sciences and Engineering Research Council of Canada, the Steel Structures Education Foundation, Petro-Canada Inc., The O'Brien Foundation, and the Faculty of Graduate Studies of the University of Alberta. The report contained herein is based on the Ph.D. Dissertation of the senior author.

The assistance of technicians in the Department of Civil Engineering, the Department of Mechanical Engineering, and the Department of Mining, Petroleum and Metallurgical Engineering of the University of Alberta is acknowledged with thanks.

The interest shown by John Robertson of National-Oilwell Canada Ltd. is appreciated. Mr. Robertson educated the authors into field practice of the drilling industry and helped to establish valuable contacts with persons in that industry. Thanks are also extended to Mr. Maurice Slack of the Centre for Frontier Engineering Research, Edmonton, for his helpful advice during the initial stage of the test program, and especially for suggesting the method of prestressing used to axially preload the test specimens. Dr. M.L. Wayman of the Department of Mining, Petroleum and Metallurgical Engineering gave freely of his time to instruct and assist in the metallurgical examinations.

Table of Contents

List of Symbols

General

c_o = Curvature of drill pipe adjacent to a support.

c_d = Curvature of dogleg.

D_o, D_i = Atomic plane spacing in the unstressed and stressed state, respectively.

E = Modulus of elasticity.

k_s = Axial stiffness of a stiff radial truss member.

L_b = Average gage length before sectioning.

L_a = Average gage length after sectioning.

m_φ = Stress function defined by Eq. (3-13).

T = Axial load on drill pipe in a dogleg.

T_h = Horizontal component of axial tension force in drill pipe.

T_v = Vertical component of axial tension force in drill pipe.

δ = Deflection at the middle tool joint used in the finite element analysis.

ε_{rupt} = Strain at rupture.

$\varepsilon_{\varphi,\psi}$ = Strain in a direction defined by angles φ and ψ.

φ = Angle between the major principal stress and σ_φ on the plane of the surface.

λ = Wavelength.

σ_b = Bending stress resulting from curvature c_o (Eq. (6-48)).

σ_r = Residual stress.

σ_U = Ultimate strength.

σ_Y = Yield strength.

σ_φ = Stress on the plane of the surface.

σ_1, σ_2 = Major and minor principal stresses parallel to the surface.

Θ_o = Angle between incident beam and atomic planes.

ψ = Angle between strain vector and normal to the surface.

Fracture Mechanics

a = Half length of major axis of an elliptical crack.

a_{cr} = Through-thickness crack size at onset of unstable crack propagation.

a_i = Size of initial through-thickness crack.

A,n = Crack growth rate constants for Paris model.

c = Half length of minor axis of an elliptical crack.

c_{cr} = Critical part-through crack size (given by Eq. (6-17)).

c_i = Initial part-through crack size.

c_f = Final part-through crack size.

F = Boundary correction factor (given by Eq. (6-33)).

K_c = Fracture toughness for material and thickness.

K_{Ic} = Plane strain fracture toughness for opening mode crack loading.

K_P = Stress intensity factor for part-through crack (given by Eq. (6-31)).

N = Fatigue life in number of cycles.

N_f = Total fatigue life.

N_P = Part of the fatigue life expended to propagate a part-through crack.

N_{ref} = Reference fatigue life.

N_T = Part of the fatigue life expended to propagate a through-thickness crack.

Q = Crack shape correction factor given by Eq. (6-13).

Q' = Shape factor for an ellipse (given by Eq. (6-32)).

R = Ratio of minimum stress to maximum stress in a loading cycle.

S_a = Alternating stress, equivalent to half the stress range.

S_b = Bending stress at outer surface of pipe.

S_f = Fully reversed fatigue strength.

S_m = Mean stress.

S_r = Stress range.

t = Drill pipe wall thickness.

w = Finite width of a flat plate.

α, m = Crack growth rate constants for Forman's model.

ΔK_P = Range of stress intensity factor for a part-through crack.

ΔK_T = Range of stress intensity factor for a through-thickness crack.

ϕ = Crack geometry factor given by Eq. (6-14).

σ_{max} = Maximum stress in a loading cycle.

Statistical Analysis

a = Intercept of the regression line on the logN axis.

b = Slope of regression model.

$\bar{b}$ = Common estimate of the slope of two regression lines (given by Eq.(6-7)).

b_1, b_2 = Multiple linear regression constants.

F = Statistical F ratio given by Eq. (6-3).

n = Sample size.

r^2 = Coefficient of determination.

s = Standard deviation of the sample.

s_b = Standard deviation of the slope (given by Eq.(5-4)).

s_e = Standard error of estimate given by Eq.(5-6).

$s_{\bar{b}}^2$ = Estimated variance of $\bar{b}$ given by Eq. (6-8).

$t_{\alpha/2}$ = Student's t value for a level of confidence of $(1-\alpha)$.

x_i = ith value of independent variable x.

$\bar{x}$ = Mean value of x.

y_i = ith measured value of logN.

$\hat{y}$ = predicted y (logN) from regression model.

$\bar{y}$ = Mean value of y.

ε = Error term in regression model.

Chapter 1

Introduction

1.1 Background

1.1.1 The Drill String

A critical part of the rotary drilling system is that portion which physically creates the hole: the drill string. The main components of a drill string are the kelly, the drill pipes, drill collars, accessories including heavy-wall drill pipe, jars, stabilizers, reamers, shock subs and bit subs, and the drill bit. A typical drill string assembly is illustrated in Figure 1.1.

The kelly is a four or six-sided piece of pipe used to transmit rotation and weight to the drill bit via the drill pipes and drill collars. The shape of the kelly allows it to transfer the rotating motion of the rotary table to the drill string. The kelly is mounted in an opening of similar shape contained in a device called the kelly bushing. The kelly is free to move up and down through the rotary table while it is being turned. In this manner, the drill string is allowed to move steadily down the hole as it rotates and drills deeper. The kelly must also carry the total weight of the drill string, and it is therefore the most heavily loaded item of the drill string. Kellys are manufactured from high grades of chrome-molybdenum steel and are heat treated.

Attached to the kelly is the drill pipe. The main function of drill pipe is to transmit rotary motion and drilling mud under high pressure to the drill bit. Drill pipe comes in lengths of approximately 10 meters. These are called joints. The wall thickness of the drill pipe is increased near the pipe end, where a coupling has been attached by welding. The region of increased wall thickness is called the upset. According to the type of upset, drill pipe can be described as internal upset (IU), external upset (EU), or internal-external upset (IEU). The couplings, also called tool joints, are short, cylindrical pieces attached to each end of a drill pipe joint. Tool joints are threaded either externally or internally. The externally threaded end of the drill pipe tool joint is described as the 'pin', whereas the internally threaded end is described as the 'box'. As the drill string is assembled, the pin of one length of pipe is threaded into the box of another length. Drill pipe is manufactured in three length ranges: Range 1 is from 5.5 to 6.7 m, Range 2 is from 8.2 to 9.1 m, and Range 3 is from 11.6 to 13.7 m. Range 2 drill pipes are, by far, the most widely used.

Five grades of drill pipe are also available to suit different loading requirements. The American Petroleum Institute specifies grades D, E, X95, G105, and S135. The five grades are also manufactured in different sizes, ranging from 60.3 mm to 168.3 mm O.D. More information about the manufacture of drill pipe is given in a later section.

Drill collars are used to provide weight on the bit and to keep the drill pipe in tension. Consequently, drill collars are placed directly above the drill bit. Because of their relatively large bending rigidity, drill collars help keep the borehole straight and provide the strength needed to run in compression. Drill collars are available in many sizes and shapes, such as round, square, triangular, and spiral grooved. Because of the large thickness of the body of drill collars, they are not provided with welded-on tool joints. Instead the pins and boxes that make up the joint are simply cut from the pipe body.

Heavy-wall drill pipe is placed between standard drill pipe and the drill collars in order to provide a more gradual transition in drill string stiffness. The heavy-wall drill pipe has the same outside diameter as standard drill pipe, but has a much reduced inside diameter and has an extra long tool joint. Heavy wall drill pipe can be distinguished by an integral center wear pad which acts as a stabilizer. The heavy-wall drill pipe is also used to provide weight on the drill bit in addition to the weight provided by the drill collar.

Drilling jars are used during operations to free stuck pipe when an upward or downward pull is required to free the pipe. Stabilizers are tools placed above the bit and along the bottom hole assembly to control hole deviation and minimize dogleg severity. Dogleg severity is defined as the amount of angular deviation of the borehole per 30 m of hole. Stabilizers achieve these functions by centralizing the drill string and providing extra stiffness to the bottom hole assembly. Shock subs are placed between the drill collars and the drill bit to absorb vibrations and impact loads caused by the movement of the drill string. The drill bit, attached at the end of the drill string, is generally designed with three cone-shaped wheels equipped with hardened teeth for cutting the rock. All bits have passages that allow drilling fluid to pass through and sweep away the rock cuttings as the bit drills deeper.

1.1.2 The Drilling Environment

Corrosion in various forms is probably the major cause of drill pipe failures. The trends toward drilling of deeper wells, use of higher strength steels, operation at higher

stress levels, and use of lower pH drilling fluids contribute to increased susceptibility of metals to failure due to corrosion.

The drill pipe operates in a drilling fluid which serves many purposes, including removal of the cuttings from the bottom of the borehole and cooling and lubrication of the drill bit and the drill string. Many types of drilling fluids are used by the industry. The major categories include air-based, water-based, and oil-based fluids. Water-based fluids can make use of either fresh or salt water. Although fresh water has been used extensively as a drilling fluid, salt water has become more common because of its availability in offshore drilling. The density of the drilling fluids is usually adjusted by addition of solids such as clay minerals and salts. Other chemicals are also often added to drilling fluids to obtain properties considered desirable for improvement of the drilling efficiency. The type of drilling fluid used depends on factors specific to the drilling conditions encountered in the field. Indeed, the properties of the drilling fluid can vary within the same borehole.

The corrosivity of the drilling fluid will change with time due to dissolution of gases and minerals from the formations through which drilling is performed. The principal corrosive elements that can enter the drilling fluids include oxygen, hydrogen sulfide, carbon dioxide, and chlorides.

Oxygen

Oxygen dissolved in drilling fluids is the major cause of drill pipe corrosion. Because it acts as a depolarizer and electron acceptor in cathodic reactions, oxygen accelerates the anodic destruction of the metal. Oxygen is supplied to the metal by the high velocity flow of drilling fluids over the surfaces of the drill pipe. Aeration of drilling fluids, done to improve the penetration rate during drilling, also provides more oxygen to the environment surrounding the pipe. Oxygen corrosion of drill pipe also occurs while the pipe is out of the hole. The main form of corrosion in the presence of oxygen is pitting. Pitting can develop rapidly under particles of mud solids which are left on the pipe. Pits provide sites for further local attack of the drill pipe while it is on the surface. Because oxygen is a depolarizer, it will drastically increase the corrosivity resulting from other dissolved gases such as hydrogen sulfide or carbon dioxide.

Hydrogen Sulfide

Hydrogen sulfide is very soluble in water and, when dissolved, behaves as a weak acid. Hydrogen sulfide damages drill pipe by promoting sulfide cracking or embrittlement. It can be present as a result of the reaction of acids on metal sulfides or it can be found as a

component of formation gases dissolved in water or hydrocarbons. Thermal cracking of organic material can create hydrogen sulfide along with other gases. The presence of sulfate-reducing bacteria is one of the original sources of sulfur as these reduce sulfates to sulfur.

Carbon Dioxide

When carbon dioxide dissolves in water it forms carbonic acid and, consequently, the corrosivity increases as the pH decreases. Although carbon dioxide is not as corrosive as oxygen, it can cause pitting on the drill pipe surface.

Chlorides

Chlorides can be present in the drilling fluid as a result of dissolution of formation materials or because it is introduced as an additive to drilling fluids when drilling through a salt formation in order to prevent the formation of large cavities in the salt formation. Brine fluids are also used for other purposes, such as inhibition of clay hydration. In addition, in offshore drilling seawater fluids are more economical than freshwater fluids. The most commonly used chlorides as a drilling fluid additive are potassium chloride, sodium chloride, and calcium chloride. The sodium chloride system is probably the most common brine water used in drilling due to its availability.

Addition of chlorides to the drilling fluid increases the conductivity of the electrolyte and, as a result, increases the corrosivity. The form of corrosion most likely to take place in the presence of chlorides is pitting. Chloride ions form metal chlorides with metal ions formed during the oxidation process. The metal chlorides hydrolyze in water and result in the formation of an insoluble hydroxide and free acid, which in turn accelerates the dissolution of metal (Fontana, 1986).

1.1.3 Manufacture of Drill Pipe

Drill pipe is manufactured in four different grades (grades D, E, X95, G105, and S135), and they are identified by tensile yield strength, size and end geometry. The tensile yield strength varies from 380 MPa for Grade D drill pipe to 930 MPa for Grade S135 drill pipe.

The manufacturing process of a drill pipe consists of the following stages: forming of the drill pipe body, forging of an upset at each end of the pipe body, welding of tool

joints, and application of a wear-resistant surface on the tool joint. Inspection of the pipe is carried out at various stages of the production.

In order to meet requirements of the American Petroleum Institute (1988) the drill pipe body must be a seamless pipe. The seamless pipe is manufactured by hot working steel using a piercing process and, if necessary, by subsequently cold-finishing the hot-worked tubular product to produce the desired shape, dimensions, and properties (American Petroleum Institute, 1988; Adams and Charrier, 1985). Low alloy steel of grades AISI 4135 to AISI 4145 is used in order to meet the chemical composition and mechanical property requirements (American Petroleum Institute, 1988). Immediately after hot-forming of the pipe body, both ends of the pipe are hot-forged to form an upset to which a tool joint will be welded later. Following the upsetting operation, the full length of pipe must be heat treated. Although minimum strengths for drill pipe steel are specified, the heat treatment process used to achieve those strengths is left to the discretion of the drill pipe manufacturer. Commonly, grade E drill pipe is subjected to a normalize and temper heat treatment and the higher grades drill pipe are subjected to a quench and temper heat treatment (Vingoe, 1972).

Inspection of the finished drill pipe is carried out before welding of the tool joints, which are often welded by a processor other than the drill pipe manufacturer. Inspection is performed in compliance with specified procedures outlined by the American Petroleum Institute (1988). Any linear imperfection (seams, laps, cracks, cuts, gouges) or nonlinear imperfection, such as a pit, having a depth greater than 12.5 percent of the specified wall thickness is considered a defect. When a defect is detected it may be removed by grinding (provided the remaining wall thickness is not less than 87.5 percent of the specified wall thickness), or the section of pipe containing the defect may be cut off (within the limits of length requirements), or the pipe in which the defect was detected is rejected. In addition to visual inspection, drill pipes are inspected over their full length for longitudinal defects using either magnetic particle, ultrasonic, or electromagnetic methods. The ends of upset pipe are also inspected for transverse defects, using the magnetic particle method. Typically, most drill pipes are inspected three to four times before the operator is satisfied to run the pipe downhole (Stanley, 1987). Often, such inspections are conducted by different companies.

Following the upsetting operation and after passing the inspection, the upset drill pipe is ready for attachment of a tool joint. Tool joints are machined separately from the drill pipe body and are welded to the upset end in the neck assembly. There are three

accepted methods of welding tool joints to drill pipe: flashweld, inertia welding, and friction welding. A controlled heat treatment is necessary after welding in order to prepare the welded joint for oilfield service. The minimum heat treatment is to normalize and temper the weld and the heat affected zone. The minimum heat treatment process has been found to be satisfactory for the flashwelded tool joint but not acceptable for the inertia welded and friction welded drill pipes (Smith, 1978). A better heat treatment process is to austenitize, quench, and temper the weld and heat affected zone to make the three welding techniques completely interchangeable from a standpoint of service (Smith, 1978).

The final stage of the manufacturing process is protection of the tool joint against accelerated wear by applying a wear resistant hard band on tool joint boxes close to the elevator shoulder (Best, 1983; Gooch, 1977; True, 1975; Williamson and Bolton, 1983). The hardfacing bands are composites of steel and tungsten carbide. Since the welding is done on steels which have a carbon equivalent beyond that which is generally considered weldable, it is necessary to preheat the weld region before welding and to follow the welding with a post-heat treatment to prevent cracking of the heat affected zone. Tool joints often need to be resurfaced during the life of a drill pipe. The same procedure used on new tool joints is also employed on used tool joints. In addition to protecting the tool joint from wear, the interior of the pipe is usually protected from corrosion by application of a plastic coating on the inner surface of the pipe and tool joint.

1.2 Statement of the Problem

Fatigue damage occurs to drill pipe when it is subjected to sufficiently large alternating stresses such as those created when the drill pipe rotates in a curved portion of the well bore. The well bore may be curved as a result of accidental or otherwise unintentional deviation, which gives rise to a dogleg. On the other hand, the well bore may be curved intentionally, such as is done for deviated and horizontal wells. Deviated holes are drilled to get around obstacles between the drilling rig and the reservoir, or in order to permit the drilling of more than one hole from the same platform (see Figure 1.2). The main reasons for drilling horizontal wells is to improve recovery and increase productivity by drilling a horizontal hole at the bottom of a gravity drainage reservoir (Moritis, 1990; Holbert, 1985). Deviation in borehole can be as low as 1 degree per 30 m of borehole or less for straight drilling, and it can be as large as 50 degrees per 30 m of borehole for horizontal drilling (Moritis, 1990). Although some horizontal holes have been drilled by using small deviations (less than 3 degrees per 30 m), the incentive for using a more severe

deviation is great since the portion where the borehole goes from near vertical to horizontal has a large influence on the cost of the well (Holbert, 1985).

Rotation of a drill pipe in the curved portion of a hole induces cyclic stresses in the drill pipe because of the bending reversal of any given point on the pipe wall. Stress cycling in the drill pipe can also take place as a result of vibration of the drill string. Three different types of vibration have been identified through field measurements using instrumented drill strings, namely, axial vibration due to bouncing of the drill bit as it rotates on a hard formation, torsional vibration due to friction forces developed between the wall of the borehole and the drill string, and bending vibration. As a result of those different sources of cyclic stresses, the stress spectrum for a drill pipe in a crooked hole is complex.

In addition to bending of the drill pipe as it is forced through the curved portion of a borehole, axial loads are also applied to the drill pipe. In a vertical hole, the axial load results from the weight of the drill pipe below the dogleg, which puts the drill pipe in tension. In vertical or moderately deviated drilling it is the practice to keep the drill pipe in tension in order to prevent buckling and excessive vibration of the drill pipe. The drill pipe is kept in tension by using more drill collar than that required to provide the desired force on the drill bit. However, when drilling a horizontal well, the portion of the drill string located in the horizontal portion of the well bore will be subjected to compression. Under such a condition , buckling of the slender drill pipe in the horizontal portion of the borehole can take place. Although compressive forces are known to extend the fatigue life, the additional bending stresses created in the drill pipe when buckling takes place more than offsets the beneficial effect of the compressive force.

In addition to the forces created in a drill pipe as it rotates in the curved portion of the borehole, drill pipes are also subjected to a corrosive environment. The nature of the corrosive medium is highly variable since the corrosive environment is provided by the drilling mud which contains various chemical additives depending on the drilling conditions. As discussed earlier, the environment not only depends on the mud composition used for drilling but also on the nature of the formations through which drilling is performed. Dissolution of formation materials and gases constantly modifies the characteristics of the drilling mud.

1.3 Scope and Objectives

The oil industry has developed guidelines for the fatigue life evaluation of a drill string (American Petroleum Institute, 1989). The rules identify the maximum level of dogleg severity below which no fatigue failure should take place. If this level cannot be met, the rules will allow for monitoring of the fatigue damage. The guidelines originated from experimental work performed in the 1930's and the 1940's by Hughes Tool Co., and presented in the early 1950's by Bachman (1951). Although the tests presented by Bachman served the purpose for which they were designed (to evaluate the fatigue resistance of tool joints and drill pipe affected by the presence of the tool joint) they were neither performed in a corrosive environment nor under a superimposed axial load, two factors considered important in the fatigue life of drill pipe. As the search for petroleum moves into more hostile environments, requiring drilling to greater depths and in more corrosive media, the drilling contractor is again confronted with fatigue problems of drill pipes. It is estimated that 14 percent of all rigs experience drill string failures (Moyer and Dale, 1984) and recent publications show that failure of drill strings is still a major concern to drilling contractors (Marion, 1987; Joosten et al., 1985; Dale, 1986). In order to address the present concerns of the drilling industry, the research program presented herein was designed with the following objectives:

1. To review the existing literature on fatigue and field loading of drill pipe.

2. To design a testing apparatus capable of testing full-size drill pipes in rotating bending, under a superimposed axial load, and in a corrosive environment.

3. To obtain fatigue test results in air and in a corrosive environment on drill pipes representative of the ones presently in use by the industry.

4. To determine experimentally the effect of stress range, mean stress, and corrosive environment on the fatigue life of drill pipes.

5. To investigate the significance of residual stresses in drill pipes and their effect on the fatigue strength.

6. To identify the most prominent origins of fatigue failures in drill pipe in order to identify the area where most significant improvement in drill pipe can be made.

7. To investigate the effect of drill pipe upset geometry on fatigue life.

8. To assess the existing fatigue design guidelines for drill pipes in light of the recently obtained test results.

The main test program was conducted on API Grade E 114 mm O.D., 24.7 kg/m drill pipe with an external-internal upset geometry. The experimental program in a corrosive environment was carried out in a 3.5 percent sodium chloride solution. This represents a simplification of the field environment, which is very complex compared to the environment used for the test program. To obtain quantitative evaluation of the effect of the different types of drilling environment encountered in the field represents a formidable task and such a task is not included within the scope of this study. Consideration of dynamics of the drill string as it affects cyclic loading of the drill pipe is also beyond the scope of the work presented herein.

1.4 Organization of the Thesis

A literature review is presented in Chapter 2. This outlines the research done in the area of fatigue of drill pipe since the beginning of the century and also presents the work done to measure loading in drill pipe under field conditions. Having identified the need for further research, Chapter 3 then presents a description of a test setup and testing procedure used to investigate the effect of stress range, mean stress, and corrosion on the fatigue resistance of drill pipe. Chapter 3 also presents the procedure used to measure residual stresses in drill pipes. The test results are then presented in tabular and graphical form in Chapter 4. The analysis performed on the test results in order to quantify the effect of the various parameters investigated in the test program is presented in Chapter 5. Chapter 6 presents a comparison of the present test program with results of test programs and analytical work presented by other investigators. A comparison of test results with the current design guidelines is also present in Chapter 6. Finally, a summary, conclusions, and recommendations for further research are presented in Chapter 7.

Characteristic dimensions of the drill pipes used in the experimental program are tabulated in Appendix A. Details of the end fixtures used to test drill pipes in cyclic tension are presented in Appendix B. The details and dimensions of drill pipe prestressing hardware are presented in Appendix C. The finite element analysis performed to investigate the effect of upset geometry on stress concentration in a drill pipe is presented in Appendix D. Appendix E presents the analysis performed to estimate the effect of bearing pressure on the state of stress in a drill pipe.

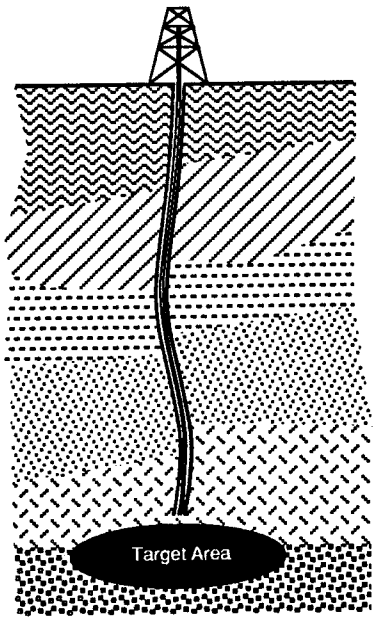

(a) Dogleg (Accidental Deviation)

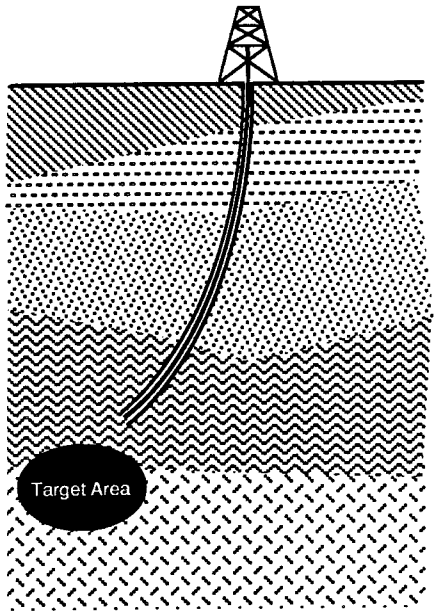

(b) Deviated Drilling (Intentional Deviation)

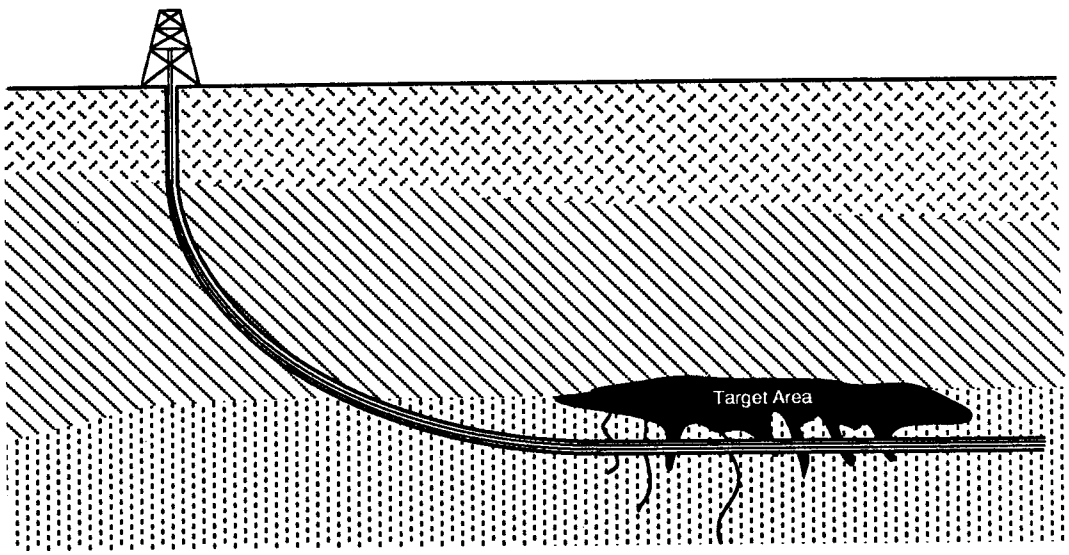

(c) Horizontal Drilling (Intentional Deviation)

Figure 1.2 Causes of Borehole Deviation in Oil Well Drilling

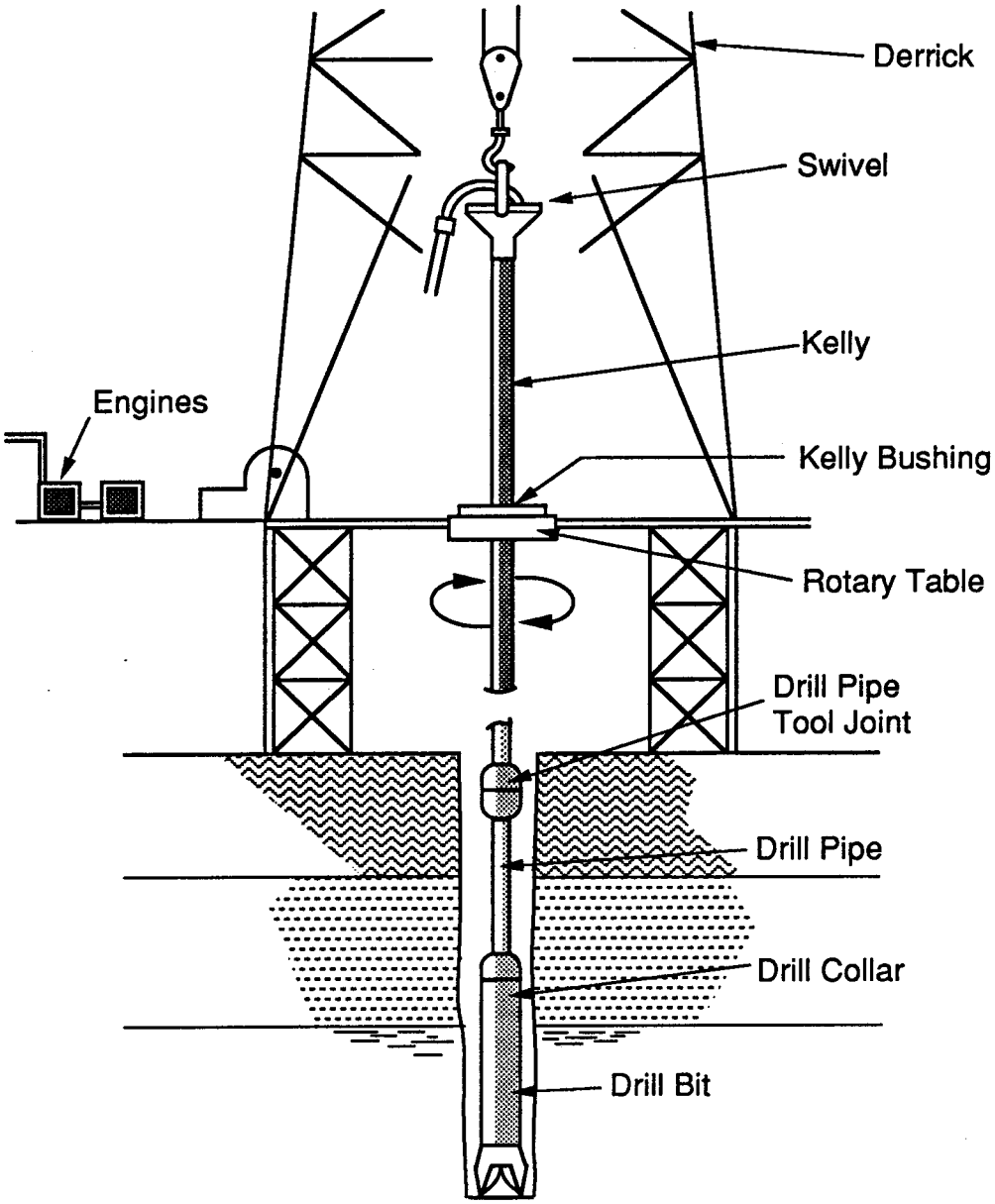

Figure 1.1 Rotary Drilling System

CHAPTER 2

Literature Review

2.1 Development of Tool Joint

As the depth of drilling increased beyond a single length of drill pipe, the need to join lengths of drill pipe became an obvious necessity. Equally obvious, the presence of joints in the drill string creates local stress concentration where fatigue failures will take place preferentially. Furthermore, in the early days of oil well drilling drill pipes were being used in compression in order to apply the necessary downward force on the drill bit. Buckling of the drill pipe in compression induced large bending stresses, thus accentuating the effect of stress concentration at the joints. Typically, early drill pipes failed at the last engaged thread of the threaded joint. When the use of drill collar became more widespread as a means of applying the necessary downward force on the drill bit, leaving the drill pipe in tension, the oil well drilling industry saw a net decrease in drill pipe fatigue failures (Grant and Texter, 1941; Shutts, 1934). However, the number of drill pipe failures in the joint area remained a major concern of the industry for many years.

Early research on fatigue of drill pipe paralleled the development of the connection used to join lengths of drill pipe (Fletcher, 1935; Graham, 1935). One of the first joint configurations used for drill pipe was a short, fine thread coupling (Shutts, 1934) (see Figure 2.1). Fine V-threads were machined on the pipe ends, thus reducing the effective wall thickness at the joint. Because of the necessity of continually making-up and breaking-out the joints, it soon became apparent that the fine thread coupling could neither stand hard usage nor be made-up and broken-out fast enough. Furthermore, if handling damage and galling of the threads did not put the drill pipe out of service, fatigue failure at the last engaged thread did. Several alternative types of joints were investigated largely to overcome the notching effect of the V-thread. In about 1910 the first heavy section tool joints were introduced (Figure 2.2). The coarse tapered threads meant the make-up and break-out were faster, but galling of the threads was still a problem. In 1918 the first tool joints made of alloy steel were introduced, and in 1925 they were adopted as a standard by the American Petroleum Institute (Bachman, 1951). The tool joints were now more durable but they were still connected to the pipe with sharp V-threads and, as a consequence, failure of the pipes occurred at the last engaged thread. In an effort to eliminate failures at the last engaged thread, the pipe was upset on the ends enough to

compensate for the material removed by threading and later the upset thickness became up to 2.5 time the body wall thickness. Threads were also changed from sharp to rounded crests and roots in an effort to reduce stress concentration. Failures in the last engaged thread did persist, however. Oxy-acetylene welding of the threaded tool joint to the drill pipe body was also attempted in an effort to reduce the stress concentration at the last engaged thread but the success was minimal.

This shortcoming in the threaded tool joint pointed the way for the next drill string improvement. Flash weld tool joints were introduced in 1938, first with the welds made in the heavy portion of the tool joint; this required that a heavy and costly upset to be forged on the pipe ends (Smith, 1978) (Figure 2.3(a)). To reduce the cost of the upset, the flashweld was later located in the neck assembly (Figure 2.3 (b)). Before the seamless or piercing method of making pipe was introduced, the welding method of manufacturing pipe necessitated low-carbon content, which means that the early drill pipe was of this type. When the piercing method was introduced, the low-carbon analysis was still adhered to but failures in drilling and greater depths of hole brought recognition of the possibilities of the seamless method for making drill pipe of higher carbon content and, consequently, of greater strength. Flash welding tool joints to higher carbon content drill pipe created problems in the heat affected zone. The lower toughness of the heat affected zone was even more problematic when the weld was moved into the neck assembly. It took the industry 40 years to develop the flash welded drill string as it is used today (Smith, 1978).

2.2 Reports of Field Failures

Early reports of field failures of drill pipes indicate that cyclic stresses resulting from rotating a pipe in a dogleg, coupled with the action of a corrosive environment, caused premature failure of the pipes at the last engaged thread and sometimes in the pipe body (Grant and Texter, 1941; Shutts, 1934; Bachman, 1951). The literature often refers to failures simply as washouts or twistoffs, without reference to the exact cause of the failure. A washout takes the form of a hole in the pipe as a result of a crack formed under stress and then enlarged by the eroding action of the drilling mud stream. Another common type of washout results from a bad seal in the threaded joint where mud flow quickly erodes the threads. A twistoff results when the crack propagates to such an extent that a complete failure or break occurs.

A paper by Grant and Texter (1941) outlined the different causes of fatigue failure. Although most of the causes identified in the paper have now been eliminated by better field

practice, some of the causes identified still seem to be present today. The many possible causes of failures include (Casner, 1961; Grant and Texter, 1941; Rollins, 1966; Shryne and Smith, 1986; Speller, 1935; Vingoe, 1972) the presence of surface damage such as slip marks, gouges, welding arc spots, stenciled numbers, etc, when failures originate from the outside surface. Many times failures have also been reported to originate from the inside surface of the pipe, and these have been associated with severe pitting of the inside of the pipe (Grant and Texter, 1941; Vingoe, 1972; Rollins, 1966; Jackson et al., 1947; Speller, 1935). Field research carried by Thompson and Texter (1948) on a drill string made up of mill rejects showed that corrosion fatigue was the major cause of drill pipe failure and that mechanical or geometrical defects resulting from the manufacturing process which would lead to drill pipe rejection were not the cause of any of the failures observed on the experimental drill string. However, it is considered that the outcome of their experiment could have been different if the pipes had been coated to lower the corrosion severity.

Despite the effort made by the oil well drilling industry in the past 80 years to alleviate the problem of fatigue failures in drill pipe, recent literature indicates that it remains a major concern of the industry (Anon., 1990; Chinese Petroleum Standardization Committee, 1987; Dale, 1988a; Gensmer, 1986; Hampton, 1987; Helbig and Vogt, 1987; Joosten et al., 1985; Marion, 1987; Raseev and Ulmann, 1983; Shryne and Smith, 1986; Tumuluru, 1987). Very few statistical data concerning the location of failures in drill pipe, the type of failures, or their probable causes have been accumulated and published by the manufacturers of drill pipe, by those involved in inspection of used drill pipe, or by major users of drill pipe.

Bush et al.(1966) presented a summary of field failure records of some 3478 drill pipe joints accumulated over a seven year period. The results showed that corrosion played a major role (74 percent of the drill pipe loss), while corrosion fatigue cracks penetrating the tube wall while drilling accounted for 19 percent of the loss. It was noted that 80 percent of the drill pipe failures were located within one metre of the pin or box end of the joint near the upset area.

More recently, published reports of field failures indicate that fatigue cracks can originate in the drill pipe body, typically 75 to 125 mm from the end of the upset transition (Marion, 1987; Tumuluru, 1987). Marion (1987) reports that 80 percent of the observed fatigue cracks start from the outside surface. The distance of 75 to 125 mm from the upset corresponds generally to the area where slips are used (Shryne and Smith, 1986). (Slips secure the drillstring in the rotary table during each connection of a drill pipe to the drill

string. The outer diameter of the slips is tapered and the inner diameter has a set of jaws for "biting" into the pipe. When slips are used to hold the drill string during a connection, circumferencial notches are made on the pipe surface). A recent Chinese study (Chinese Petroleum Standardization Committee, 1987) indicated that approximately 70 percent of the observed washouts are located in the internal upset region of the drill pipe and failures in that area are usually associated with severe corrosion of the inside surface of the drill pipe. The same study also indicated that the failure location is independent of the grade of pipe and drilling site. Thus, it appears that there is reason to believe that tool joint design has arrived at the stage where the location of fatigue failures has been forced into the body of the pipe.

2.3 Experimental Investigations

One of the first attempts to quantify the effect of the corrosiveness of an environment on fatigue life of drill pipe was presented in 1941 by Grant and Texter. A number of bending fatigue tests were performed on small samples of drill pipe, all cut from the same pipe and stressed to the same degree. The only variation in conditions was the medium in which the specimens were stressed and no attempt was made to duplicate field conditions. Various environments were used to obtain different degrees of corrosiveness: distilled water as a non-corrosive medium, salt water as mildly corrosive, magnesium chloride as a definitely corrosive solution, and dilute hydrochloric acid as very corrosive. The test results showed clearly that the life of a fatigue specimen is decreased as the corrosiveness of the fluid is increased. A reduction of fatigue life of 35 percent was reported as the environment changed from distilled water to salt water and a reduction of more than 90 percent was reported for drill pipe steel tested in dilute hydrochloric acid.

In 1947 the Battelle Memorial Institute (Jackson et al., 1947) reported the results of an investigation initiated as a result of frequent drill pipe failures in the Permian Basin. Laboratory tests were performed on Grade D drill pipe steel, the most popular grade of steel for drill pipe at that time. Small steel rotating beam fatigue test specimens were subjected to accelerated corrosion conditions and loaded at a speed of nearly 28 Hz. The failures obtained from these tests were reported to have every feature characteristic of those on used drill pipe, and the actual operating lifetimes obtained under these test conditions were reported to be identical with prior results of a long time, slow speed, full-scale corrosion fatigue test of a joint of Grade D drill pipe. No details of the full-scale test program was given nor the nature of the corrosive environment used for accelerated corrosion tests on small rotating beam specimens identified. As a result of this

investigation recommendations were made to provide protection against corrosion by use of protective coatings, use of inhibitors in the drilling mud, periodic cleaning of drill pipes to prevent crevice corrosion at locations on a drill pipe where mud or other substance tends to adhere, or a combination of these preventive measures.

Thompson and Texter (1948) studied the effect of mill defects on the effective service life of drill pipe. They presented the results of field experimentation in which a 1620 m string of 114 mm drill pipe, made up entirely of mill rejects, was used to drill wells. The lengths of drill pipe were not internally coated, no inhibitors were added to the drilling fluids, and only a minimum of drill collars was employed. In drilling 20 wells totalling 14160 m of hole, 21 drill pipe failures occurred, none originating at a mill defect. Each failure was the result of corrosion fatigue. It was concluded that mill defects, even up to twice the depth allowed by API specifications at that time, had no effect on the service life of drill pipe.

The results of a 15-year investigation performed at Hughes Tool Company were presented by Bachman (1951). These results still represent a major contribution to the understanding of the fatigue strength of drill pipe. The size of test specimen and its geometry were recognized as important factors affecting fatigue life. For this reason the tests were performed on full-size specimens of 114 mm diameter drill pipe. Furthermore, these tests were performed to assess the fatigue resistance of different types of tool joints. Consequently, the test specimens took the form of cantilever beams tested in rotating bending. The tool joint was located at the fixed end of the cantilever. The scatter band of the test results, representing the difference in fatigue strength between the best and the worst specimens, was wide. In addition to the effect of surface pits and mill scale, the hardness of the test specimens was also believed to contribute to the scatter. Among all the various kinds of tool joints investigated, the integral joint with a flash weld was found to be able to develop the fatigue life of the drill pipe body. Regular API threaded connections similar to the one shown in Figure 2.2, widely used at the time the investigation was carried out, all failed in the pipe at the last engaged thread. All the test results presented by Bachman were obtained from tests performed in air without the presence of a superimposed axial load (i.e. under zero mean stress).

Experimental work presented by Battelle Memorial Institute in 1964 was reported in a paper presented by Rollins (1966). The effect of surface finish on fatigue resistance of drill pipe steels was investigated using notched and unnotched specimens. It was found that notched specimens could tolerate 138 MPa alternating stress while the unnotched

specimens could tolerate a stress range of 586 MPa at 5 million cycles. In the same investigation the effect of mean stress was studied on S-135 steel under cyclic tension. Without any tensile preload the notched specimens sustained a stress range of 138 MPa for a life of 5 million cycles, while the unnotched specimens sustained a stress range of 586 MPa for a life of 5 million cycles. For a 276 MPa tension preload, the 5 million cycle life was obtained with a stress range of 470 MPa and 103 MPa for unnotched and notched specimens, respectively. At a 550 MPa tension preload the values were 380 MPa for unnotched specimens and 62 MPa for notched specimens.

Starting in the mid 1970's multiple experimental investigations on fatigue of drill pipe have emerged as a result of a reported increased frequency of drill pipe failures. Azar and Lummus (1976) conducted experiments to determine the effect of drilling fluid pH on the corrosion fatigue performance of Grade D drill pipe. Actual drilling fluids were used for the investigation. Fatigue test specimens were machined from steel sheets meeting Grade D drill pipe mechanical properties requirements. The tests were conducted at 200 rpm and the pH was adjusted periodically by adding sodium hydroxide (NaOH) to the mud system. A range of pH between 8 to 11 was investigated. No appreciable difference was found in drill pipe material fatigue performance in the various corrosive environments. A similar investigation was presented later by Azar (1979) studying the effect of oxygen, carbon dioxide, and chlorides on drill pipe fatigue. Mud systems containing O_2, CO_2, and chlorides were used for the test environment and test samples were made of Grade E material. The results showed a decrease in life expectancy as the amount of O_2, CO_2, and chlorides in the mud increased. Again, the test results did not show significant influence of pH.

A significant number of new test data on drill pipe fatigue in a corrosive environment were published in the 1980's. Joosten et al. (1985) presented data collected during drilling of 20 wells that enabled a comparison to be made between field observations and a fatigue damage analysis. Field data on pipe sequence, hole deviation, and drilling conditions were compiled for each trip into each well so that a complete drill pipe history was obtained. In order to calculate cumulative drill pipe fatigue damage, baseline corrosion fatigue tests were conducted on Grade G-105 drill pipe. Lengths of 89 mm diameter drill pipe 0.9 m long were tested in three point bending. The specimens were tested both in air and in a potassium chloride - seawater solution (simulated drilling mud). Test frequency and mean stress used for testing were not reported, and only the results of the tests conducted in a corrosive environment were published. Consequently, no

comparison between resistance in air and resistance in a corrosive environment can be made from the published data. During drilling of the 20 wells included in the study no fatigue failure was experienced. Results of cumulative fatigue calculations showed that the maximum cumulative fatigue experienced by any one drill pipe ever used for the operation was 16.3 percent. Study of collected field data and predicted cumulative fatigue did not show a strong correlation between distance drilled for drill pipe and fatigue accumulation. Evidence pointed to the fact that the position of the drill pipe in the string is more influential than the length drilled.

Helbig and Vogt (1987) recently presented the results of more than ten years of investigation on fatigue of drill pipe. Both full-size sections of drill pipe body and small bending specimens were tested under conditions encountered in practice. These tests were conducted with special emphasis on the loading frequency and the effect of corrosion. The test programme was established to study the behaviour of drill pipe of various material grades and of different manufacture under corrosion fatigue, and the manner in which high strength grades can be utilized under this kind of load. Tests on small bending specimens were performed in air, tap water, and a 20 percent sodium chloride (NaCl) solution. The test results from small bending specimens showed that the speed of testing has a significant influence on fatigue life when testing in a corrosive environment. Quenched and tempered steels yielded lower values of fatigue strength than did normalized steels. However, no well-defined effect of the strength level was recognizable. All the tests on small bending specimens were conducted under rotating bending and zero mean stress. Full-size drill pipe specimens consisted of four point rotating bending specimens with a constant moment region 800 mm long. A corrosive fluid consisting of tap water or a 20 percent NaCl solution was circulated inside the pipe. All tests on full-size specimens were conducted under a zero mean stress and at a speed of 100 rpm (1.67 Hz). The test results from full-size specimens did not show a clear difference with respect to the state of treatment - normalized versus quenched and tempered. The reverse bending fatigue strength, referred to 10^7 loading cycles, varied from 34 MPa to 68 MPa for exposure to corrosion, and no endurance limit was observed for tests conducted in a corrosive environment. No full-size specimen was tested in air.

A paper presented by Dale (1988a) outlined the results of an investigation on fatigue failure in drill collars. Although the study focussed on drill collar behaviour, corrosion fatigue crack growth data on API drill pipe steels in air and in three representative water-base drilling fluid environments were also presented. API grades E, X, G, and S drill pipe

steels were tested in air, fresh water mud, seawater mud, and potassium chloride mud. The tests were run under a load ratio of 0.6 and frequency of 5 Hz. A total of 16 fatigue crack growth rate material tests were completed. One test each was conducted for API grades E, X, G, and S drill pipe in air and each of the three water-base drilling fluid environments. The test results showed that the crack growth rate of all the grades of steel was not influenced by the water-base drilling fluid environments under the conditions tested.

Despite its common use, 114 mm O.D., 24.7 kg/m (4.5-in., 16.6 lb/ft) pipe is the only grade E, internal-external upset drill pipe that does not have an industry specification relating to a minimum length of the internal taper. Field study by Gensmer (1988) on drill pipes that failed prematurely (failures occurred after 2800 rotating hours instead of the commonly experienced 18 000 hours) indicated that short taper length was the most probable cause of the failures observed. Although the taper geometry was not proven to be the cause of the field failures studied, a strong enough correlation was established to support further industry investigation of the phenomenon. Short tapers allow an extremely sharp angle in the interior wall surface and a corresponding increase in the stress concentration. The short taper lengths were not found to be common to just one manufacturer or national origin. The taper length was also found to affect the integrity of the internal protective plastic coating, causing early cracking of the coating and accelerated corrosion in some cases.

The geometry of the drill pipe upset to drill pipe body transition zone has been the object of recent investigations. In addition to the work of Gensmer (1988) discussed above, Tsukano et al. (1986) investigated the internal upset geometry of a drill pipe. The finite element method was used to analyze stress concentration in the upset transition zone of the pipe body for different combinations of length of taper and radius of runout (see Figure 2.4). A combination of length of taper and radius of runout was sought for which the stress concentration factor would be less than unity, i.e. which would indicate failure in the pipe body rather than in the transition. Tests on full-size specimens with a length of taper varying from 80 mm to 130 mm and a radius of runout varying from 300 mm to 800 mm were conducted to confirm the findings of the finite element analysis. The tests were performed in a four-point rotary bending type fatigue tester. Full-size 127 mm x 29.0 kg/m (5 in.x 19.5 lb/ft) IEU Grades G-105 and S-135 drill pipes incorporating the tool joint and upset region were tested in air. Tests were conducted at a high stress range since the location of the crack initiation was the factor investigated. None of the specimen tested

failed near the upset and no distinction could be made between the two grades of steel tested. Recommendations were made for suitable internal upset geometry to prevent drill pipe failure in the upset region.

In 1987 the Chinese Petroleum Standardization Committee presented the results of an investigation of the effect of geometry of the transition zone between pipe upset and pipe body. Full-size drill pipes with a transition zone of varying length and radius were tested in air as cantilever rotating beams under no axial load. It was found that the fatigue resistance improved with an increase in length of the transition zone. The minimum length of the transition zone recommended was 80 mm, with a taper radius of at least 300 mm.

Studies on impact toughness of drill pipe steel were recently presented. Tumuluru (1987) presented a study of toughness of API Grades E and G pipe that used instrumented impact tests on Charpy V-notch specimens. The use of instrumented impact testing made it possible to distinguish the stage of crack initiation from that of propagation during the impact tests. Charpy specimens were sampled from the pipe body, upset region, and transition from upset to non-upset region of the drill pipe. Because of the small thickness of the pipe body sub-standard size Charpy specimens were used for the investigation. Standard and sub-standard size Charpy specimens were sampled from the upset region. The test results showed that the energy required to propagate a crack in Grade E pipe was almost equal to or less than the energy required to initiate the crack. This suggests that once a crack initiates it propagates quickly. The toughness behaviour varied from upset to non-upset regions in Grade E pipe. Lowest energy was observed in the non-upset region while energy was similar in upset and transition zones. Greater toughness was obtained from quenched and tempered Grade E of the same hardness as normalized and tempered. Grade G drill pipe exhibited higher toughness and uniform properties throughout the length of the drill pipe.

The following year Buscemi and co-workers (1988) presented a study of Charpy impact toughness on pipes that suffered downhole failure, as well as samples of sound drill pipe and tool joints taken from the field. Three-quarter size Charpy test specimens were taken from the drill pipe body while full-size specimens were taken from the tool joint. The study was conducted on seven failed specimens of drill pipe and 23 sound samples. The results indicated that a minimum Charpy impact toughness requirement of 54 J at 24 ^{o}C appeared to eliminate many brittle failures and parted strings in the field. The investigation showed that the date of manufacture of drill pipe was unrelated to toughness. The pipe samples used in the investigation were manufactured between 1972 and 1985. It had been

postulated that most low toughness products were manufactured in the late 1970's and early 1980's, a time when manufacturers were having difficulty meeting demand.

More recently, the results of an investigation by Shell Canada Limited (Szklarz, 1990) showed that an impact toughness of 80 J at room temperature from three-quarter size Charpy test specimens is required to ensure that washout can occur before parting of the drill pipe. The toughness criterion was based on a fracture mechanics, leak before break, concept for a pipe body containing fatigue cracking, and on field observations of parted pipe and washouts in pipe. An empirical relationship between fracture toughness and impact properties was proposed to allow use of fracture mechanics and leak before break philosophy.

2.4 Existing Guidelines for Fatigue Control

Guidelines for the design of drill pipes have been set forth by the American Petroleum Institute (API) in order to assist the drilling engineer to select the proper size and grade of drill pipe for specific drilling conditions. These guidelines are presented in the form of bulletins of calculation formulas (API, 1989b), bulletins of recommended practice (API, 1989a), and specifications (API, 1988). Usual design criteria for drill pipe include factors related to its ability to withstand tensile loads under static conditions. The factors considered are yield strength, ultimate strength, maximum hook load, and average cross-sectional area. Fatigue life of drill pipe is not usually considered to be a significant design criterion and its importance in the design of a drill string is sometimes overlooked.

2.4.1 Guidelines for Operation in a Non-Corrosive Environment

The first guidelines towards establishing quantitative values for fatigue damage in curved holes resulted from early work by Lubinski (1961). The theoretical analysis performed by Lubinski (1961) to evaluate bending stresses in a pipe rotating in a dogleg of constant curvature also considered the effect of axial tension and the lateral component of the submerged weight of the drill pipe. In this way, dogleg severity (a geometric consideration) was converted to stress range. The theoretical stress range was then compared to the endurance limit for drill pipe to determine whether fatigue damage would occur. To account for the effect of axial load on the endurance limit, a modified Goodman diagram was used. The endurance limit used, 250 MPa, was obtained from laboratory tests conducted in air on drill pipe under no axial load (Bachman, 1951). From this early work Lubinski presented charts from which a dogleg severity below which no fatigue

damage would take place could be selected for a specified value of axial tension on the drill pipe. Consideration was also given to other problems encountered while drilling through dog legs (keyseats, casing wear, excessive drag) by limiting the side load on tool joints to 8.9 kN.

An API Mid-Continent District study committee on straight hole drilling (1963) presented an analysis of approximately 1100 dog legs which occurred in wells drilled in both hard and soft formations. Plots of dogleg severity versus distance of dogleg above total depth for various types of trouble were presented. The types of trouble considered in the study were those encountered during drilling operations, such as keyseats, excessive drag or torque, casing wear, and, to some extent, fatigue failures of drill pipe and drill collar. Fatigue failures were attributed to a dogleg if the failure occurred at or within a reasonably small distance below the dogleg. This necessarily limited the consideration of fatigue failures to very severe cases. An empirical curve of permissible dogleg severity was developed from field data so as to exclude most of the troublesome dog legs. The empirical curve showed reasonable agreement with the limits of dogleg severity proposed by Lubinski (1961).

Further work by Hansford and Lubinski (1964, 1966) extended the earlier work of Lubinski (1961) in an effort to account for cumulative fatigue damage if dogleg severity limits presented by Lubinski (1961) were exceeded. In order to estimate fatigue damage, a stress range versus number of cycles to failure (S-N) curve, representing a lower bound of laboratory test results presented by Bachman (1951), was used in conjunction with Miner's law to account for cumulative fatigue. The results were presented in the form of a chart that could be used to predict the percentage of the total fatigue life expended in a dogleg interval as a function of dogleg severity and tension in drill pipe at the dogleg. The work of Hansford and Lubinski was intended to be applied to Grade E drill pipes and aluminum drill pipes. The guidelines for aluminum drill pipe were derived using fatigue test data presented by Boice and Dalrymple (1963).

In the 1970's, Nicholson (1974) generalized Lubinski's (1961) findings to Grade S-135 drill pipe. Guidelines presented for S-135 drill pipe are based on an endurance limit of 276 MPa. The findings of Lubinski (1961), Hansford and Lubinski (1964, 1966), and Nicholson (1974) have been adopted as recommended practice by the American Petroleum Institute (1984).

2.4.2 Guidelines for Operation in a Corrosive Environment

When the fatigue guidelines for drill pipe outlined in Section 2.4.1 were developed, test results for fatigue of drill pipe in a corrosive environment were non-existent. To account for the detrimental effect of a corrosive environment on fatigue life, the fatigue curve obtained from tests conducted in air was lowered by 40 percent (Hansford and Lubinski, 1964). Although this simplified approach to account for the detrimental effect of a corrosive environment was recognized to be conservative at high stress levels and not conservative at low stress levels, the proposed guidelines are still used today.

Particular consideration has been given to steel components operating in environments containing hydrogen sulfide (H_2S). During the early 1950's, the oil industry in both the USA and Europe experienced failures of wellhead equipment in gas and oil wells containing hydrogen sulfide (NACE Committee 1-G, 1952; NACE Committee T1G, 1954). As a result of these failures, extensive research programs were introduced to provide means of overcoming the problem. A compilation of classic papers outlining research done on sulfide corrosion cracking and sulfide corrosion until the late 1970's has been prepared by the National Association of Corrosion Engineers in 1981 (Tuttle and Kane, 1981).

The type of failure generally observed in an environement containing hydrogen sulfide has been simply termed sulfide stress cracking so as to avoid specifying a mechanism of cracking. However, it is now generally accepted (Snape, 1967; Phelps, 1967) that failure occurs as a result of hydrogen embrittlement cracking.

Many investigators have demonstrated that resistance to sulfide cracking decreases with increase in strength level (Snape, 1967; Carter and Hyatt, 1977; Frazer and Treseder, 1952). The importance of strength level has been well recognized by the petroleum industry in the selection of materials for service in H_2S environments. On the basis of laboratory and field tests and service experience, the National Association of Corrosion Engineers (NACE) has published recommendations (NACE Standard MR-01-75, 1984) aimed at providing materials that are highly resistant to sulfide stress cracking. Essentially, it states that the hardness should not exceed 22 HRC, although there are additional limitations concerning cold work and nickel content of the steel. The hardness limit corresponds to a tensile strength of about 800 MPa.

Existing literature contains considerable evidence supporting the 22 HRC criterion.

Treseder and Swanson (1968), Ishizuka and Onishi (1967), Warren and Beckman (1957) have shown that various steels of various chemical compositions were not susceptible to cracking when HRC was 15 to 21. In spite of all the evidence that supports the NACE recommendations, some studies have demonstrated that cracking can occur at lower strength levels. Hudgins et al. (1966) concluded that a conservative hardness of notched C-ring specimens in high hydrogen sulfide systems would be 16 HRC. Baldy (1961) also found that 0.2 C-Mn-Mo-V steel normalized and tempered to a hardness of 17 HRC was susceptible to cracking.

It has been established that cold working has a detrimental effect on sulfide cracking resistance. This is recognized in NACE recommendations for selection of materials for use in sulfide environments (NACE Standard MR-01-75, 1984). Cold worked materials must be tempered at 595 °C, minimum, to a hardness of 22 HRC or less. The adverse effect of cold working has been associated with at least two factors: (1) production of potential sites for crack initiation, and (2) increasing the hydrogen solubility of steel (Darken and Smith, 1949; Boniszewski and Moreton, 1967).

In order to minimize susceptibility to sulfide stress cracking, NACE recommendations (NACE Standard MR-01-75, 1984) also limit the nickel content of steel to one percent. There has been controversy regarding the effect of nickel on sulfide stress cracking resistance. Many investigators consider that nickel has an adverse effect, particularly when the content exceeds one percent. Treseder and Swanson (1968), after testing different steels with various nickel contents, pointed out that the steels having a hardness lower than 22 HRC which failed in a 0.5 percent acetic acid solution saturated with H_2S all contained more than one percent nickel. Kihara and co-workers (1967) have also reported that nickel is undesirable. In contrast, extensive studies by Snape (1967, 1968) indicated that nickel has no detrimental effect on sulfide stress cracking resistance. Snape pointed out that nickel lowers the lower critical temperature and untempered martensite could result from tempering at high temperature, resulting in a material more susceptible to sulfide stress cracking.

2.5 Analytical Investigations

Stress analysis of drill pipe in a dogleg and analysis of fatigue data from the literature has been used to calculate the fatigue damage suffered by drill pipe in a dogleg (Zeren, 1986). Bending moment, shear, deflection distributions along the pipe, and reaction forces at contact points were considered. Charts for cumulative fatigue calculation

similar to the ones derived earlier by Hansford and Lubinski (1964, 1966) were presented. To account for the effects of tension in using bending fatigue data, the Gerber equation (Fuchs and Stephens, 1980) was used to obtain an equivalent bending stress. Analysis showed that the use of pipe protectors which prevent the pipe from coming in contact with the wall of the borehole substantially decreases bending stresses in a drill pipe when they are place at equal intervals along the length of a drill pipe. The effect of pipe protectors was found to be more beneficial in reducing bending stresses in drill pipe when used in severe doglegs (above 8^{o}/100 ft). Oversized protectors near tool joints to protect the tool joint from wear were found to be detrimental to the fatigue life of drill pipe.

Attempts have been made to use the fracture mechanics approach to estimate the fatigue life of a drill pipe under the combined action of bending and axial cyclic loading (Kral et al., 1984a, 1984b). The investigators made use of a simple flat plate model and the Paris crack growth law to calculate the expected fatigue life in terms of the number of cycles for a crack to grow to critical dimensions. No account was taken of the effect of the drilling environment on the rate of crack propagation in the pipe material.

More recently, Dale (1988b) presented the development and application of a fracture mechanics model, verified by extensive full-scale testing, to predict fatigue crack growth behaviour in both the pipe body and connections of drill collars. The Paris model for crack growth prediction was used. Stress intensity factors were based on a modified solution for an edge crack in a semi-infinite sheet under combinations of tension and bending loads. The research work resulted in recommendations for determining inspection intervals for drill collar.

2.6 Drill String Dynamics

The magnitude of motion and forces at both the drill bit and at various points along the drill string has concerned the drilling industry for many years. Field measurements have been taken mostly to evaluate the weight on the bit as the drill string rotates. The interest in these measurements was motivated by a need to optimize the drilling rate through control of the force on the drill bit. Although not specifically addressed, the problem of drill pipe vibration and accelerated fatigue as the drill pipe is rotated near its resonance frequency is one of considerable importance when investigating downhole loading conditions which may affect fatigue of drill pipe. Cycles of loading accumulate at a faster rate as a pipe vibrates in a longitudinal, torsional, and bending mode.

Research on drill string dynamics started in the 1960's. The 1980's have seen an increase in research being performed in an attempt to gain a better understanding of drill stem dynamics. The following summarizes the work done to obtain field data and some of the analytical work done on drill stem dynamics in the past three decades.

The work of Finnie and Bailey (1960) is the first published attempt to measure forces in a drill string in operation. Measurement of axial force, torque, and axial and rotational motions at the top of the drill string was performed. The recordings showed a large number of frequencies of vibration. An analytical study of drill string vibration by Bailey and Finnie (1960) was performed to develop a method of determining natural frequencies of drill strings. The effect of any damping of the vibrations that may occur in practice was neglected. Lateral motions of the string were neglected and it was assumed that the torsional and longitudinal motions were independent. Comparison of predicted natural frequencies with those measured in the top of the string (Finnie and Bailey, 1960) did not show good agreement.

Paslay and Bogy (1963) presented an analytical investigation to determine if bit force can be predicted by measurements taken at the top of the drill string at the kelly. An idealized model of a typical drill string, part drill pipe and part drill collar, was considered. A very simple type of viscous damping was assumed, recognizing that extensive field measurements should be obtained to adjust the assumption made. The theoretical work showed that bit force can be obtained from measurements taken at the kelly. No comparison of analytical results with field measurements was presented.

The work of Deily et al. (1968) led to the development of a downhole recorder to provide quantitative data at various points along the drill string. The research program presented by Deily et al.. and discussed by Cunningham (1968) and Miller and Rollins (1968), resulted in many recordings of measurements in a number of different wells. These recordings include measurements of weight on bit, torque, bending moment, axial acceleration, angular acceleration, and radial acceleration, pressure inside the drill string, and pressure in the annulus. Magnitude of forces and motions at the drill bit and in the drill string were measured for a wide variety of drilling conditions. Large amplitude variations of weight on bit reached ±50 percent of the mean weight as a result of bouncing of the drill string. This variation was found to be dependent on drilling depth and rotary speed. Axial excitation was found to develop mainly in hard formations and the excitation frequency was measured as three times the rotary speed when tricone drill bits are used.

Many other investigations of longitudinal and torsional vibration modes for general drill string configurations have been presented in the literature (Dareing and Livesay, 1968; Halsey et al., 1986; Dawson et al., 1987; Kyllingstad and Halsey, 1988; Dareing, 1983). Halsey et al. (1986) concluded that torsional resonance frequencies in the drill string are nearly independent of drilling parameters such as weight on bit and rotary speed so long as the drill string rotates freely. They observed that only the intensities of the torsional resonances are affected by downhole conditions, at least in normal drilling.

Dawson et al. (1987) and Kyllingstad and Halsey (1988) treated the special case of slip and stick motion of the drill collar section. This phenomenon is associated with a large amplitude, saw-tooth-like variation in the applied torque. Slip and stick motion refers to the belief that the amplitude of the torsional oscillations can become so large that the drill collar section periodically comes to a complete stop and does not come free until enough torque is developed to overcome the static friction. The dynamic model used by Dawson et al. (1987) and Kyllingstad and Halsey (1988) assumed that the drill collar is acting as a pendulum suspended by drill pipes. One important conclusion from the Dawson et al.. investigation is that slip and stick motion is lost above a certain critical rotary speed. The same phenomenon was reported to occur in the field (Kyllinstad and Halsey, 1988).

Aarrestad et al. (1986) studied axial vibrations in drill strings using a linear elastic theory and experiments in a 1000 m deep vertical well. The study showed that the response at the top of the drill string is strongly dependent on damping along the drill string and the suspension parameters such as the mass, spring stiffness and damping coefficient in the moving equipment at the top of the drill string. By including frequency-dependent damping, the theoretical results agreed better with experimental results than was obtained assuming constant damping.

Recent work has emphasized a simpler approach to the axial and torsional vibration problem: drill pipe and rig equipment are ignored and only the bottom hole assembly is considered (Dareing, 1982, 1983, 1984). Using this assumption, very simple equations for critical rotating speeds were presented. According to the work of Dareing (1982) the natural frequency of the fundamental drill string longitudinal mode is between 5.0 and 5.8 Hz. Hence, the drill string should resonate while drilling in a hard formation at 100 to 115 rpm. Field measurements presented by Wolf et al. (1985) showed that the maximum longitudinal vibrations occurred while drilling at 70 to 80 rpm.

The finite element method has been used for dynamic analysis of drill string.Using a three dimensional beam element, the finite element method solves for all modes of vibration (axial, torsional, and lateral). The method can account for several factors that are generally ignored in the simpler models, such as lateral vibration modes, buoyancy forces, the presence of stabilizers, and well bore trajectory. The work of Mitchell and Allen (1985) on dynamic behaviour of drill collar indicated that lateral vibrations in a straight hole could induce large bending stresses, reaching twice the fatigue endurance limit in drill collar. According to the same authors, axial and torsional vibration analysis of bottomhole assembly could not explain the cause of repeated washouts and twistoffs observed in three drill strings. Lateral vibration was identified as the most probable cause. Furthermore, lateral motion, especially near the drill bit, was shown to affect hole direction and probably the initiation of bottom hole formation patterns which produce periodic axial and torsional loads on the drill bit (Dareing, 1984; Millheim and Apostal, 1981).

Lateral vibration in drill pipe has not received much consideration. This is probably due to the fact that only axial and torsional oscillations can be detected uphole, despite the predominant bending vibrations downhole. Wolf et al. (1985) noted that downhole bending moments cannot be observed at the surface. Chin (1988), using a mathematical formulation, demonstrated that bending vibration waves can not propagate in the drill string above the neutral point where the drill string goes from compression to tension. Any bending disturbances originating above the neutral point, where the drill string is in tension, as a result of drill string bore hole contacts will propagate towards the neutral point rather than uphole.

2.6 Summary

A survey of the literature showed that fatigue of drill pipe has been a problem of major concern to the oil industry ever since sections of drill pipe had to be joined together to permit drilling at depths greater than one length of drill pipe. Current design guidelines for fatigue of drill pipe are based on test results obtained before the 1950's. Those tests were all conducted in air, and corrosion was dealt with by making simplifying assumptions. The effect of mean stress was dealt with by using a modified Goodman equation. The Goodman equation was originally obtained from tests conducted on small residual stress free specimens (Fuchs and Stephens, 1980) and, as a consequence, it may not apply to a full-size structure where residual stresses may affect the behaviour of drill pipes under cyclic loading.

Published fatigue test data on full-size drill pipe are very limited. Although the effect of corrosive environment on fatigue life of drill pipe has been investigated through the use of small steel samples, its effect on full-size drill pipe has not been compared with results from tests on similar drill pipes tested in air. Experimental investigation of speed of testing on fatigue life of drill pipe steel in a corrosive environment showed conclusively that the speed of testing has a very determinant effect on fatigue life. No experimental investigation to date has specifically addressed the problem of the effect of mean stress on the fatigue life of full-size drill pipe operating in air or in a corrosive environment.

Investigations of drill string dynamics have dealt mostly with the bottom hole assembly where the drill string is in compression. The very complex nature of formation and bit interaction and contact between drill string and wall of the borehole explains why an accurate dynamic analysis has not been developed yet.

Recent articles published in the literature indicate that fatigue failure of drill pipe is still a major concern of drilling contractors as an increased frequency of drill pipe failure has been reported in the past few years. It seems that design guidelines presently available are not suitable for current drilling practice. As drilling moves to more hostile environments the problem of fatigue in a corrosive environment is becoming more crucial. Furthermore, as depth of drilling increases, the mean stress on drill pipes increases and it becomes essential to be able to evaluate the true effect of mean stress on the fatigue life of drill pipes. More research is therefore required to determine the effect of mean stress on full-size specimens. The investigation of the effect of mean stress has to address both the external axial load applied on the drill pipe and residual stresses present in the drill pipe.

Because drill pipes are being used in a corrosive environment, testing should be carried out in a corrosive environment. It must however be recognized that field conditions cannot be exactly duplicated in a laboratory and, even if this was possible, the numerous different environment conditions present in the field would make it a formidable task to investigate all the different field conditions encountered in practice. The present state of knowledge in the field of corrosion fatigue does not enable one to predict test results in one environment from results of tests in another environment. With these limitations in mind, an experimental program aimed at investigating the effect of controlled test environments on fatigue life is timely. Simultaneous effect of a corrosive environment and axial load has to be considered. Although such a program would represent only a modest attempt to solve a problem that will remain for many years to come, it is believed that such a test program

would provide a sound basis from which better design guidelines can be developed.

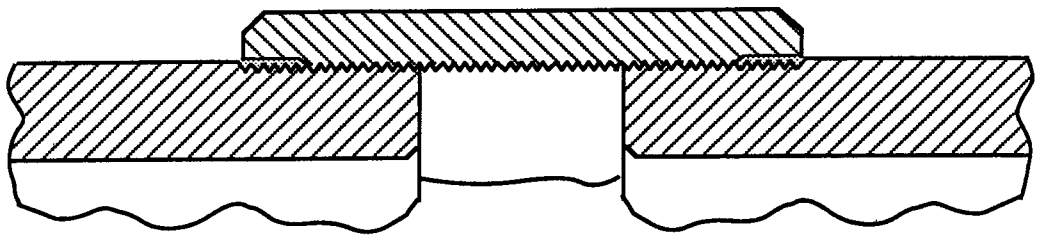

Figure 2.1 Early Drill String, Non Upset Line Pipe and Coupling With Sharp "V" Threads

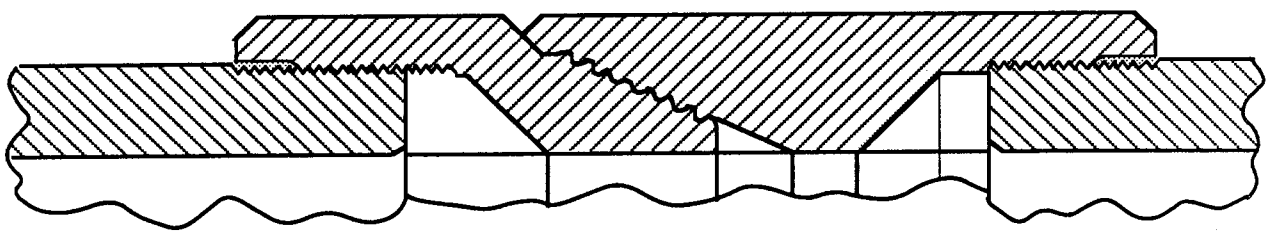

Figure 2.2 Early Heat Treated Tool Joint

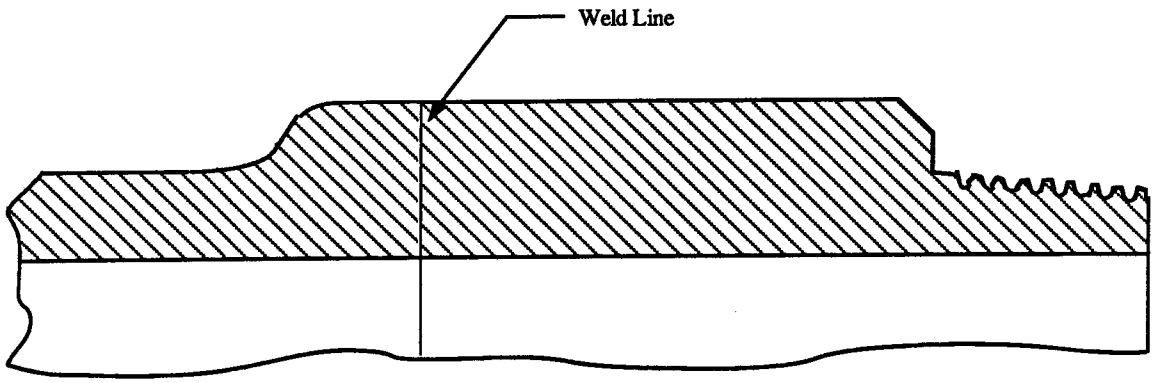

(a) Flash weld in heavy portion of tool joint

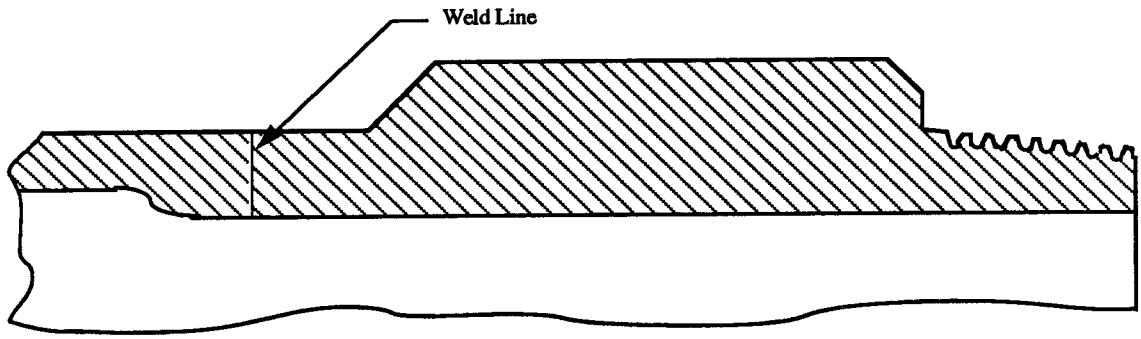

(b) Flash weld in neck assembly

Figure 2.3 Flash Welding of a Tool Joint

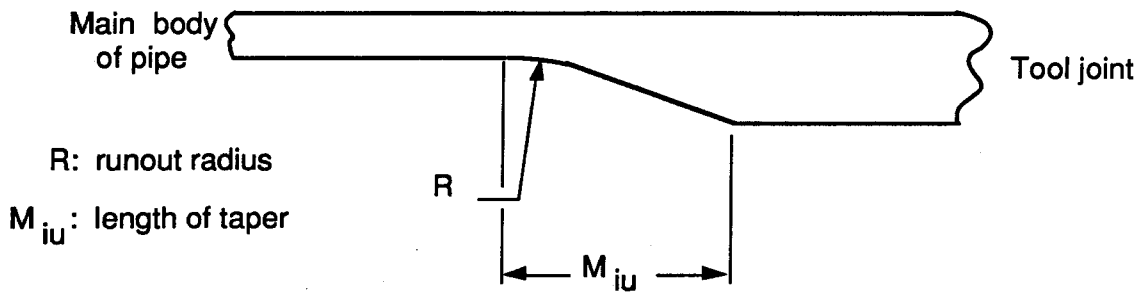

Figure 2.4 Internal Upset Geometry Investigated by Yazaki et al. (1986)

CHAPTER 3

Experimental Program

3.1 Introduction

The literature review has identified that the direct stress in a drill pipe resulting from its self-weight has been considered to be an important parameter in establishing the fatigue life of the pipe. Existing specifications (API 1984) use a modified Goodman approach to account for the effect of mean stress. However, the literature review did not identify that there has been any test program that examined this parameter using full-size pipe. Thus, it was appropriate that the study reported herein examine the influence of mean stress on the fatigue life of drill pipe.

The presence of a corrosive environment obviously has the potential for affecting fatigue life. The literature review indicates that test results from full-size specimens do not show clearly the effect of a corrosive environment on fatigue life. A comparative study of fatigue life in air and a corrosive environment was performed by Helbig and Vogt (1987) on small steel specimens only. Joosten et al. (1985) conducted fatigue tests on short sections of drill pipe in air and in a corrosive environment, but only the test results obtained in a corrosive environment were presented. No direct comparison between fatigue life in air and fatigue life in a corrosive environment can therefore be made for full-size drill pipes. In addition, tests on full-size specimens conducted in a corrosive environment presented in the literature did not include the geometry effect. Therefore, the test program reported herein was designed to include the effect of mean stress on fatigue life of full-size specimens both in air and in a corrosive environment.

3.2 Preparation of Test Specimens

In a preliminary test program, full-size drill pipe specimens were tested to determine the location of fatigue failures in drill pipes and to confirm that failures observed in the field could be duplicated in the laboratory. The preliminary test program consisted of one test done using cyclic tension and seven tests conducted in cyclic bending. Once the location of fatigue failure in the drill pipe was identified, the main test program designed to study the effect of mean stress and corrosive environment on fatigue life was initiated.

Test specimens were fabricated using lengths of drill pipe obtained through normal purchasing channels. Three test specimens in the preliminary test program were API Grade E 89 mm O.D., 19.8 kg/m (3-1/2 in. O.D., 13.3 lb/ft) drill pipe with external upset geometry. Other specimens in the same series were obtained from two different suppliers. These were API Grade E 114 mm O.D., 24.7 kg/m (4-1/2 in. O.D., 16.6 lb/ft) drill pipes with internal - external upset. Dimensions of the tool joint and upset, and the pipe wall thickness were measured for each specimen. The measured dimensions are presented in Appendix A. Figure 3.1 shows the location of test specimens in a length of drill pipe. Each drill pipe was flame cut in three sections and the connection was made up between the two end pieces (A and E in Figure 3.1) using the API (1989) recommended torques of 9.90 kN.m for the 89 O.D., 19.8 kg/m drill pipes and 16.4 kN.m for the 114 mm O.D., 24.7 kg/m drill pipes. This procedure for preparing test specimens was adopted so that the tool joint, upset ends, and a portion of pipe body could be incorporated in the test section.

As will be discussed in the next chapter, the main test program indicated that the majority of failures took place in the body of the pipe, not at the tool joint or in the upset region. This observation is consistent with field observations. For this reason, and also for economic reasons, many tests in this report were done on lengths of pipe with no tool joint or upset.

Tension coupons or sections of pipe tested as stub-columns used to obtain the mechanical material properties and sections used for residual stress measurement were also obtained from the middle portion (C and D in Figure 3.1) of the drill pipe. Material samples for metallographic study and chemical analysis were obtained from the pipe body, upset region, and tool joint of broken fatigue test specimens.

3.3 Fatigue Test Program

Full-size drill pipe specimens were tested in cyclic tension, cyclic bending, and rotating bending. Cyclic tension and cyclic bending tests were conducted as preliminary tests in order to establish the location of fatigue failure in a drill pipe tested in the laboratory. The test program used to study the effect of mean stress and corrosive environment was conducted using a rotating beam test setup that closely simulates field operating conditions.

3.3.1 Tension Fatigue

One 89 mm O.D., 19.8 kg/m, test specimen was tested in cyclic tension. The test specimen was mounted by means of pin connections into a MTS 6000 universal testing machine capable of applying cyclic loading at a frequency of 0.3 Hz. The test setup is illustrated in Figure 3.2. End attachments consisted of solid steel cylinders welded to the test specimen and mounted in the testing machine through a set of clevises to provide pin connections at both extremities of the specimen. Dimensions of end pieces for attachment of the test specimen to the universal testing machine are presented in Appendix B. The weld between the drill pipe and steel cylinder was a full penetration groove weld. Because the drill pipe material is a medium carbon low alloy steel, special precautions were required during the welding process. The base metal was preheated and post weld heat treated to prevent cracking of the heat affected zone. A high nickel welding electrode was used to provide more ductility in the weld metal. The weld region was preheated to decrease the cooling rate of the heat affected zone in order to prevent formation of brittle martensite and consequent cold cracking due to hydrogen embrittlement. Post weld heat treatment was used to temper the martensite formed during cooling of the weld and heat affected zone and to remove hydrogen absorbed by the steel during the welding process. The surface of the weld was ground smooth in order to reduce stress concentration around the weld. Although welding was performed carefully under controlled conditions, fatigue cracks developed in the heat affected zone and the welds had to be redone at regular intervals.

During testing, strains were measured on the outer surface of the drill pipe body with electrical resistance strain gages placed at two different sections along the length of the test specimen. Four strain gages, placed at quarter points around the circumference, were placed at each section. Strain readings were monitored with a strain indicator and the load on the test specimen was cycled between a minimum and maximum load such that the minimum stress was 10 MPa and the maximum stress was 270 MPa. The number of cycles of loading and unloading was recorded by a cycle counter.

3.3.2 Simple Bending Fatigue

Two 89 mm O.D. and seven 114 mm O.D. drill pipe specimens were tested in flexure using a 2400 mm span with two-point loading in the central portion of the span. The distance between the loading points was 1500 mm. The constant moment region

between the loading points included the upset ends, tool joint, and a portion of drill pipe body. One 114 mm O.D. specimen consisted of a section of pipe body only.

A schematic of the test setup for simple bending fatigue testing is shown in Figure 3.3. The cyclic loading was applied on a distributing beam with a Pegasus servo-load simulation system. Rocker and roller assemblies were used to transfer the load from the distributing beam onto the test specimen. The load was cycled at a frequency of 3 to 4 Hz such that the stress at the bottom fiber of the specimen in the constant moment region varied from minimum to maximum tension. The setup did not allow for reversed bending.

Electrical resistance strain gages were placed on the surface of the pipe at two sections 900 mm apart in the constant moment region. At each section, the gages were mounted at the top and bottom fibers of the pipe. Strain gage readings were taken with a strain gage indicator and monitored with an oscilloscope. The trace on the oscilloscope served as a guide to maintain the strain range when cyclic loading was applied to the test specimen. After the oscilloscope had been calibrated by running a static test on a drill pipe specimen, the cyclic load was adjusted to give the desired minimum and maximum strains indicated on the oscilloscope within a testing frequency of 3 to 4 Hz. Testing was stopped when the stiffness of the pipe dropped to about one third of the stiffness at the beginning of the test, i.e. when the maximum deflection at the loading points reached about three times the maximum deflection at the beginning of the test. This was observed to correspond to the presence of a crack in the pipe with a length of about one third to half of the pipe circumference. At that stage, the crack growth rate was very rapid and the maximum load could not be reached without going through large deflection. All the simple bending fatigue tests were conducted under load control.

In a simple cyclic bending test setup the mean stress in the test specimen can be varied by varying the mean load applied on the beam specimen. Nevertheless, a prestressing system was developed to vary the mean stress on the drill pipe without having to adjust the applied mean load. The prestressing system shown in Figure 3.4 was developed so that it could also be used in the rotating bending test setup designed for the main test program. One end of the pipe was plugged with a threaded end plug and a prestressing rod was inserted in the pipe and compressed using a flange fitting and flat plate assembly located at the other extremity of the drill pipe. The prestressing rod was 75 mm diameter and it was made of high strength steel (SAE 4140 HT). Load in the rod was induced by bolting the flat plate to the flange fitting using high-strength bolts. This put the prestressing rod in compression and the drill pipe in tension. Buckling of the prestressing

rod was prevented by supporting the rod with plastic centralizers along its length. The preload induced in this way was monitored by means of strain gages mounted on the load rod and on the surface of the test specimen. Detailed dimensions of the prestressing hardware are given in Appendix C.

Two 114 mm O.D. drill pipe specimens were tested in simple bending fatigue with a superimposed static axial load of 430 kN (inducing a tensile stress of 150 MPa in the body of the drill pipe). The axial load was kept constant throughout the duration of the test.

As has already been noted, one of the specimens tested in simple bending did not incorporate a tool joint and upsets in the constant moment region. This specimen was tested in a corrosive environment consisting of a 3.5 percent sodium chloride solution. The test region was kept wet during the test by pumping the corrosive fluid on the surface of the pipe. The corrosive solution was changed every day in order to keep the corrosivity of the solution approximately constant during the test.

3.3.3 Rotating-Bending Fatigue

Tests performed under simple cyclic bending have the major disadvantage that the maximum stress range is limited to the bottom fiber of the test specimen. For beams of circular cross-section, the volume of material stressed to the maximum stress range will therefore be relatively small. Because surface flaws causing nucleation of a fatigue crack can be expected to be randomly distributed on the surface of a drill pipe, it is expected that the fatigue life from a simple bending test would be longer than an equivalent rotating pipe unless the most critical surface flaw is uniquely located at the bottom fiber of the test specimen. It is reasonable to anticipate that test results from simple bending tests would be dependent on the position in which the specimen is placed in the test setup. For this reason, and also to obtain a better simulation of field operating conditions, the majority of full-size fatigue tests conducted in the program were carried out in a rotating-bending test frame.

The test frame, shown schematically in Figure 3.5, uses a simply supported rotating beam under two-point loading to provide a region of constant moment 1500 mm long. The tensile axial load, if present, was introduced using the preloading scheme described for the bending specimens with the exception that the threaded end plug was fitted with a shaft for power transmission. Three levels of axial load were investigated; no

axial preload, which represents testing conditions used by other investigators conducting research in this area; 125 MPa (axial load of 350 kN), which corresponds to the stress at the top of the string if drilling is carried 1525 m in a 15 lb/gal drilling mud; and 250 MPa (axial load of 700 kN), which corresponds to the stress at the top of the string when drilling is carried out at 3050 m. Transverse loading was applied by deflecting the pipe using loading rods passing through the laboratory strong floor (see Figure 3.6). Stiff springs were placed between the strong floor and loading rods to maintain the load at approximately the same level as a fatigue crack propagated in the test specimen and its stiffness changed. The deflection was introduced by turning the nut on the loading rod that passed through the strong floor. Load was transferred from the loading rods to the distributing beam using square tubular sections tied together with smaller steel rods, as shown in Figure 3.6. The top tubular section was seated on a bed of steel balls placed on the distributing beam so as to minimize friction and allow vertical alignment of the loading rods in order that any horizontal force transferred to the distributing beam would be negligible.

The loading and reaction points must transfer the applied load from the distributing beam to the test specimen and from the test specimen to the floor. An important feature required by the loading and reaction points is that there be free flexural bending at the loading and reaction points while the specimen is rotating in a deflected position. For these reasons, spherical roller bearings were selected for the loading points. Spherical roller bearings are self-aligning and insensitive to minor angular misalignments of the shaft relative to the outer ring of the bearing, (i.e. insensitive to shaft bending). Under normal loads (the basic load rating for the size of bearing used on the drill pipes in this investigation is 730 kN) and operating conditions and in a case where the inner ring of the bearing rotates, the permissible angular misalignment is about 5 degrees. This represents a dogleg severity of approximately 125 degrees per 30 m length of drill pipe. This is in excess of the maximum recommended value of 10 degrees allowed for in the present recommendations (API, 1989).

Bearings were selected to fit on a 127 mm O.D. drill pipe. To facilitate the mounting and dismounting of the bearings on a drill pipe, tapered adapter sleeves with tapered bore bearings to fit a maximum shaft diameter of 135 mm were selected. Adapter sleeves also have the advantage of having a wider seating diameter tolerance than for bearing seatings. Bearings were mounted on a drill pipe by pushing the bearing on the tapered adapter sleeve with a locknut screwed on the adapter sleeve. Semi-circular steel

sleeves and rubber pads were used to fill the space between the 135 mm diameter adapter sleeve and 114 mm O.D. drill pipe. Nylon reinforced rubber pads were used primarily to prevent fretting fatigue problems at the loading points which could occur if a stiffer material was used.

During the course of the test program fatigue cracks developed under the load bearings in a few cases. Because the effect of bearing pressure on fatigue crack initiation and propagation is not well known, and because this situation does not correspond to field conditions, the surface of the pipe under the two load bearings subsequently was peened in an attempt to prevent local fatigue failure under the bearings. As only the surface is plastically deformed by the shot peening process, an inhomogeneous deformation takes place which induces compressive residual stresses in a thin surface layer (Roth et al., 1987). It is well known that high surface compressive residual stresses will prevent initiation of fatigue cracks (Desvignes et al., 1987). After peening of the pipe surface under the bearings was adopted as part of the procedure in specimens preparation, no more fatigue cracks started under the bearings.

Electrical resistance strain gages were used to measure strains in the drill pipe body within the test portion. A data logger, mounted at one extremity of the pipe, was used to read the strain gages. Wiring between the strain gages and data logger was fed across the bearings through gaps left between the two semi-circular steel sleeves used as spacers (see Figure 3.7).

A minimum of six electrical resistance strain gages were used on each test specimen. The location of the strain gages on test specimens is shown in Figure 3.8. Four strain gages were mounted at section A-A to monitor the stress distribution around the circumference as the axial load was applied. Two additional strain gages were placed at section B-B to check the constant moment condition in the test portion as the transverse load was applied. For slightly crooked pipes, or pipes with varying wall thickness along the length and around the circumference, application of an axial load created a secondary bending moment which resulted in a non-uniform strain distribution around the circumference and along the length. For any specimen that showed a variation in axial strain of more than five percent of the average strain, more strain gages were subsequently applied. The strain range and mean strain at the origin of the fatigue crack were obtained by linear interpolation between strain gages closest to the fatigue crack.

During the loading stage, strains were monitored with an electronic strain indicator. After loading, the test specimen was rotated manually to determine the maximum and minimum strains at every strain gage location. The mean strain and strain range were thus obtained for a specimen rotating at low speed. An electronic datalogger containing four channels to read four strain gages wired in a quarter bridge configuration was attached to the rotating pipe and was used to read strain gages when the test specimen was rotated at testing speed. The datalogger was battery operated and could record and store voltage readings of all four channels at a rate of one reading per second. Readings were kept in memory until they were retrieved by downloading the memory into a personal computer. The datalogger has a storage capacity of 1200 readings for each channel. The calibration was performed by recording strain gage readings from the test specimen while it was rotated very slowly (at approximately two cycles per minute). The minimum and maximum voltage outputs recorded were compared with the minimum and maximum strains measured with a strain indicator. Once the calibration of every channel was completed, the test specimen was rotated at the desired test speed while data was recorded by the datalogger. Because of the inertia of the system, the strains had a tendency to decrease as rotating speed increased. Loading on the specimen was adjusted to obtain the desired strain range at the testing speed. Specimens tested in air were rotated at a frequency of 3 to 7 Hz. For all tests conducted in air, the maximum rotary speed at which no vibration problems occurred was used.

In the field, a drill pipe is not subjected to the maximum stress range for the entire duration of its life. Consequently, a pipe in the field would suffer more corrosion than a pipe in a laboratory running at the same rotary speed under maximum stress range for the duration of the test. For this reason, tests conducted in a corrosive environment were run at a frequency of one hertz, which is lower than the rotary speed of 1.5 Hz (90 rpm) commonly used in drilling practice. Another factor taken into consideration in determining the rotary speed of testing was the desired duration of a test. From an examination of Helbig and Vogt's (1987) test data, the rotary speed was selected so that a drill pipe tested at a stress range of 130 MPa would have a test life of about one month. The number of cycles that a test specimen underwent was recorded by a magnetic proximity sensor connected to a cycle counter. An electrical signal is produced by the proximity sensor every time a magnetic object, mounted on the drill pipe, passed close to the sensor. Every cycle was thus recorded by the cycle counter.

A schematic representation of the hydraulic power drive used to rotate the test specimens is shown in Figure 3.9. A hydraulic motor was powered by a 91 litres per minute hydraulic pump. A hydraulic actuator module controlled the flow of hydraulic fluid to the motor and also regulated the pressure to the motor through an accumulator. The hydraulic actuator module was controlled by an electronic control module which included a push button emergency switch mounted on the distributing beam. As a crack propagated in a specimen, its stiffness decreased and there was a resultant downward displacement of the distributing beam. The push button switch was positioned so that the hydraulic actuator module was shut off when the fatigue crack has propagated through about one third of the specimen circumference. The speed of the motor was adjusted by controlling the flow of hydraulic fluid with a needle valve placed between the hydraulic actuator module and the hydraulic motor. In order to develop the higher torques required to turn slightly crooked pipes at low speed, a 12 to 1 ratio gear box speed reducer was used. The output shaft from the gear box was coupled to the test specimen end shaft by a double universal joint.

Corrosion fatigue tests were run in a 3.5 percent sodium chloride solution. The solution was placed in a container under the test specimen and was pumped on the surface of the specimen, allowing for good aeration of the corrosive solution. Figure 3.10 shows a schematic representation of the corrosive fluid circulation system. The corrosive fluid was pumped using a varistaltic pump at a rate of two liters per minute.

3.4 Measurement of Residual Stresses

3.4.1 Definition of Residual Stresses

Residual stresses are self-equilibrating stresses that commonly exist in materials under uniform temperature conditions without external loading. The resultant force and the resultant moment produced by residual stresses must be zero. Residual stresses are produced if regions of a member are inhomogeneously deformed in such a permanent manner that strain incompatibilities occur. Residual stresses are classified according to some criteria as the origin of residual stresses (thermal, mechanical, chemical, etc.) or the fabrication process (welding, forging, thermal treatment, surface treatment, etc.). A standardized system of designation widely used classifies residual stresses in three different categories called type I, type II, and type III residual stresses (Macherauch and Kloos, 1987).

- Type I residual stresses (macro residual stresses) are nearly homogeneous across large areas (several grains) of a material and are equilibrated over the whole body.

- Type II residual stresses are nearly homogeneous across microscopic areas (one grain or part of a grain) of material and are equilibrated across a sufficient number of grains. The random orientation of the crystal lattice in different grains causes different deformations in certain grains under a unidirectional stress. When the material is composed of different phases, type II residual stresses can develop as a result of different mechanical properties in different phases.

- Type III residual stresses are inhomogeneous across submicroscopic areas of a material, say several atomic distances within a grain, and are equilibrated over a small part of a grain. Type III residual stresses will be created in the presence of a dislocation in a crystal which disturbs electrical forces between atomic particles near the dislocation.

3.4.2 Measurement Techniques

Although various procedures have been developed over the years, cheap, simple, and reliable methods for the quantitative determination of residual stresses do not exist. Various techniques of residual stress measurement have been developed. In general, residual stresses can be obtained from:

- measurement of macroscopic strains which are released when material is removed from parts loaded with residual stresses. This is the basis of destructive methods, which measure type I residual stresses.

- measurement of uniform crystal lattice strain distributions. This is the basis of the X-ray diffraction method, which measures type I and type II residual stresses.

- effects of residual stresses on some distinct physical properties. This is the basis of ultrasonic and magnetic methods, which yield quantities influenced by all three types of residual stresses.

It is evident that each technique of residual stress measurement, destructive or non-destructive, finds a field of application which can be defined by the geometry of the part

under study, the type of material and its crystal structure, or by the volume of material affected by the measurement.

3.4.2.1 Measurement of Residual Stresses by Sectioning Technique

The method of sectioning was used to determine the residual stress distribution in some of the drill pipe sections tested in fatigue. The method of sectioning is based on the principle that type I residual stresses in a material are relieved when a specimen is cut into strips of small cross-sectional area (Tebedge et al., 1971). The residual stress distribution in a cross-section is determined by measuring the change in length of each strip due to sectioning and applying Hooke's law. Two basic assumptions are made when this method is used, namely that the transverse stresses are negligible and that the method of cutting the strips produces no appreciable strain. Improper sectioning, and also existence of strong residual stress gradients beneath the surface can lead to uncertainties in the results (Hauk et al., 1987).

Preparation of Test Specimen

To avoid the influence of end effects on the magnitude and distribution of residual stresses, the specimens were taken in the central portion of the drill pipe body, at least 100 mm away from the flame cut edge made when the fatigue test specimen was cut from the extremities of a drill pipe. A section of drill pipe 1000 mm long was used for residual stress measurement. A gage length of 250 mm was used for all the specimens used for measurements except for one specimen for which a gage length of 500 mm was used. The gage holes were carefully prepared using a 1.6 mm drill bit. Measurements over the gage length were taken with a Demec gage extensometer modified as shown in Figure 3.12. A mechanical strain gage extensometer is believed to be particularly suitable since it is not damaged during sectioning and the same device can be used to measure repeatedly. Because measurements had to be taken on both the external and internal surfaces of a specimen, the standard dial gage indicator on the extensometer was replaced by a linear variable differential transformer (LVDT) so that readings could be monitored on a voltmeter located outside the pipe. To minimize the variation due to positioning of the extensometer, a spring-loaded holder, shown in Figure 3.12, was placed on the extensometer to hold the extensometer at the same angle to the pipe surface every time a reading was taken. Lead weights were fixed to the extensometer to exert the same pressure on the contact points of the extensometer when readings were taken. To prevent any error from changes in

temperature, a reference bar, made of drill pipe steel, was used to calibrate the extensometer. The bar was placed on the specimen to be tested for at least two hours before starting the measurements.

To decrease experimental errors attributed to mechanical and human factors, ten sets of readings were taken for each set of gage holes. Before any statistical analysis was performed on the data, the smallest and largest values were discarded. The sample size, n, required to obtain a maximum error in measured change in length of about 5 MPa, was calculated based on the assumption that the sample was normally distributed. Because the population standard deviation is not known, a t-distribution was used to obtain the required number of data points as follows (Kennedy and Neville, 1986)),

$$n = \left(\frac{t_{\alpha/2}\, s}{\text{Error}} \right)^2 \tag{3-1}$$

where: $t_{\alpha/2}$ = t value for a level of confidence of $(1 - \alpha)$

s = standard deviation of the sample

For a level of confidence of 95 percent and a number of degrees of freedom of seven, $t_{\alpha/2} = 2.365$. If an error of 0.0025 mm on the measured distance between gage points, which corresponds to a strain of 10 $\mu\varepsilon$, is accepted, the sample size needed can be obtained as,

$$n = (876\, s)^2 \tag{3-2}$$

where s is the sample standard deviation in millimeters. For a given set of ten readings, the calculated value of n was compared to the actual number of readings taken (8 readings which corresponds to the 10 readings recorded minus 2 rejected readings), and if the calculated value of n was larger than the actual sample size, a new set of 10 readings was obtained. The process was repeated until a valid set of readings was obtained.

After a valid set of 10 readings was obtained on the exterior surface, the 1000 mm long specimen was cut to a shorter length to allow easier access to the inside surface of the pipe. The effect of shortening the pipe on residual stresses was monitored by measuring the gage length on the exterior surface every time the section was gradually cut shorter until the length of the specimen had reached 350 mm. None of the specimens obtained from pipes of the preliminary test program showed any change in gage length on the exterior surface of the pipe as it was shortened from 1000 mm to 350 mm. However, specimens

from the second set of pipes (manufactured by Mannesmann) showed a different behaviour. The gage length on those specimens changed when the test specimen was cut shorter than 625 mm. Therefore, a gage length of 500 mm was used for one of those specimens so that the test specimen could be cut 650 mm long.

After initial extensometer readings were taken on the outside and inside surfaces of a test specimen, a band saw was used to section the test specimen into narrow strips. Twenty-nine strips of equal width were cut around the circumference. After sectioning of a specimen, extensometer readings were taken on both the outer and inner surfaces of each strip. To ensure the same positioning of the Demec extensometer on each strip as existed before sectioning, the strips were placed on semi-circular supports, as shown in Figure 3.13, so that each strip would be seated in the same position with respect to adjacent strips on which the extensometer holder was sitting when the measurements were taken.

Residual stresses released by sectioning were calculated using the measured gage length before and after sectioning. An elongation of a strip after sectioning indicates that a compressive residual stress has been released by sectioning, while shortening of a strip results from release of tensile residual stresses. Stresses can be calculated from:

$$\sigma_r = \frac{L_b - L_a}{L_b} E \qquad (3\text{-}3)$$

where, σ_r = the residual stress magnitude. A negative value corresponds to compressive residual stress

L_b = average gage length before sectioning

L_a = average gage length after sectioning

E = modulus of elasticity.

3.4.2.2 Measurement of Residual Stresses by X-Ray Diffraction

Measurement of residual stresses by X-ray methods has become, along with destructive methods, one of the most widely used techniques both in research and practice. Some of the main advantages of the techniques are as follows:

- it is a nondestructive method

- the volume of material considered in the measurement is small (only a few hundredths of a mm^3)
- it can be used on parts with complex geometries
- the possibility exists to perform in-situ measurements.

The major disadvantages of the technique are:

- the results can be influenced by the presence of microscopic residual stresses (type II and III)
- the procedure can be time consuming

- if residual stresses need to be measured below the surface, the technique becomes destructive.

Measurement of residual stresses using X-ray diffraction is based on the measurement of crystal lattice spacing. This distance is a function of stresses acting on the crystal, therefore on residual stresses present in the material. During the study of the diffraction spectrum of an X-ray beam, only one phase of the material can be considered. Furthermore, for a given type of crystal, the study concerns only one atomic plane, a plane which repeats itself n times in the crystal and is defined by the position of three atoms in Cartesian space. The distance between those planes, measured on a normal to the planes, influences the observed angle of interference, the angle which defines the direction of a strong concentration of diffracted rays. The theoretical background to X-ray diffraction and its relation to macroscopic stresses is briefly summarized in the following. For more details refer to Noyan and Cohen (1987).

If an X-ray beam (I) located in a plane perpendicular to the crystal lattice planes impinges on those planes at an angle Θ_o, constructive interference, that is, diffraction, will occur when (Figure 3.14)

$$n\lambda = 2 D_o \sin\Theta_o \tag{3-4}$$

where n = multiple of the radiation wavelength
λ = wavelength
D_o = atomic plane spacing
Θ_o = angle between incident beam and atomic planes

In other words, if two X-ray beams are diffracted at the same angle but have traveled different distances, the difference in traveled paths is an even multiple of the wavelength. This relation is called Bragg's law. Differentiating Eq. (3-4), we obtain the following expression for the change in diffraction angle in terms of the change in distance between atomic planes

$$d\Theta = - \tan \Theta_o \frac{dD}{D_o} \tag{3-5}$$

For practical reasons, Eq. (3-5) can be transformed as follows:

$$\frac{D_1 - D_o}{D_o} = - \cot\Theta_o \left(\Theta_1 - \Theta_o\right) \tag{3-6}$$

where subscript 1 refers to a state of deformation due to uniform and unidirectional stresses and subscript 0 refers to the unstressed state. The development presented so far relates the deformation between planes of atoms caused by uniform external stress (residual or other), to the angular change of diffracted X-rays.

The relation between microscopic deformation ($D_1 - D_0$) and macroscopic stresses is based on the theory of elasticity. The generalized Hooke's law, relating stresses to deformations in an elastic, homogeneous, and isotropic material is applicable to deformations in the crystal lattice (Noyan and Cohen, 1987).

Since only a very thin layer of material on the surface is affected by the measurement, the stress in the direction perpendicular to the surface is assumed to be zero. Using Hooke's law and various trigonometric transformations, the basic equation for determination of stresses by X-ray diffraction can be obtained from (Noyan and Cohen, 1987):

$$\varepsilon_{\varphi,\psi} = \sigma_\varphi \frac{\nu + 1}{E} \sin^2\psi - \frac{\nu}{E} \left(\sigma_1 - \sigma_2\right) \tag{3-7}$$

where $\varepsilon_{\varphi,\psi}$ = strain in a direction defined by angles φ and ψ shown in Figure 3.15

σ_φ = stress on the plane of the surface

ψ = angle between strain vector and normal to the surface

φ = angle between the major principal stress and σ_φ measured on the plane of the surface

σ_1, σ_2 = major and minor principal stresses parallel to the surface

In other words, material deformation in a given direction, $\varepsilon_{\varphi,\psi}$, is expressed in terms of the stress projected onto the strain vector and principal stresses parallel to the surface.

In order to determine a stress using X-rays and Eq. (3-7), different values of ψ have to be considered for a given direction φ. The equation now defines a linear relation between elongation and the term $\sin^2\psi$. Partial differentiation of Eq. (3-7) with respect to $\sin^2\psi$ gives the following result:

$$\frac{\partial \varepsilon_{\varphi,\psi}}{\partial \sin^2\psi} = \frac{\nu + 1}{E}\,\sigma_\varphi = m_\varphi \tag{3-8}$$

Solving for σ_φ

$$\sigma_\varphi = \frac{m_\varphi\, E}{\nu + 1} \tag{3-9}$$

The parameter determined from X-ray measurements is the diffraction angle Θ for a given angle of incidence of the X-ray beam. Equation (3-9) can be transformed using Eq. (3-6) as follows:

$$\sigma_\varphi = -\frac{\cot\Theta_o\ \Delta\Theta}{\sin^2\psi}\,\frac{E}{\nu + 1} \tag{3-10}$$

where Θ_o is the diffraction angle for the non-deformed state. Finally, Eq.(3-10) can be rewritten as

$$\sigma_\varphi = k\ \Delta\Theta \tag{3-11}$$

where k is a stress constant for a given material. The constant k can be determined from a calibration test.

A check on the calibration of the instrumentation was performed using a piece of drill pipe steel. The sample was loaded in tension in the setup shown in Figure 3.16. Applied stress was measured using electrical resistance strain gages mounted on both sides of the irradiated surface. These measurements were compared to the value obtained from X-ray diffraction in order to confirm the calibration.

At every location on a specimen where residual stresses were measured, a total of six X-ray exposures (three exposures at each of two different tilts, ψ) were taken to get a better estimate of the average. Only longitudinal residual stresses were measured.

Because the depth of penetration of X-rays is very small (only about 5 μm in steel), surface preparation of the specimen is very important. Techniques to measure residual stresses on a rough surface are not well developed, and it is therefore preferable to remove the surface roughness at locations where measurements are to be made. Any type of surface preparation, such as milling, grinding, turning, etc., which changes the state of residual stresses is not recommended. For specimens with a rough surface, a surface layer of 0.1 mm was removed using strong acid. The depth of penetration below the surface was carefully monitored using an optical micrometer.

To investigate the variation of residual stresses with depth, greater thickness of material had to be removed. Since it required approximately one hour to remove a 0.1 mm layer with strong acid, grinding and sanding, followed by strong acid etching, was used to remove thicker layers, such as 0.5 mm. A procedure used to remove a thick layer of material was investigated on a strip of AISI 4140 steel annealed at 650 °C for two hours and furnace cooled. The surface on which an initial stress measurement was to be taken was cleaned with dilute nitric acid to remove all trace of oxide. The measured residual stress was 55 MPa in compression. A layer of material 0.36 mm thick was then removed by grinding. Sanding was used to remove an additional 0.30 mm layer, and a final layer 0.15 mm thick was removed by strong acid etching. A total of 0.81 mm was removed over a surface of approximately 100 mm^2. The residual stress measured after this process was 35 MPa in compression. The difference of 20 MPa is considered to be within the precision of the equipment used for residual stress measurement and therefore the same procedure for layer removal was used to remove layers thicker than 0.15 mm. Layer removal by mechanical means (grinding or sanding) was always followed by removal of a 0.15 mm layer with strong acid.

A theoretical investigation of layer removal in residual stress measurement by Moore and Evans (1958) showed that correction to measured stresses can be neglected when the total material thickness removed does not exceed 10 percent of the specimen thickness. The work of Moore and Evans considered the case where a layer is removed over the entire surface of a tubular specimen. Since the drill pipe wall thickness is about 8.2 mm, a layer 0.8 mm thick can be removed over a small area without having to make any correction to the measured value.

Except for one specimen, all residual stress measurements were taken in the body section of the drill pipe. Stresses were measured at ten equally spaced locations around the circumference, and at one of these locations residual stress variation with depth was investigated. One of the specimens on which residual stress measurements were made incorporated the tool joint and upset region. Figure 3.17 shows the locations where measurements were taken, namely, in the body of the drill pipe, the external upset runout, and within the upset.

3.5 Ancillary Tests

Standard tensile coupons were tested to obtain the material properties of every drill pipe used in the experimental investigation. Tension coupons were cut from a 300 mm length of drill pipe. The dimensions of the tensile coupons were as specified by ASTM A370-88a (1989) except that the grip length was increased to 100 mm, which is double the grip length specified by ASTM (1989). The gage section width was 12.5 mm and the gage length 50 mm. The coupons were milled flat to remove grinding marks and other surface imperfections that prevented an accurate measurement of the cross-sectional area.

The testing was done in a MTS 1000 Universal testing machine. The elongation of the coupons was measured by an electric clip-on extensometer of 50 mm gage length. Two punch marks were made on the specimens at 50 mm spacing to measure the rupture strain. The tests were run at a stroke rate of about 3 mm/min, corresponding to a strain rate of about 15 $\mu\varepsilon$/sec (microstrain per second) in the elastic range. During the test, the load versus elongation diagram was continuously plotted on a X-Y recorder and load and elongation from the clip-on extensometer were recorded at regular intervals using a multichannel data acquisition system. When the specimen had started to yield, the loading was stopped to obtain a static stress value. This procedure was repeated several times during a test. Shortly after the ultimate stress level was reached, the extensometer was

removed and then loading continued until the specimen ruptured. The maximum elongation at rupture was measured after removal and reassembly of the specimen.

3.6 Metallography

Preparation of metallographic specimens required five operations; sectioning; mounting; grinding; polishing; and etching.

The microstructure of a drill pipe is anticipated to be different along its length because of the different processes used to fabricate different parts of the drill pipe. For this reason, many metallographic specimens were sampled along the length of the drill pipe. A band saw was used to remove a strip of material along part of the body of the drill pipe, the upset, and tool joint. Water soluble oil was used as a cutting fluid in order to minimize frictional heat which may alter the microstructure of the specimen below the cut surface.

Once a strip of material had been removed from a drill pipe, small samples were cut for mounting. The sectioning of the strips was performed with an abrasive cutoff machine. Sectioning was done wet with an ample flow of water soluble oil coolant directed onto the cut in order to guard against excessive surface damage caused by overheating.

The primary purpose of mounting metallographic specimens is to facilitate handling of the specimens during subsequent steps of metallographic preparation and examination. Both compression mounting and cold mounting were used for metallographic preparation. Compression mounting involves molding around the metallographic specimen by heat and pressure using a molding material such as Bakelite. Since Bakelite is a thermosetting material, the mounted specimens can be ejected from the mold at maximum molding temperature. The specimens which were too large to be mounted in a standard 31 mm diameter mold were prepared using cold mounting with epoxy resin.

After a specimen was mounted, the mechanical surface damage was removed by grinding and subsequent polishing operations. Grinding was accomplished by abrading the specimen surface through a sequence of operations using progressively finer abrasive grit. Grit sizes from 40 mesh through 150 mesh are usually regarded as coarse abrasive, and grit sizes from 180 mesh through 600 mesh as fine abrasives. The purpose of grinding is to lessen the depth of deformed metal to the point where the last vestiges of damage can be removed by a series of polishing steps. Each grinding step completely removed the deformed metal produced by the previous step.

Polishing is the final step in producing a surface that is flat, scratch free, and mirrorlike in appearance. Polishing was done in two stages. The first stage consisted of polishing with a diamond compound abrasive and the final polishing was done with 0.05 micron particle size aluminum oxide.

As the final step towards metallographic specimen preparation for observation with the optical microscope, etching is necessary in order to reveal the structure. The principle of etching is based on preferential attack of one or more phases and grain boundaries because of differences in chemical composition, and, to a lesser extent, because of differences in orientation. A two percent nital solution was used for etching the metallographic samples.

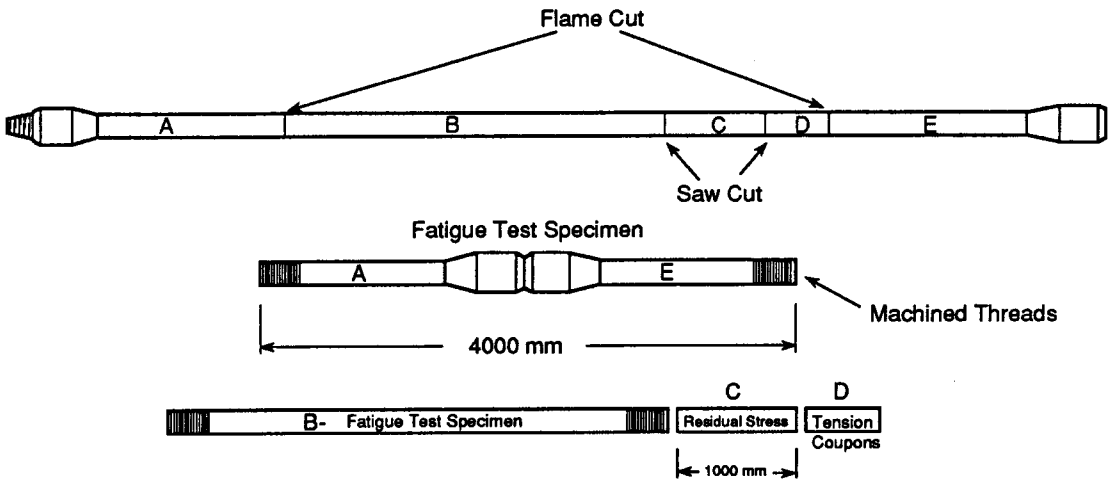

Figure 3.1 Partioning of a Length of Drill Pipe Into Test Specimens

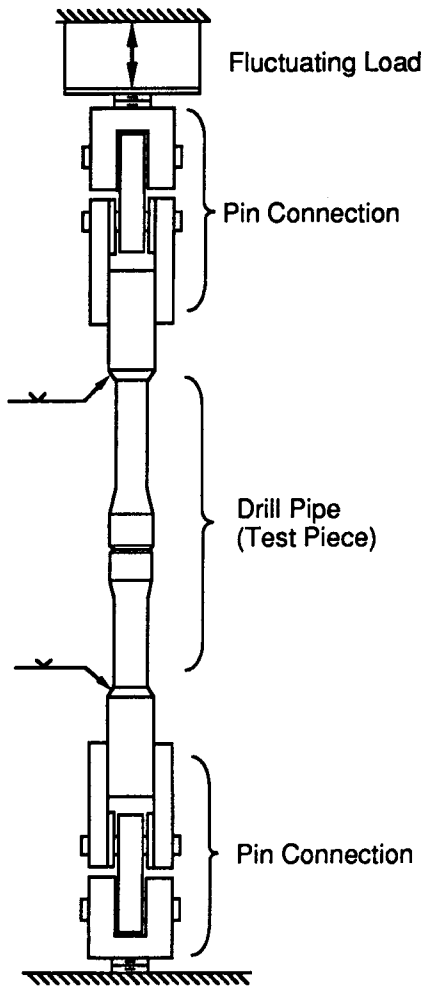

Figure 3.2 Setup for Tension Fatigue Test

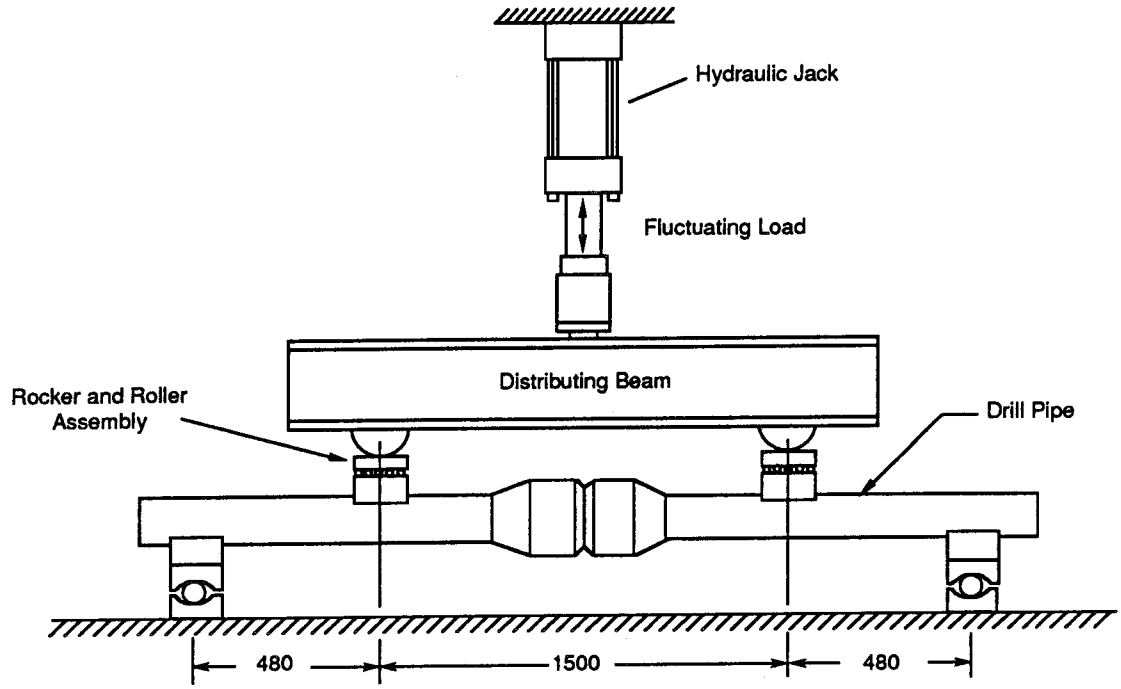

Figure 3.3 Simple Bending Fatigue Test Setup

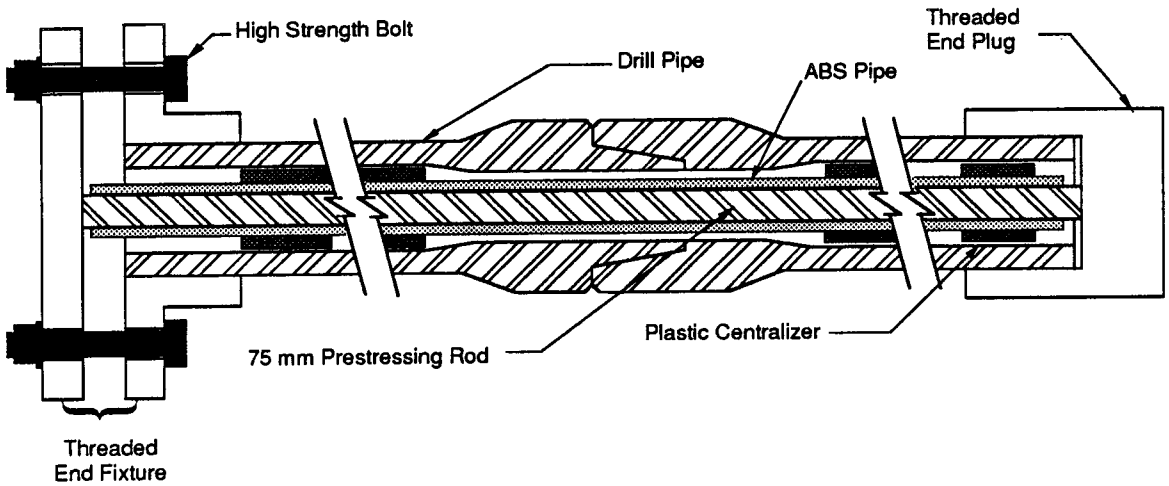

Figure 3.4 Section Through Drill Pipe With Prestressing Arrangement

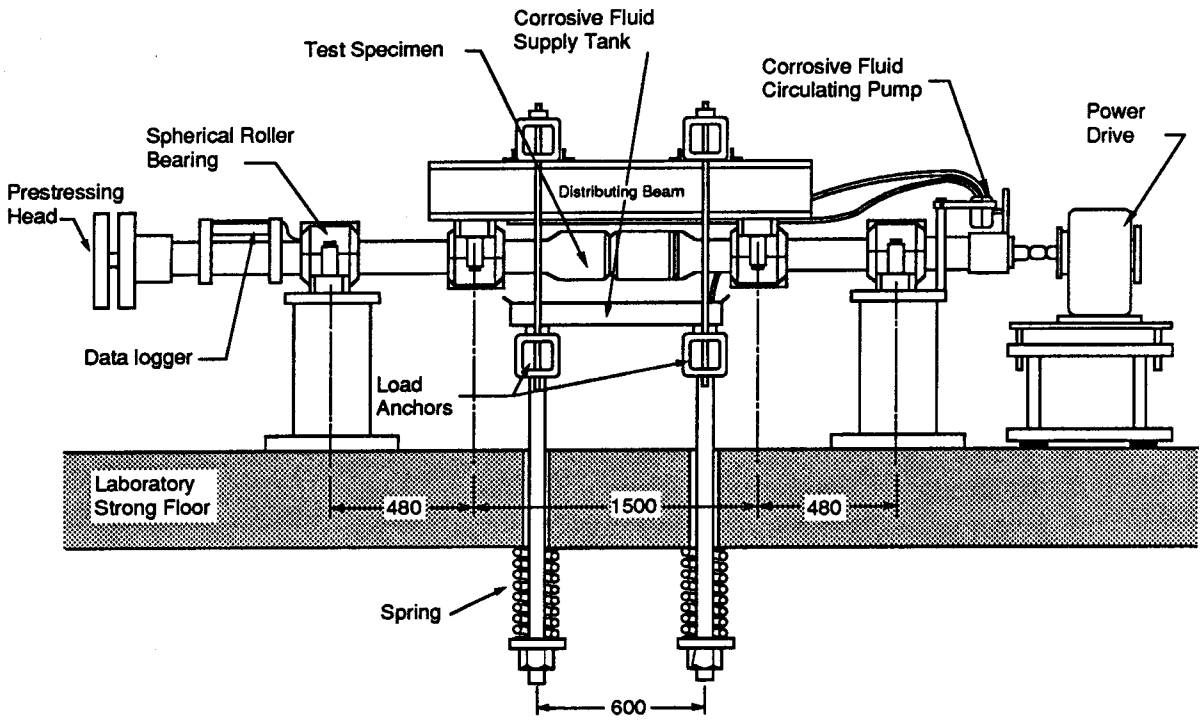

Figure 3.5 Rotating - Bending Test Setup

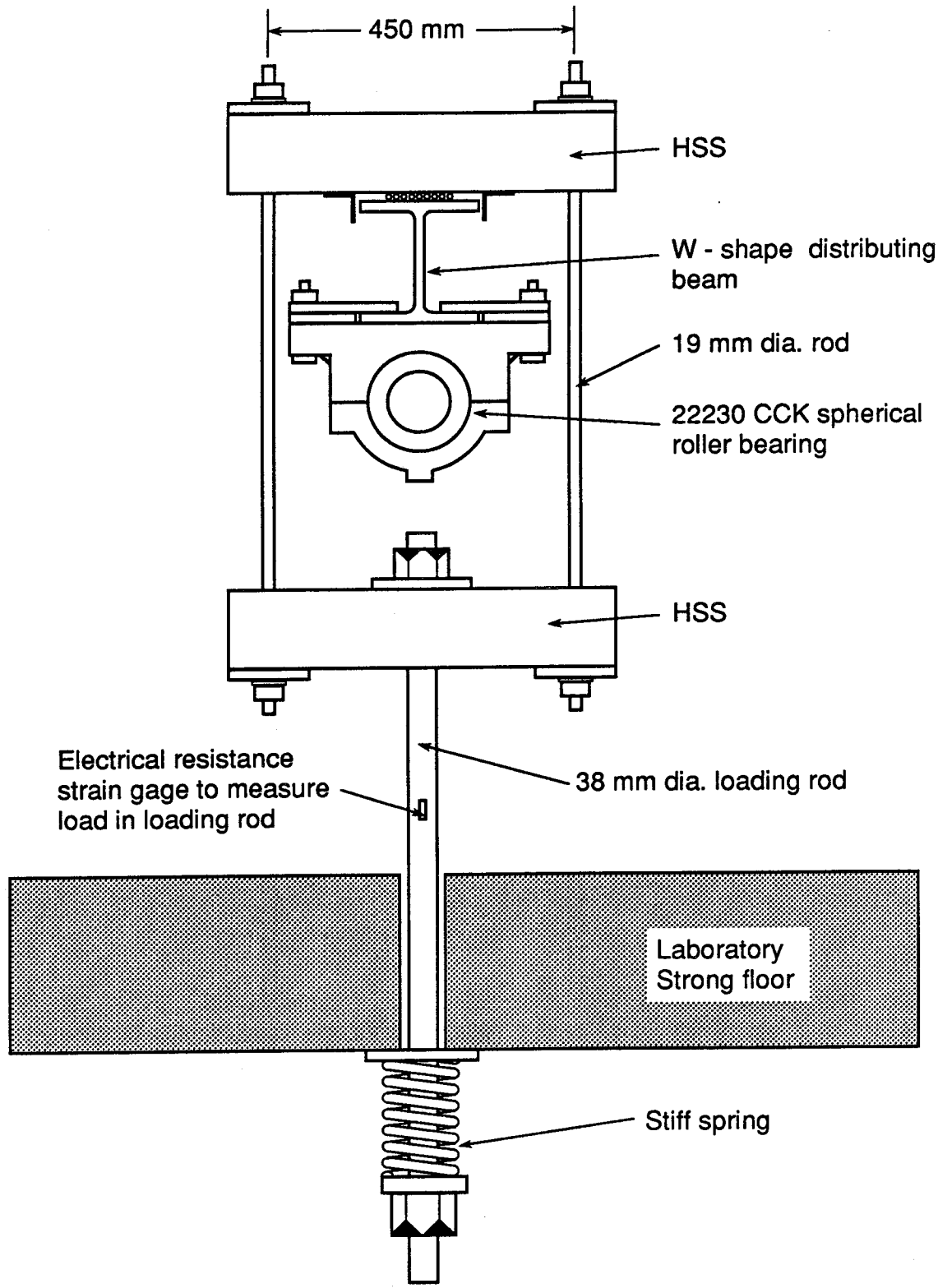

Figure 3.6 Detail of Loading Point Assembly

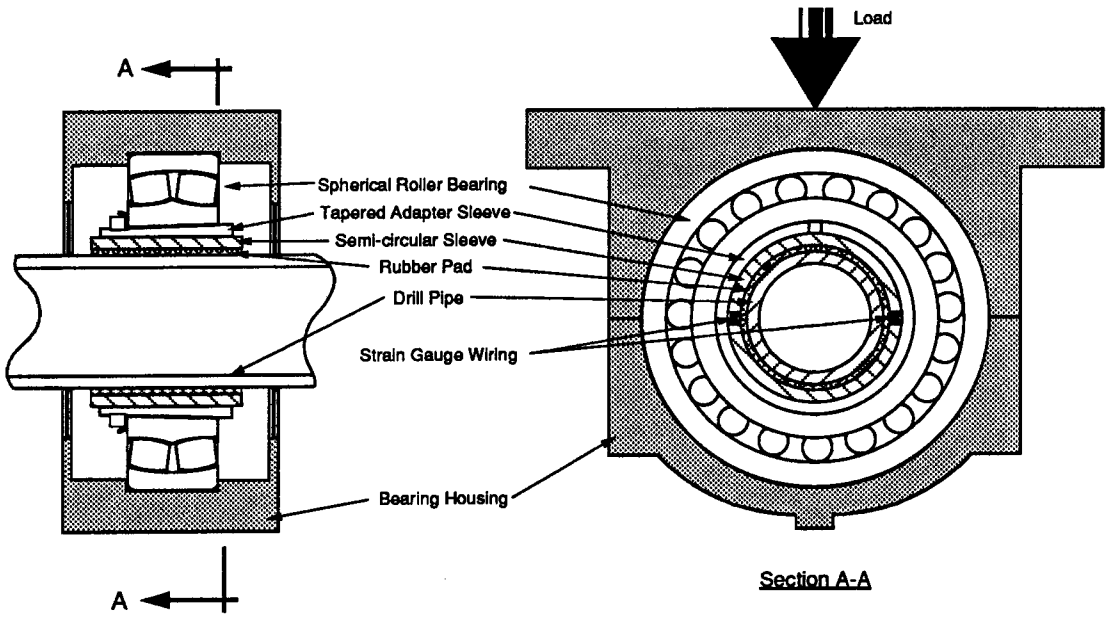

Figure 3.7 Loading Point Assembly

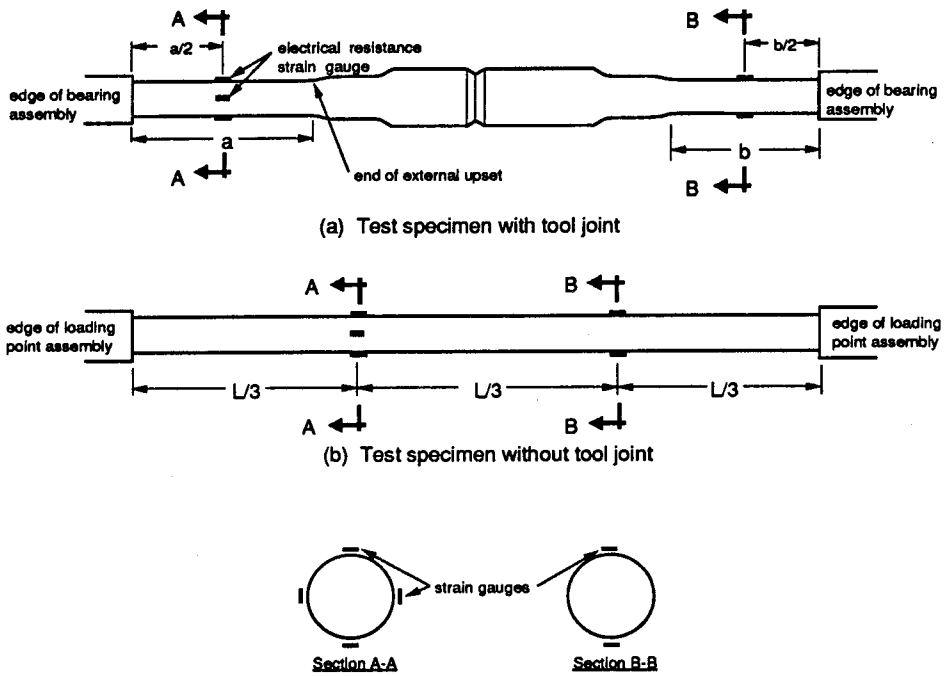

Figure 3.8 Strain Gaging of Test Specimens

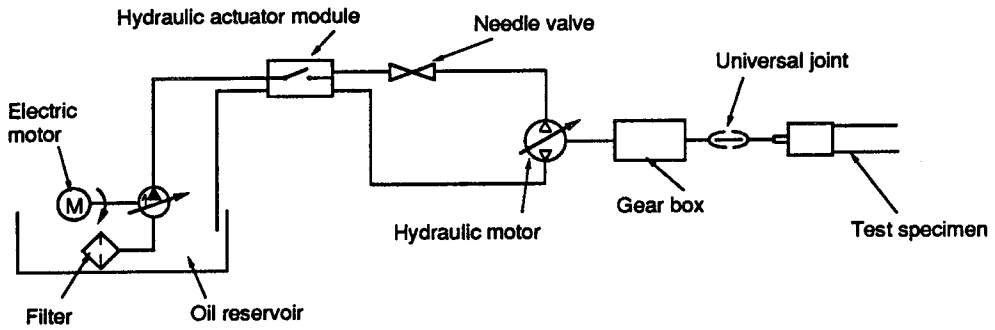

Figure 3.9 Hydraulic Power Drive for Rotating Bending Tests

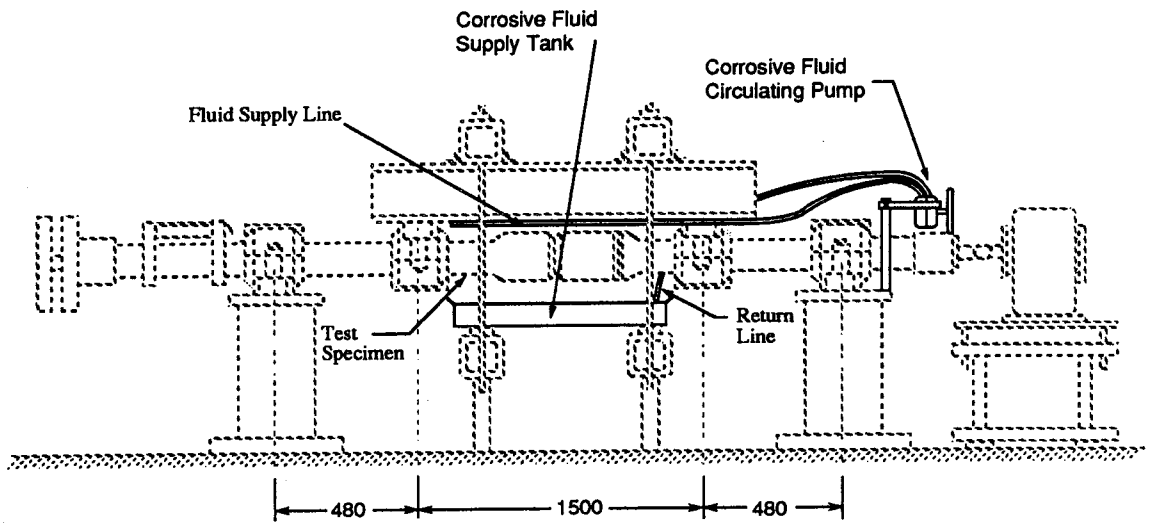

Figure 3.10 Corrosive Fluid Circulation System

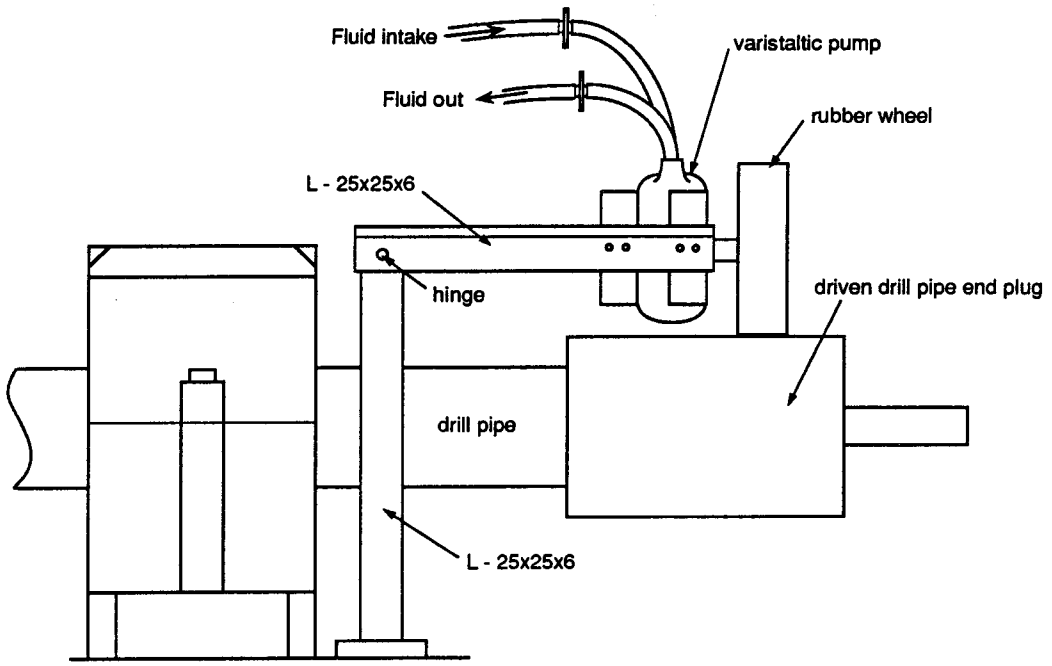

Figure 3.11 Salt Water Pump Arrangement

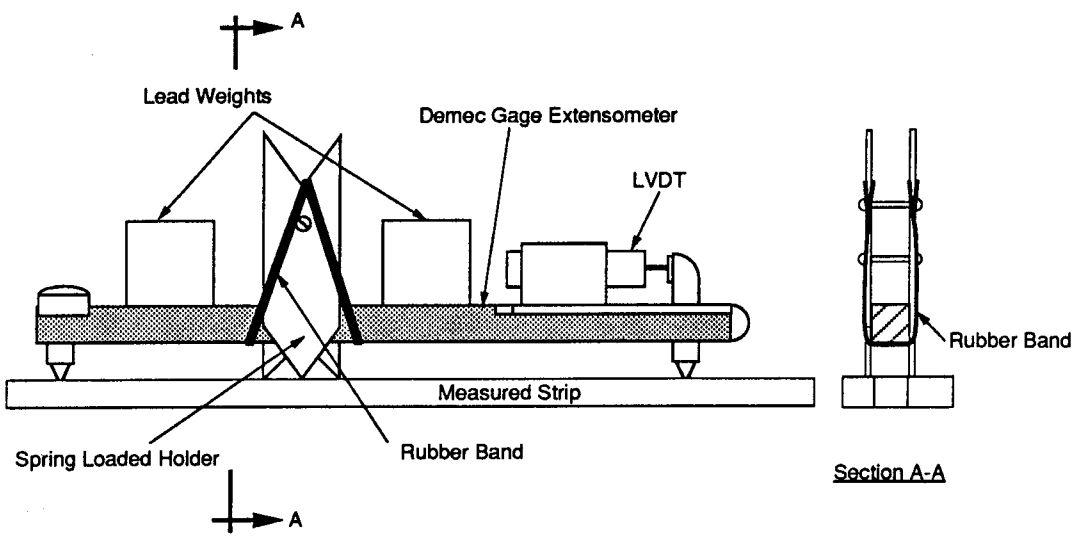

Figure 3.12 Demec Gage Extensometer Modified for Residual Stress Measurement

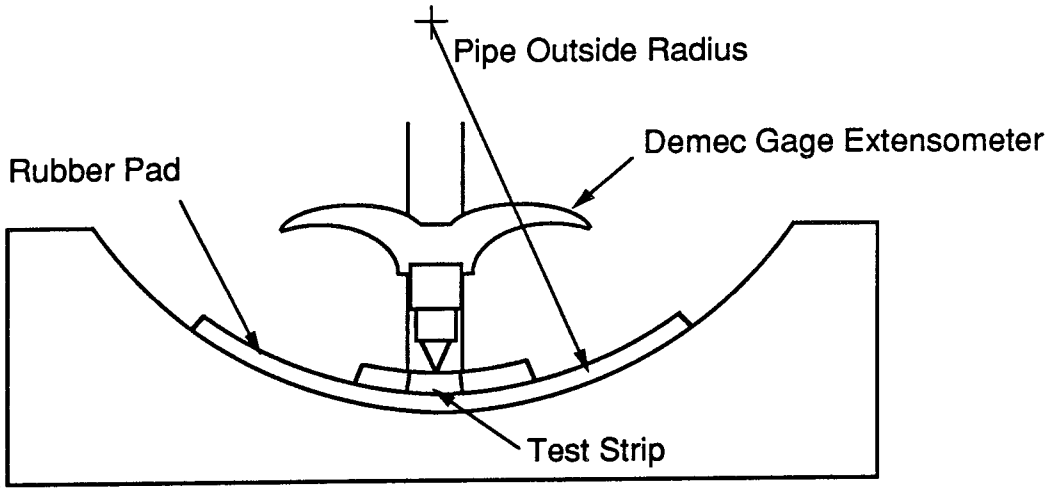

(a) Measurement on Inside Surface

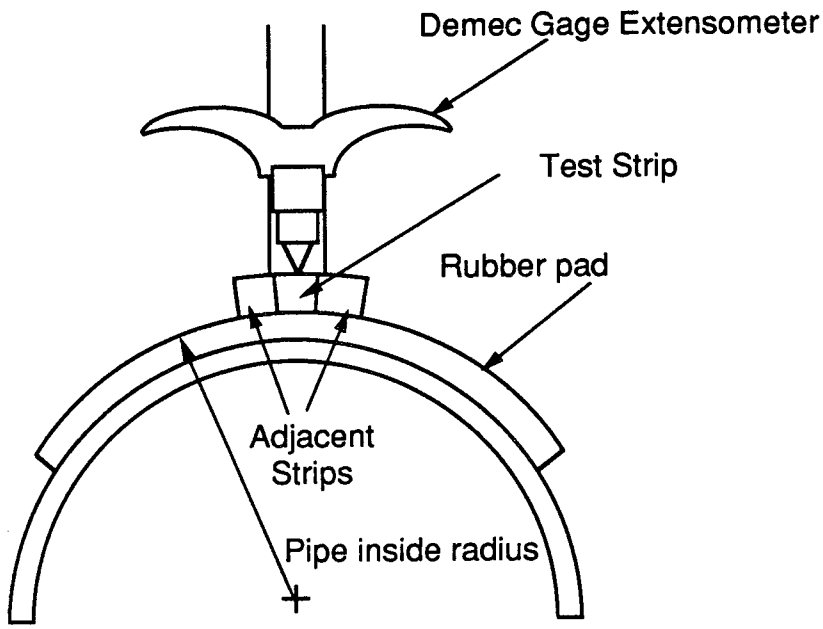

(b) Measurement on Outside Surface

Figure 3.13 Measurement of Gage Length After Sectioning

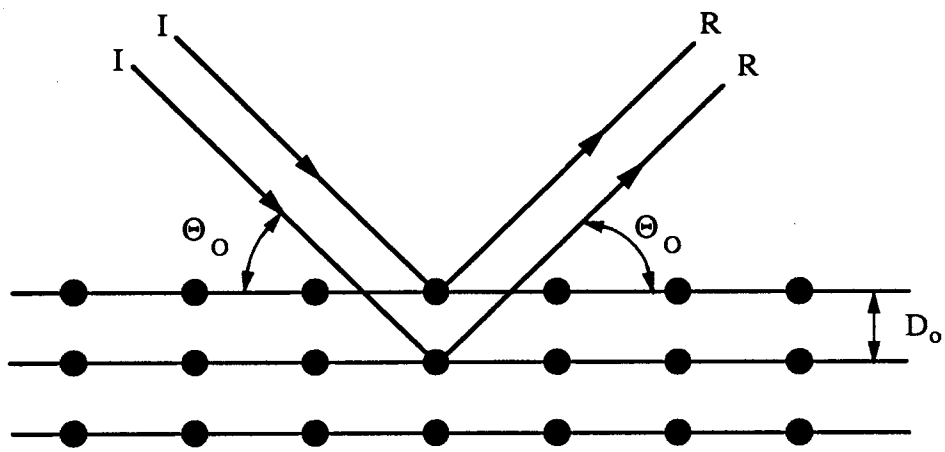

D_o = distance between planes of atoms

I = incident beam

R = reflected beam

Figure 3.14 Diffraction of X-Rays Within a Crystal

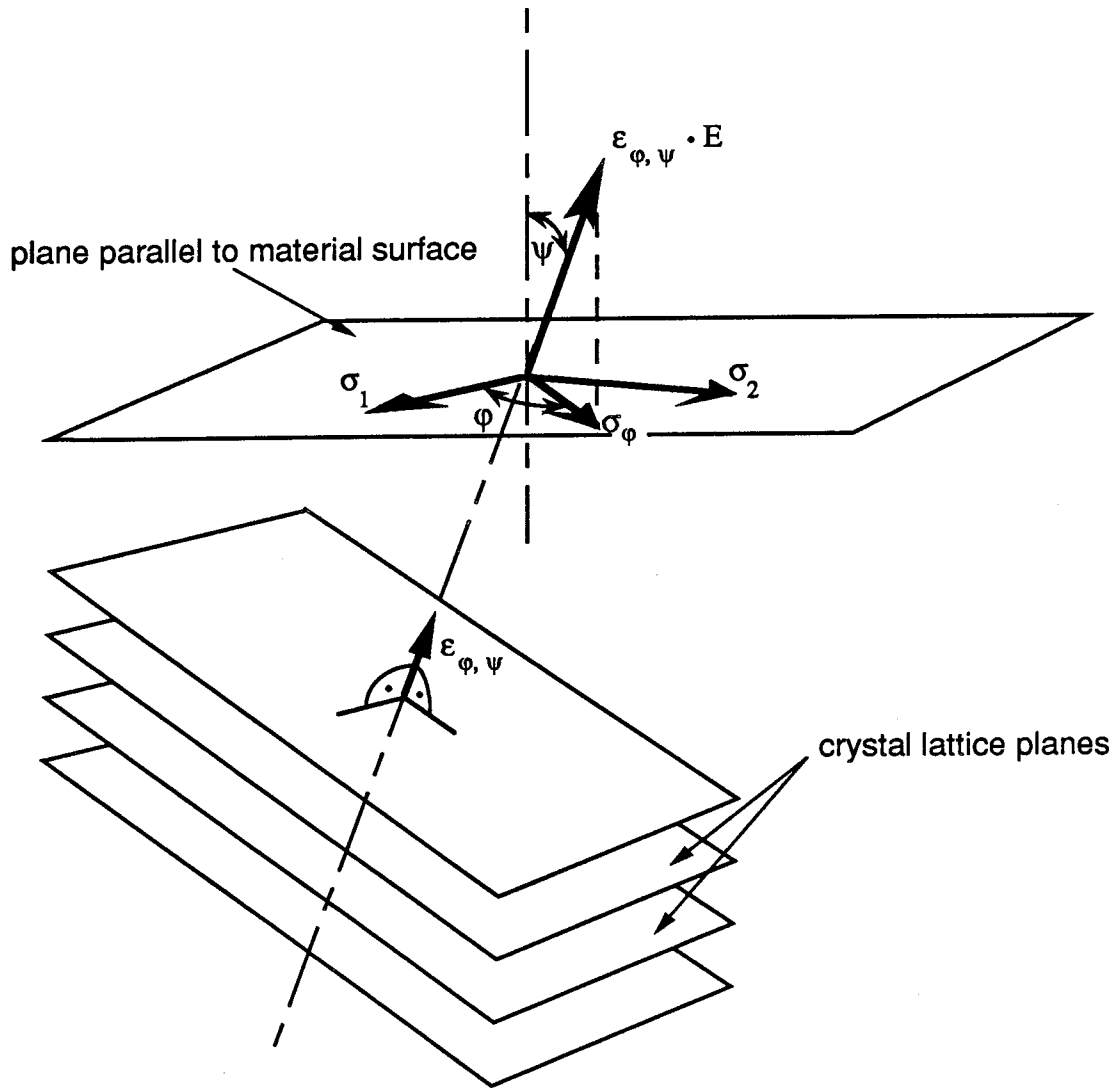

Figure 3.15 Relation Between Atomic Planes Deformation, $\varepsilon_{\varphi,\psi}$, And Stress At the Surface of the Material

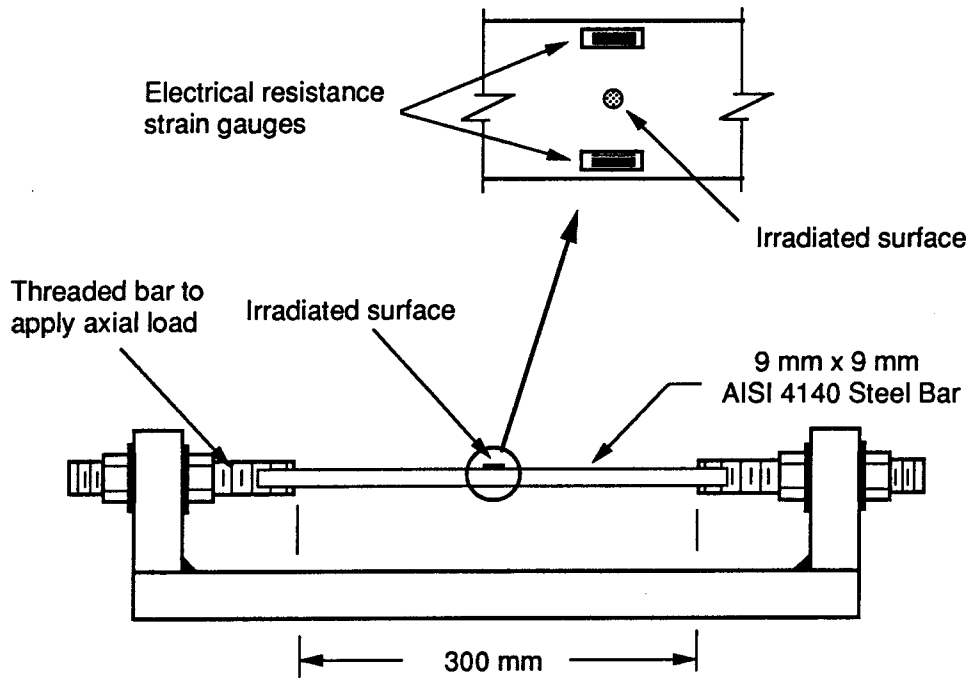

Figure 3.16 X-Ray Calibration Test Setup

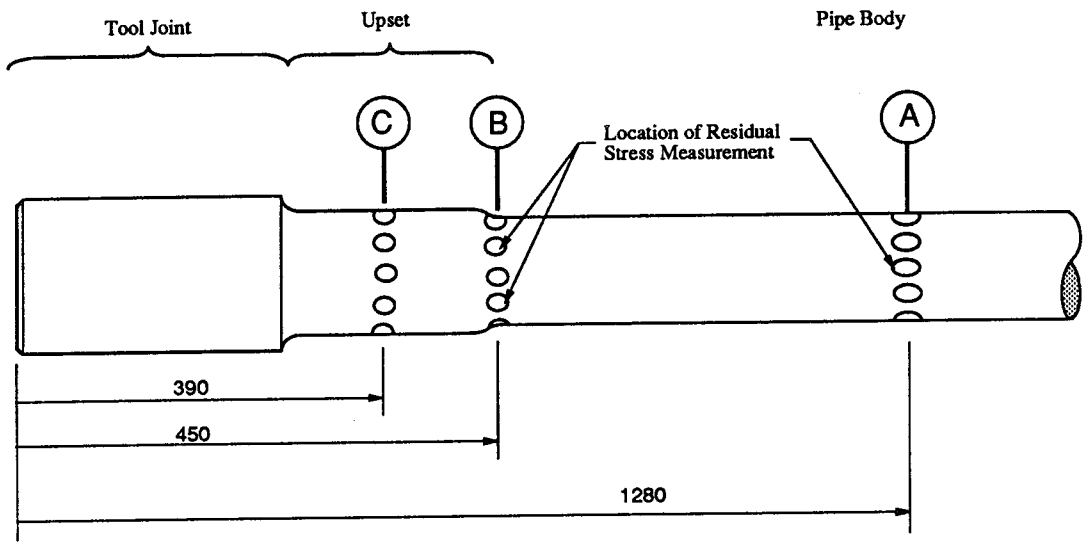

Figure 3.17 Locations of X-Ray Residual Stress Measurements

Chapter 4

Results of Experimental Program

4.1 Fatigue Tests

Fatigue tests were conducted on full-size specimens of drill pipe. Some of the test specimens incorporated the tool joint and upset regions as well as drill pipe body in the test portion, while other specimens consisted of drill pipe body only. A preliminary test program was conducted to verify that failures similar to the ones observed in the field could be duplicated in the laboratory. In the preliminary test program, drill pipes were tested under cyclic tension and cyclic bending. Once the mode of failure in specimens tested in the laboratory was found to be comparable to the mode of failure observed in the field, a more detailed test program, using rotating beam specimens with a variable mean stress, was initiated. In this chapter, the results obtained from both the preliminary and main test programs are described. In presenting these results, the intention is to give the factual information, provide an overview of the trends of fatigue life, etc., but not to enter into a detailed examination on any of the issues. The latter is presented in Chapter 5.

4.1.1 Preliminary Test Program

The results of tests on full-size tension and simple cyclic bending specimens are summarized in Table 4.1. All the test specimens presented in the table were obtained from a local supplier and all were drill pipes manufactured by Ohio Drill Pipe. The test frequency was 0.3 Hz for the cyclic tension test and varied between 3 to 4 Hz for the tests performed under cyclic bending. Except for specimen DST1, a test in cyclic tension, all the test specimens from the preliminary test program were tested in cyclic bending and are designated by a prefix BT, followed by the number of the specimen. Specimen designation with a suffix C designates a test specimen tested in a corrosive environment. Three drill pipes in the preliminary test program were 89 mm O.D. drill pipes with external upset. All the other specimens in the preliminary test program were 114 mm O.D. drill pipes with internal-external upset. Specimen BT1, tested in simple cyclic bending, was inadvertently deformed plastically in bending before testing and had to be straightened. Plastic deformation of the drill pipe before and during straightening resulted in a change in residual stresses which may have affected the fatigue life of the specimen.

Testing of DST1, the only test specimen tested in cyclic tension, was abandoned after 535 000 cycles because comparable specimen BT1, tested at the same stress range but in cyclic bending, had not failed after more than 18 million cycles of loading.

Examination of the last column of Table 4.1 indicates that the majority of the test specimens failed in the upset region. This correlates well with observed failure locations in the field (Marion, 1987). With the exception of specimen BT3, all the test specimens failed from a crack originating on the outer surface. The fracture surface of BT3 showed three different crack nuclei, one of which originated from the inner surface of the drill pipe.

The results of the preliminary test program are plotted in Figure 4.1. A significant amount of scatter can be observed. Specimens BT3, BT7 and BT8, tested at a stress range of 350 MPa and a mean stress of 215 MPa to 230 MPa, show a scatter in fatigue life of about 90 000 cycles, representing 25 percent of their mean fatigue life. At a stress range of 290 MPa and mean stress of 320 MPa the fatigue life of BT5 and BT6 differed by about 34 000 cycles. Specimen BT4 shows no significant difference in fatigue life when the mean stress is decreased to 170 MPa and the stress range kept at 290 MPa.

Specimen BT6C-B, tested in a 3.0 percent NaCl solution, showed a reduction in fatigue life of about 30 percent over comparable specimen BT4 tested in air under the same stress range and mean stress. BT6C-B did not have a tool joint in the constant moment region, however.

4.1.2 Rotating Bending Test Program

The main test program was conducted with drill pipes tested in rotating bending with a superimposed axial load. This closely simulates field conditions. The parameters investigated were the effect of mean stress, stress range, and the effect of a corrosive environment on the fatigue life. Although field conditions cover a wide range of corrosive environments, the testing environment for the test program was limited to a 3.5 percent NaCl solution.

The results from the rotating bending test program are presented in Table 4.2 for tests conducted in air and Table 4.3 for tests conducted in a corrosive environment. The first column of Tables 4.2 and 4.3 indicates the specimen designation. Specimens from the main test program were all tested in rotating bending and are designated by a prefix RB. Specimen designation with a prefix RBT indicates that the test specimen was obtained from

drill pipes purchased for the preliminary test program. The letter C in the specimen designation indicates that the test specimen was tested in a corrosive environment. Test specimens were formed both from the part of a drill pipe length containing the tool joint and from drill pipe body only. Those specimens consisting of drill pipe body only are designated by the suffix B. This identification scheme was adopted in order to keep track of the origin of each test specimen. Drill pipes used for the investigation came from three different manufacturers. The second column of tables 4.2 and 4.3 identifies the manufacturer of each specimen tested. Most of the test specimens used in this investigation were manufactured by Mannesmannrohren-Werke (M). Other pipes used in the test program were manufactured by Ohio Drill Pipe (O) and Sumitomo Metal Industries (S). All the drill pipes tested were Grade E, 114 mm O.D., 24.7 kg/m, with an internal-external upset configuration. Tables 4.2 and 4.3 also report the stress range, mean stress, and number of cycles to failure. Remarks about the test conditions, specimen description and the location of fatigue failure with respect to the tool joint are reported in the last column of Tables 4.2 and 4.3.

4.1.2.1 Tests in Air

With the exception of specimen RB16, the data in Table 4.2 show that all the test sections which incorporated a tool joint, a total of 10, failed from a crack developing in the body of the drill pipe away from the upset runout. This indicates that the tool joint and upset regions are stronger than the body section and, consequently, they do not affect the fatigue strength of the drill pipe. For this reason, and also for reasons of economy, specimens consisting of drill pipe body only were also tested. Figure 4.2 (a) shows the extent of crack growth in the drill pipe body when testing was stopped. Figure 4.2 (b) shows the fatigue crack that developed at the internal upset runout of drill pipe RB16.

The lowest fatigue life of all specimens tested in air, 82 100 cycles, came from specimen RB16, which is also the only specimen in the main test program to fail in the upset runout region. Examination of the fracture surface under a scanning electron microscope revealed a region at the crack initiation site where many magnesium silicates were present in the form of inclusions.

The effect of mean stress on fatigue life was investigated at a stress range of 290 MPa. Three tests were run at each of the mean stress levels 250 MPa, 125 MPa, and 0 MPa. The test results are presented in Figure 4.3 in the form of mean stress versus number of cycles to failure. Testing was discontinued in some specimens after

approximately 10 million cycles if there was no apparent crack. (These results are identified by the arrows attached to the data point.) Even given that there is a relatively large amount of scatter at each mean stress level, the test results indicate that the fatigue life decreases as the mean stress is increased.

The effect of stress range on fatigue life was investigated using a mean stress of 125 MPa. The results presented in Figure 4.4 cover stress ranges varying from 180 MPa to 350 MPa. A large amount of scatter in the data can be observed. For example, for specimens at a stress range of 290 MPa the fatigue life varied from 468 500 cycles to more than 10 million cycles. A similar scatter is observed at a stress range of 250 MPa. As expected, the test results plotted in Figure 4.4 indicate that the fatigue life decreases as the stress range increases.

4.1.2.2 Tests in Corrosive Environment

The results from tests run in a corrosive environment are presented in Table 4.3. The test data show that all the test sections incorporating a tool joint, a total of seven, failed from a crack developing in the body of the drill pipe away from the upset runout. As was the case for tests conducted in air, the upset geometry and tool joint do not seem to affect the fatigue strength of drill pipe. The results presented in Table 4.3 show significantly less scatter than do the results obtained in air.

The effect of mean stress on fatigue life was investigated at two different stress ranges. The mean stress levels used for the investigation were 0, 125, and 250 MPa and the stress range levels were 290 MPa and 130 MPa. Figure 4.5 indicates a decrease of fatigue life as the mean stress increases.

With the exception of one test, all the tests done in the corrosive environment were conducted at a frequency of 60 rpm (1.0 Hz). One drill pipe, specimen RB9C, was tested at a frequency of 90 rpm (1.5 Hz). The stress range and mean stress for this specimen were 290 MPa and 250 MPa, respectively. As indicated in Figure 4.5, the fatigue life was longer at a higher test frequency. Although this observation is based on only one test result, it is consistent with observations made by other investigators on the effect of testing frequency on the fatigue life in a corrosive environment (Helbig and Vogt, 1987).

The effect of stress range was investigated using a mean stress of 125 MPa. Stress ranges varying from 290 MPa to 80 MPa were used in the investigation. Figure 4.6 shows

the effect of stress range on fatigue life for a constant mean stress in a 3.5 percent NaCl solution.

The effect of a corrosive environment in itself on fatigue life is illustrated in Figure 4.7, where the test results for specimens tested at a mean stress of 125 MPa and varying stress range are presented. Figure 4.7 indicates that the corrosive environment reduces the fatigue life. As the stress range decreases, the effect of corrosive environment is more noticeable. A greater number of test specimens tested in air reached a fatigue life of over 10 million cycles. At a stress range of 290 MPa the tests conducted in a corrosive environment lasted only 55 to 171 hours. Under a longer period of exposure it is expected that the corrosive environment would have a more detrimental effect because of the time dependent nature of the corrosion process. Therefore, it can be expected that the influence of the corrosive environment will be more significant in decreasing the fatigue life when a specimen is tested at a low stress range.

4.2 Fractography

Macroscopic examination of fracture surfaces from specimens tested in air revealed three distinct regions, as shown in Figure 4.8. Region I, which contains the crack initiation site, consists of a smooth flat surface of semi-elliptical shape, perpendicular to the loading direction. The smooth flat surface is indicative of the slow propagation rate of the fatigue crack. Once the semi-elliptical crack reached the inner surface of the drill pipe, the fracture surface became somewhat coarser (region II), indicating a faster crack propagation rate. The fracture surface gradually tilted and, in region III, the crack propagated at an angle of approximately 45 degrees from the surface. At this stage, the state of stress at the crack tip has become predominantly a state of plane stress and the propagation rate has increased further.

The fracture surface for each test specimen was examined with a stereomicroscope and a scanning electron microscope in order to identify the cause of crack initiation. Specimens from the preliminary test program were coated with a clear lacquer to prevent corrosion of the fracture surface before it could be examined. It was later found that the protective lacquer could not be removed without damaging the fracture surface. For this reason, only the observations made on the specimens from the main test program are presented herein. The corrosion fatigue fracture surfaces were cleaned with inhibited hydrochloric acid to remove the corrosion products accumulated on the surface.

Table 4.4 presents a listing of the fatigue crack origins identified in the test specimens. It is readily apparent from Table 4.4 that surface grinding has a detrimental effect on the fatigue strength of drill pipes since those marks were identified to be at the origin of most fatigue failures. Figure 4.9 shows a typical fatigue crack that initiated from a surface groove produced by grinding. Fatigue cracks were observed to start preferentially at the bottom of the grooves made by grinding. Grinding was also observed to have a detrimental effect on the fatigue life of drill pipes tested in a corrosive environment. As shown in Figure 4.10 several fatigue cracks started from surface scratches left by grinding, although only one of those cracks led to failure of the test specimen. Figure 4.11 shows the appearance of typical corrosion fatigue fracture surface. Extensive corrosion and pitting at the crack origin masks the grinding mark usually observed on fatigue specimens tested in air.

As shown in Figure 4.12, fatigue cracks also started from surface pits. Although all the specimens tested had surface pits, the pits were seldom identified as the origin of fatigue failure. Specimens such as the one shown in Figure 4.13, where many deep surface pits were observed, still failed at grinding marks, indicating that grinding is more detrimental than surface pits. As shown in Figure 4.14 (a), corrosion pits are not only found on the outer surface, but can also be found on the inner surface. It is probable, as evidenced by Figure 4.14 (b), that corrosion pits on the inner surface of the pipe are formed by water trapped inside the pipe. Because of the presence of the internal upset, water that gets into the pipe cannot drain out. However, no specimen failed from a fatigue crack initiating on the inner surface of the drill pipe.

Two specimens (RB14-B and RB20-B) showed a fatigue crack initiating at a surface notch produced during handling of the pipe either during or after manufacturing. The presence of paint detected on the notch surface indicates that the notch which led to failure of the pipes was not detected during pipe inspection. Figure 4.15 shows the fatigue cracks in specimens RB14-B and RB20-B, which originated at a surface notch. Inasmuch as any transverse mark can be a dangerous stress-concentration point, steel stencil marks on the body of the drill pipe can initiate a fatigue crack wherever any part of the letter is transverse to the pipe. Although recommendations against this practice were made in the early forties (Grant and Texter, 1941), steel stenciling on the drill pipe body is still used, as evidenced by Figure 4.16 (a). However, this practice does not seem to be general since only one specimen in the test program was marked in this way. Specimen RB28C-B failed from a fatigue crack originating at the vertical line of the numeral 1 stamped transverse to

the pipe axis (see Figure 4.16 (b)). Specimen RB28C-B had a fatigue life of only 25 percent of the fatigue life of specimens RB21C and RB23C, all tested under the same conditions.

In few instances, crack initiation was caused by surface inclusions. Figure 4.17 shows the origin of fracture in specimen RB16 at an impurity worked into the surface during the forming process of the drill pipe. Figure 4.17 (a) shows the extent of penetration of the inclusion below the surface. The interface of the inclusion and the intact material is indicated by a triangular marker on the right. Above the marker, the inclusion, shown at a greater magnification in Figure 4.17 (b), shows precipitates of magnesium silicates, while a normal clean fatigue fracture surface is detected below the marker (see Figure 4.17 (c)).

4.3 Residual Stresses

Residual stresses were measured in drill pipes taken from the different manufacturing sources. Both the method of sectioning and X-ray diffraction were used to measure residual stresses in the body of the drill pipe, the external upset runout, and the upset. Residual stress measurements on the upset and the upset runout were performed on one specimen only because specimens used for residual stress measurements could not be used subsequently for testing in fatigue. Residual stress measurement was not performed on specimens already tested in fatigue because of the potential for the presence of fatigue cracks that would release some of the residual stresses originally present in the drill pipe. Because a long gage length is required when the method of sectioning is used for residual stress measurement, only X-ray diffraction could be used to measure residual stresses in the upset and upset runout regions.

Figure 4.18 shows the distribution of residual stresses on the outer and inner surfaces of drill pipe BT4, as well as the average of the inner and outer surface residual stresses. The test section was obtained from the body of the drill pipe and the sectioning method was used to obtain the residual stress values. Residual stresses are small both on the exterior and interior surfaces, and they vary from tension to compression. The maximum residual stress measured on the exterior surface is approximately 25 MPa in compression, while the maximum stress measured on the interior surface is about 35 MPa in tension. These values are 3.0 percent and 4.0 percent of the measured tensile strength of the pipe, respectively. Figure 4.18(c) shows the average of the stresses measured on the

outer and inner surfaces of the pipe. The figure indicates that equilibrium is satisfied on the cross-section.

In order to assess the variation of residual stresses along the length of a drill pipe, a second section of drill pipe body was taken from BT4. Residual stresses measured in BT4-2, a replicate of BT4-1, are presented in Figure 4.19. The stresses measured on the outer and inner surfaces show the same characteristics as section BT4-1 presented in Figure 4.18. Stresses are small and vary from tension to compression. Figure 4.19(c) shows the distribution of average residual stresses around the circumference of BT4-2. Although the figure indicates that equilibrium of forces is not satisfied, the out-of-balance force is within the accuracy of the technique used.

Figure 4.20 shows the residual stress characteristics for drill pipe BT6, a pipe originating from the same manufacturer (Ohio Drill Pipe) as drill pipe BT4. Electrical resistance strain gages were mounted on the exterior and interior surfaces of the pipe before sectioning to confirm the reliability of the measurements taken with a Demec gage extensometer. A total of nine strips were instrumented in this way. Gage readings were taken before and after sectioning to obtain the amount of residual stresses released by the sectioning operation. Figures 4.20(a) and 4.20(b) show good agreement between stress measured with a mechanical Demec gage extensometer and by using electrical resistance strain gages. Specimen BT6-1 also shows low residual stresses, varying from tension to compression, on both surfaces of the pipe. Figure 4.20(c) shows that the distribution of average residual stresses satisfies equilibrium within the accuracy of the technique employed.

A second section from drill pipe BT6 was also used for residual stress measurements. Measured stresses on the exterior and interior surfaces and the average of inner and outer stresses are presented in Figure 4.21. Figure 4.21(a) indicates that residual stresses are again very low (a maximum of 25 MPa in compression), but this time residual stresses are compressive all around the circumference. Measured residual stresses on the interior surface are close to zero and the average shown in Figure 4.21(c) shows an overall compressive stress distribution around the circumference of the pipe.

Figures 4.22 and 4.23 present residual stresses measured in drill pipes RB5 and RB8, both manufactured by Mannesmannrohren-Werke. Unlike the pipes from the preliminary test program (pipes BT4 and BT6), the length of the specimen was found to be influential on measured residual stresses in these cases. Decreasing the length of specimen

from 1000 mm to 625 mm did not affect the residual stresses significantly. However, when the length of the specimen was decreased below 625 mm, significant change in residual stresses was observed. Figures 4.22(d) and 4.23(d) show the amount of residual stresses released by cutting the specimen to a length of 415 mm (from an original length of 1000 mm). No measurement could be taken on the interior surface until the specimen was cut down to a length of 415 mm. Figures 4.22(a), (b) and (c) for specimen RB5 and figures 4.23 (a), (b) and (c) for specimen RB8 show residual stresses released by sectioning a 415 mm long specimen. The total residual stresses measured on the exterior surface of a full length drill pipe consists of the sum of the residual stresses released by shortening the specimen and subsequent released stresses due to sectioning of the short specimen. Total residual stresses released on the exterior surface of specimens RB5 and RB8 are presented in figures 4.22(e) and 4.23(e), respectively. Exterior surface residual stresses in specimen RB5 vary between 30 MPa in tension and 70 MPa in compression. These values are 4.0 percent and 9.0 percent of the measured tensile strength of the pipe, respectively. Residual stresses measured on the exterior surface of drill pipe RB8 varied between 15 MPa and 65 MPa in compression. Because no reading could be taken on the interior surface until the test specimens were cut 415 mm long, the total amount of residual stresses released on the interior surface by sectioning and shortening could not be measured or estimated.

Since the minimum length at which a section had to be cut in order to retain all the residual stresses was approximately 625 mm, the gage length was increased to 500 mm and subsequent specimens were cut no shorter than 650 mm before sectioning.

Residual stresses were measured in one section of drill pipe using both X-ray diffraction and the method of sectioning. The test section was obtained from drill pipe RB13 (Mannesmannrohren-Werke). Drill pipe RB13 was used for measurement of residual stresses in the upset region and therefore could not be used for fatigue testing, as explained above. Measurements were first taken using X-ray diffraction and the same section was then used to measure residual stresses by the method of sectioning. This was done in order to obtain a direct comparison between the two methods. Figure 4.24(a) shows the residual stress distribution measured using X-ray diffraction. Measurements were taken 0.1 mm and 0.5 mm below the surface. At 0.1 mm below the surface, residual stresses vary from 100 MPa to 300 MPa in compression (13 percent to 38 percent of the tensile strength). At 0.5 mm below the surface, residual stresses vary from compression to tension. It is evident from Figure 4.24(a) that a high stress gradient exists near the

surface. Figure 4.24(b) shows the measured residual stress distribution using the method of sectioning on the same length of drill pipe. Stresses measured by this technique are significantly lower than those measured using X-ray diffraction. The discrepancy between the two residual stress measuring techniques can be explained by several factors. Measurements using a mechanical device sitting in drilled holes do not represent measurements on the surface but are representative of values somewhere below the surface. Measurements made using the sectioning method represent an average value over a relatively large volume of material and, consequently, cannot detect high stress gradients near the surface, as are apparently present in the drill pipes used in this investigation. Measurements made using X-ray diffraction reflect the presence of Type I and Type II residual stresses while the method of sectioning does not reflect the presence of Type II residual stresses. In addition, cutting of the strips may not release all the residual stresses and could also introduce additional stresses by plastic deformation of the material near the saw cut edge. A combination of all the above factors is most likely the cause of the discrepancy between the results obtained by X-ray diffraction and the method of sectioning.

Figure 4.24(c) shows measured residual stress distribution on the interior surface of drill pipe RB13 measured by the method of sectioning. Stresses are mostly compressive, with a maximum magnitude of 35 MPa. Average stresses in the cross-section are presented in Figure 4.24(d). Again, the average residual stress distribution closely satisfies equilibrium. Since fatigue cracks most often start from surface features, residual stresses at or near the surface are more influential than average stresses through the thickness. For this reason, it is believed that X-ray diffraction methods yield more valuable results than the method of sectioning. (It should be noted that both methods are time-consuming. Typically, measurement of residual stress by the method of sectioning took about 150 man-hours per pipe sample, while measurement by X-ray diffraction took about 90 hours).

Residual stresses were measured in a section of drill pipe incorporating the tool joint (box section), upset and part of the drill pipe body. Stresses were measured in the pipe body, the upset runout, and the upset. These are referred to as sections A, B, and C and are shown in Figure 3.17. Stresses measured at section A were presented in Figure 4.24(a) and were used as a basis for comparison with the method of sectioning. Stresses measured at the upset runout (section B in Figure 3.17) are plotted in Figure 4.25. Although the magnitude of residual stresses is smaller here than in the drill pipe body, the

stresses are compressive both at 0.1 mm and 0.5 mm below the surface. Figure 4.26 shows the measured stress distribution in the upset region (section C in Figure 3.17) measured 0.1 mm and 0.5 mm below the surface. Again, measured residual stresses are all compressive. The maximum residual stress measured at section C was about 350 MPa (44 percent of the tensile strength) at a depth of 0.1 mm below the surface. The specimen on which those X-ray measurements were performed was obtained from a drill pipe manufactured by Mannesmannrohren-Werke.

Residual stresses measured in drill pipe RB11, also from Mannesmannrohren-Werke, are presented in Figure 4.27. Figure 4.27(a) shows that residual stresses measured 0.1 mm below the surface are all compressive, with a maximum value of about 430 MPa and a minimum value of approximately 90 MPa. The distribution of residual stresses below the surface in drill pipe RB11 is presented in Figure 4.27(b). A large stress gradient, about 700 MPa/mm, exists near the surface. At a depth of about 0.5 mm residual stresses change from compression to tension.

Residual stresses measured by X-ray diffraction in a pipe manufactured by Ohio Drill Pipe (test specimen BT4) are shown in Figure 4.28. Figure 4.28(a) shows the residual stress distribution around the circumference of the pipe body. Stresses vary from about 180 MPa in compression to about 200 MPa in tension. Stresses were measured at a depth of 0.1 mm below the surface. Figure 4.28(b) shows the stress distribution below the surface down to a depth of 0.76 mm. Stresses vary with depth from tension to compression.

As discussed in section 4.1.2, several drill pipe specimens failed from fatigue cracks originating at surface grinding marks. To investigate the effect of grinding marks on the distribution of surface residual stresses, a section of drill pipe taken from drill pipe RB6 was used for X-ray diffraction. Grinding marks were present at three different locations around the circumference of the section. Figure 4.29 shows measured stresses on the surface and identifies locations where grinding marks were located. The figure shows that the unground surface is subjected to high compressive residual stresses. On the other hand, areas where grinding marks were present displayed mostly tensile residual stresses with the exception of one point where a residual stress of 20 MPa in compression was measured.

Residual stresses were also measured on a section of drill pipe body taken from specimen RB14 (manufactured by Mannesmannrohren-Werke), which was ground at two

different locations. The measured residual stresses on the unground and ground surfaces are presented in Figure 4.30. High compressive residual stresses, approaching 300 MPa, were measured on the unground surface. Residual stresses measured on the ground surface vary between 130 MPa in compression and 125 MPa in tension.

Figure 4.31 presents residual stresses measured in a section of drill pipe manufactured by Sumitomo Metals Industries (test specimen RB23). Figure 4.31(a) shows residual stresses on the outer surface measured on ground and unground surfaces. Locations where grinding marks were present show both compressive and tensile residual stresses while the unground surface shows compressive residual stresses only. Stress distribution below the surface at a grinding mark is presented in Figure 4.31(b).

4.4 Metallography

Examination of metallographic specimens sampled from drill pipes manufactured by Ohio Drill Pipe, Mannesmannrohren-Werke, and Sumitomo Metal Industries did not reveal anything unusual about the microstructure of the normalized and tempered steel. However, the following observations were made:

- Drill pipes manufactured by Ohio Drill Pipe showed a microstructure in the body section consisting of approximately 90 percent tempered martensite with small bands of ferrite and pearlite for the remaining 10 percent. Figure 4.32 shows the typical microstructure in the drill pipe body. The microstructure in the body near the upset and about 20 percent of the upset length adjacent to the pipe body consists of ferrite and pearlite with no trace of tempered martensite (see Figure 4.33). The remaining portion of the upset and tool joint consist of tempered martensite, as shown in Figure 4.34. The surface layer of the pipe body is decarburized, as evidenced by Figure 4.35.

- Some drill pipes manufactured by Mannesmannrohren-Werke showed a microstructure in the drill pipe body consisting of about 60 percent ferrite-pearlite and 40 percent tempered martensite (see Figure 4.36). The upset and the tool joint consisted of tempered martensite (see Figure 4.37). As seen in Figure 4.38, the surface layer of the pipe body is decarburized.

- Some of the drill pipes manufactured by Mannesmannrohren-Werke had a drill pipe body consisting mostly of tempered martensite, with very little trace of ferrite and pearlite.

- Drill pipes manufactured by Sumitomo Metal Industries showed a microstructure consisting of approximately 50 percent ferrite and pearlite and 50 percent tempered martensite.

4.5 Ancillary Test Results

Typical stress versus strain curves for drill pipe steel are shown in Figure 4.39. Tables 4.5 to 4.7 give values of significant parameters. The modulus of elasticity was determined using the method of least squares on strain gage extensometer readings and load readings recorded during the test. The static yield level was determined by decreasing the strain rate to zero in the initial portion of the nonlinear part of the stress versus strain curve. The 0.2 percent offset method was used to determine the yield level. The ultimate stress, σ_u, was obtained by dividing the maximum load recorded during the test by the initial cross-sectional area of the tension coupon. Finally, the rupture strain, ε_{rupt}, was measured using a caliper over a gage length of 50 mm.

Strength requirements according to API Specification 5A for grade E drill pipe steel require that σ_y be between 517 MPa and 724 MPa, with a minimum ultimate strength of 689 MPa. Table 4.5 shows that specimen DST1 meets the requirements for Grade E drill pipe while BT2 slightly exceeds the requirements. The average of the material properties presented in Table 4.6 shows that the 115 mm O.D. drill pipes used in the preliminary test program met the strength requirements for Grade E drill pipe. It is evident from the average values presented in Table 4.7 that the drill pipes used in the main test program were also Grade E drill pipes.

4.6 Chemical Analysis

A wet chemical analysis of drill pipe steel from a drill pipe manufactured by Ohio Drill Pipe, a drill pipe manufactured by Mannesmannrohren-Werke, and one manufactured by Sumitomo Metal Industries was performed in order to determine the grade of steel used for the drill pipes used in this investigation. The results of this analysis are presented in Table 4.8. Carbon, manganese, nickel, chromium, and sulfur contents were determined from the chemical analysis. The phosphorous content could not be determined from the

chemical analysis. The composition of the steels indicates that they are low alloy steels of the AISI 4100 series. Their carbon content indicates that they are 4135 steels.

4.7 Summary

Fatigue tests were conducted on full-size drill pipes to study the effect of mean stress and corrosive environment on the fatigue life. A preliminary test program conducted on drill pipes loaded in cyclic tension or cyclic bending showed that most of the fatigue failures took place in the upset region of the drill pipe. The main test program was conducted using a rotating beam test setup. The setup allowed for variation of the mean stress. Tests were conducted either in air or in a corrosive environment consisting of a 3.5 percent NaCl solution. The results of the main program indicate that the mean stress has an effect on fatigue life; it is observed that fatigue life decreases as the mean stress is increased. Mean stresses of 0 MPa, 125 MPa, and 250 MPa were investigated. The effect of mean stress on fatigue life for pipe tested in a corrosive environment was similar. The damaging effect produced by grinding of the pipe surface was observed in several specimens. This effect was observed in both air and the corrosive environment. Sources of fatigue crack initiation other than grinding marks include surface inclusions and surface notches. Generally, under the same stress conditions tests conducted in a corrosive environment showed a significantly lower fatigue life than tests conducted in air.

Residual stresses were measured in sections of drill pipe obtained from two different manufacturers. Two methods were used, sectioning and X-ray diffraction. Comparison indicates that the method of sectioning consistently gives much lower values of residual stresses than does the X-ray diffraction method.

Measurements using X-ray diffraction indicate that a steep stress gradient exists near the surface of the drill pipe. Drill pipes manufactured by Ohio Drill Pipe had residual stresses on the exterior surface varying from tension to compression. In contrast, residual stresses on the outer surface surface of drill pipes manufactured by Mannesmannrohren-Werke are compressive. Stresses up to 440 MPa in compression were measured on the outer surface of specimens of Mannesmannrohren-Werke pipes.

Surface grinding performed during the inspection process at the pipe mill was found to induce moderate tensile stresses on the surface of drill pipes where the outer surface had been in compression prior to grinding. Tensile stresses of up to 250 MPa were measured on ground surfaces.

Metallographic examination of drill pipes taken from the preliminary test program showed that part of the upset region and the body of the drill pipe near the upset had a microstructure consisting of ferrite and pearlite. Tempered martensite and ferrite-pearlite was observed in the drill pipe body. The drill pipes manufactured by Mannesmannrohren-Werke showed only tempered martensite in the upset region of the drill pipe. The body of some of the drill pipes consisted of tempered martensite or tempered martensite with ferrite and pearlite. A chemical analysis of the drill pipe steel confirmed that the drill pipes were made of low alloy steel AISI 4135.

Table 4.1

Fatigue Test Results From Preliminary Test Program

Specimen Designation	Type of Test	Stress Range (MPa)	Mean Stress (MPa)	No. of Cycles to Failure	Remarks
DST1 (89 mm O.D.)	Cyclic Tension	260	142	—	No failure at 535 000 cycles.
BT1 (89 mm O.D.)	Cyclic Bending	260	159	—	No failure at 18 630 000 cycles.
BT2 (89 mm O.D.)	Cyclic Bending	350	218	544 410	Rupture at upset runout (L_p* = 370 mm)
BT3 (114 mm O.D.)	Cyclic Bending	350	230	338 590	Rupture in pipe body (L_b = 640 mm)
BT4 (114 mm O.D.)	Cyclic Bending	290	170	438 870	Rupture in upset (L_b = 385 mm)
BT5 (114 mm O.D.)	Cyclic Bending	290	320	467 280	Rupture in upset (L_b = 410 mm)
BT6 (114 mm O.D.)	Cyclic Bending	290	320	432 860	Rupture in pipe body (L_p = 595 mm)
BT7 (114 mm O.D.)	Cyclic Bending	350	215	418 330	Rupture in upset (L_p = 370 mm)
BT8 (114 mm O.D.)	Cyclic Bending	350	215	328 310	Rupture in upset (L_p = 300 mm)
BT6C (114 mm O.D.)	Cyclic Bending	290	170	296 700	Specimen without tool joint tested in a 3% NaCl solution.

*

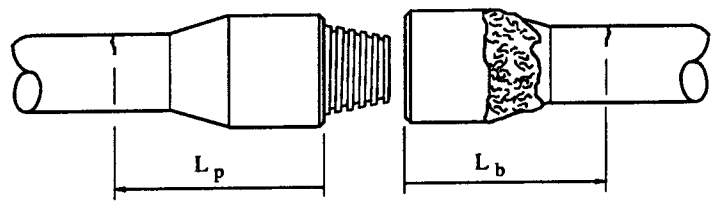

Table 4.2

Fatigue Test Results From Rotating Bending Test Program in Air

Specimen Designation	Manufacturer *	Stress Range (MPa)	Mean Stress (MPa)	No. of Cycles to Failure	Remarks
RBT4-B (114 mm O.D.)	O	302	144	472 600	Specimen without tool joint. Taken from same drill pipe as BT4.
RBT5-B (114 mm O.D.)	O	267	126	1 181 500	Specimen without tool joint. Taken from same pipe as RBT5.
RB1 (114 mm O.D.)	M	290	0	—	No failure at 10 066 800 cycles.
RB1-B (114 mm O.D.)	M	249	124	—	Specimen without tool joint. Taken from same pipe as RB1. No failure at10 000 000 cycles.
RB2 (114 mm O.D.)	M	290	125	468 500	Failure in pipe body under bearing. (L_b**= 750 mm)
RB2-B (114 mm O.D.)	M	335	125	189 800	Specimen without tool joint. Taken from same pipe as RB2.
RB3 (114 mm O.D.)	M	290	126	882 800	Failure in pipe body (L_b = 550 mm)
RB3-B (114 mm O.D.)	M	267	125	1 876 000	Specimen without tool joint. Taken from same pipe as RB3. Failure under bearing.
RB6 (114 mm O.D.)	M	287	0	1 389 900	Failure in pipe body (L_b = 665 mm)
RB7 (114 mm O.D.)	M	293	126	—	No failure at 10 107 400 cycles.

Table 4.2 (Cont'd)

Specimen Designation	Manufacturer *	Stress Range (MPa)	Mean Stress (MPa)	No. of Cycles to Failure	Remarks
RB7-B (114 mm O.D.)	M	273	127	508 500	Specimen without tool joint. Taken from same pipe as RB7.
RB8 (114 mm O.D.)	M	290	0	4 771 100	Failure in pipe body (L_p = 730 mm). Failure under bearing.
RB9-B (114 mm O.D.)	M	335	125	259 900	Specimen without tool joint. Taken from same pipe as RB9. Failure under bearing.
RB13-B (114 mm O.D.)	M	250	125	568 800	Specimen without tool joint. Taken from same pipe as RB13.
RB14 (114 mm O.D.)	M	340	126	511 200	Failure in pipe body (L_b = 590 mm)
RB14-B (114 mm O.D.)	M	320	127	300 400	Specimen without tool joint. Taken from same pipe as RB14. Failure simultaneously under bearing and at midspan.
RB15 (114 mm O.D.)	M	290	250	262 800	Failure in pipe body (L_p = 525 mm)
RB16 (114 mm O.D.)	M	292	252	82 100	Failure in upset (L_p = 350 mm)
RB18 (114 mm O.D.)	M	294	257	352 900	Failure in pipe body (L_b = 645 mm)
RB18-B (114 mm O.D.)	M	251	125	461 600	Specimen without tool joint. Taken from same pipe as RB1.

Table 4.2 (Cont'd)

Specimen Designation	Manufacturer *	Stress Range (MPa)	Mean Stress (MPa)	No. of Cycles to Failure	Remarks
RB19-B (114 mm O.D.)	S	200	123	586 000	Specimen without tool joint. Taken from same pipe as RB19.
RB20-B (114 mm O.D.)	S	220	126	1 237 500	Specimen without tool joint. Taken from same pipe as RB20.
RB21-B (114 mm O.D.)	S	180	123	982 000	Specimen without tool joint. Taken from same pipe as RB21.
RB22-B (114 mm O.D.)	S	181	127	—	Specimen without tool joint. Taken from same pipe as RB22. No failure at 10 158 000 cycles.
RB22-BR (114 mm O.D.)	S	201	127	1 451 800	Specimen RB22-B retested at a stress range of 200 MPa.
RB23-B (114 mm O.D.)	S	177	124	—	Specimen without tool joint. Taken from same pipe as RB23. No failure at 10 000 000 cycles.
RB23-B1R (114 mm O.D.)	S	200	124	—	Specimen RB23-B retested. No failure at 10 000 000 cycles.
RB23-B2R (114 mm O.D.)	S	220	124	—	Specimen RB23-B1R retested. No failure at 10 000 000 cycles.

Table 4.2 (Cont'd)

Specimen Designation	Manufacturer *	Stress Range (MPa)	Mean Stress (MPa)	No. of Cycles to Failure	Remarks
RB23-B3R (114 mm O.D.)	S	250	124	1 289 500	Specimen RB23-B2R retested.

* M : Mannesmannrohren-Werke
O : Ohio Drill Pipe
S : Sumitomo Metal Industries

**

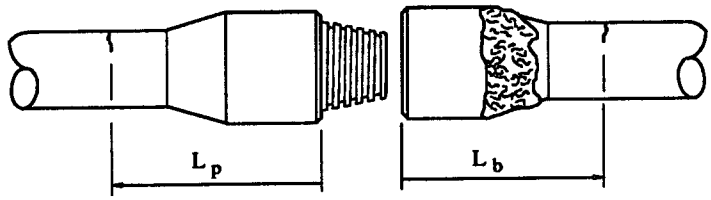

Table 4.3

Fatigue Test Results From Rotating Bending Test Program in Corrosive Environment (3.5 percent NaCl Solution)

Specimen Designation	Manufacturer *	Stress Range (MPa)	Mean Stress (MPa)	No. of Cycles to Failure	Remarks
RBT3C-B (114 mm O.D.)	O	132	123	2 345 200	Specimen without tool joint. Taken from same pipe as BT3.
RB4C (114 mm O.D.)	M	296	250	196 400	Failure in pipe body. (L_b** = 440 mm)
RB4C-B (114 mm O.D.)	M	130	250	1 455 600	Specimen without tool joint. Taken from same pipe as RB4-C.
RB5C (114 mm O.D.)	M	288	122	565 300	Failure in pipe body. (L_b = 600 mm)
RB5C-B (114 mm O.D.)	M	129	0	3 383 200	Specimen without tool joint. Taken from same pipe as RB5.
RB6C-B (114 mm O.D.)	M	132	252	1 783 200	Specimen without tool joint. Taken from same pipe as RB6.
RB8C-B (114 mm O.D.)	M	130	0	5 395 700	Specimen without tool joint. Taken from same pipe as RB8.
RB9C (114 mm O.D.)	M	290	253	448 400	Test conducted at 1.5 Hz. Failure in pipe body. (L_b = 580 mm)
RB10C (114 mm O.D.)	M	290	255	234 600	Failure in pipe body. (L_b = 605 mm)
RB11C (114 mm O.D.)	M	291	125	486 600	Failure in pipe body. (L_b = 625 mm)
RB12C (114 mm O.D.)	M	290	0	613 900	Failure in pipe body. (L_b = 495 mm)

Table 4.3 (Cont'd)

Specimen Designation	Manufacturer *	Stress Range (MPa)	Mean Stress (MPa)	No. of Cycles to Failure	Remarks
RB15C-B (114 mm O.D.)	M	126	127	2 240 800	Specimen without tool joint. Taken from same pipe as RB15.
RB17C (114 mm O.D.)	M	288	0	578 500	Failure in pipe body. (L_b = 585 mm)
RB19C	S	90	125	7 899 600	Failure in pipe body. (L_p = 445 mm)
RB21C (114 mm O.D.)	S	158	125	1 605 700	Failure in pipe body. (L_b = 575 mm)
RB23C (114 mm O.D.)	S	158	125	1 792 500	Failure in pipe body. (L_p = 495 mm)
RB24C-B (114 mm O.D.)	S	130	0	4 356 200	Specimen without tool joint. Taken from same pipe as RB24.
RB25C-B (114 mm O.D.)	S	210	123	564 200	Specimen without tool joint. Taken from same pipe as RB25.
RB26C-B (114 mm O.D.)	S	209	125	627 800	Specimen without tool joint. Taken from same pipe as RB26.
RB27C-B	S	90	125	7 899 000	Specimen without tool joint. Taken from pipe RB27.
RB28C-B (114 mm O.D.)	S	159	126	422 300	Specimen without tool joint. Taken from same pipe as RB28.

Table 4.3 (Cont'd)

* M : Mannesmannrohren-Werke ; O : Ohio Drill Pipe ; S : Sumitomo Metal Industries

**

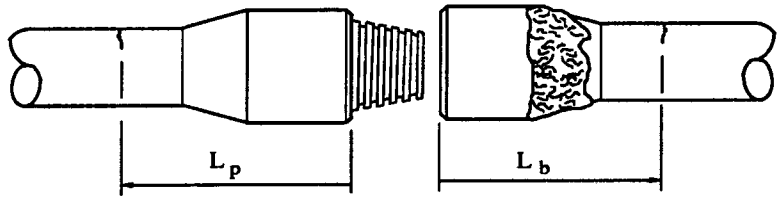

Table 4.4
Origin of Fracture

Specimen	Origin of Fracture
RBT3C-B	Fatigue crack originated at surface grinding marks.
RBT4-B	Fatigue crack originated at a surface pit.
RBT5-B	Fatigue crack originated at surface grinding marks.
RB1	No failure
RB1-B	No failure.
RB2	Fatigue crack originated at surface grinding marks.
RB2-B	Fatigue crack originated at surface grinding marks.
RB3	Fatigue crack originated at surface grinding marks.
RB3-B	Fatigue crack originated at surface grinding marks.
RB4C	Fatigue crack originated at surface grinding marks.
RB4C-B	Fatigue crack originated at surface grinding marks.
RB5C	Fatigue crack originated at surface grinding marks.
RB5C-B	Fatigue crack originated from surface pit.
RB6	Fatigue crack originated at surface grinding marks (see Figure 4.9 (a)).
RB6C-B	Fatigue crack originated at surface grinding marks.
RB7	No failure.
RB7-B	Fatigue crack originated at surface grinding marks.
RB8	Fatigue crack originated from surface pit (see Figure 4.12 (a)).
RB8C-B	Fatigue crack originated at surface grinding marks.
RB9C	Fatigue crack originated at surface grinding marks.
RB9-B	Fatigue crack originated at surface grinding marks (see Figure 4.9 (b)).
RB10C	Fatigue crack originated at surface grinding marks (see Figure 4.10).

Table 4.4 (Cont'd)

Specimen	Origin of Fracture
RB11C	Fatigue crack originated at surface grinding marks.
RB12C	Fatigue crack originated at surface grinding marks.
RB13-B	Fatigue crack originated at surface grinding marks.
RB14	Fatigue crack originated at surface grinding marks.
RB14-B	Fatigue crack originated from surface notch (see Figure 4.15 (a)).
RB15	Fatigue crack originated at the bottom of a pit on a ground surface.
RB15C-B	Fatigue crack originated from surface pit.
RB16	Fatigue crack originated from a surface inclusion (see Figure 4.17).
RB17C	Fatigue crack originated at surface grinding marks.
RB18	Fatigue crack originated at surface grinding marks.
RB18-B	Fatigue crack originated at surface grinding marks.
RB19-B	Crack originated from surface inclusion.
RB20-B	Fatigue crack originated from surface notch (see Figure 4.15 (b)).
RB21C	Fatigue crack originated at surface pit.
RB21-B	Fatigue crack originated at the bottom of a pit on a ground suraface.
RB22-BR	Fatigue crack originated at surface pit.
RB23C	Fatigue crack originated at surface pit.
RB23-B3R	Crack originated at surface silicate inclusion ($\approx$ 100 μm deep).
RB24C-B	Crack started from surface notch.
RB25C-B	Crack started from surface pit.
RB26C-B	Crack started from surface pit.
RB27C-B	Fatigue crack originated at surface pit.
RB28C-B	Fatigue crack originated at stenciled number on pipe surface (see Figure 4.16 (b)).

Table 4.5

Ancillary Test Results (Preliminary Test Series on 89 mm O.D. Drill Pipe)

Specimen Designation	E (MPa)	σ_Y (MPa)	σ_U (MPa)	ε_{rupt}
DST1	191 000	650	937	---
	195 000	650	901	---
BT1	192 000	740	1025	---
	191 000	735	966	---
Average	192 000	694	957	---

Table 4.6

Ancillary Test Results (Preliminary Test Series on 115 mm O.D. Drill Pipe)

Specimen Designation	E (MPa)	σ_Y (MPa)	σ_U (MPa)	ε_{rupt}
BT3	190 000	488	835	0.234
	201 000	421	762	0.279
	190 500	436	782	0.237
	198 700	426	771	0.226
BT4	202 600	639	926	0.189
	199 300	660	920	0.183
	194 900	641	919	0.170
	208 000	681	907	0.158
BT5	199 500	709	943	0.183
	206 400	702	947	0.173
	192 000	679	936	0.171
	199 000	724	909	0.177
BT6	210 000	591	878	0.200
	198 500	553	841	0.203
	197 700	608	882	0.190
	193 800	585	860	0.188

Table 4.6 (Cont'd)

Specimen Designation	E (MPa)	σ_Y (MPa)	σ_U (MPa)	ε_{rupt}
BT7	198 000	614	890	0.184
	208 300	545	845	0.197
	191 700	511	821	0.242
	238 600	731	1067	0.246
BT8	202 000	538	850	0.201
	204 000	448	750	0.219
	207 000	582	887	0.186
	197 000	636	930	0.182
Average	201200	590	877	0.201
Std. Deviation	9820	97	72	0.030

Table 4.7

Ancillary Test Results (Main Test Program on 115 mm O.D. Drill Pipe)

Specimen Designation	E (MPa)	σ_Y (MPa)	σ_U (MPa)	ε_{rupt}
RB1	201 500	540	764	0.226
	207 400	520	757	0.250
	195 000	505	774	0.221
RB2	193 000	450	730	0.248
	199 400	495	730	0.233
	193 700	460	718	0.238
RB3	209 100	490	744	0.236
	199 500	490	735	0.231
	196 900	495	737	0.239
RB4	196 100	535	795	0.233
	195 300	525	789	0.208
	196 800	530	806	0.226

Table 4.7 (Cont'd)

Specimen Designation	E (MPa)	σ_Y (MPa)	σ_U (MPa)	ε_{rupt}
RB5	210 600	475	758	0.235
	195 200	545	764	0.228
	199 700	520	739	0.230
RB6	199 180	552	754	0.223
	202 100	545	794	0.221
	191 200	570	782	0.218
RB7	202 800	500	762	0.185
	210 200	510	760	0.225
	200 000	500	767	0.221
RB8	205 500	550	805	0.197
	198 600	540	805	0.208
	200 960	605	809	0.221
RB9	201 000	580	854	0.191
	195 200	550	825	0.210
	196 800	550	815	0.215
RB10	210 000	487	752	0.228
	194 000	522	754	0.209
RB11	202 300	495	813	0.195
	202 200	534	800	0.216
RB12	210 300	533	755	0.223
	211 500	532	753	0.226
RB14	197 000	498	780	0.208
	204 900	493	775	0.226
RB15	198 000	492	743	0.207
	199 000	513	752	0.234
RB16	210 000	526	740	0.248
	189 000	520	737	0.228
RB17	204 300	522	743	0.238
	212 300	500	751	0.222

Table 4.7 (Cont'd)

Specimen Designation	E (MPa)	σ_Y (MPa)	σ_U (MPa)	ε_{rupt}
RB18	204 300	515	727	0.245
	194 200	513	726	0.228
RB19	203 000	600	792	0.205
	203 000	580	790	0.217
RB20	209 000	600	759	0.307
	200 800	580	756	0.233
RB21	199 000	560	747	0.230
	201 400	545	750	0.219
RB22	207 900	590	773	0.211
	201 300	585	767	0.204
RB23	211 940	570	749	0.242
	200 810	545	755	0.240
RB24	197 600	570	755	0.223
	200 500	569	766	0.219
RB25	203 400	572	782	0.212
	204 500	592	779	0.209
RB26	199 710	540	727	0.246
	203 800	545	733	0.242
RB27	204 400	600	803	0.188
	202 310	610	815	0.194
RB28	200 400	591	788	0.207
	213 000	590	792	0.184
Average	201 500	537	767	0.223
Std. Deviation	5470	38	29	0.019

Table 4.8

Chemical Analysis of Drill Pipe Steel

Drill Pipe Manufacturer	%C	%Mn	%Cr	%Ni	%S
O*	0.36	0.89	0.92	0.14	0.04
M*	0.38	0.79	0.81	0.10	0.03
S*	0.36	0.90	0.82	0.12	0.04

* O: Ohio Drill Pipe

M: Mannesmannrohren-Werke

S : Sumitomo Metal Industries

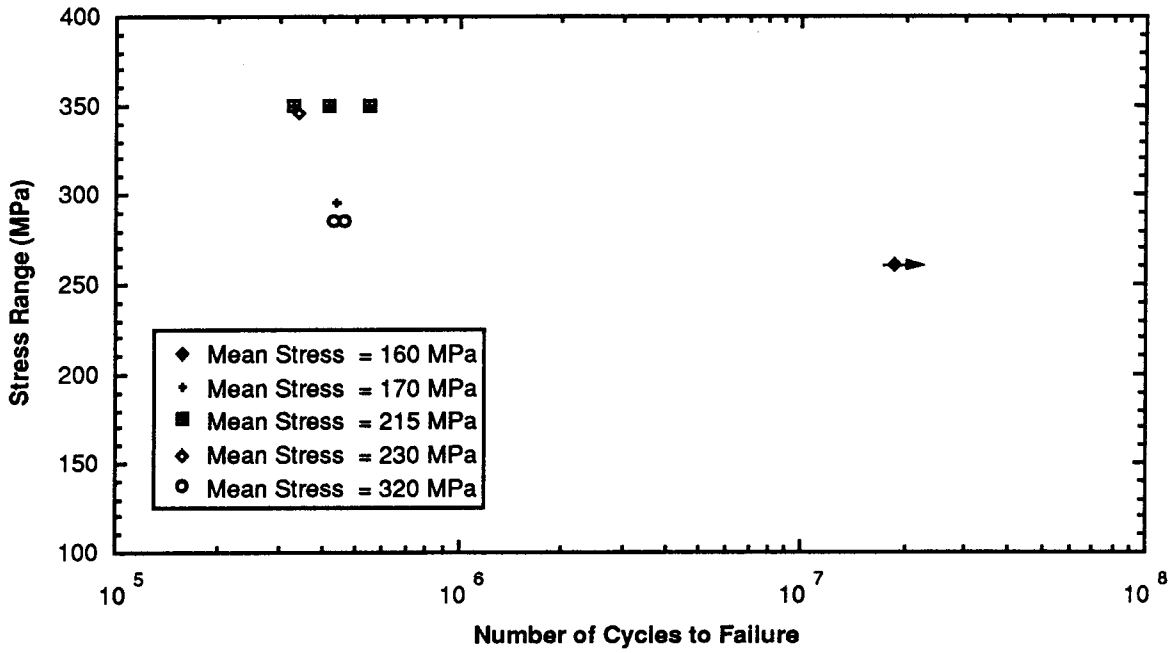

Figure 4.1 Results of Cyclic Bending Test Program

(a) Fatigue Failure in Drill Pipe Body

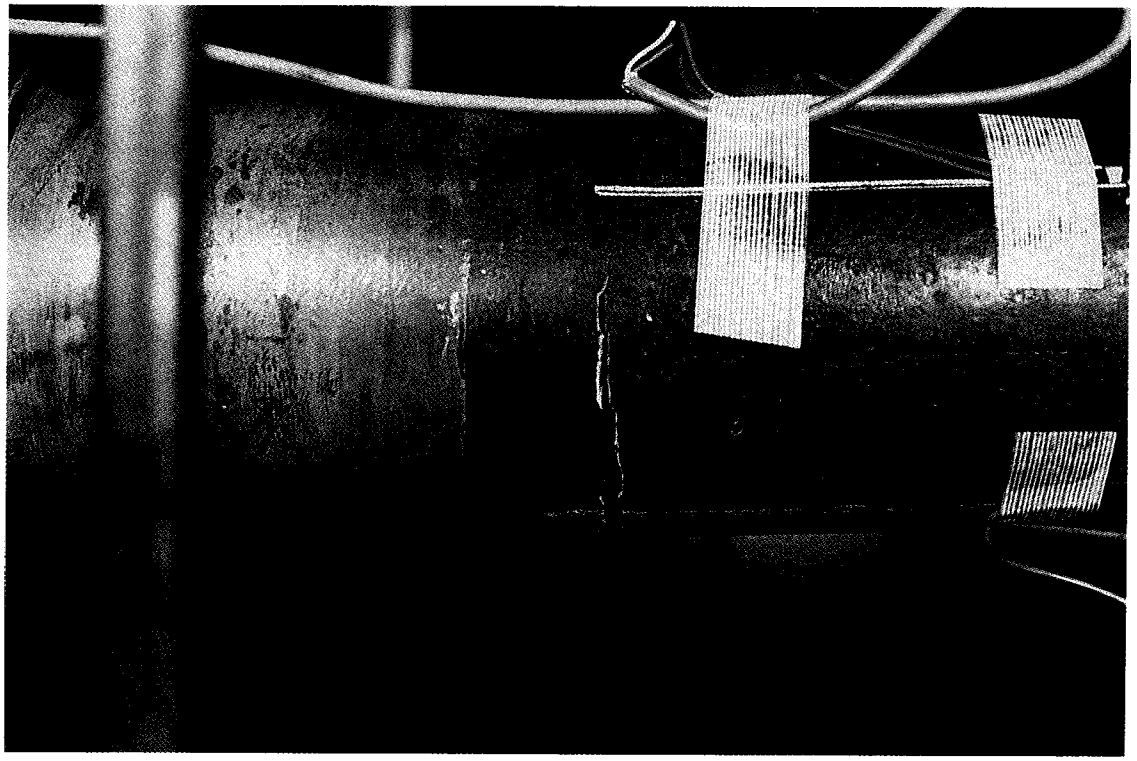

(b) Failure at Internal Upset Runout (Drill Pipe RB16)

Figure 4.2 Typical Failure of Drill Pipe in Test Setup

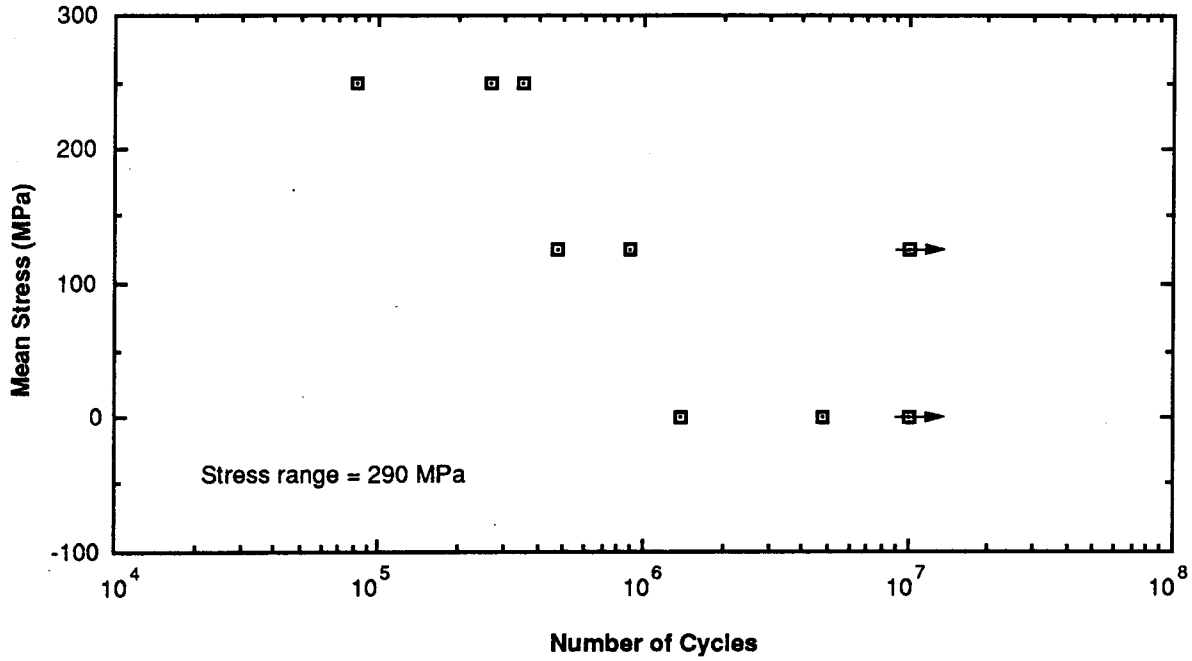

Figure 4.3 Effect of Mean Stress on Fatigue Life in Air

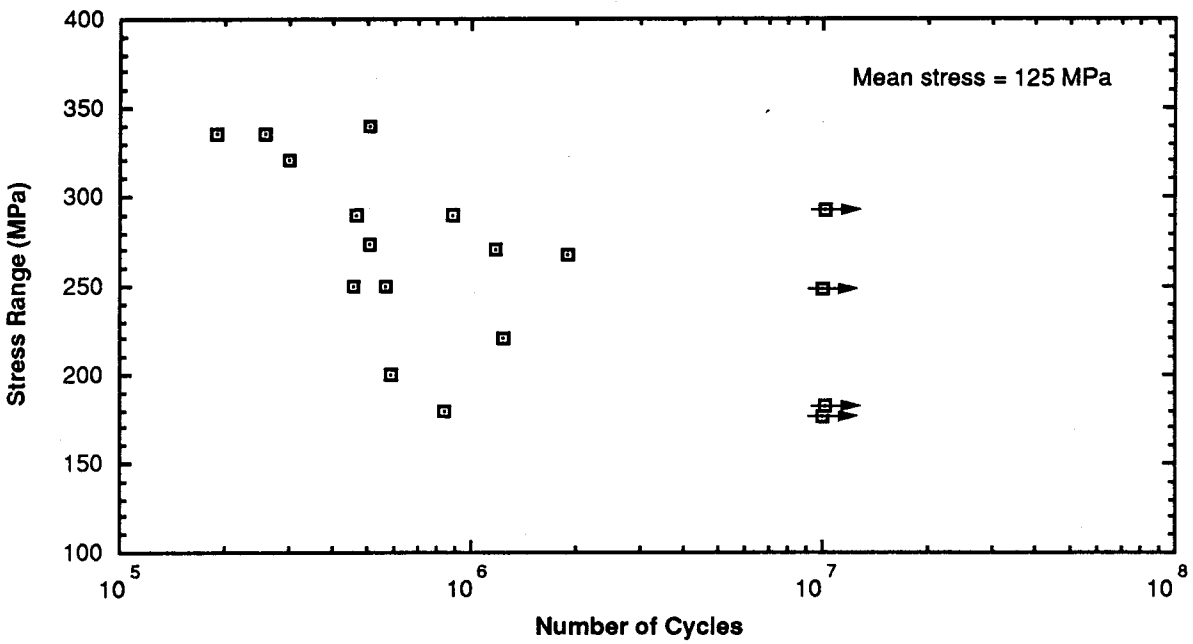

Figure 4.4 Effect of Stress Range on Fatigue Life in Air

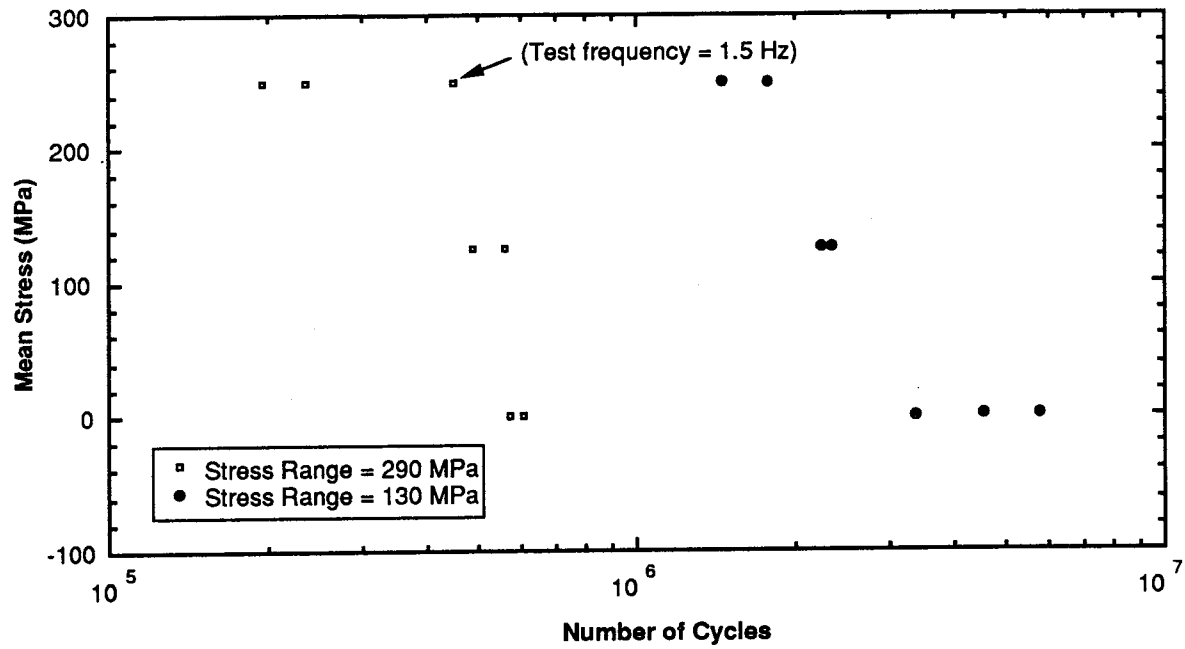

Figure 4.5 Effect of Mean Stress on Fatigue Life in a Corrosive Environment

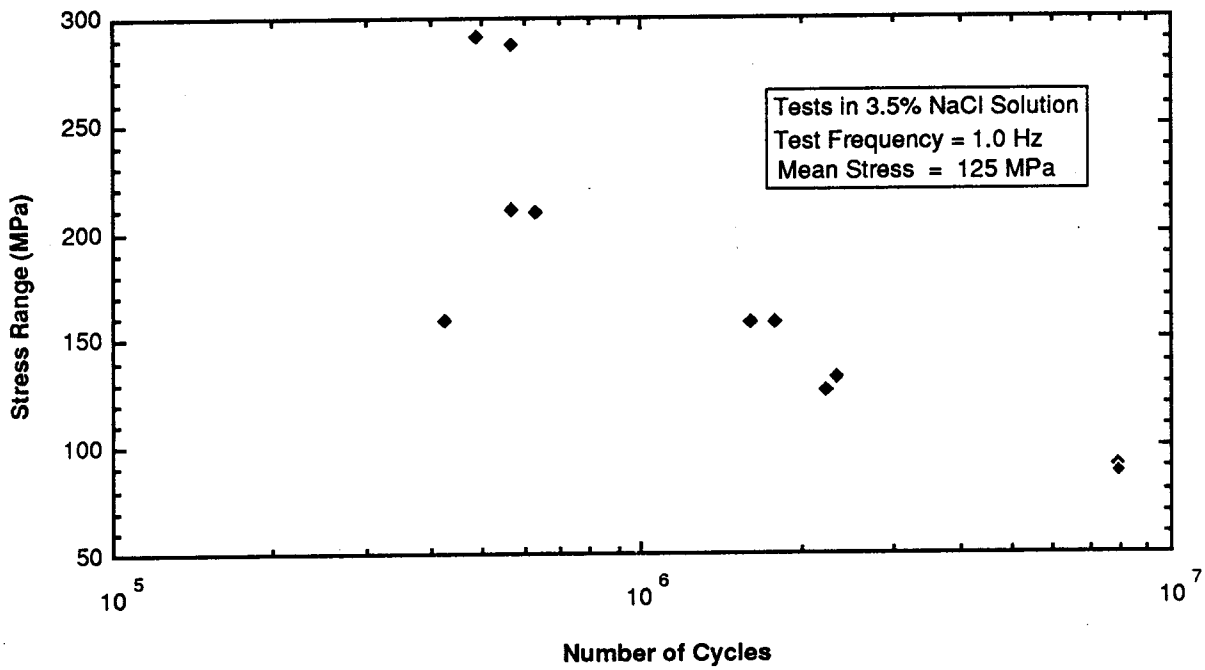

Figure 4.6 Effect of Stress Range on Fatigue Life in a Corrosive Environment (Mean Stress = 125 MPa)

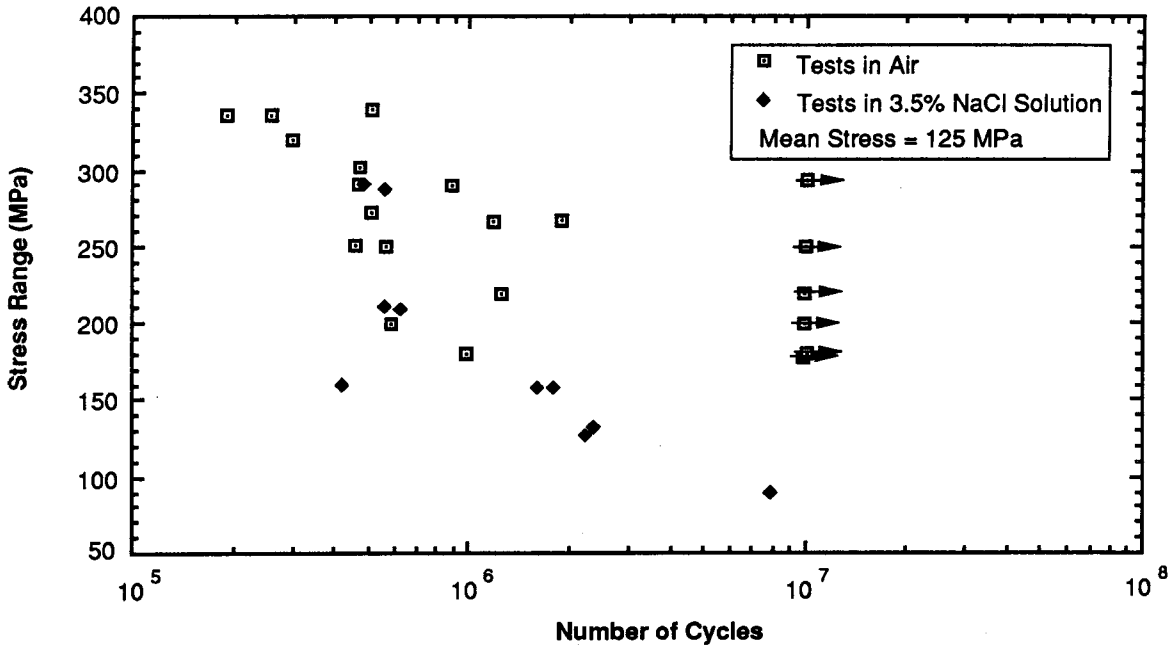

Figure 4.7 Effect of Corrosive Environment on Fatigue Life

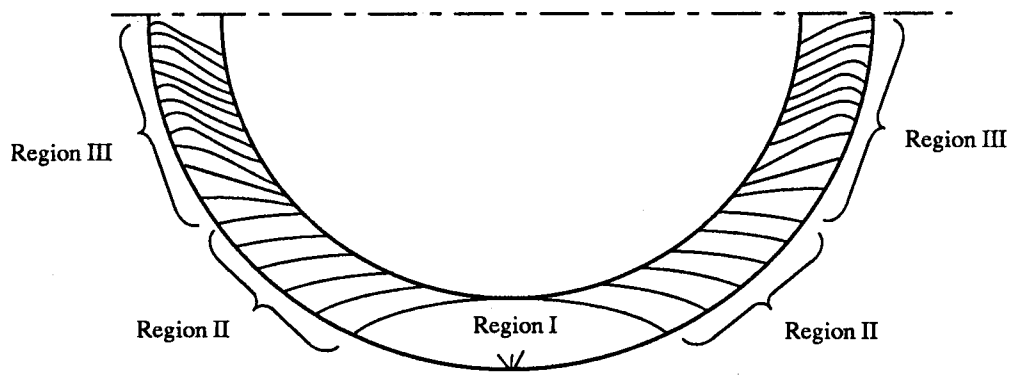

Figure 4.8 Macroscopic Appearance of Fracture Surface

(a) Test Specimen RB6

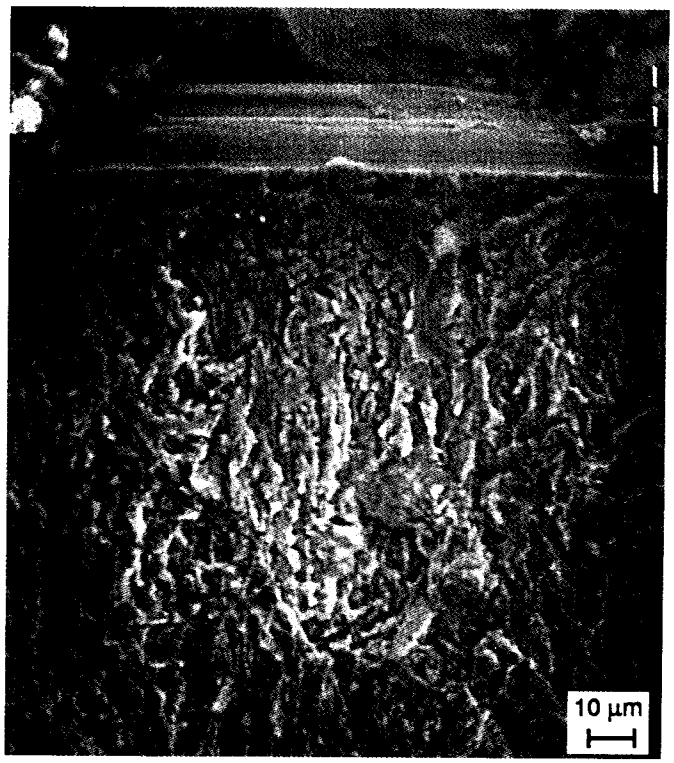

(b) Test Specimen RB3

Figure 4.9 Fatigue Crack Initiation From a Surface Groove Introduced by Grinding

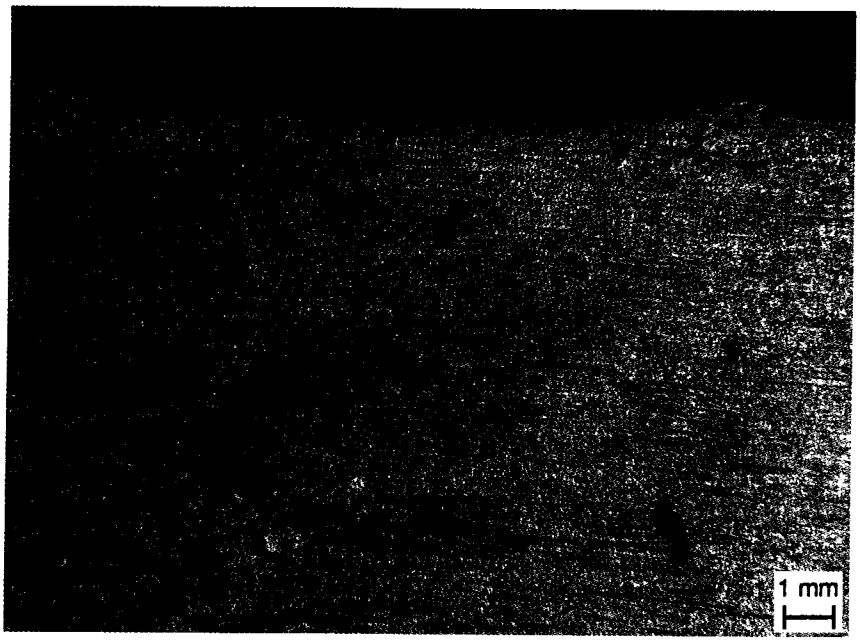

(a) Test Specimen RB10C

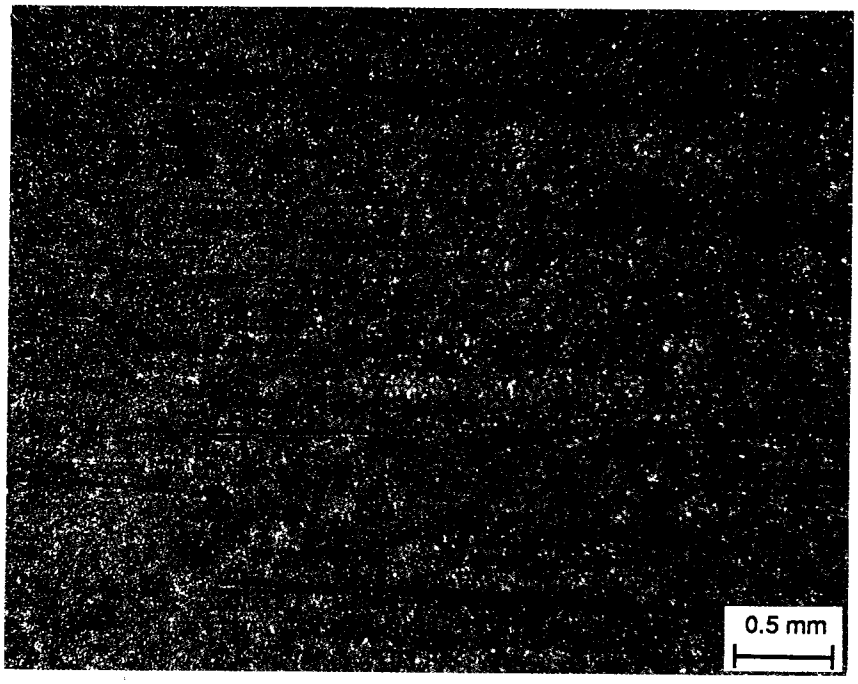

(b) Multiple Cracks on Test Specimen RB10C

Figure 4.10 Corrosion Fatigue Cracks From Surface Grooves Introduced by Grinding

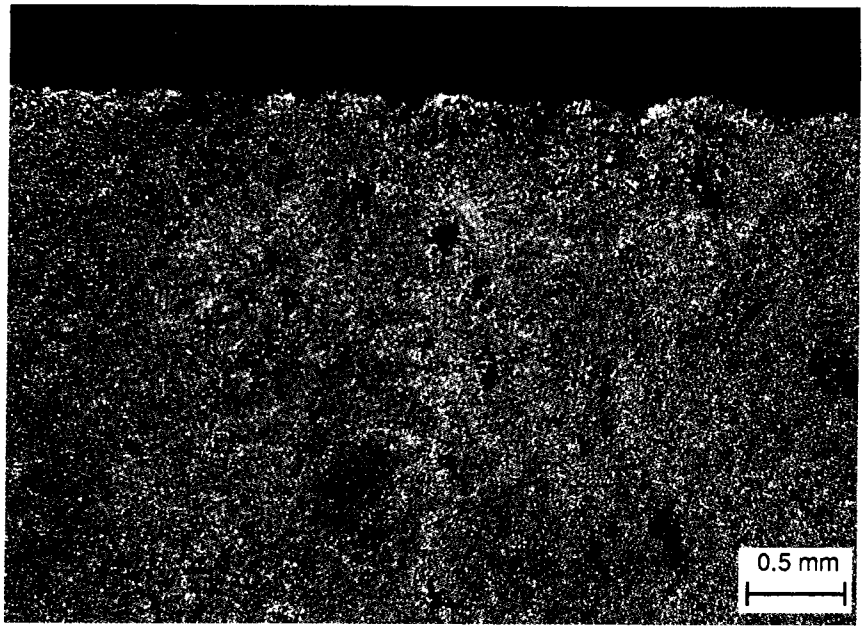

(a) Photomicrograph of Corrosion Fatigue Crack Surface

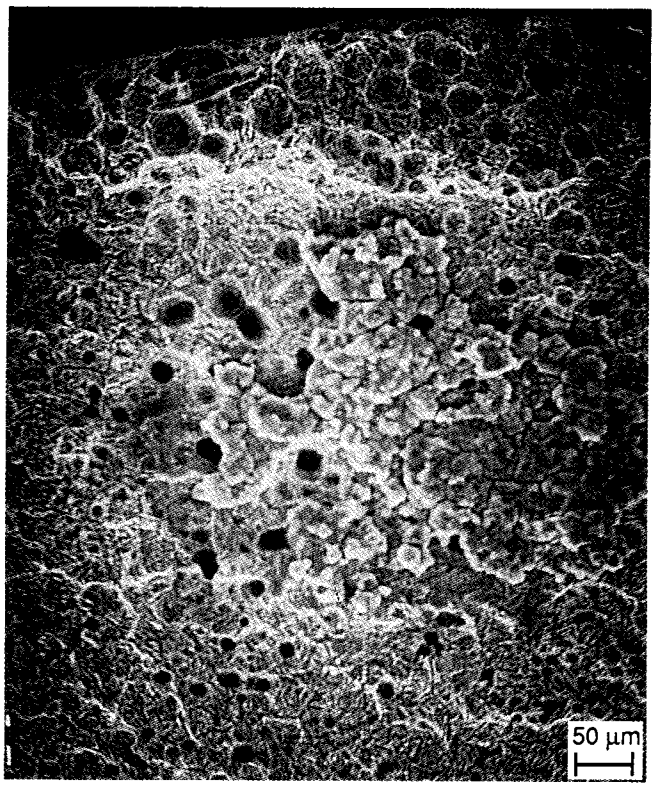

(b) Electron Photomicrograph of Corrosion Fatigue Crack Surface

Figure 4.11 Typical Corrosion Fatigue Crack Surface

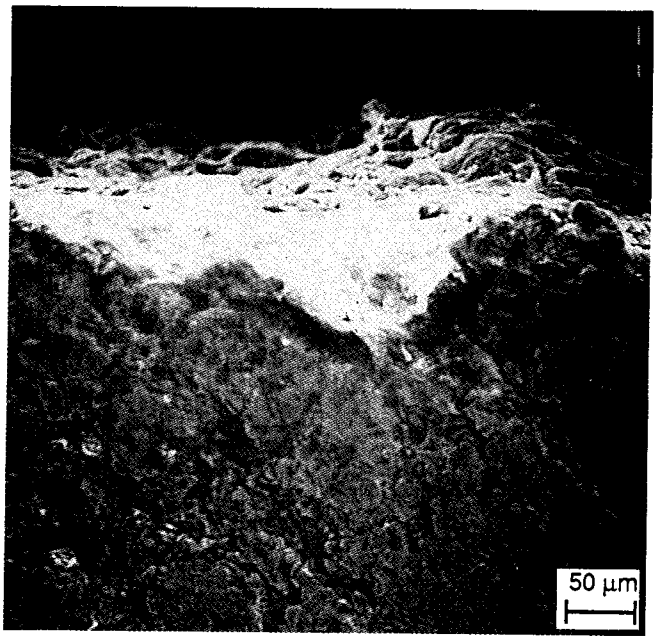

(a) Test Specimen RB8

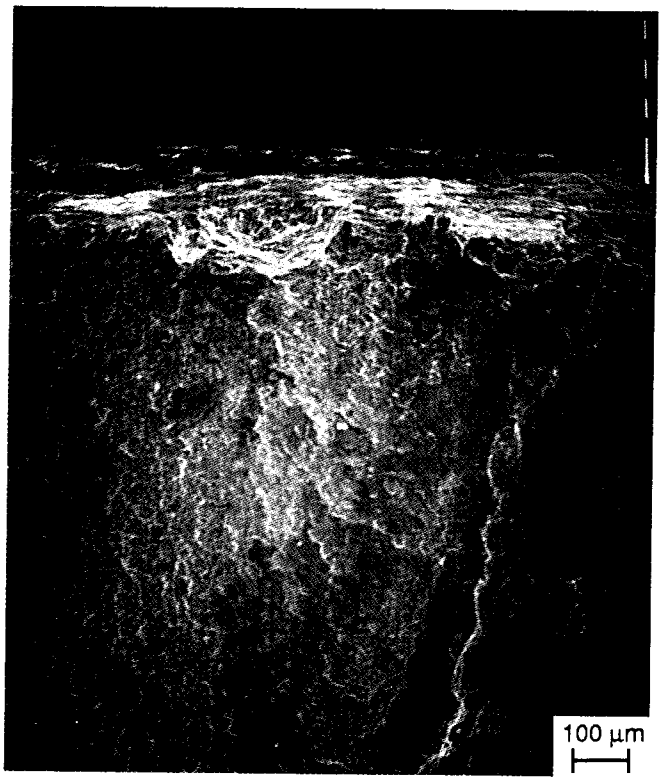

(b) Test Specimen BT7

Figure 4.12 Fatigue Crack Initiation From Surface Pits

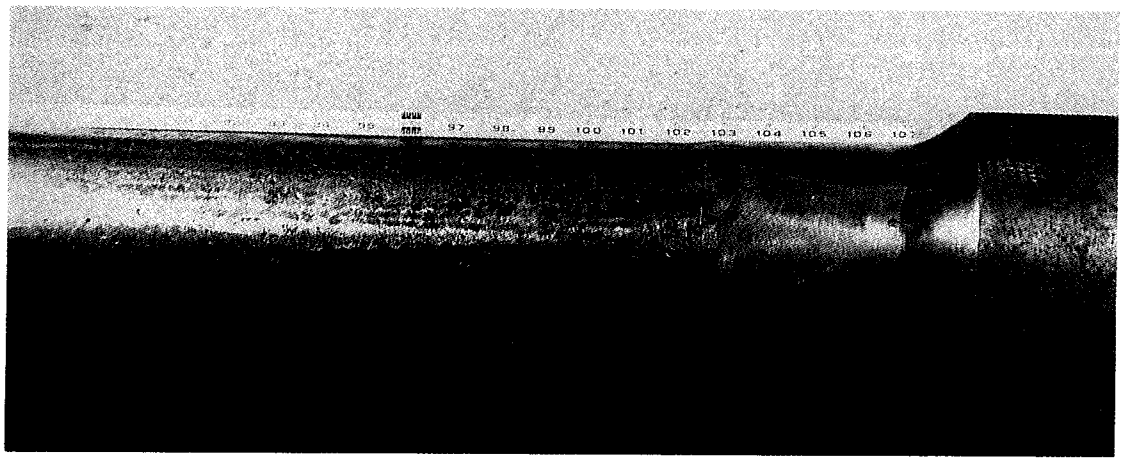

(a) Surface of Test Specimen RB2

(b) Body Section of Test Specimen RB2

Figure 4.13 Rough Surface Condition With Multiple Pits and Grinding Marks

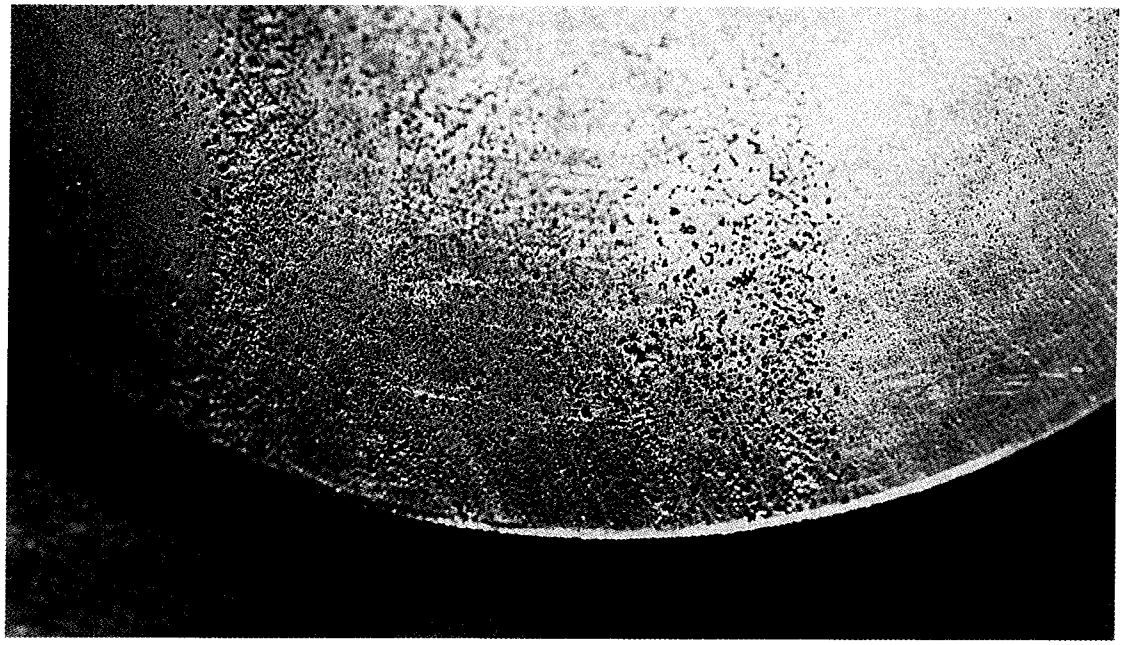

(a) Corrosion Pits on Inner Surface of RB6

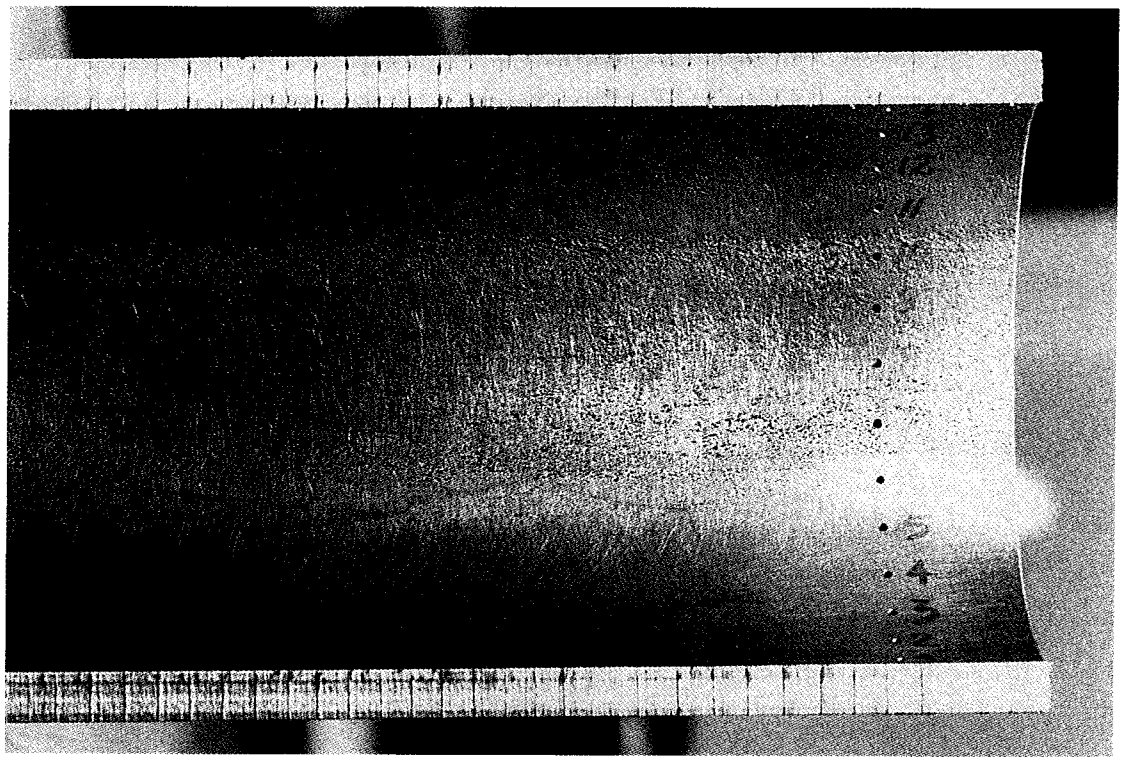

(b) Inner Corrosion Pits from Water Accumulation Inside Drill Pipe

Figure 4.14 Corrosion Pits on Inner Surface of Drill Pipe

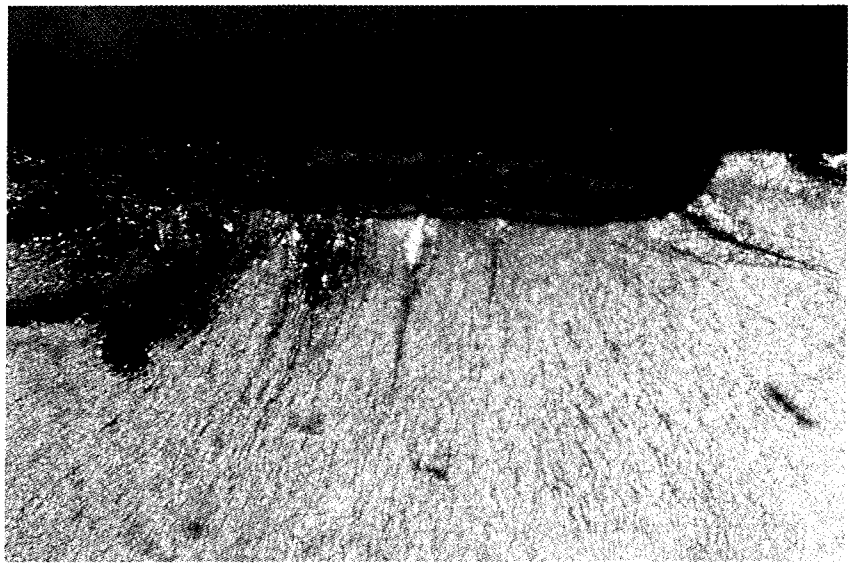

(a) Test Specimen RB14-B

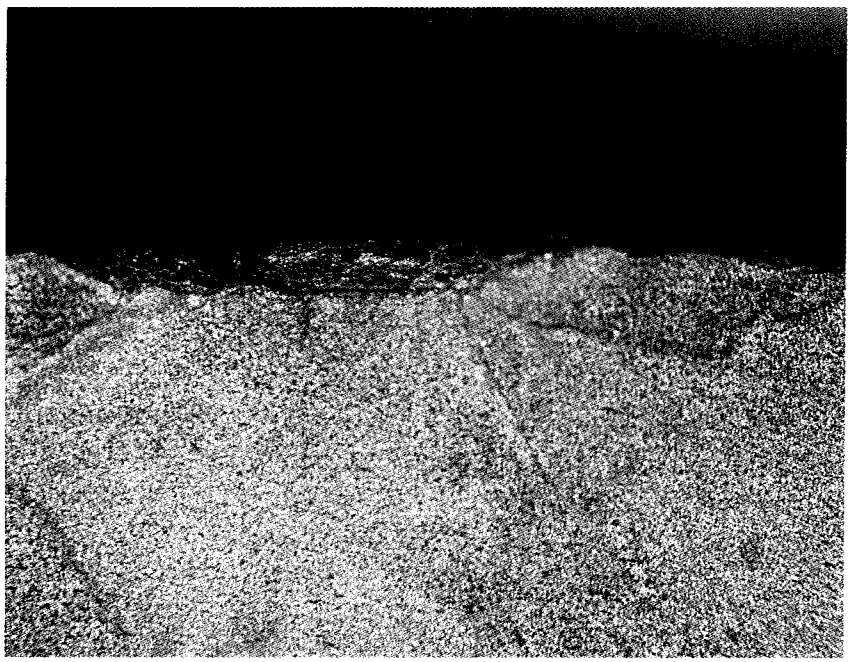

(b) Test Specimen RB20-B

Figure 4.15 Crack Initiation From Surface Notch

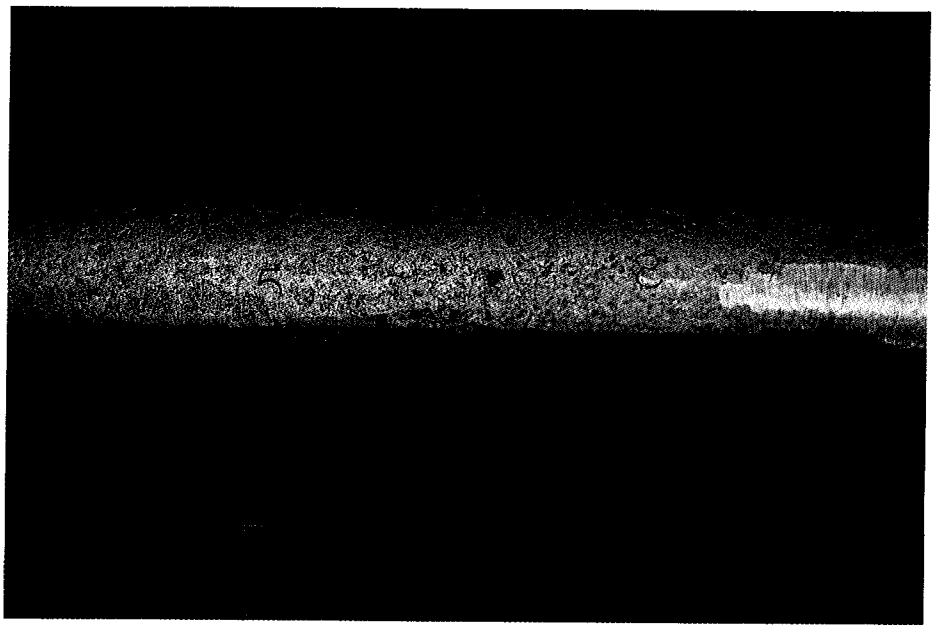

(a) Steel Stencil Marks on Drill Pipe Body

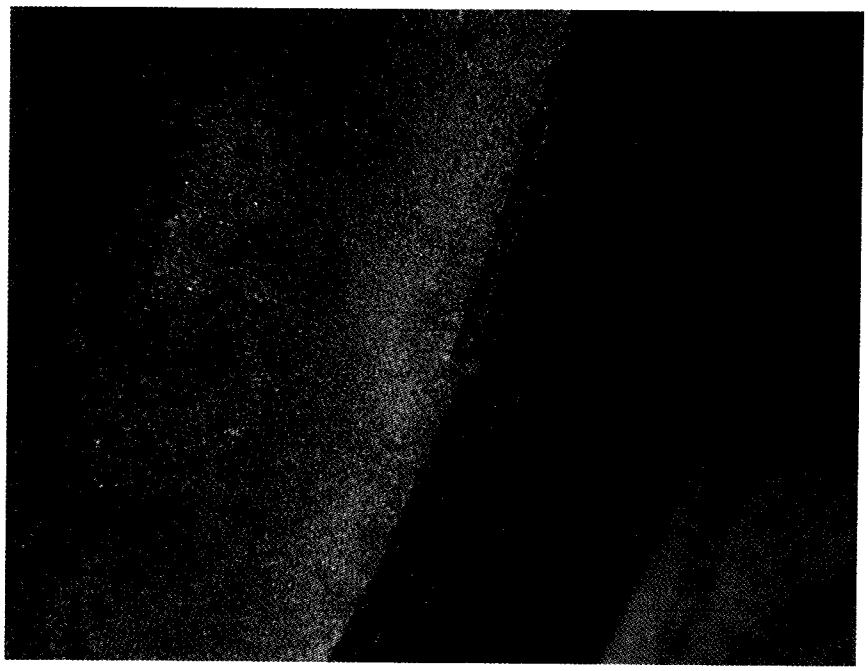

(b) Fatigue Failure From Numeral 1 Stamped on Pipe Surface

Figure 4.16 Steel Stencil Marks on Drill Pipe Body (Specimen RB28C-B)

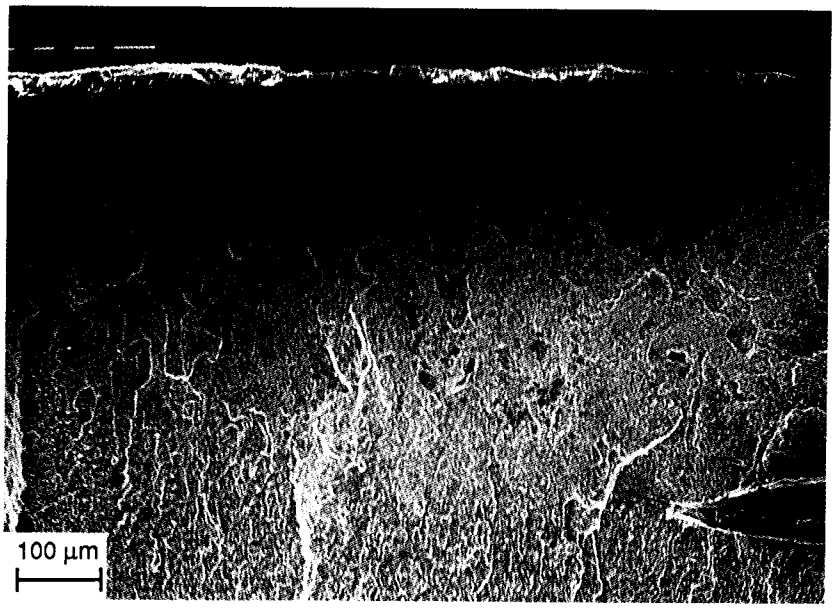

(a) Boundary Between Inclusion and Clean Regions

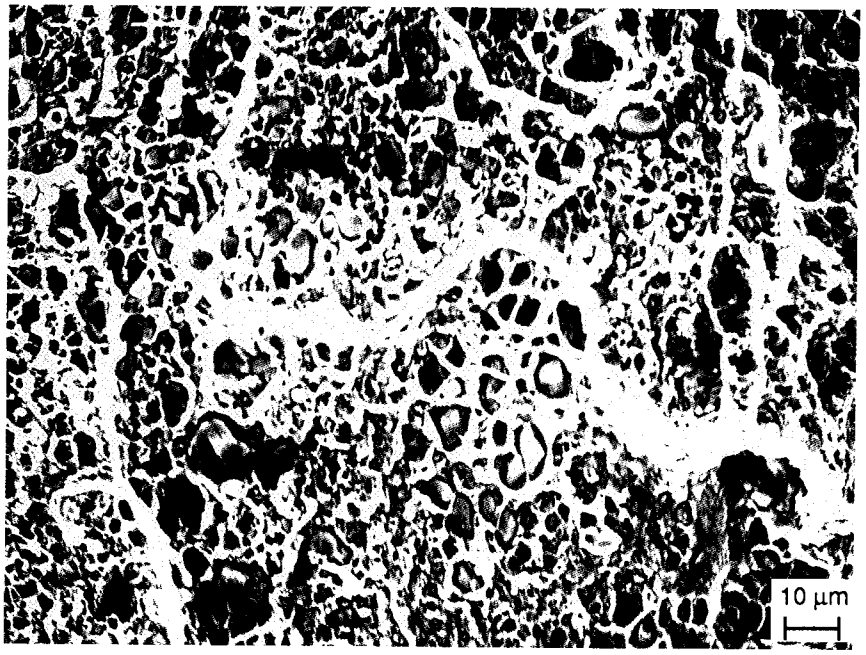

(b) Aluminum Silicate Inclusions

Figure 4.17 Crack Initiation From Surface Inclusion

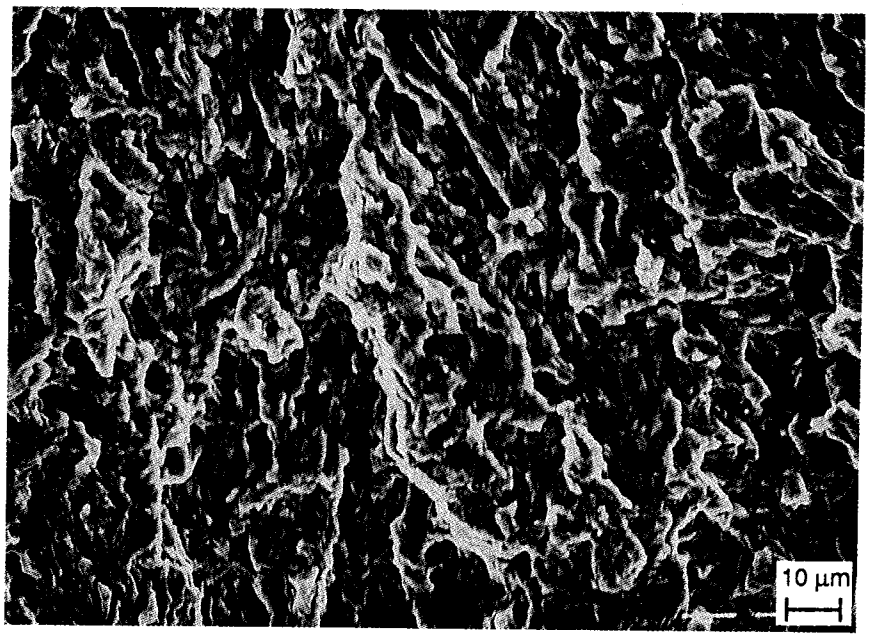

(c) Clean Fracture Surface

Figure 4.17 (Cont'd)

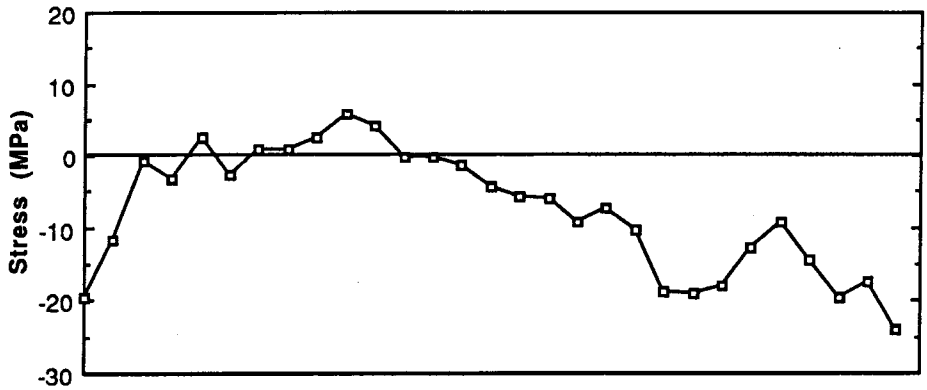

(a) Residual Stresses on Outer Surface

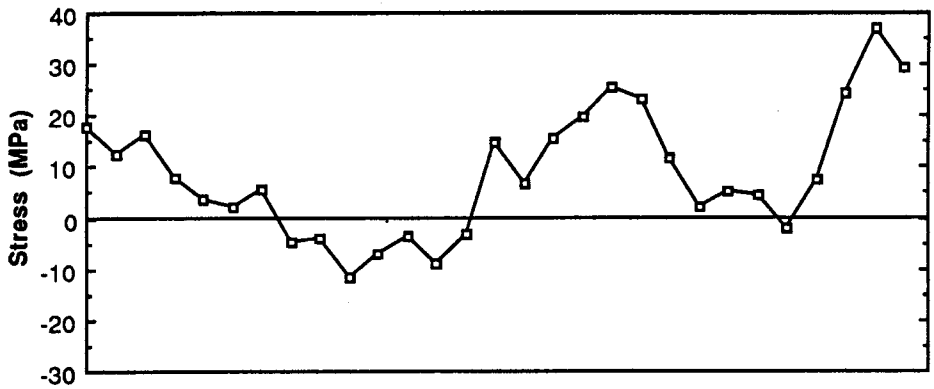

(b) Residual Stresses on Inner Surface

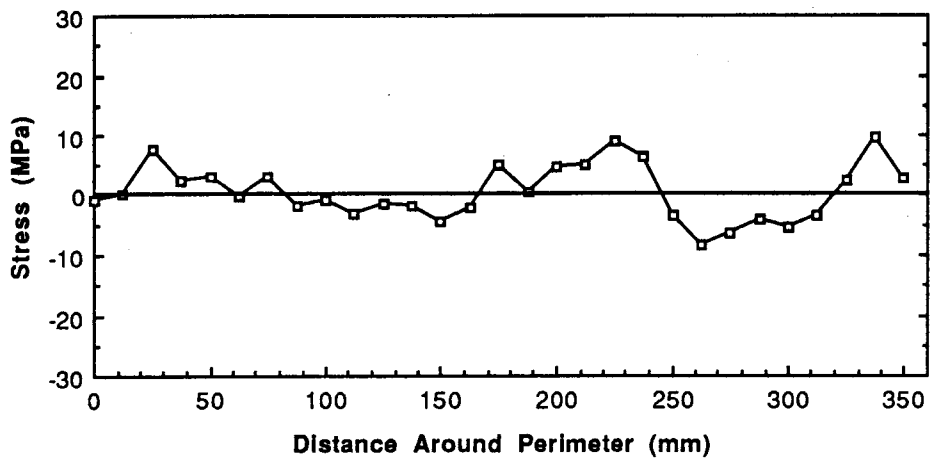

(c) Average of Outer Surface and Inner Surface Residual Stresses

Figure 4.18 Residual Stresses in Drill Pipe BT4-1

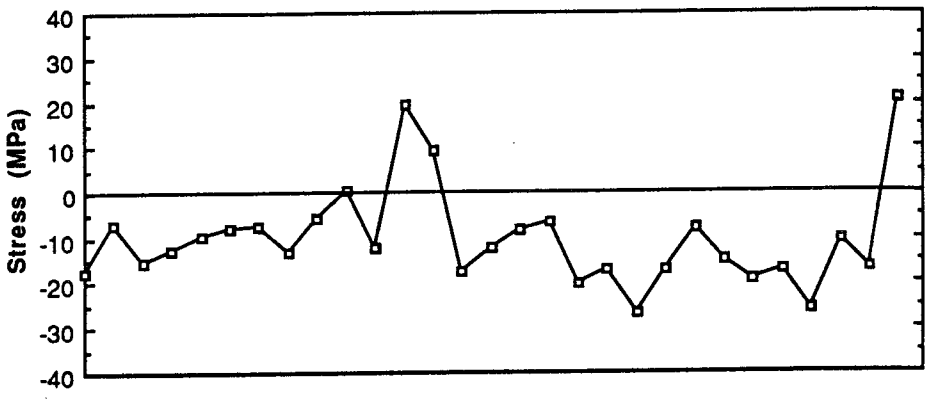

(a) Residual Stresses on Outer Surface

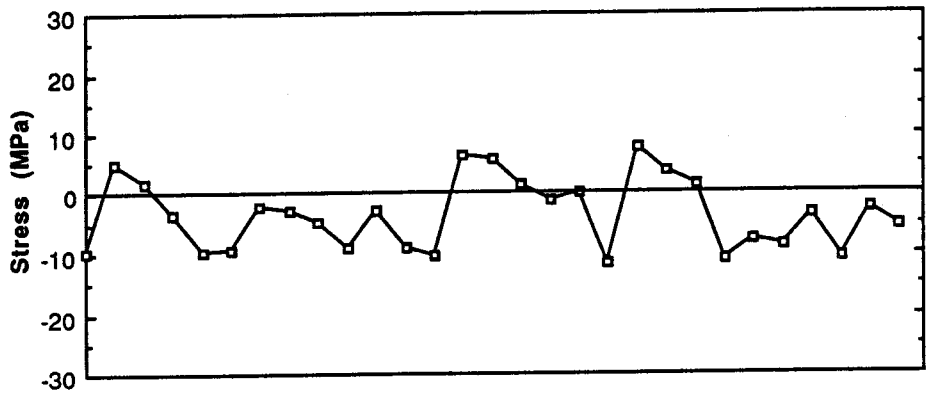

(b) Residual Stresses on Inner Surface

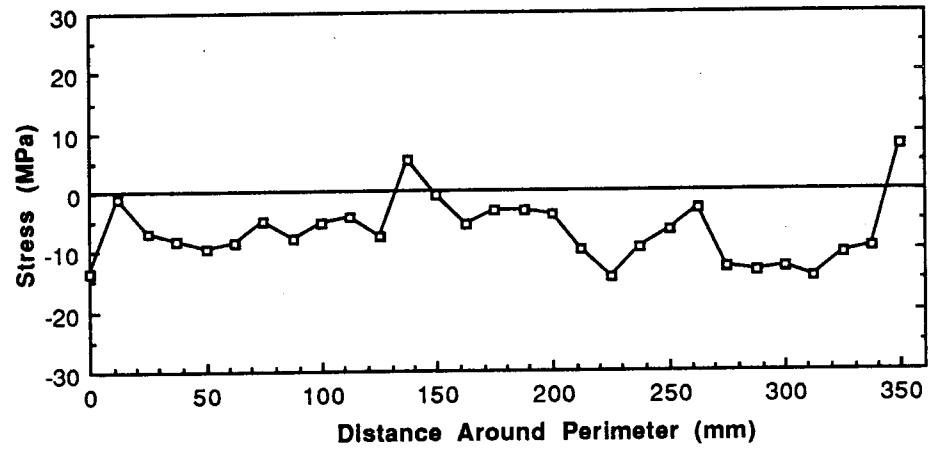

(c) Average of Outer Surface and Inner Surface Residual Stresses

Figure 4.19 Residual Stresses in Drill Pipe BT4-2

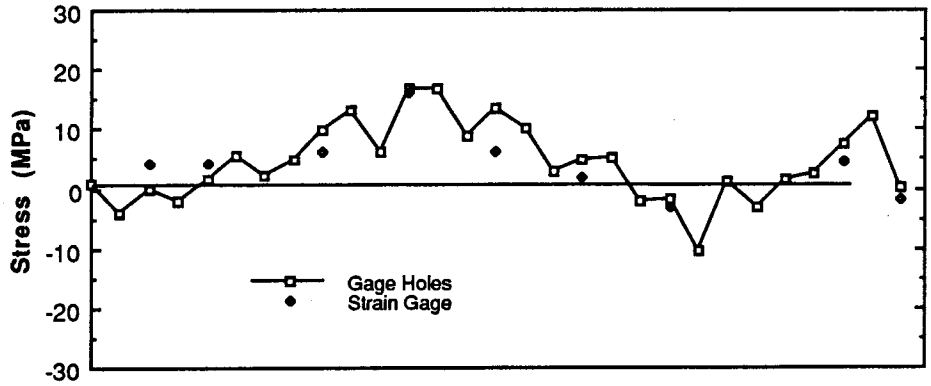

(a) Residual Stresses on Outer Surface

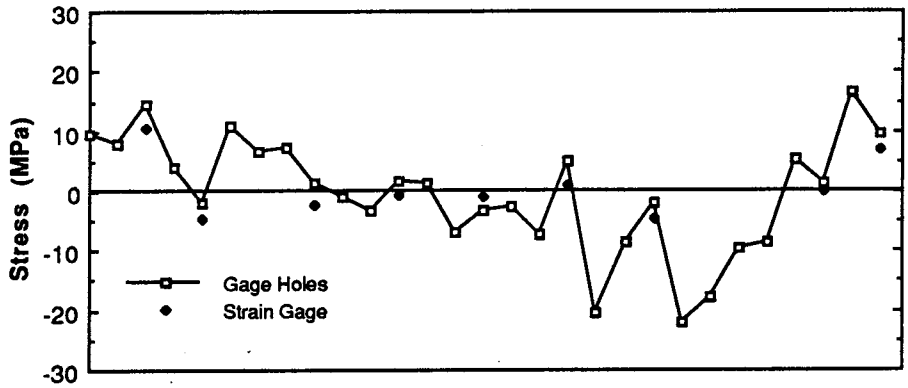

(b) Residual Stresses on Inner Surface

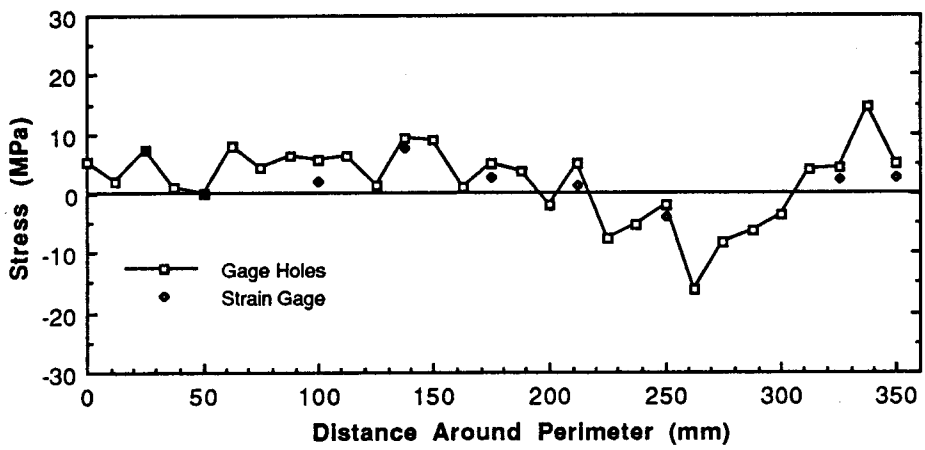

(c) Average of Outer Surface and Inner Surface Residual Stresses

Figure 4.20 Residual Stresses in Drill Pipe BT6-1

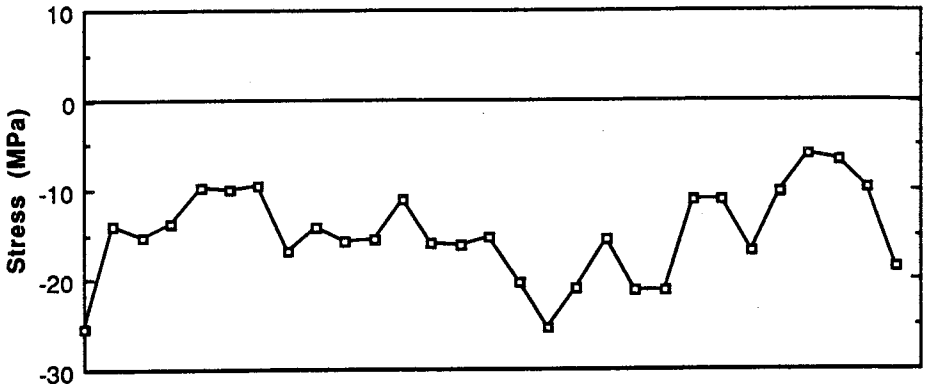

(a) Residual Stresses on Outer Surface

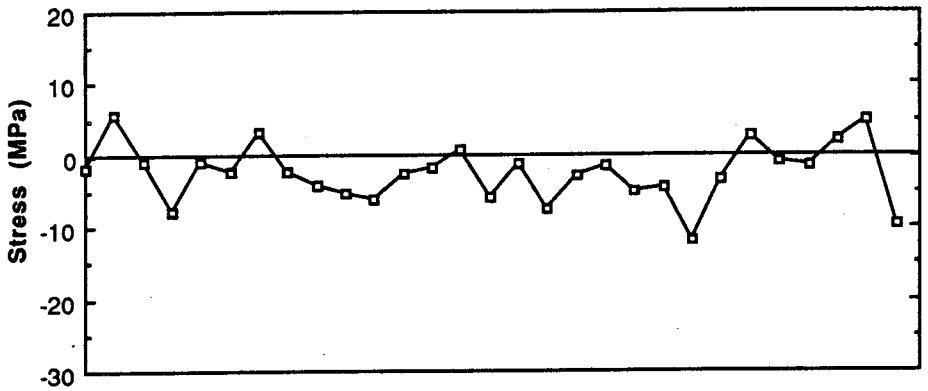

(b) Residual Stresses on Inner Surface

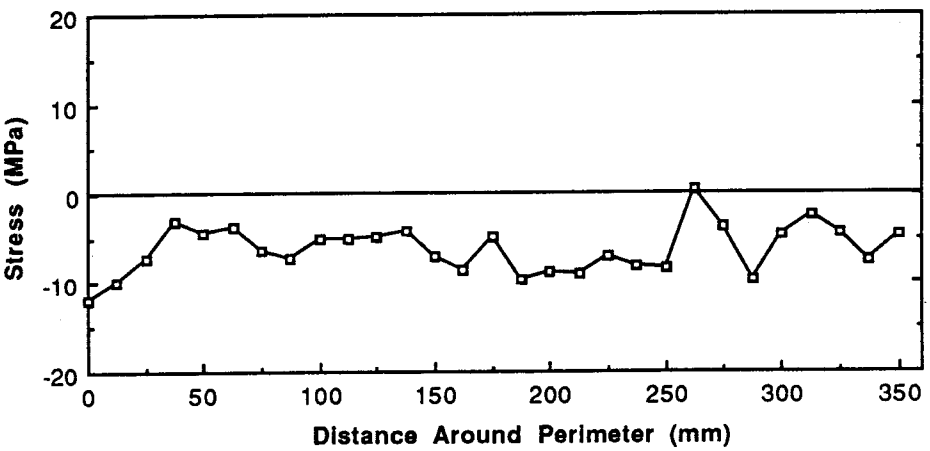

(c) Average of Outer Surface and Inner Surface Residual Stresses

Figure 4.21 Residual Stresses in Drill Pipe BT6-2

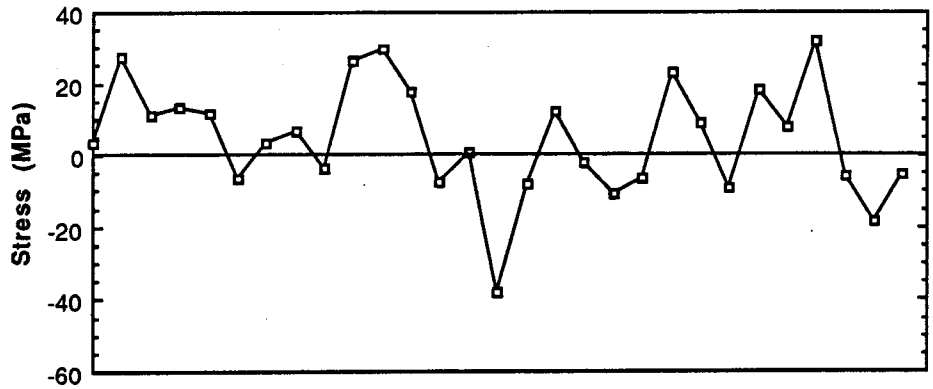

(a) Residual Stresses on Outer Surface

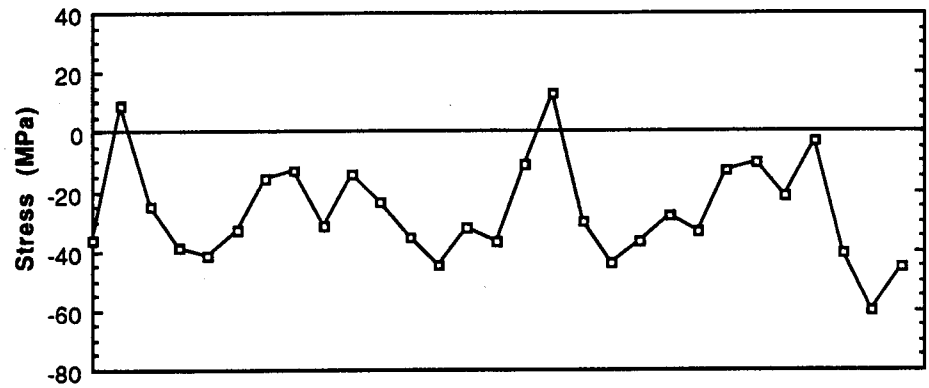

(b) Residual Stresses on Inner Surface

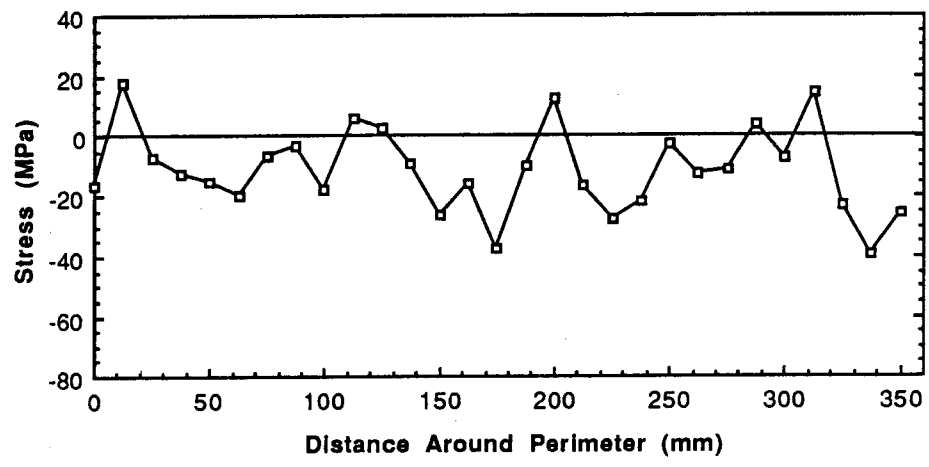

(c) Average of Outer Surface and Inner Surface Residual Stresses

Figure 4.22 Residual Stresses in Drill Pipe RB5

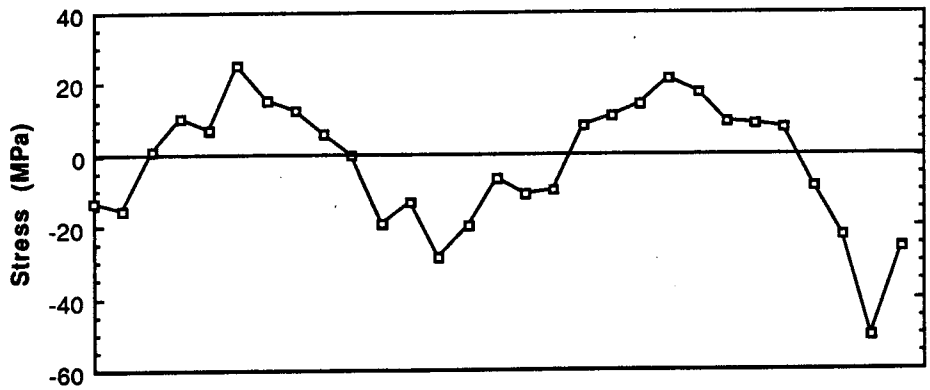

(d) Residual Stresses on Outer Surface Released by Shortening the Test Specimen

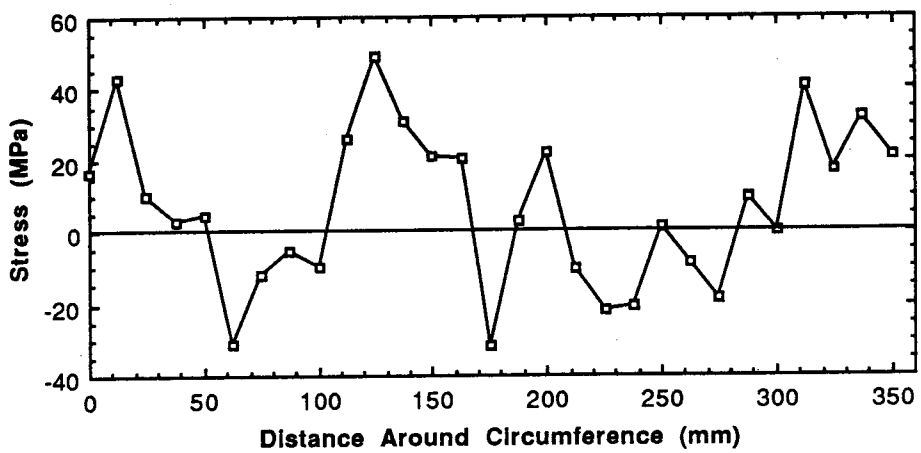

(e) Total Residual Stresses on Outer Surface

Figure 4.22 (Cont'd)

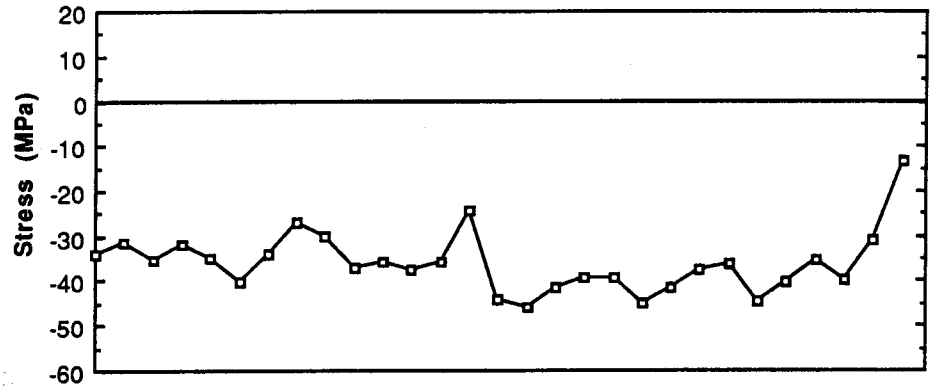

(a) Residual Stresses on Outer Surface

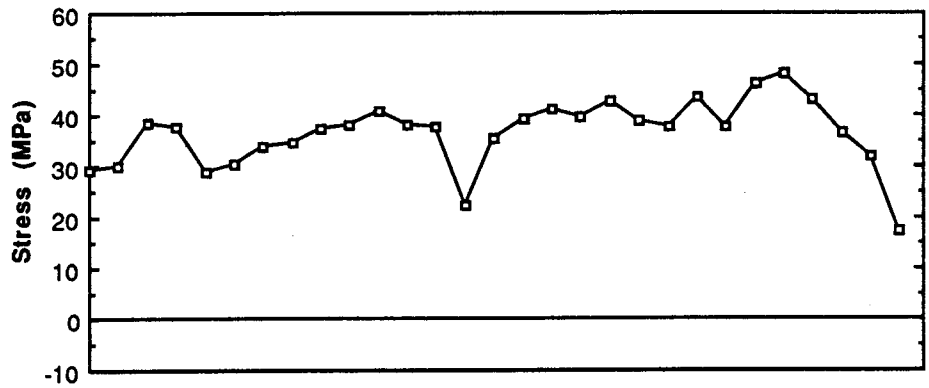

(b) Residual Stresses on Inner Surface

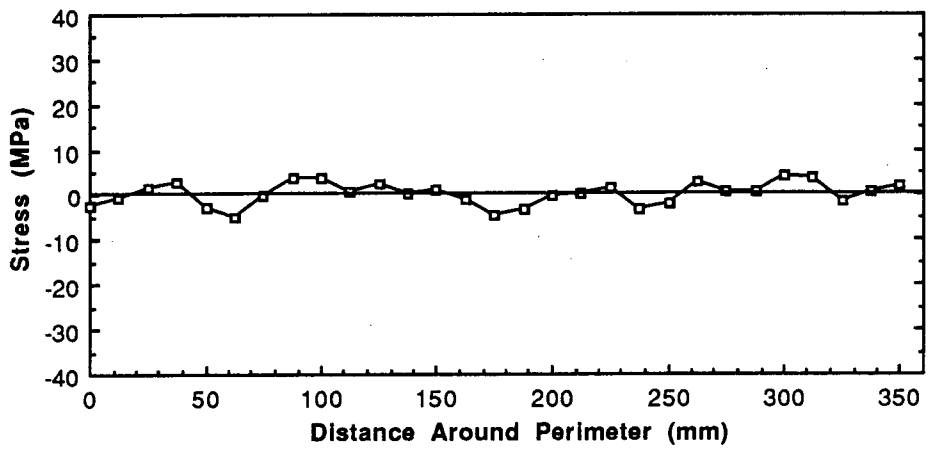

(c) Average of Outer Surface and Inner Surface Residual Stresses

Figure 4.23 Residual Stresses in Drill Pipe RB8

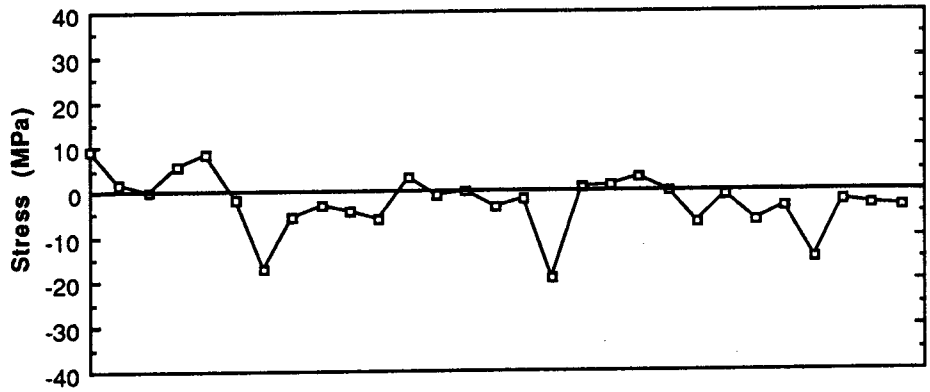

(d) Residual Stresses on Outer Surface Released by Shortening the Test Specimen

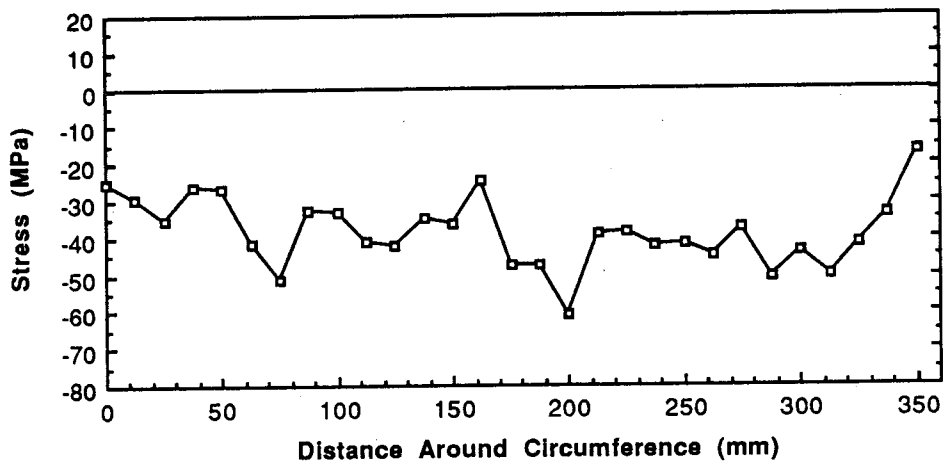

(e) Total Residual Stresses on Outer Surface

Figure 4.23 (Cont'd)

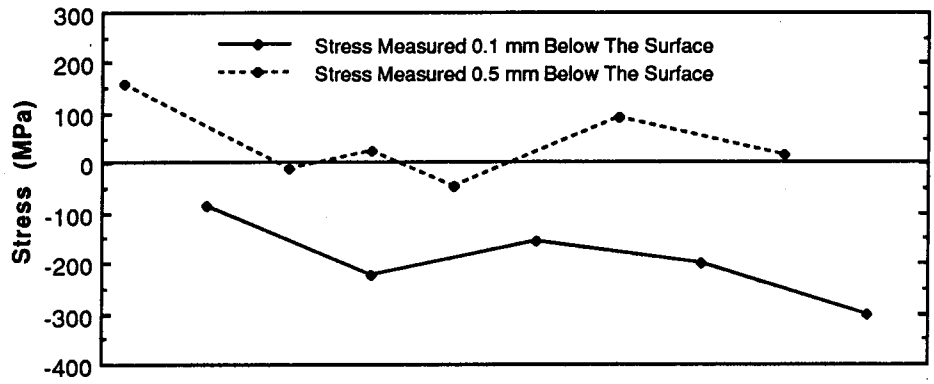

(a) Outer Surface Residual Stress Distribution in Body of Drill Pipe RB13 Measured by X-Ray Diffraction

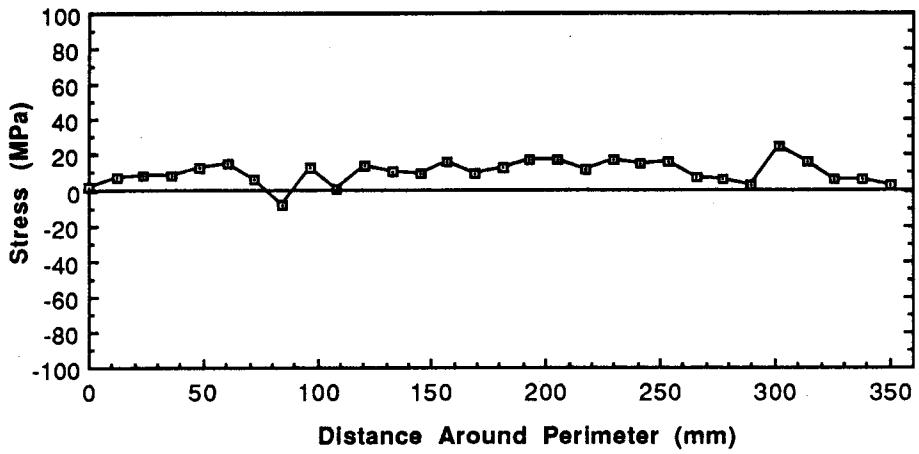

(b) Outer Surface Residual Stresses in Body of Drill Pipe RB13 Measured by Sectioning Technique

Figure 4.24 Residual Stresses in Body of Drill Pipe RB13

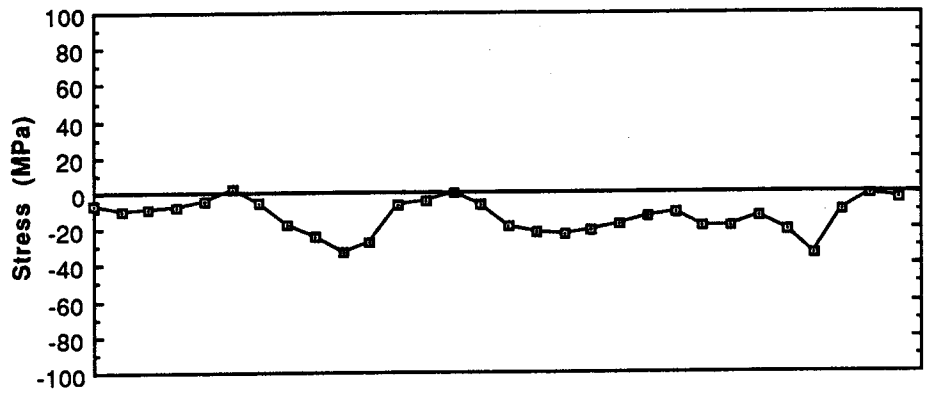

(c) Inner Surface Residual Stresses in Body of Drill Pipe RB13
Measured by Sectioning Technique

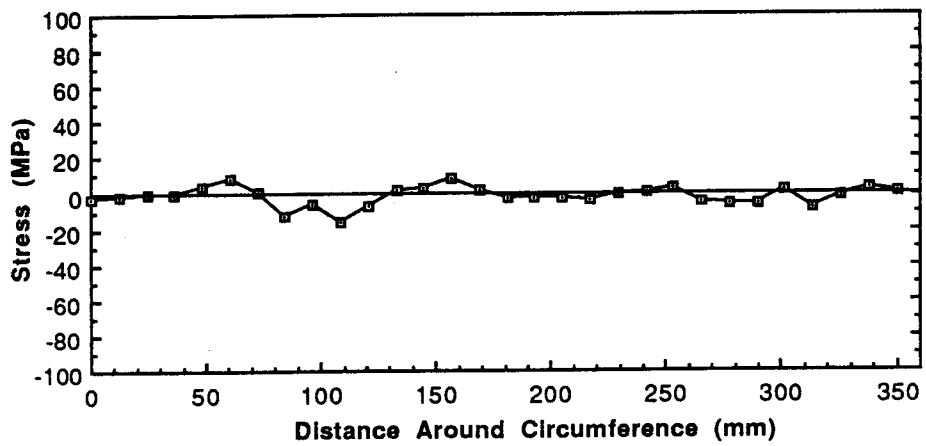

(d) Average Residual Stresses in Body of Drill Pipe RB13
Measured by Sectioning Technique

Figure 4.24 (Cont'd)

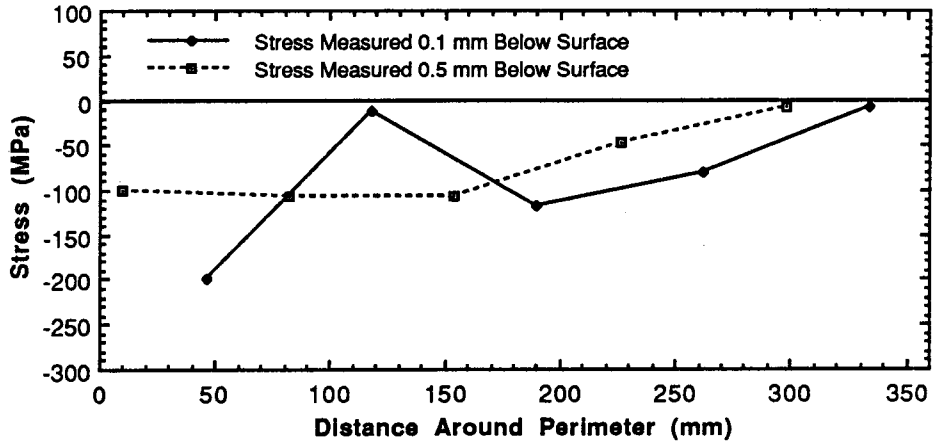

Figure 4.25 Residual Stress Distribution on Outer Surface of Upset Runout in Drill Pipe RB13

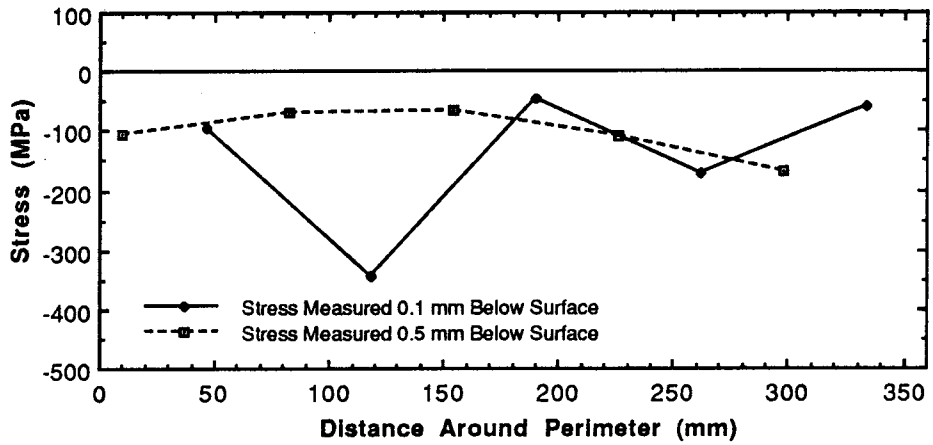

Figure 4.26 Residual Stress Distribution on Outer Surface of Upset in Drill Pipe RB13

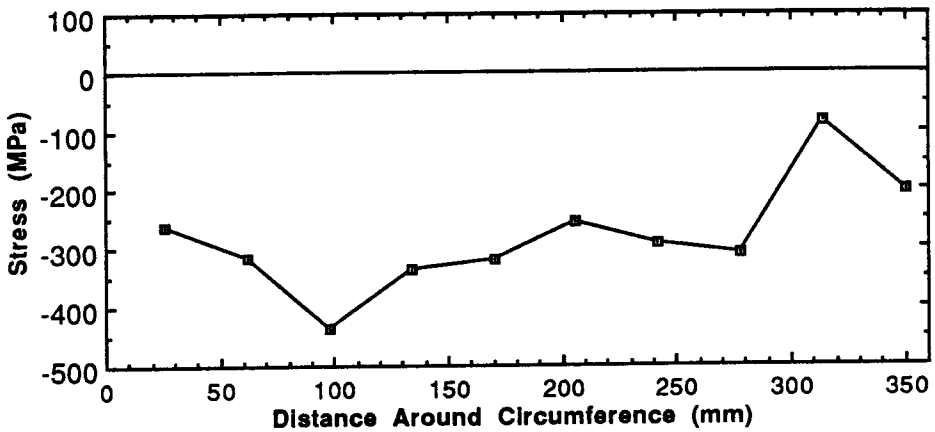

(a) Residual Stresses on Outer Surface

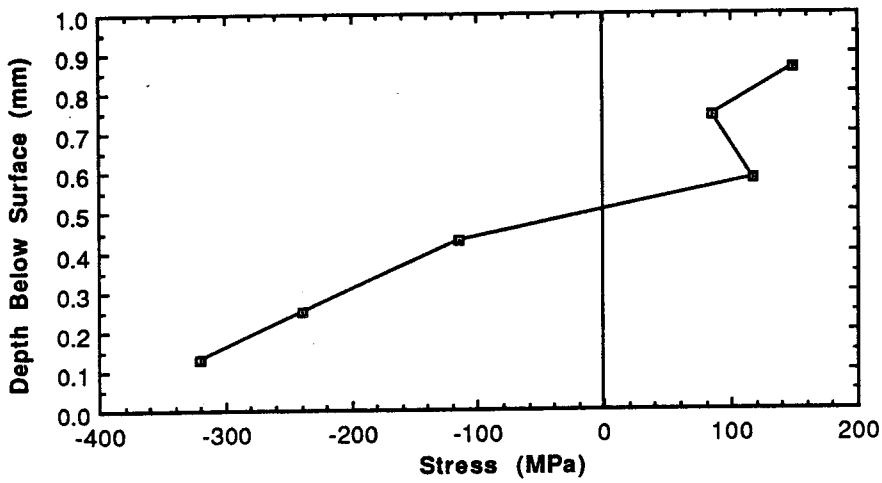

(b) Residual Stress Distribution Below the Surface

Figure 4.27 Residual Stress Distribution in Drill Pipe RB11

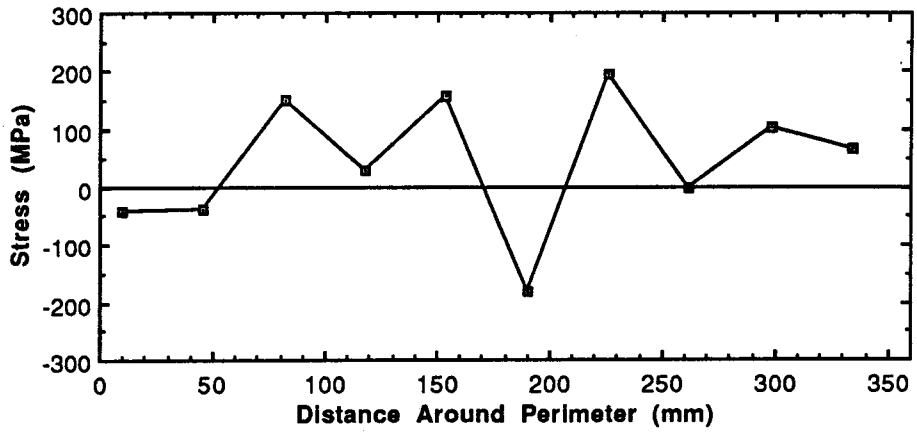

(a) Residual Stress Distribution Measured 0.1 mm Below the Surface

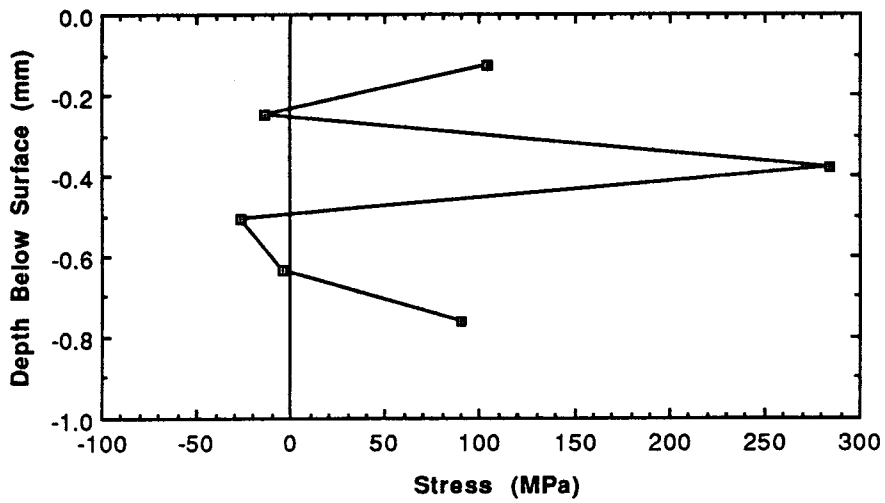

(b) Residual Stress Distribution Below the Surface

Figure 4.28 Residual Stress Distribution in Drill Pipe BT4

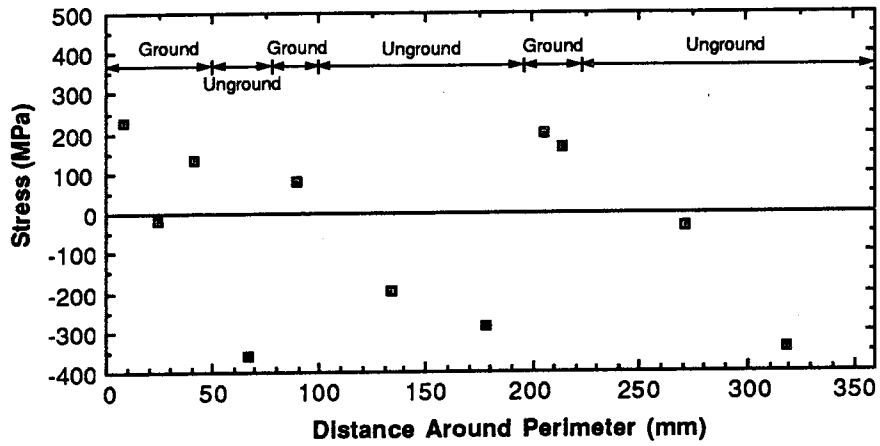

Figure 4.29 Residual Stress Distribution on Outer Surface of Drill Pipe RB6

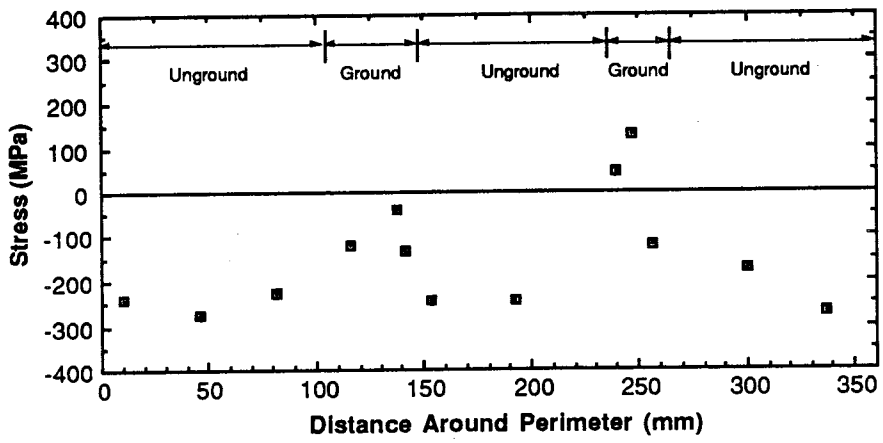

Figure 4.30 Residual Stress Distribution on Outer Surface of Drill Pipe RB14

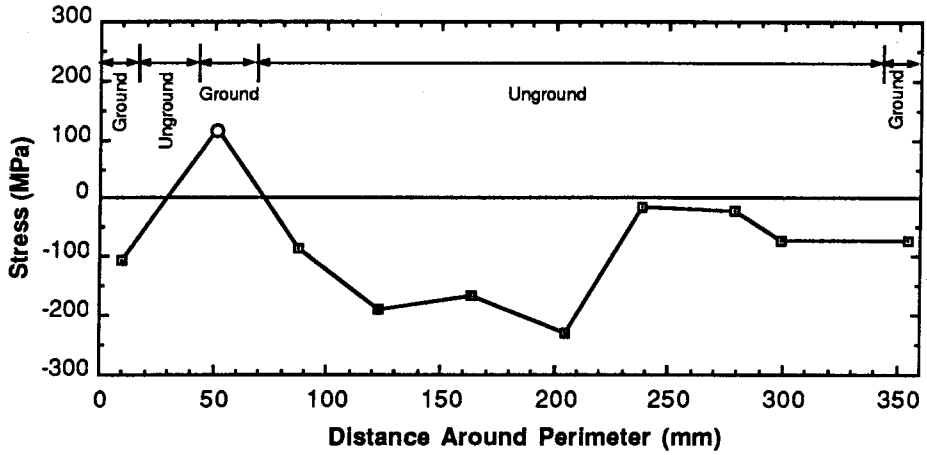

(a) Residual Stress Distribution on Outer Surface

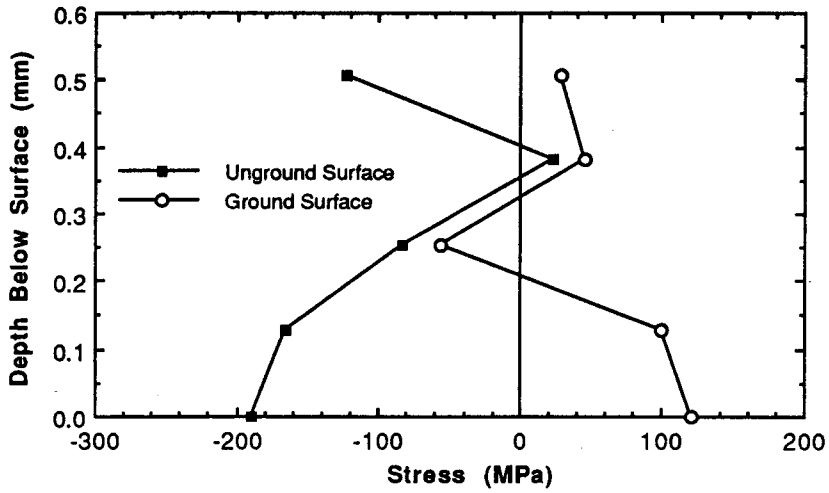

(b) Residual Stress Distribution Below the Surface

Figure 4.31 Residual Stress Distribution in Drill Pipe RB23

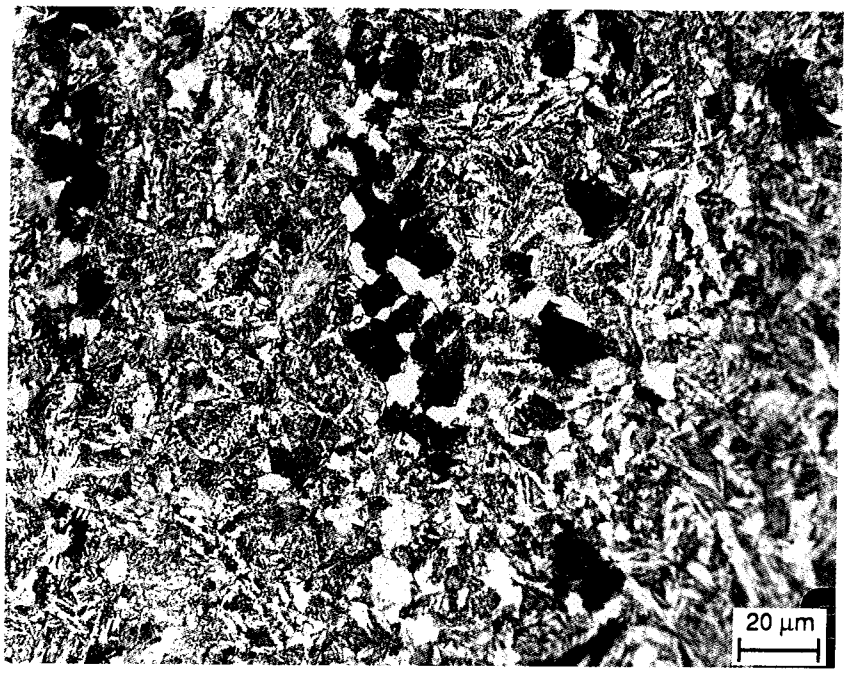

Figure 4.32 Microstructure in Body of Drill Pipe Manufactured by Ohio Drill Pipe

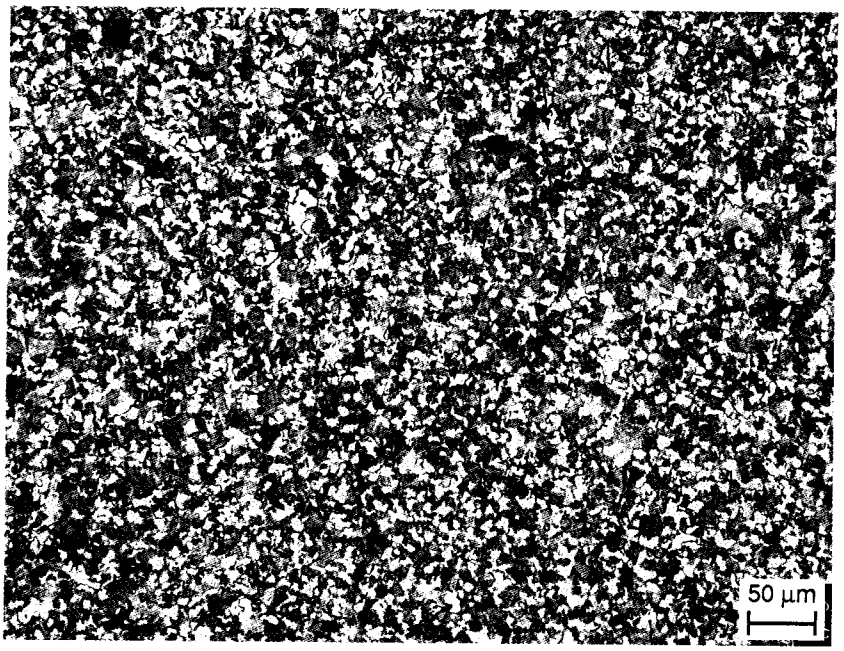

Figure 4.33 Microstructure in Upset of Drill Pipe Manufactured by Ohio Drill Pipe

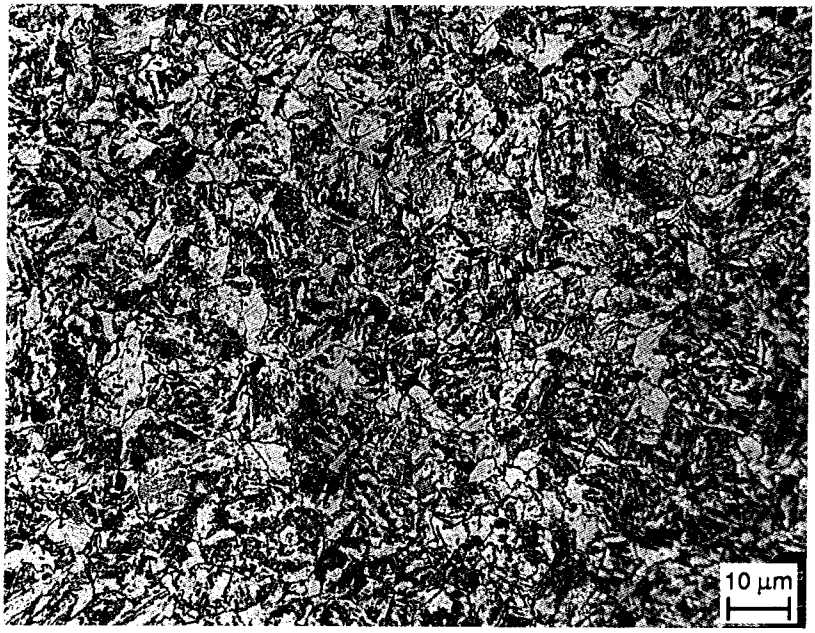

Figure 4.34 Tempered Martensite in Upset and Tool Joint of Drill Pipe Manufactured by Ohio Drill Pipe

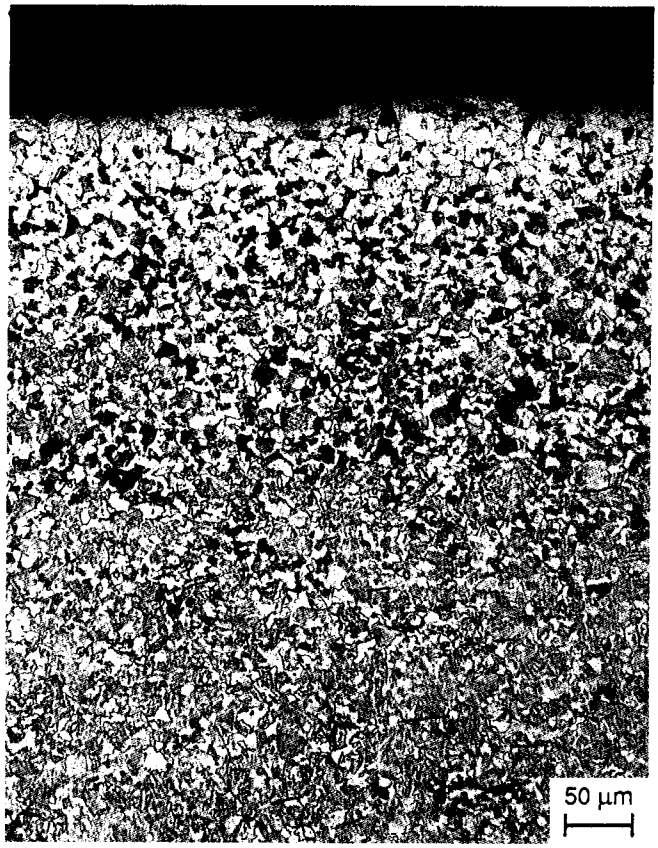

Figure 4.35 Decarburized Surface Layer on Outer Surface of Drill Pipe Manufactured by Ohio Drill Pipe

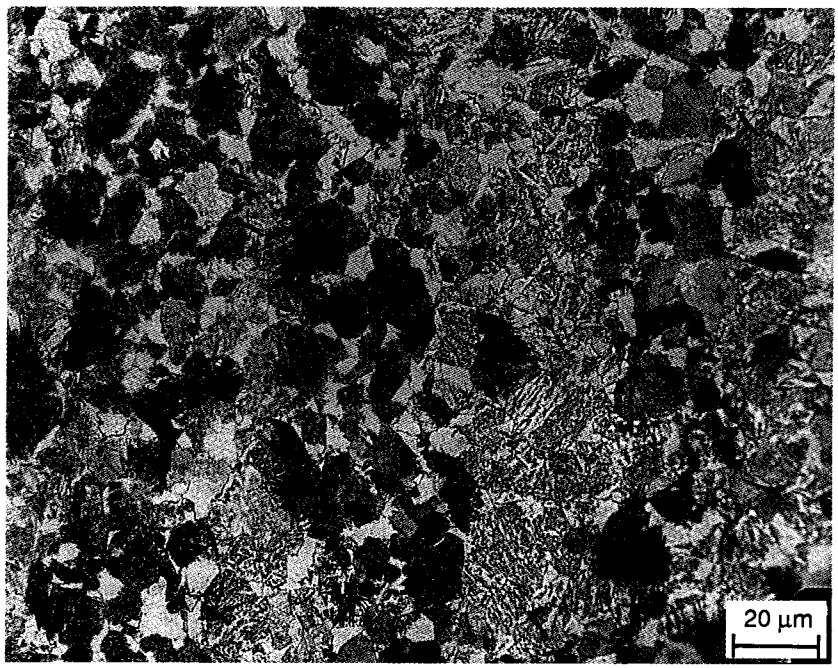

Figure 4.36 Microstructure in Drill Pipe Body Manufactured by Mannesmannrohren-Werkes

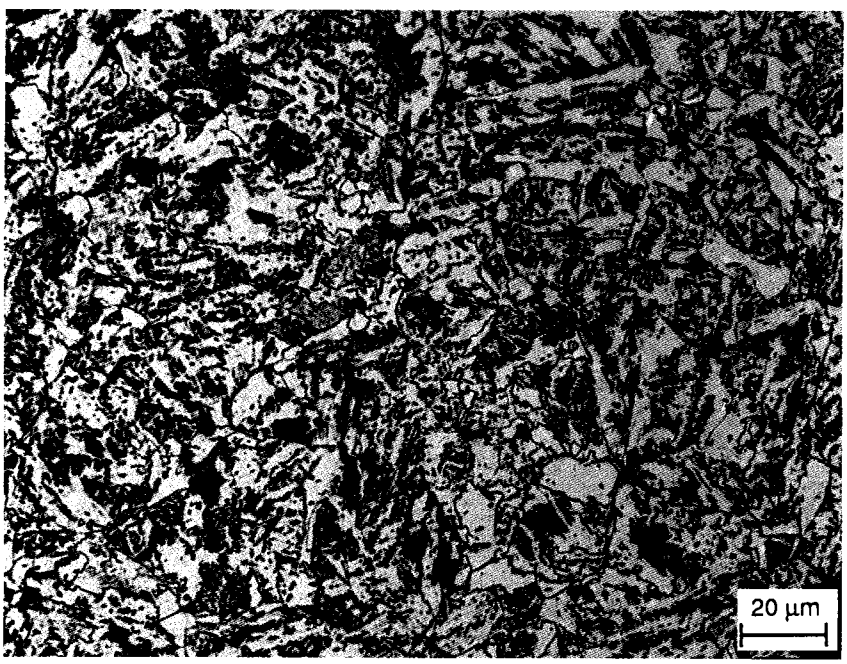

Figure 4.37 Tempered Martensite Microstructure in Upset of Drill Pipe Manufactured by Mannesmannrohren-Werke

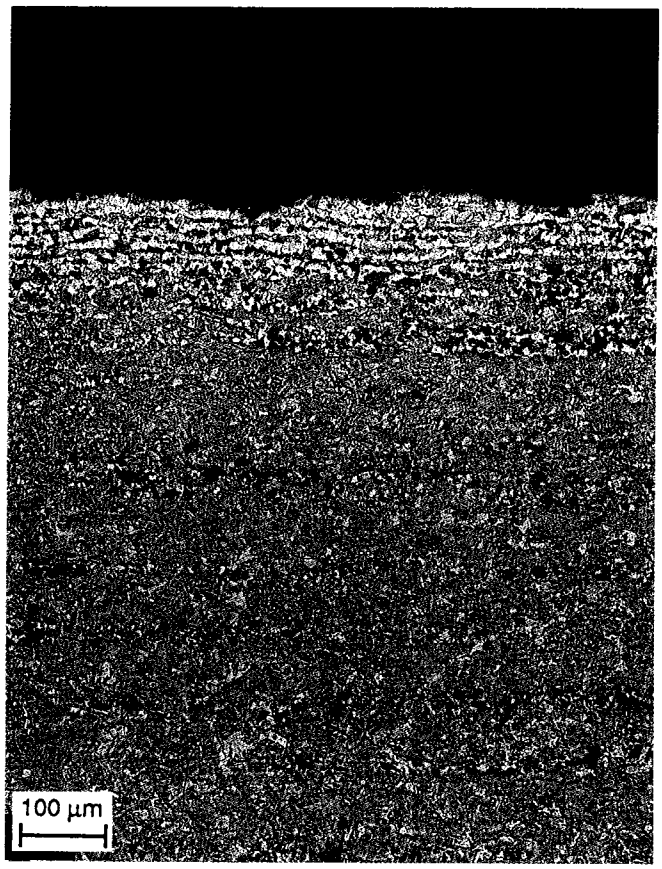

Figure 4.38 Decarburized Outer Surface Layer in Drill Pipe Manufactured by Mannesmannrohren-Werke

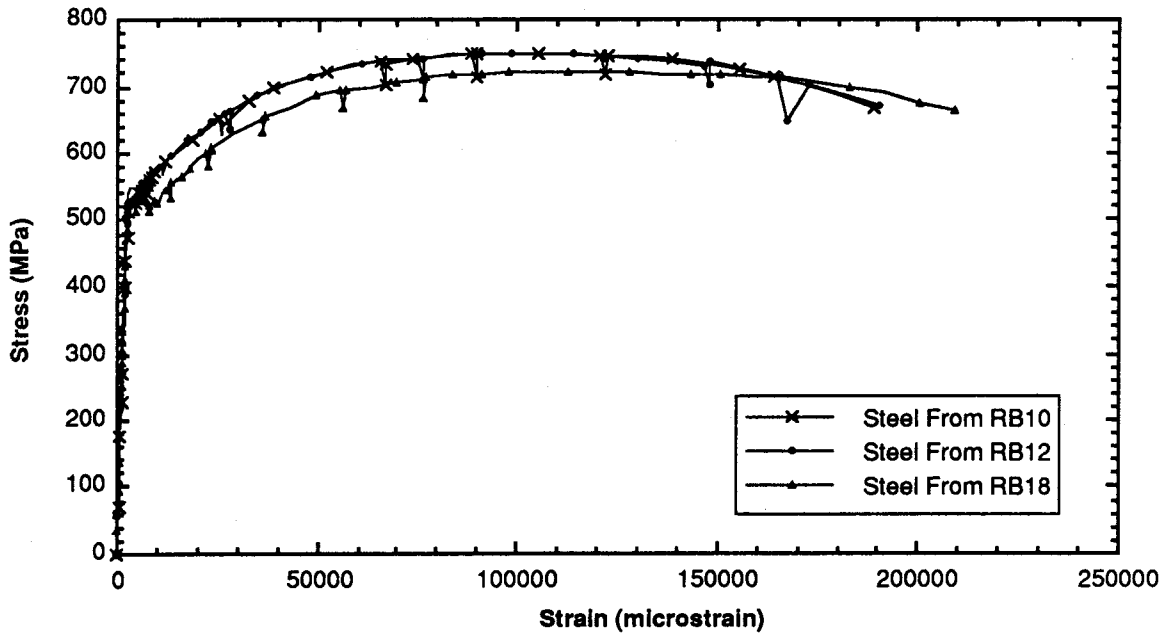

Figure 4.39 Typical Stress Versus Strain Curves for Drill Pipe Steel

Chapter 5

Discussion of Test Results

5.1 Test Results in Air

5.1.1 Effect of Stress Range on Fatigue Life

The effect of stress range was investigated experimentally at a mean stress of 125 MPa. The stress range levels used varied from 180 MPa to 350 MPa. To obtain information concerning the variability of the test specimens and test procedure, three replicates were tested at each stress level. ASTM Committee E-9 on Fatigue (1963) recommends at least four replicates at each stress level in order to be able to estimate the variability of the data. A minimum of ten specimens at each stress level was also recommended to obtain some indication as to the shape of the distribution of fatigue values. Because of time and financial constraints, only three specimens, instead of four, were tested at every stress range level.

Because of the limited number of specimens tested at each stress level, assumptions had to be made regarding the shape of the distribution of fatigue life values. Based on statistical test results discussed by other authors (Reemsnyder, 1969; Fuchs and Stephens, 1980; Dieter, 1986) it was concluded that a log-normal distribution of fatigue life could be assumed.

Regression analysis of the test data was used to provide information on the quantitative effect of stress range on fatigue life under a constant mean stress. Consequently, only the test data obtained under a mean stress of 125 MPa, a total of 20 test results, were used in the regression analysis. For specimens that did not fail, the total number of cycles applied on the specimen was used. This will provide a conservative estimate of their fatigue life for the analysis. In the statistical method used to analyze the results, the fatigue lives were transformed using the logarithm of the cyclic lives. Two different models were investigated in the effort to find a best fit for the test data and the coefficient of determination was used as a measure of goodness of fit of the regression line to determine the best model. The coefficient of determination represents the portion of the total variability in the dependent variable that is accounted for by the fitted simple linear regression model (Harnett, 1982), and therefore a value of unity would be expected if the model fits perfectly the test data. In the first model, the stress range was left untransformed

and in the second model the stress range was transformed using the logarithm of the stress range. Only the second model, which showed a slightly better fit of the test data, is presented here. This model is expressed as

$$\log N = a + b \log S_r + \varepsilon \tag{5-1}$$

where N is the number of cycles to failure, S_r is the stress range, and ε is an error term. The constants a and b are determined from a least squares regression analysis (Kennedy and Neville, 1976). Values of a and b were determined to be 15.62 and -3.95, respectively (see Appendix F for details of the regression analysis). The model of Eq. (5-1) can therefore be expressed as

$$N = 10^{15.62} \; S_r^{\,-3.95} \tag{5-2}$$

where S_r is given in MPa and N is given in cycles.The large scatter observed in the test data is reflected by a low coefficient of determination, r^2, of 0.35. It should be emphasized that Eq. (5-2) applies for values of stress range from 180 MPa to 350 MPa.

A significance test for the slope was performed (Kennedy and Neville, 1976) in order to determine whether log N is dependent upon log S_r . To test whether the slope differs significantly from zero, the t test is applied to the slope of the regression equation. The value of t is given by (Kennedy and Neville, 1976)

$$t = \frac{|b|}{s_b} \tag{5-3}$$

where b is the slope of the regression line and s_b the standard deviation of the slope given by (Kennedy and Neville, 1976)

$$s_b^{\,2} = \frac{\sum \varepsilon_i^{\,2}}{(n-2)\sum (x_i - \bar{x})^2} \tag{5-4}$$

and ε_i is the error of the estimate for a value of the independent variable x_i. The values of ε_i can be found using Eq. (5-1). The sample size is n and $\bar{x}$ is the mean value of x. For the present case, x is taken as log S_r.

The calculated value of t from Eq.(5-4) is compared with the tabulated value for a level of significance of $\alpha = 0.05$ and a number of degrees of freedom of n-2. If the

calculated t is greater than the tabulated value of t, it can be concluded that log N is dependent on log S_r. For the present case, the calculated value of t is 3.12 and the tabulated value is 2.10. Therefore, it can be concluded that, with a risk of $\alpha = 0.05$, the stress range has a significant effect on the fatigue life of the specimen. This conclusion is consistent with experience in other areas of fatigue testing, for instance, fabricated steel flexural members (Fisher et al., 1970).

Eq. (5-2) represents an estimate of the mean fatigue life for values of stress range between 350 MPa and 180 MPa and a mean stress of 125 MPa. Confidence limits of the estimate can be formed using the variance of the estimate. The variance of log N, estimated by the regression line of Eq.(5-1), is defined as the sum of the squares of the deviations divided by the number of degrees of freedom available for calculating the regression line (Kennedy and Neville, 1976).

A confidence interval delimited by a number of standard error of estimate from the mean can be constructed as

$$\log N \pm n\, s_e \tag{5-5}$$

where n is an arbitrary number and s_e is the standard error of estimate (equivalent to the standard deviation for a set of data) given as (Kennedy and Neville, 1976)

$$s_e = \sqrt{\frac{1}{n-2} \sum (y_i - \hat{y})^2} \tag{5-6}$$

where y_i is a measured value of log N, and $\hat{y}$ is the corresponding value of log N predicted by the regression line. The term $(y_i - \hat{y})$ is equivalent to the error term ε_i of Eq. (5-4). The interval delimited by two standard errors of the estimate can be expressed as,

$$\log N = 15.62 - 3.95 \log S_r \pm 1.03 \tag{5-7}$$

or

$$10^{14.59} S_r^{-3.95} \leq N \leq 10^{16.65} S_r^{-3.95} \tag{5-8}$$

Figure 5.1 shows the test data for a mean stress of 125 MPa along with the mean regression line of Eq. (5-2) and the interval described by Eq. (5-8).

As mentioned earlier, the regression analysis was performed with all the test data

obtained when the applied mean stress was 125 MPa. It was therefore assumed that the fatigue limit, defined as the stress below which failure does not occur and above which failure occurs, is below the minimum stress range (180 MPa) used in the experimental investigation. The statistical problem of accurately determining a fatigue limit is complicated by the fact that the value of the fatigue limit for any given specimen cannot be measured. A specimen can only be tested at a particular stress range and, if failure occurs, it is known that the fatigue limit is somewhere below the stress range of the test. When determining the fatigue limit, it must be recognized that each test specimen has its own fatigue limit. The variation of this stress level above which a specimen fails and below which it does not fail is different from specimen to specimen for very obscure reasons. Two statistical methods have been recommended for making a statistical estimate of the fatigue limit (Committee E-9 on Fatigue, 1963). These methods are called Probit analysis and the staircase method. A minimum of 50 test specimens is recommended in order to determine the fatigue limit using the Probit method, while a minimum of 30 specimens is recommended when using the staircase method (Committee E-9 on Fatigue, 1963). Because of the large number of test specimens required to obtain a good estimate of the fatigue limit, no attempt was made to determine a fatigue limit using statistical analysis. Assuming the fatigue limit to lie at the minimum stress range used in the experimental program would be unconservative and, therefore, in order to get a reliable estimate of the fatigue limit, more test data are required.

5.1.2 Effect of Mean Stress on Fatigue Life

The effect of mean stress was investigated experimentally at a stress range of 290 MPa. Specimens were tested at three different mean stress levels, namely, 0, 125, and 250 MPa. Three specimens were tested for each value of mean stress. A total of nine specimens were therefore available for the regression analysis.

Because of the limited number of specimens tested at each mean stress level, a log-normal distribution of fatigue life was assumed in the statistical analysis presented in the following. Three different models were investigated to find a best fit for the test data. The models were:

$$\text{Model I}: \log N = a + b\, S_m \tag{5-9}$$

$$\text{Model II}: \log N = a + b\, (S_m)^2 \tag{5-10}$$

$$\text{Model III}: \log N = a + b\, (S_m)^3 \tag{5-11}$$

where N is the number of cycles to failure, S_m is the mean stress, and a and b are regression constants. A least square regression analysis applied to each of the above models showed that the coefficients of determination are 0.60, 0.63, and 0.61 for models I, II, and III, respectively. Model II was therefore retained since it gave the largest value of correlation coefficient, indicating the best fit of the three models. The values of a and b for Model II, obtained by a least square regression analysis, are 6.57 and -2.00×10^{-5}, respectively (see Appendix F). Thus, the relation between the fatigue life and mean stress can be expressed as

$$\log N = 6.57 - 2.00 \times 10^{-5} (S_m)^2 \qquad (5\text{-}12)$$

where N is expressed in cycles and S_m in MPa. A significance test for the slope was performed. The value of t calculated using Eq. (5-3) is 3.38 and the tabulated value of t for a level of significance α of 0.05 and a number of degrees of freedom of 7 is 2.36. Therefore, it can be concluded that the slope of the regression line is significantly greater than zero and the mean stress has a significant effect on the fatigue life of drill pipe.

The interval delimited by two standard deviations can be expressed as

$$5.60 - 2.07 \times 10^{-5} (S_m)^2 \leq \log N \leq 7.54 - 2.07 \times 10^{-5} (S_m)^2 \qquad (5\text{-}13)$$

The test data used to obtain the regression line of Eq. (5-12) are presented in Figure 5-2. The mean regression line and the interval given by Eq. (5-12) and Eq. (5-13), respectively, are also shown in the figure.

5.1.3 Combined Effect of Stress Range and Mean Stress on Fatigue Life

Since it has now been established that both stress range and mean stress are influential in determining the fatigue life of a drill pipe, a multiple linear regression analysis can be performed on the test results obtained in air during the main test program in order to identify the combined effect. Having used Eq. (5-1) for the effect of stress range and Eq. (5-10) for the effect of mean stress on the fatigue life, the following model was used for the combined effect of stress range and mean stress

$$\log N = a + b_1 \log S_r + b_2 (S_m)^2 \qquad (5\text{-}14)$$

where a, b_1, and b_2 are constants determined by the regression analysis. S_r and S_m are the

stress range and the mean stress, respectively, expressed in MPa. Multiple linear regression analysis (Kennedy and Neville, 1976) of the data from the main test program in air yields values of 14.6, -3.40, and -1.67×10^{-5} for a, b_1, and b_2, respectively. (See Appendix F for details of calculation of regression constants). Eq. (5-14) can be rewritten as

$$\log N = 14.8 - 3.47 \log S_r - 1.65 \times 10^{-5} (S_m)^2 \qquad (5\text{-}15)$$

A significance test was performed on the partial regression coefficients b_1 and b_2. The calculated t value for b_1 is 3.03 and for b_2 is 2.87 for b_2. (See Appendix F for details of these calculations). The tabulated t value for $\alpha = 0.05$ and $n-3 = 24$ degrees of freedom is 2.06. Therefore, it can be concluded, with a probability of error of 5 percent, that b_1 and b_2 are significant that is, the stress range and the mean stress have a marked effect on the fatigue life. This is consistent with the observations made in the previous sections when the effect of mean stress and stress range was investigated independently.

The significance of interaction between the effect of mean stress and the effect of stress range cannot be checked because in the experimental program the mean stress was investigated at only one level of stress range and the effect of stress range was investigated at only one level of mean stress. It is assumed that there is no significant interaction between the effect of stress range and the effect of mean stress in a non-corrosive environment. This means that S-N curves are assumed to be parallel for different levels of mean stress. This is consistent with work presented by other investigators (Fuchs and Stephens, 1980).

The confidence interval for Eq. (5-15), delimited by two standard deviations, can be expressed as

$$\log N = (14.8 \pm 2\, s_e) - 3.47 \log S_r - 1.65 \times 10^{-5} (S_m)^2 \qquad (5\text{-}16)$$

where s_e is the standard error of the estimate given by Eq. (5-6). Upon substituting the the value of s_e obtained using Eq. (5-16), the confidence interval can be expressed as

$$\log N = (14.8 \pm 1.0) - 3.47 \log S_r - 1.65 \times 10^{-5} (S_m)^2 \qquad (5\text{-}17)$$

Equations (5-15) and (5-17) are valid for the range of mean stress and stress range covered in the experimental investigation, namely for a mean stress of 0 to 250 MPa in tension and stress range of 180 MPa to 340 MPa.

5.1.4 Crack Initiation and Growth

Fatigue failure of the test specimens tested in air was observed to originate on the outer surface of the drill pipe. This is in contradiction with reported field failures which originate on the inner surface of the drill pipe (Hansford and Lubinski, 1964; Grant and Texter, 1941; Chinese Petroleum Standardization Committee, 1987). However, it must be recognized that drill pipes tested in air are more likely to fail from cracks originating from the outer surface where bending stresses are largest. Because the wall of a drill pipe is relatively thin, the bending stress on the inner pipe surface is not much smaller than that on the outer surface. For this reason, other factors such as fluid velocity, amount of entrained oxygen and presence of scale may overshadow the stress difference between the outer and inner surfaces of the pipe when they are operated in the corrosive environment present in the field. Furthermore, the cleansing action resulting from the drill pipe outer surface rubbing against the wall of the borehole is believed to make corrosion conditions less severe on the outer surface than on the inner surface (Patton, 1974). In the laboratory, where environmental conditions are the same on the inner and outer surfaces of the drill pipe, fatigue cracks start on the outer surface where bending stresses are larger.

A majority of the test specimens from the preliminary test program (four out of six 114 mm O.D. drill pipes) failed in the internal upset runout region. In addition, personal discussion with a drilling contractor suggests that, although 89 mm O.D. drill pipe with an external upset detail are frequently used, few failures have been reported with that size of drill pipe. The upset geometry was therefore investigated numerically to determine their stress concentration effect and to see whether certain upset geometries would cause a more severe stress concentration. High stress concentration near the upset could cause fatigue cracks to start prematurely in that region.

The finite element method was used to determine the magnitude of stress concentration in the upset region when the drill pipe is subjected to pure axial tension or pure bending. Three different upset geometries were investigated, namely, internal upset (IU), external upset (EU), and internal-external upset (IEU). Upset geometries specified by the American Petroleum Institute (API Spec. 5A, 1987) were used for the analytical investigation. Details of the analysis can be found in Appendix D.

Axial stress distributions in the three different upset geometries are presented in Figure 5.3 for drill pipe in uniaxial tension. A stress concentration factor, defined as the

ratio of maximum stress to stress in the body of the drill pipe, was calculated for each type of upset geometry investigated. Stress concentration factors of 1.21, 1.19, and 1.17 were calculated for the IU, EU and IEU geometries, respectively. The stress contour lines presented in Figure 5.3 represent the stress distribution in the upset area when the uniform stress in the drill pipe body is 100 MPa.

The stress distribution in a drill pipe subjected to pure bending is generally similar to that obtained for uniaxial tension. Figure 5.4 shows the longitudinal stress distribution on the tension side of the drill pipe for different upset geometries. Stress concentration factors of 1.05, 1.13, and 1.10 were obtained for the internal upset, external upset, and internal-external upset, respectively.

It appears that the location of fatigue crack initiation cannot be reliably predicted from calculated stress distribution in a drill pipe. Although the highest level of stress concentration in a IEU drill pipe takes place on the inner surface of the drill pipe, test specimens from the preliminary test program failed from fatigue cracks originating on the outer surface of the drill pipe. However, under field conditions, where the corrosive environment is believed to be more severe on the inner surface of the drill pipe, stress concentration on the inner surface is not desirable. For this reason, the external upset might give better performance than the internal upset or the internal-external upset drill pipe, for which stress concentration occurs on the inner wall of the drill pipe. However, this in itself does not explain completely the better performance of the 89 mm EU drill pipe that is reported from field observations. It is believed that the lower bending stress produced in a smaller diameter pipe as it is bent in a given dogleg is the major factor accounting for the superior performance of the 89 mm drill pipe. The maximum stress in a 89 mm O.D. drill pipe body is only 78 percent of the maximum bending stress in a 114 mm O.D. drill pipe body when both drill pipes are bent in a dogleg of the same severity.

Except for one test specimen (RB16), all the specimens from the main test program failed in the drill pipe body away from the upset runout. An explanation for this difference in behaviour as compared to the pipes from the preliminary test program can be found from observations made during metallographic examination of test specimens. Drill pipes from the preliminary test program showed a ferrite and pearlite microstructure in the upset and upset runout region, while drill pipes from the main test program showed a tempered martensite microstructure in the same region. In a study of the effect of typical alloy steel microconstituents on toughness, Low (1959) concluded that finer microstructures, such as lower bainite or martensite, provide higher toughness than the coarser high-temperature

transformation products, such as ferrite and pearlite. Consequently, pipes from the preliminary test program, which contained ferrite and pearlite in the upset region and tempered martensite in the body, were predisposed to fail in the upset region. In contrast, pipes from the main test program showed a martensitic microstructure in the upset region. Some specimens from the main test program showed some traces of ferrite and pearlite in the pipe body.

The fatigue crack in many of the test specimens from the main test program was found to initiate from grinding marks on the outer surface. When considering the effect of grinding on fatigue resistance of drill pipe, two features are considered to be of major importance; the surface roughness and the residual stress in the surface layer. Experimental work by Suhr (1986) on residual stress free specimens containing grinding marks showed that fatigue cracks almost invariably initiated at the root of one of the grooves introduced by grinding when the grinding marks were oriented transverse to the direction of loading. A notch effect was found to exist when a surface is ground. Fractographic examination of the test specimens in the study reported herein showed that fatigue cracks did initiate at the root of grooves left by grinding marks.

Surface grinding was found not only to introduce surface roughness, but also to modify residual stresses in the surface layer. Residual stresses measured by X-ray diffraction along the grinding marks showed that residual stresses varied from high tension to low compression. In contrast, unground surfaces were found to be under a compressive residual stress that sometimes exceeded 400 MPa. This effect of grinding on residual stresses in drill pipe is in agreement with recent observations by Flavenot (1987) and Scholtes (1987) on steel plates. Flavenot showed that hard-grinding (i.e. hard grinding wheel material and high grinding pressure) resulted in high tensile residual stresses, whereas for soft and medium grinding conditions only very low levels of residual stresses were observed. Scholtes demonstrated that residual stresses due to grinding are determined by all parameters influencing heat production and/or plastic deformations during grinding. Scholtes also demonstrated that residual stresses introduced by grinding can vary from high tension to high compression, depending on grinding conditions. The work of Flavenot (1987) showed a reduction in fatigue life of about 26 percent for hard grinding compared with soft grinding. The orientation of the grinding marks in relation to the axis of loading was also found to be influential, grinding marks transverse to the direction of loading being more damaging than longitudinal grinding marks.

Changes in surface properties such as decarburization of the surface are known to

be particularly detrimental to fatigue performance (Dieter, 1986; Hertzberg, 1983). Metallographic examination of test specimens reported herein showed more extensive decarburization on the outer surface layer than on the inner surface. This could predispose the outer surface to earlier crack initiation.

Out of 25 specimens tested in air, five specimens failed from fatigue cracks that developed at a loading point under a bearing. Amongst those five specimens, drill pipe RB14-B failed from cracks developing simultaneously at midspan of the test specimen and in the bearing area.

As has been mentioned, bearings were pressure-fitted on a test specimen and, as a result, a radial pressure of unknown magnitude is exerted on the outer surface of the drill pipe. To prevent fretting (a surface damage resulting when two surfaces in contact experience a slight periodic relative motion) rubber pads were placed between the pipe and bearing surface. This measure was found to be effective since no test specimen suffered surface damage from the bearings. Although no physical damage to the pipe resulted from the bearings, radial pressure exerted by the bearings on the pipe modifies the state of stress in the pipe and may adversely affect fatigue resistance.

The effect of bearing pressure on the state of stress in the drill pipe body in the bearing area was investigated using the finite element method. The bearing pressure due to pressure fitting of a bearing was simulated by an axisymmetric radial pressure (see Figure 5.5 (a)). However, when a test specimen is loaded through the bearings, the pressure distribution at the bearing is no longer uniform, as depicted in Figure 5.5(b). The uniform pressure distribution was assumed in the analysis in order to simplify the model and to permit a qualitative rather than a quantitative evaluation of the bearing pressure effect.

All the fatigue cracks that developed under a bearing were perpendicular to the pipe axis. Therefore, longitudinal stresses were of greater interest in the analysis since they are normal to the crack front. More details about the finite element analysis are presented in Appendix E. The analysis showed that the stiffness of the rubber pads and the coefficient of friction between the pipe surface and the rubber pad were not influential. Variable longitudinal stresses are introduced in the pipe wall as a result of the radial pressure. Compressive stresses about 1.7 times the magnitude of the radial pressure are induced on the outer surface of the pipe under the bearing at about 20 mm from the edge of the bearing contact surface. Likewise, tensile stresses of about 1.7 times the magnitude of the radial pressure are found on the outer surface about 20 mm from the bearing contact area. At a

distance of about 70 mm from the bearing contact area, longitudinal stresses are found to be only a small fraction of the bearing pressure.

5.2 Test Results in a Corrosive Environment

5.2.1 Effect of Stress Range on Fatigue Life

The effect of stress range on fatigue life in a 3.5 percent saline solution was investigated at a mean stress level of 125 MPa. Stress ranges varying from 130 MPa to 290 MPa were used for the investigation. Although it is expected that the effect of stress range on fatigue life is also affected by the mean stress, it is assumed in the work presented below that the mean stress has a negligible influence on the effect of stress range. This means that S-N curves are assumed to be parallel for different levels of mean stress.

Regression analysis was performed on all the test data obtained for a mean stress of 125 MPa except for specimen RB28C-B, which failed prematurely because of the presence of a stencil mark on the pipe body. This test specimen was excluded from the analysis since the practice of steel stencil marking is not generally used on the drill pipe and the presence of those markings on one of the test specimens is considered to be an exception. Furthermore, such practice has been recognized to be detrimental for a long time (Grant and Texter, 1941) and the industry has been warned against such a practice. With good mill practice, steel stenciling on the drill pipe body can be easily prevented. As for the tests in air, the test results in a 3.5 percent NaCl solution were assumed to be normally distributed for each value of stress range. The model described by Eq. (5-1) was used to correlate the fatigue life to the stress range and the constants a and b from the regression model were determined from a least squares analysis. With values of a and b of 11.24 and -2.29, respectively, the fatigue life in a 3.5 percent NaCl solution under a mean stress of 125 MPa and a testing frequency of 1.0 Hz can be expressed as

$$\log N = 11.24 - 2.29 \log S_r \qquad (5\text{-}18)$$

The coefficient of determination is $r^2 = 0.92$. A significance test on the slope of Eq. (5-18) indicated that, with a risk of α=0.05, the stress range has a significant effect on the fatigue life of a drill pipe in a corrosive environment. The interval delimited by two standard deviations from the mean can be expressed as

$$11.00 - 2.29 \log S_r \leq \log N \leq 11.48 - 2.29 \log S_r \qquad (5\text{-}19)$$

The test data used for the regression analysis, the mean regression line, and the interval delimited by two standard deviations are illustrated in Figure 5.6.

5.2.2 Effect of Mean Stress on Fatigue Life

The effect of mean stress in a 3.5 percent NaCl solution was investigated at two different stress range levels, namely 130 MPa and 290 MPa. Three levels of mean stress, 0, 125 MPa, and 250 MPa were used for each stress range. Because of the reduced scatter observed in the corrosion fatigue test results and because of the time-consuming nature of tests in a corrosive environment (a single test can take from 1 to 20 weeks testing time), only two replicates of each test were performed.

Stress range of 290 MPa

Assuming a log-normal distribution, the models of Eq. (5-9), (5-10) and (5-11) were investigated for a best fit of the test data. Values of the coefficient of determination, r^2, of 0.82, 0.96, and 0.97 were obtained for Models I, II, and III, respectively. Although Model III gives the best fit for the analyzed data, Model II was retained in order to be consistent with the analysis performed on specimens tested in air. From a least squares analysis, Model II can be expressed as

$$\log N = 5.80 - 7.19\times10^{-6} (S_m)^2 \qquad (5\text{-}20)$$

where N is the fatigue life in cycles and S_m is the mean stress in MPa. Eq. (5-20) is applicable for a mean stress ranging from 0 to 250 MPa in tension, a stress range of 290 MPa, an environment consisting of a 3.5 percent NaCl solution, and a rate of testing of 1.0 Hz.

To determine whether log N is dependent on the square of the mean stress, a significance test was performed. The value of t calculated using Eq. (5-3) is 9.67: the tabulated value of t for a number of degrees of freedom n-2 of 4 and a level of significance α of 0.05 is 2.78. Therefore, it can be concluded that the slope of the regression line is significantly greater than zero and that the mean stress has a significant effect on the fatigue life of drill pipes. The interval delimited by two standard deviations from the mean can be expressed as

$$\log N = (5.80 \pm 0.10) - 7.19\times10^{-6} (S_m)^2 \qquad (5\text{-}21)$$

Eq. (5-21) is subjected to the same limitations as is Eq.(5-20). Figure 5.7 shows the test

data, the mean regression line, and the interval delimited by two standard errors from the mean regression line for the effect of mean stress on fatigue life at a stress range of 290 MPa.

Stress range of 130 MPa

The same model used above for a stress range of 290 MPa was used to establish the effect of mean stress at a stress range of 130 MPa. A least squares regression analysis was performed on the data obtained at a stress range of 130 MPa (see Appendix F). The coefficient of determination obtained from the regression analysis was 0.75, which is significantly lower than the value of 0.96 obtained at a stress range of 290 MPa. This lower value of coefficient of determination may reflect the larger scatter usually observed in fatigue test data at low stress ranges. A least squares fit of Model II from Eq.(5-10) to the test data gives

$$\log N = 6.57 - 6.29\text{x}10^{-6} (S_m)^2 \qquad (5\text{-}22)$$

A significance test performed on the slope of the regression equation indicates that, with a probability of error of 5.0 percent, the mean stress has a significant influence on the fatigue life. The calculated and tabulated value of t were 3.89 and 2.57, respectively. The interval delimited by two standard deviations from the mean can be expressed as

$$\log N = (6.58 \pm 0.23) - 6.29\text{x}10^{-6} (S_m)^2 \qquad (5\text{-}23)$$

The test data, mean regression line, and the interval delimited by two standard deviations from the mean for the effect of mean stress on fatigue life at a stress range of 130 MPa are shown in Figure 5.8.

Comparison of Eq. (5-20) with Eq. (5-22) shows that the fatigue life of a drill pipe was less sensitive to a change in mean stress when the pipe was tested at a stress range of 130 MPa than when it was tested at a stress range of 290 MPa. This indicates that the effect of mean stress on fatigue life is also dependent on the stress range level at which the tests were conducted. To study the effect of stress range on the sensitivity of fatigue life to the mean stress, the following two models were investigated

$$\text{Model A: } \log N = a + b\ S_r (S_m)^2 \qquad (5\text{-}24)$$

$$\text{Model B: } \log N = a + b\ \log S_r (S_m)^2 \qquad (5\text{-}25)$$

By multiplying the mean stress term, $(S_m)^2$, by a function of the stress range, a relationship is obtained whereby the effect of mean stress on the fatigue life varies with varying stress range. A least squares regression analysis of the test data can be used to obtain values of the constants *a* and *b* for both models. The independent variable in model A is $S_r (S_m)^2$ and in model B it is $\log S_r (S_m)^2$. A least squares fit of models A and B to the data obtained at a stress range of 290 MPa results in the following:

$$\text{Model A: } \log N = 5.80 - 2.46\text{x}10^{-8} S_r (S_m)^2 \tag{5-26}$$

$$\text{Model B: } \log N = 5.80 - 2.91\text{x}10^{-6} \log S_r (S_m)^2 \tag{5-27}$$

Fitting models A and B to the data obtained at a stress range of 130 MPa results in

$$\text{Model A: } \log N = 6.58 - 4.78\text{x}10^{-8} S_r (S_m)^2 \tag{5-28}$$

$$\text{Model B: } \log N = 6.58 - 2.97\text{x}10^{-6} \log S_r (S_m)^2 \tag{5-29}$$

It can be observed that model A gives a significantly different value of *b* for the two different stress ranges investigated. The value of *b* in Eq. (5-28) is almost twice that in Eq. (5-26). On the other hand, Model B yields almost identical values of *b* for both stress ranges. A difference of only 2.0 percent is observed between the value of *b* for the two different stress ranges. This indicates that, under the test conditions used in this investigation, the fatigue life depends on the value of $\log S_r (S_m)^2$ and not uniquely on the square of the mean stress. This interaction of the stress range and the mean stress is believed to be the consequence of the time-dependent nature of corrosion. Any factor which may affect the duration of exposure of a test specimen to the corrosive environment is also likely to affect the influence of other factors on the fatigue life. This complex interaction between chemical, mechanical, and metallurgical factors makes a quantitative fatigue life prediction for conditions other than the ones in which the fatigue data were obtained almost impossible. Therefore, equations (5-27) and (5-29) have to be viewed as not applicable to test environments, testing frequency, and grades of steel other than the ones used in this investigation. Test specimen RB9C, tested at a frequency of 1.5 Hz, showed that the test frequency influences the fatigue life, for example.

5.2.3 Combined Effect of Stress Range and Mean Stress on Fatigue Life

Equations (5-27) and (5-29) show that, although both regression lines have almost the same slope, the value of the intercept on the log N axis differs for the two values of stress range investigated. Under identical environment, testing speed, and metallurgical conditions for the two series of tests, the difference in the value of the intercept is assumed to be caused by the stress range only. A study of the effect of stress range on the fatigue life showed that the logarithm of the fatigue is directly proportional to the logarithm of the stress range. For these reasons, the following model was used to correlate the fatigue life to the stress range and mean stress

$$\log N = a + b_1 \log Sr + b_2 \log S_r (S_m)^2 \qquad (5\text{-}30)$$

where a, b_1, and b_2 are constants determined by regression analysis, and S_r and S_m are the stress range and the mean stress, respectively. Although it was previously determined that the stress range has an interaction with the mean stress, it is implicit in Eq. (5-30) that the mean stress is assumed to not influence the effect of the stress range on the fatigue life. Therefore, S-N curves obtained for different values of mean stress are parallel. It is probable that this latter assumption is not valid, but, because of the limited amount of test data, it is not possible to evaluate the interaction effect of mean stress on the stress range. Therefore, the assumption is retained for the following work.

Multiple regression analysis on 18 test results obtained in a 3.5 percent NaCl solution (see Appendix F for listing of the test data used for the regression analysis) yields values of a, b_1, and b_2 of 11.43, -2.31, and -2.67×10^{-6}, respectively. Test specimen RB28C-B has been excluded from the regression analysis for reasons explained in Section 5.2.1. The fatigue life can now be expressed in terms of the stress range, S_r, and the mean stress, S_m, as

$$\log N = 11.43 - 2.31 \log S_r - 2.67 \times 10^{-6} \log S_r (S_m)^2 \qquad (5\text{-}31)$$

where S_r and S_m are expressed in MPa. A significance test was performed on the partial regression coefficients b_1 and b_2. The calculated t value is 14.8 for b_1 and 5.44 for b_2. For $n-3 = 15$ degrees of freedom and $\alpha = 0.05$, the tabulated t value is 2.13. Therefore, it can be concluded that b_1 and b_2 are significant, that is, log S_r and the interaction term log $S_r (S_m)^2$ have a marked effect on the fatigue life. This is consistent with the observations made in the previous sections when the effect of stress range and mean stress

was investigated independently. The interval delimited by two standard deviations from the mean can be expressed as

$$\log N = (11.43 \pm 2\, s_e) - 2.31 \log S_r - 2.67\text{x}10^{-6} \log S_r (S_m)^2 \qquad (5\text{-}32)$$

The standard error of the estimate, s_e, given by Eq.(5-6), is 0.110. Thus, the confidence interval delimited by two standard errors can be expressed as

$$\log N = (11.43 \pm 0.22) - 2.31 \log S_r - 2.53\text{x}10^{-6} \log S_r (S_m)^2 \qquad (5\text{-}33)$$

Eq. (5-33) is considered applicable for mean stresses from 0 to 250 MPa, stress ranges from 90 MPa to 290 MPa, and a testing frequency of 1.0 Hz in a 3.5 percent NaCl solution.

An alternative method has been used by other investigators (Fisher et al., 1970) to study the effect of stress range, mean stress, and their interaction on fatigue life. The method, called analysis of variance, is presented in Appendix F.

5.2.4 Effect of a Corrosive Environment on Fatigue Life

In order to determine the effect of a 3.5 percent NaCl solution on fatigue life of drill pipes, the test results obtained in the corrosive environment are compared to the test results obtained under similar stress conditions in air.

Shown in Figure 5.9 are the mean regression lines for the effect of stress range on the fatigue life in air and in a 3.5 percent NaCl solution. Both curves were obtained at a mean stress level of 125 MPa. It is evident from the curves that a corrosive environment has a detrimental effect on the fatigue life of drill pipes. It is also evident that the reduction in fatigue life is greater at lower stress ranges. This is believed to be the consequence of the time-dependence of the corrosion process. At lower stress ranges, test specimens are exposed for a longer time to the corrosive environment. At a high stress range, where failure occurs after a relatively small number of loading cycles, the corrosive environment cannot have such a significant effect.

The corrosive environment used for testing was also found to influence the effect of the mean stress level on the fatigue life. Figure 5.10 shows the mean regression lines for the effect of mean stress on fatigue life both in air and in a saline solution. It is seen that as the mean stress decreases, the mean fatigue life shows a greater reduction when conditions of the corrosive environment exist. This again is believed to be the effect of the time-

dependent nature of corrosion since the duration of a test is longer at lower mean stresses.

5.2.5 Crack Initiation and Growth

The surface condition of the test specimens was found to be a determining factor in crack initiation site. Several cracks were found to initiate at the root of the grinding wheel traces. Apart from being stress raisers, scratches left on the surface by grinding act as crevices and offer a restriction to the interdiffusion between the solution near the root of the scratch and the bulk corrosive solution. This restriction to interdiffusion gives rise to acidification within the grinding marks and, in turn, accelerates corrosion. This form of corrosion, similar to pitting corrosion, is particularly active in an environment containing chloride ions (Fontana and Staehle, 1967). Changing the environment from distilled water to 3.0 percent NaCl solution has been found to decrease the failure time due to stress corrosion cracking by two orders of magnitude. However, most of this reduction in life is reported to occur in weaker solutions containing approximately 0.5 percent NaCl (Carter and Hyatt, 1977). The acidification within localized corrosion cells has been accounted for by hydrolysis reactions, and the solution pH inside pits, crevices, and cracks was found to be independent of bulk solution pH (Brown, 1977). The increased corrosion activity in the bottom of grinding traces quickly gives rise to cracks which then propagate until failure.

Fatigue cracks were also found to have initiated from surface pits. However, it is not known if those pits were present before testing started or if they were formed during testing. The presence of pits on the surface of new specimens indicates that existing pits could be the origin of some of the observed failures. Existing pits provide an environment similar to the one present inside the grinding traces. Because of the stress concentration at the bottom of a pit and localized corrosion taking place in a pit, cracks can quickly emanate from those pre-existing pits. Extensive pitting observed on fracture surfaces indicates that the pitting taking place during testing might have been the origin of some of the failures. Pitting has been identified as the initiation stage of fatigue cracking by several researchers (Fontana and Staehle, 1967; Kondo, 1989; Laird and Duquette, 1973; Speidel, 1977). Furthermore, it has been shown that tensile stresses reduce the electrode potential at stress raisers such as corrosion pits much more than at other sections on metal surfaces. This leads to the formation of corrosion cells in which the stress raiser is anodic and the adjacent surfaces are cathodic (Karpenko and Vasilenko, 1977).

The scatter of test results for the corrosion fatigue condition was found to be considerably less than for fatigue in air. Although the origins of test scatter are manifold,

the most significant cause of scatter is believed to be the variation in the duration of the crack initiation stage. The exact mechanism of fatigue crack initiation in the presence of both inert and corrosive environments remains unclear. However, formation of persistent slip bands and extrusion-intrusion pairs seems to be the most widely accepted mechanism of fatigue crack nucleation in an inert environment, although their formation mechanism remains elusive (Laird and Duquette, 1973). More than one mechanism seems to be operative in corrosion fatigue. Mechanisms such as pitting, preferential dissolution of deformed areas, film rupture, and the Rebinder mechanism all play a certain role in initiating a fatigue crack in a corrosive environment (Laird and Duquette, 1973). Because of all those various mechanisms operating to initiate a crack, aqueous environments are known to dramatically affect the crack initiation process (Jaske et. al., 1981). Less scatter in test results is therefore expected when fatigue testing in carried out in a corrosive environment because of the significant reduction in the duration of the crack initiation stage.

It has been shown in a previous section (section 4.2) that mean stress is influential in a corrosive environment. Residual stresses are usually considered to be additive to the mean stress (Maddox, 1975). Although this is the case in an innocuous environment, this concept may not be applicable in a corrosive environment. Residual stresses are self-equilibrating stresses and, consequently, they remain unchanged provided the material in the structure remains unchanged. Plastification of the material by overstressing the structure of material removal will effectively change the existing state of residual stresses. Consequently, the high residual stresses measured on the surface of test specimens are likely to be influential only if corrosion does not dissolve the surface layer of the test specimens. Corrosion pits, although they do not affect a large volume of material, penetrate deeper below the surface than does uniform corrosion. Therefore, it is possible the corrosion fatigue cracks start at a depth where residual stresses are of significantly lower magnitude than the ones measured on the surface.

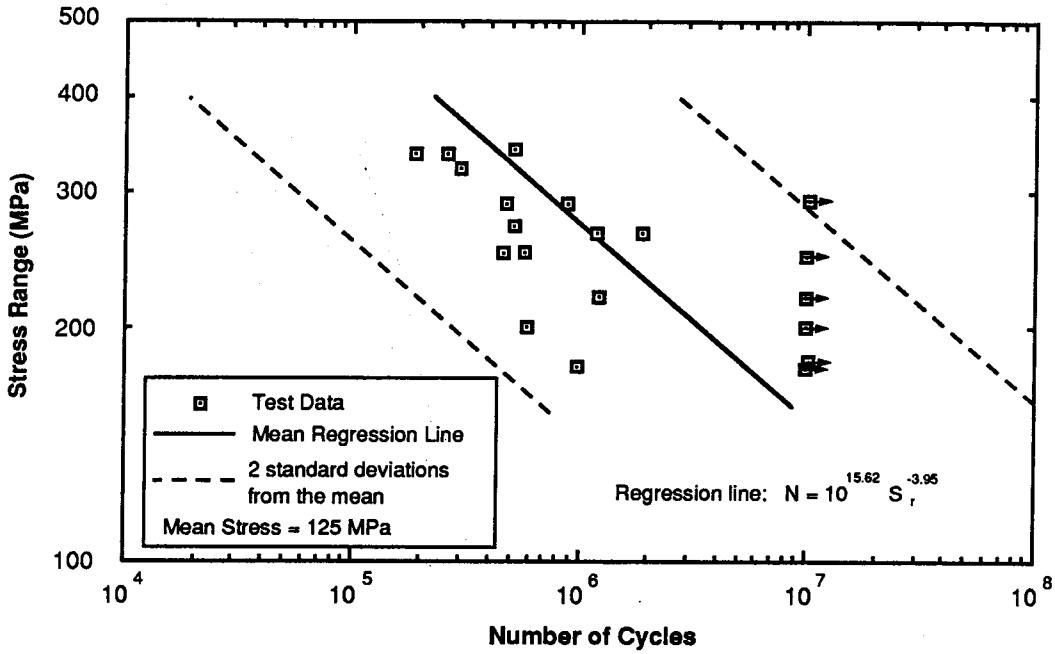

Figure 5.1 Effect of Stress Range on Fatigue Life From Tests Conducted in Air

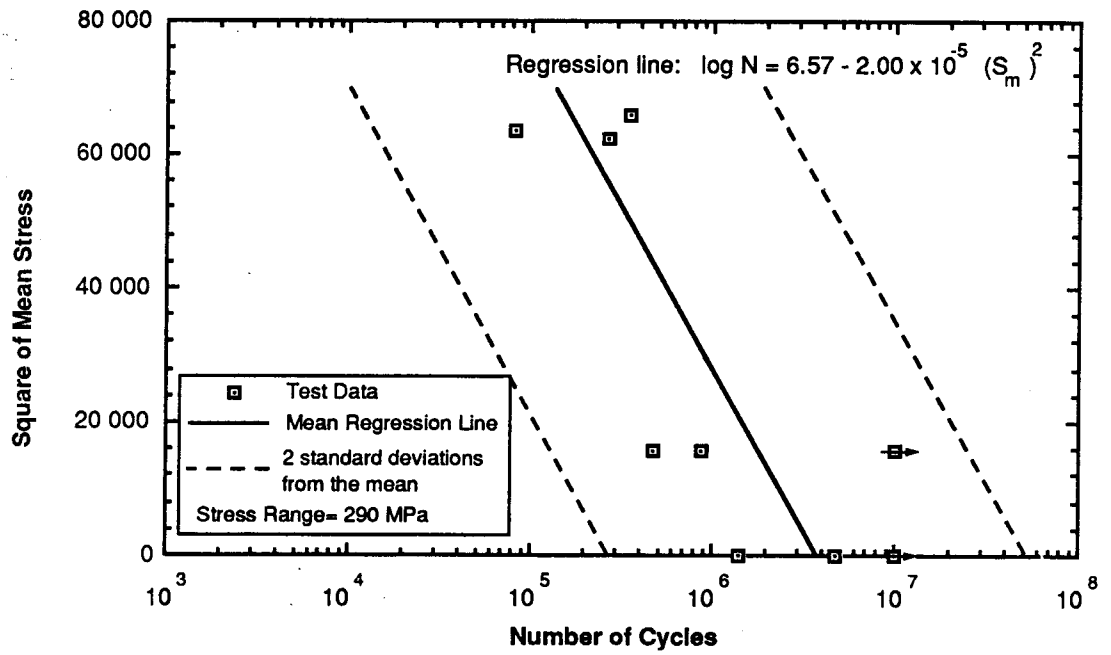

Figure 5.2 Effect of Mean Stress on Fatigue Life in Air

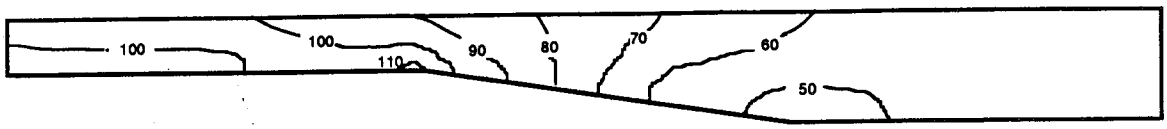

(a) Stresses in Internal Upset (SCF = 1.21)

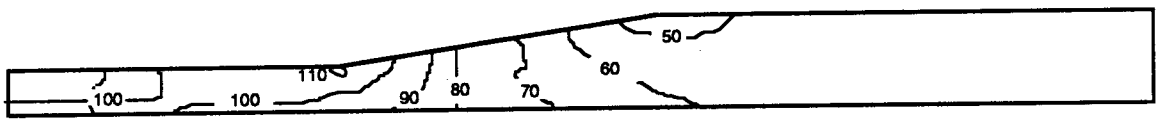

(b) Stresses in External Upset (SCF = 1.19)

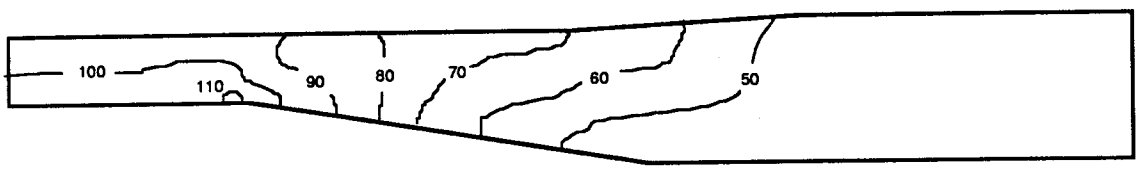

(c) Stresses in Internal-External Upset (SCF = 1.17)

Figure 5.3 Longitudinal Stress Distribution in Upsets of Drill Pipe - Axial Tension

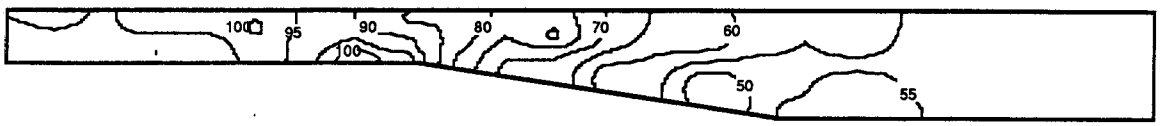

(a) Stresses in Internal Upset (SCF = 1.05)

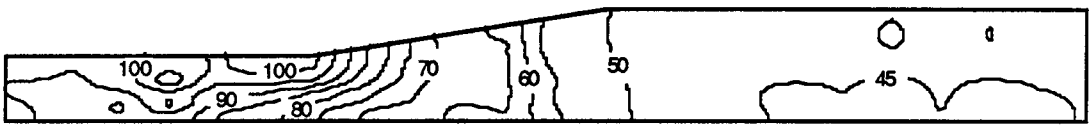

(b) Stresses in External Upset (SCF = 1.13)

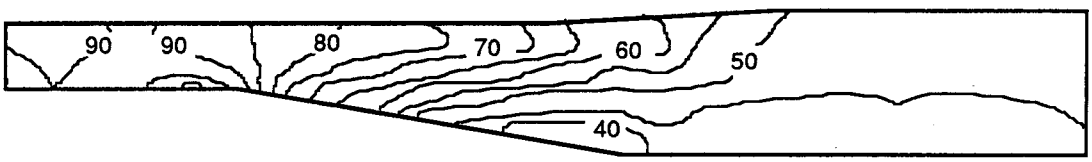

(c) Stresses in Internal-External Upset (SCF = 1.10)

Figure 5.4 Longitudinal Stress Distribution in Upsets of Drill Pipe - Pure Bending

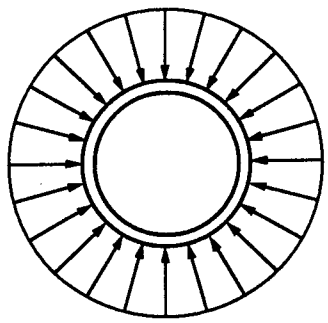

(a) Uniform Radial Pressure Before Test Specimen is Loaded

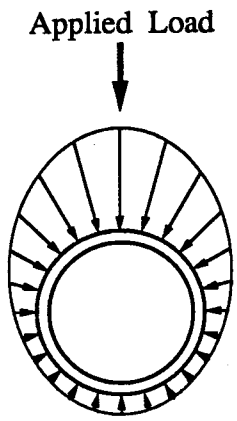

(b) Radial Pressure Distribution When Test Specimen is Loaded

Figure 5.5 Radial Pressure Distribution on Drill Pipe in Bearing Area

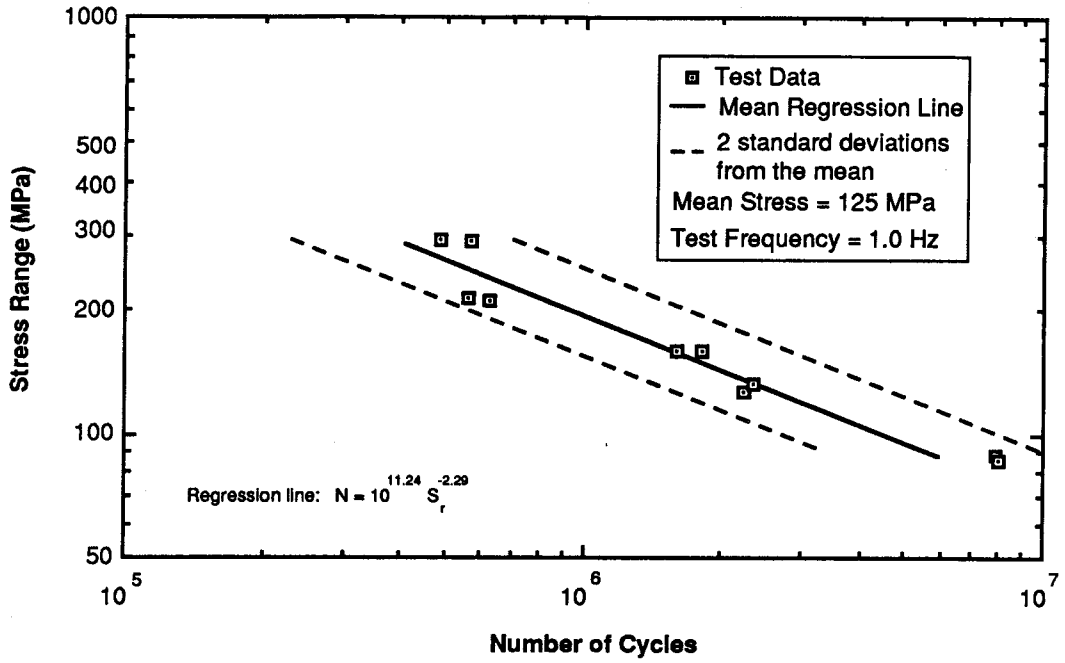

Figure 5.6 Effect of Stress Range on Fatigue Life in a 3.5 percent NaCl Solution

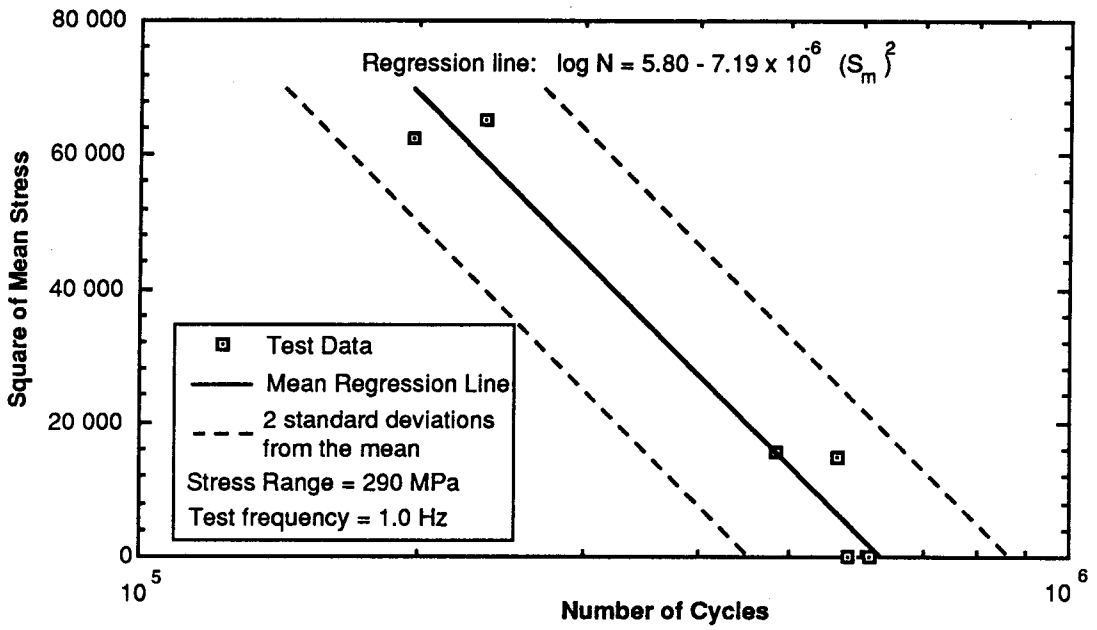

Figure 5.7 Effect of Mean Stress on Fatigue Life in NaCl Solution (Sr = 290 MPa)

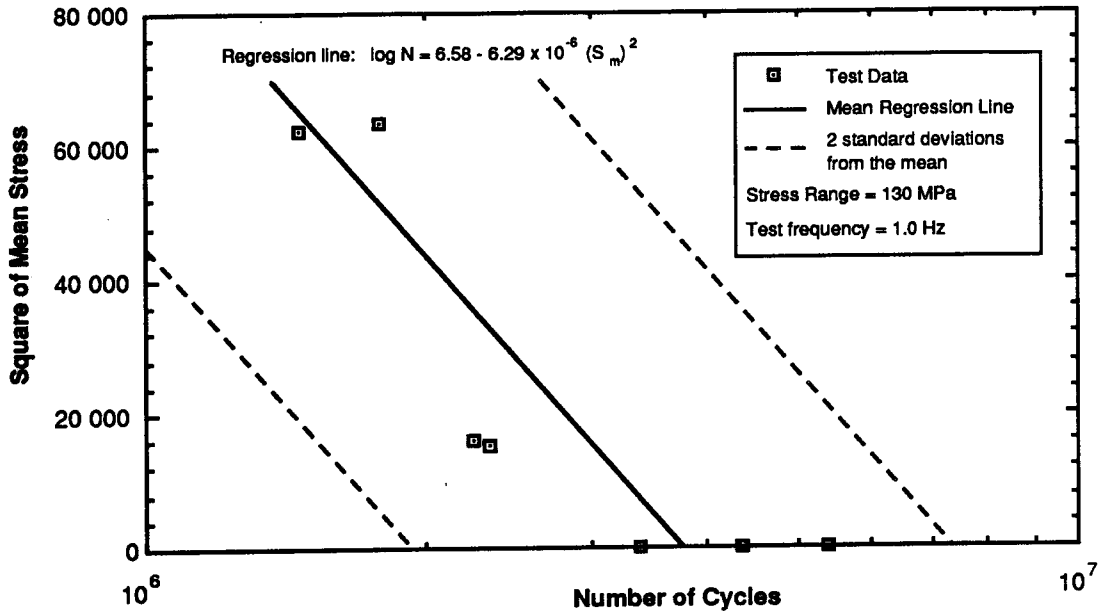

Figure 5.8 Effect of Mean Stress on Fatigue Life in NaCl Solution (Sr = 130 MPa)

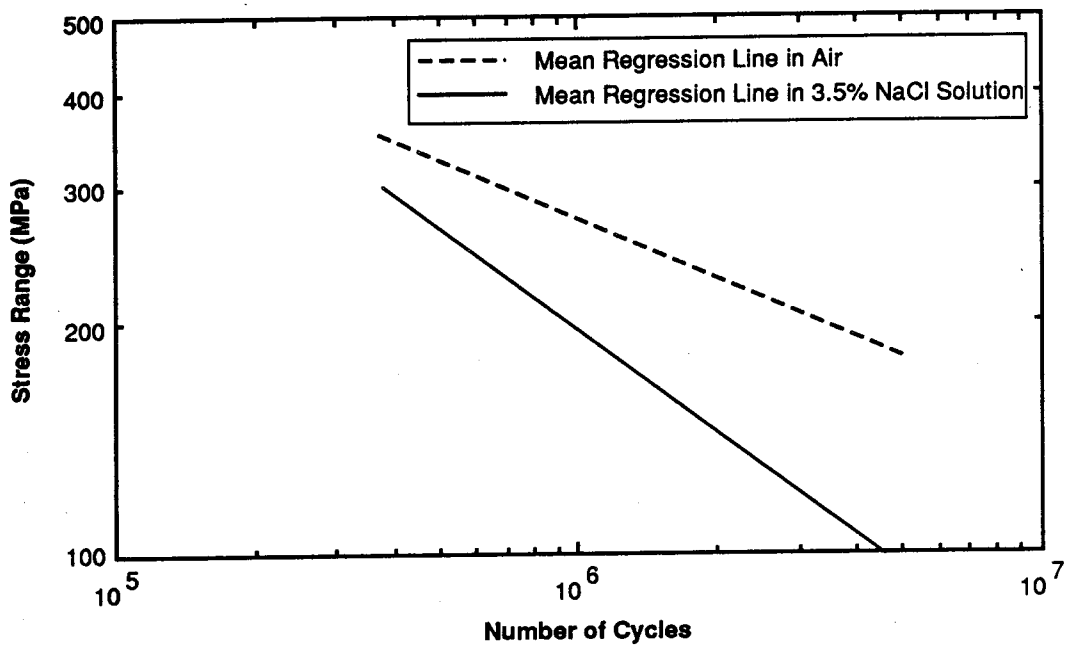

Figure 5.9 S-N Curves for Drill Pipe Tested in Air and a 3.5 Percent NaCl Solution (Mean Stress = 125 MPa)

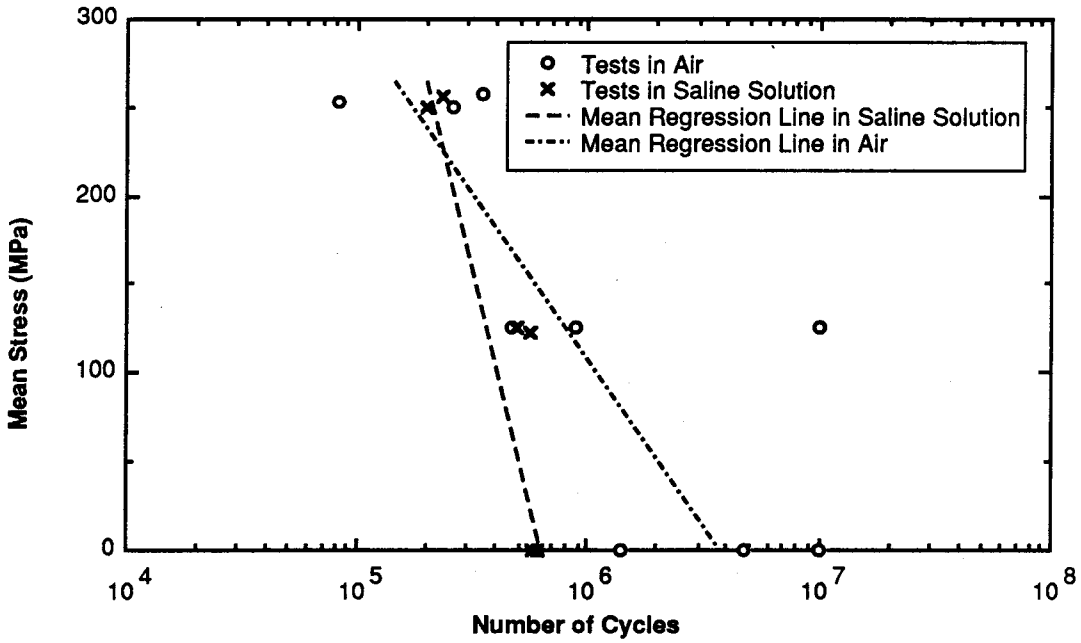

Figure 5.10 Effect of Mean Stress on Fatigue Life in Different Environments (Stress Range = 290 MPa)

Chapter 6

Comparison of Test Results With the Work of Other Investigators

6.1 Introduction

The work presented in the two foregoing chapters addressed the problem of fatigue of full size drill pipe acting under varying magnitude of mean stress and in either non-corrosive or corrosive environments. This chapter presents a comparison of the test results obtained in the present investigation with experimental and analytical work of other investigators. This comparison is made both to evaluate the work presented here in light of other work conducted in the same area, and also to attempt to pool the available fatigue data into one data base from which design guidelines can be formulated.

6.2 Fatigue of Drill Pipe in Air

6.2.1 Experimental Work of Bachman (1951)

Tests performed by Hughes Tool Company and presented by Bachman (1951) still represent a major contribution to the understanding of the fatigue strength of drill pipes. These tests were performed to assess the fatigue resistance of different types of tool joints. For this reason, the full-size test specimens took the form of cantilever beams tested in rotating bending. Thus, a severe loading condition was created at the tool joint. All the tests presented by Bachman (1951) were performed in air and without the presence of a superimposed axial load.

Regression analysis performed on the test data presented by Bachman gives the following expression for the fatigue life (see Appendix F for a listing of the test data and details of the regression analysis)

$$\log N = 12.99 - 2.80 \log S_r \qquad (6\text{-}1)$$

where N is expressed in loading cycles and S_r is the stress range expressed in MPa. The coefficient of determination was calculated to be 0.35. The standard error of the estimate, calculated using Eq. (5-6), is 0.21.

In order to compare the regression line obtained in the test program reported herein with the regression line fitted to Bachman's data, the regression line given by Eq. (5-15)

can be used if the mean stress is set to zero. Equation (5-2), which expresses the effect of stress range on fatigue life cannot be used because the data reported in the literature were obtained under a mean stress of zero while the data from which Eq. (5-2) was derived applies to tests conducted under a mean stress of 125 MPa. For a mean stress of zero, the fatigue life of the test specimens used in the current test program can be expressed from Eq. (5-15) as

$$\log N = 14.8 - 3.46 \log S_r \tag{6-2}$$

The standard error of the estimate for Eq. (6-2) is assumed to be the same as for the model of Eq. (5-15) , that is 0.50. The test data and regression line from Bachman's work are presented in Figure 6.1 along with Eq. (6-2).

An analysis of covariance is used to compare regression lines from Eq. (6-1) and Eq. (6-2). Comparison of two regression lines involves three steps: (1) testing whether the variance about the separate lines may be considered as homogeneous; (2) testing whether the two regression lines may be regarded as parallel; and (3) testing whether the two parallel lines may be considered colinear (Little and Jebe, 1975).

In order to test homogeneity of the variance about separate lines, the variance ratio test, or F test, is used. The F ratio may be calculated as (Little and Jebe, 1975)

$$F = \frac{s_{e_1}^2}{s_{e_2}^2} \tag{6-3}$$

where $s_{e_1} > s_{e_2}$ and are the standard error of the estimate for the regression lines. The calculated F value is compared to a tabulated F value associated with degrees of freedom $n_1 - 2$ and $n_2 - 2$. For comparison with Bachman's data and the data from this test program, the calculated F value is 5.44. For $n_1 - 2 = 26$ and $n_2 - 2 = 85$ and a 5.0 percent level of significance, the tabulated F value is 1.64. Therefore it may be concluded, with a probability of error of 5 percent, that s_{e_1} and s_{e_2} are not independent estimates of the same population standard error of estimate, that is, the test data presented by Bachman and the test data presented in Chapter 4 do not belong to the same population. It can therefore be concluded that significant change has taken place in the quality of drill pipe since the work presented by Bachman was performed. The drill pipes tested by Bachman failed both in the tool joint area and in the pipe body. Some of the test specimens used in Bachman's work had a pipe body with increased wall thickness in order to prevent failures in the drill

pipe body. Present day drill pipe is not comparable to drill pipe manufactured prior to the early fifties, the time at which the drill pipes used in the investigation presented by Bachman were manufactured.

6.2.2 Experimental Work of the Chinese Petroleum Standardization Committee (1987)

The Chinese Petroleum Standardization Committee (1987) presented the results of an investigation of the effect of the geometry of the transition zone between the pipe upset and the pipe body. Full-size drill pipes of Grade S-135 with a transition zone of varying length and radius were tested in air as cantilever rotating beams. No axial load was present.

A total of 16 test results were presented (Chinese Petroleum Standardization Committee, 1987). A least square regression analysis of the test data gives the following expression for the fatigue life

$$\log N = 16.90 - 4.32 \log S_r \tag{6-4}$$

The standard error of the estimate was calculated to be 0.640. The test data and the regression line from the Chinese Petroleum Standardization Committee's work are presented in Figure 6.2 along with Eq. (6-2). Using the variance ratio test to compare the test results presented in Chapter 4 with the test results presented by the Chinese Petroleum Standardization Committee results in calculated F ratio of 1.71. The tabulated F value for $n_1 - 2 = 14$ and $n_2 - 2 = 26$ and a 5 percent level of significance is 2.10. Therefore it can be concluded, with a risk of error of 5.0 percent, that the standard error of estimate for both sets of test data are both independent estimates of the population standard error of estimate.

The standard error of estimate from both sets of data (s_{e_1}, n_1 and s_{e_2}, n_2) may be pooled to form a more precise estimate of the population standard error of estimate, s_e. The estimate of the population variance is given as (Little and Jebe, 1975)

$$s_e^2 = \frac{(n_1 - 2)\, s_{e_1}^2 + (n_2 - 2)\, s_{e_2}^2}{(n_1 - 2) + (n_2 - 2)} \tag{6-5}$$

Pooling of the data presented by the Chinese Petroleum Standardization Committee and the data obtained in this study yields a value of standard error of estimate of 0.56.

In order to test whether the slopes of both regression lines are the same, Student's t test is performed where the t value takes the form (Little and Jebe, 1975)

$$t = \frac{|b_1 - b_2|}{s_e \sqrt{\frac{1}{\sum(x_{1_i} - \bar{x}_1)^2 + \sum(x_{2_i} - \bar{x}_2)^2}}} \qquad (6\text{-}6)$$

where b_1 and b_2 are the slopes for regression lines fitted to the first and second sets of data, s_e is the standard error of estimate of the pooled data (given by Eq. (6-5)), x_{1_i} and x_{2_i} are the individual x values (log Sr) for the first and second sets of data, and $\bar{x}_1$ and $\bar{x}_2$ are the mean values of x. The number of degrees of freedom is given as $[(n_1 - 2) + (n_2 - 2) + 1]$. The calculated t value for the two sets of data is 0.70. For a 5.0 percent level of significance, the tabulated t value is 2.02. This indicates that, with a probability of error of 5.0 percent, the two slopes are a common estimate of the true slope of the regression line for the population. A common estimate of the slope may therefore be obtained by forming a weighted average of the slopes of the two regression lines as follows (Little and Jebe, 1975)

$$\bar{b} = \frac{b_1 \sum(x_{1_i} - \bar{x}_1)^2 + b_2 \sum(x_{2_i} - \bar{x}_2)^2}{\sum(x_{1_i} - \bar{x}_1)^2 + \sum(x_{2_i} - \bar{x}_2)^2} \qquad (6\text{-}7)$$

with a resulting estimated variance of $\bar{b}$ given as (Little and Jebe, 1975)

$$s_{\bar{b}}^2 = \frac{s_e^2}{\sum(x_{1_i} - \bar{x}_1)^2 + \sum(x_{2_i} - \bar{x}_2)^2} \qquad (6\text{-}8)$$

All the terms in Eq.(6-7) and Eq. (6-8) have been defined previously. The variance of the pooled data, s_e^2, has been calculated from Eq. (6-5) to be 0.56. Using Eq. (6-7) and Eq. (6-8), the new pooled estimate of the regression slope, $\bar{b}$, and the variance of the slope, $s_{\bar{b}}^2$, are -3.53 and 1.52, respectively.

Whether the two parallel lines are identical, i.e., have both the same slope and same intercept can now be examined. In order to test whether the difference between the lines intercept is significant, the following t value is calculated (Little and Jebe, 1975)

$$t = \frac{\left|(\bar{y}_1 - \bar{y}_2) - \bar{b}\,(\bar{x}_1 - \bar{x}_2)\right|}{s_e \sqrt{\frac{1}{n_1} + \frac{1}{n_2} + \frac{(\bar{x}_1 - \bar{x}_2)^2}{\sum(x_{1_i} - \bar{x}_1)^2 + \sum(x_{2_i} - \bar{x}_2)^2}}} \qquad (6\text{-}9)$$

where the numerator is the difference between the line intercepts of the two regression lines and the denominator is the corresponding standard deviation. The terms $\bar{y}$, $\bar{x}$, x_i, and n are the mean value of y (log N), the mean value of x (log S_r), individual values of x, and the sample size, respectively. The subscripts 1 and 2 refer to values associated to the first and second regression lines. The number of degrees of freedom is $[(n_1 - 2) + (n_2 - 2) + 1]$. The calculated t value from Eq. (6-9) is 2.66 and the tabulated t value for a 5.0 percent level of significance is 2.02. It can be concluded, with a level of confidence of 95 percent, that the two regression lines are not colinear. In other words, after comparison of the test data presented by the Chinese Petroleum Standardization Committee with the test data presented in Chapter 4, significant difference has been found, and therefore the two sets of data cannot be pooled into one set. The test data presented by the Chinese Petroleum Standardization Committee show a longer fatigue life than the specimens tested in the test program reported herein. This higher fatigue strength observed in the test data presented by the Chinese Petroleum Standardization Committee can be attributed to the higher grade steel used for their test specimens and probably the different upset geometry that was investigated.

6.2.3 Analytical Work of Kral et al. (1984)

The only attempt at using linear elastic fracture mechanics to predict fatigue life of drill pipe presented in the open literature was presented by Kral et al. (1984). The investigators made use of a simple flat plate model of finite width, w, equal to the average of the inner and outer circumference of the pipe. The Paris crack growth law was used to estimate the fatigue life of the plate with an initial semi-elliptical surface crack with geometry as shown in Figure 6.3 (a). An aspect ratio, c/a, of 0.5 was assumed in the calculations.

The initial part-through crack is assumed to grow until it reaches a critical crack size, where unstable crack growth takes place, or until the crack front reaches the back surface of the plate. Propagation of the part-through crack is assumed to take place at a constant crack aspect ratio, c/a.

Once the crack front has reached the back surface, the part-through crack is assumed to immediately become a through-thickness crack of length 2a equal to four times the wall thickness. The through-thickness crack then propagates until it reaches its critical size. The fracture mechanics approach presented by Kral et al. (1984) is outlined below with few changes made to the notation. Equations (6-11) to (6-18) are all well established relations that can be found in standard references on fracture mechanics (Broek, 1986).

The total fatigue life of the drill pipe is given by

$$N_f = N_P + N_T \tag{6-10}$$

where N_P is the part of the fatigue life expended to propagate the part-through crack to critical size or to the back surface of the plate, whichever is smallest. N_T is the part of the fatigue life expended to propagate a through-thickness crack to critical size. The fatigue life N_P is expressed as

$$N_P = \int_{c_i}^{c_f} \frac{dc}{A\,(\Delta K_P)^n} \tag{6-11}$$

where c_i is the initial crack size, assumed to be 0.795 mm, and c_f is the final part-through crack size, taken as the smallest of the critical crack size at onset of unstable crack propagation or the plate thickness. A and n are material-dependent constants and ΔK_P is the range of stress intensity factor for a part-through crack, given as

$$\Delta K_p = 1.12\, S_r \sqrt{\frac{\pi\, c}{Q}} \tag{6-12}$$

where the factor 1.12 is the free surface correction factor, S_r is the stress range (taken as the difference between the maximum and minimum bending stress in a cycle), c is the part-through crack size as shown in Figure 6.3(a), and Q is a crack shape correction factor given as

$$Q = \sqrt{\phi^2 - 0.212 \left(\frac{\sigma_{max}}{\sigma_Y}\right)^2} \tag{6-13}$$

where σ_{max} is the maximum stress in a loading cycle, σ_Y is the static yield strength of the plate material, and ϕ is a crack geometry factor given as

$$\phi = \frac{3\pi}{8} + \frac{\pi}{8}\left(\frac{c}{a}\right)^2 \tag{6-14}$$

where a and c are as defined in Figure 6.3.

The fatigue life expended to propagate a through-thickness crack to critical size is given by

$$N_T = \int_{a_i}^{a_{cr}} \frac{da}{A\,(\Delta K_T)^n} \tag{6-15}$$

where a_i is the initial crack size equal to twice the wall thickness for a part-through crack aspect ratio of 0.5 and a_{cr} is the crack size at onset of unstable crack propagation. A and n take the same values as in Eq. (6-11) and ΔK_T is the range of stress intensity factor for a through-thickness crack, expressed as

$$\Delta K_T = S_r \sqrt{\pi\, a}\left(\frac{w}{\pi\, a}\tan\frac{\pi\, a}{w}\right)^{\frac{1}{2}} \tag{6-16}$$

The term in brackets is a correction factor that accounts for the finite width, w, of the plate. It can be recalled that Kral et al. (1984) used a width equal to the average of the inner and outer circumference of the drill pipe.

The critical crack size for a part-through crack can be calculated from Eq. (6-12), where K_{Ic}, the critical crack intensity factor, is substituted for ΔK and the maximum stress, σ_{max}, is substituted for the stress range S_r. The critical part-through crack size can thus be expressed as

$$c_{cr} = \left(\frac{K_{Ic}}{1.12\,\sigma_{max}}\right)^2 \frac{Q}{\pi} \tag{6-17}$$

where Q is given by Eq. (6-13). If c_{cr} given by Eq. (6-17) is greater than the pipe wall thickness, the final crack size to be used in Eq. (6-11), c_f, is taken equal to the wall thickness.

In a similar fashion, the size of the critical through-thickness crack can be obtained from Eq. (6-16) if the fracture toughness, K_{Ic}, is substituted for ΔK, and σ_{max} is

substituted for the stress range, S_r. The critical through-thickness crack size can thus be obtained as

$$a_{cr} = \frac{w}{\pi} \tan^{-1}\left(\frac{K_{Ic}}{\sqrt{w}\,\sigma_{max}}\right)^2 \qquad (6\text{-}18)$$

If a_{cr} given by Eq. (6-18) is less than the initial through-thickness crack size, then the crack would become unstable as soon as the part-through crack front reaches the back surface.

Kral et al. (1984) have used the method presented above for fatigue life calculation of a limited number of hypothetical cases. Values of K_{Ic}, A, and n of 61.5 MPa$\sqrt{m}$, 1.157×10^{-12}, and 3.16 (for da/dN expressed in m/cycle), respectively, were used. Those values, obtained from the open literature by Kral et al. (1984), are values suggested for AISI 4140 steel quenched and tempered to a yield strength of 620 MPa. Corresponding values for Grade E drill pipe steel have not been reported in the literature.

The method proposed by Kral et al. (1984) to calculate the fatigue life of drill pipe has been used to calculate the fatigue life at various stress ranges from 150 MPa and 350 MPa. The same assumptions with respect to initial crack size and geometry and material properties were used. A computer spread sheet was used to calculate the fatigue life at various stress ranges. Table 6.1 shows a sample spread sheet used to obtain the fatigue life at various stress ranges for a mean stress condition of 125 MPa. (The mean stress of 125 MPa was selected for the calculations presented in Table 6.1 in order to be able to compare the results with the test results presented in Chapter 4).

Columns (1) and (2) of Table 6.1 list the stress range and mean stress from which the maximum stress in a loading cycle is calculated. The first part of the table deals with propagation of a part-through crack. In column (4) the crack shape correction factor for a part-through crack is calculated using Eq. (6-13). Column (5) presents the critical crack size obtained from Eq.(6-17). Column (6) presents the fatigue life estimated using the smallest of c_{cr} in column (5) or the wall thickness in Eq. (6-11). The total stress range was used in the calculation, although part of the loading cycle might have been in compression.

The second part of the spread sheet deals with a through-thickness crack of initial size equal to

$$a_i = a/c \times t \qquad (6\text{-}19)$$

where a/c is the assumed crack aspect ratio and t is the drill pipe wall thickness. The critical through-thickness crack size, a_{cr}, calculated from Eq. (6-18) is presented in column (7) of Table 6.1. The fatigue life expended in propagating the through-thickness crack of size a_i given by Eq. (6-19) to the critical size is calculated using Eq. (6-15). If the predicted critical crack size is smaller than the initial crack size given by Eq. (6-19), then the fatigue life expended to propagate the through-thickness crack is set to zero. The fatigue life, N_T, is tabulated in Column (8). Finally, the total fatigue life is tablulated in column (9). It is the sum of the values in column (5) and column (8).

Examination of Table 6.1 shows that the portion of the total fatigue life expended to propagate the through-thickness crack to critical size is small compared to the portion expended to propagate a part-through crack through the wall thickness. At a stress range of 150 MPa, over 95 percent of the total fatigue life is expended in propagating the part-through thickness crack through the plate thickness. As the stress range increases, the portion of the total fatigue life remaining after a leak occurs (the part-through crack reaching the back surface of the plate) decreases. According to the sample calculation presented in Table 6.1 it is seen that when the stress range in the pipe model reaches 260 MPa the contribution of the through-thickness crack propagation to the total life is zero. This suggests that sudden failure by rapid crack growth would occur at the instant the part-through crack reaches the back surface of the plate and becomes a through-thickness crack. For a drill pipe in this condition, this means that twist-off would occur at the instant a washout is detected. This is an undesirable situation since fatigue cracks in drill pipe are often detected only when the fatigue crack has propagated through the wall thickness, resulting in a washout detected by a loss in mud pressure during the drilling operation.

Using the fracture mechanics model presented by Kral et al. (1984), the fatigue life of drill pipe was calculated for values of crack aspect ratio, c/a, varying from 0.2 to 1.0. The resulting curves are presented in Figure 6.4 along with the test results obtained at a mean stress of 125 MPa. It can be seen that as the crack aspect ratio is increased the predicted fatigue life increases. It is also noted that the predicted S-N curves have a slope very close to the calculated regression curve for the test results. However, the predicted fatigue life values are generally low in comparison with the test values, with a lower bound on the test results obtained for a crack aspect ratio of 0.2.

6.2.4 Effect of Mean Stress on Fatigue Life in Air

The effect of mean stress on fatigue life was not considered in the work of Kral et al. (1984) because the Paris crack growth model ignores the effect of mean stress on fatigue life. In order to account for the mean stress using Paris equation, different values of crack propagation rate constants should be used for different mean stresses. A commonly used crack growth equation that depicts mean stress effects is the Forman equation (Forman et al., 1967)

$$\frac{da}{dN} = \frac{\alpha\,(\Delta K)^m}{(1 - R)\,K_c - \Delta K} \tag{6-20}$$

where α and m are crack growth rate constants determined experimentally, K_c is the applicable fracture toughness for the material and thickness, ΔK is the range of stress intensity factor, and R is the ratio of minimum stress to maximum stress in a loading cycle. Forman's equation is a modification of the Paris equation that attempts to account for the fact that as the cyclic stress intensity factor approaches some critical value, K_c, the growth rate increases beyond the linear behaviour suggested by the Paris equation. The Forman equation shows that the growth rate depends on the cyclic stress ratio, R, and should therefore apply for all values of R.

Values of the crack growth rate constants, α and m, for Grade E steel are not available in the open literature. However, noting that fatigue crack growth data are usually referenced to the pulsating tension condition with R = 0 or approximately zero (Fuchs and Stephens, 1980), Forman's equation can be calibrated from the Paris equation for which the crack growth rate constants are known. To obtain the value of α and m in Forman's equation, Eq. (6-20) is rewritten as

$$\log\left\{[(1 - R)\,K_c - \Delta K]\,\frac{da}{dN}\right\} = \log\alpha + m\,\log\Delta K \tag{6-21}$$

This represents the equation of a straight line for $\log\{[(1 - R)\,K_c - \Delta K]\,da/dN\}$ versus $\log\Delta K$. Values of $\{[(1 - R)\,K_c - \Delta K]\,da/dN\}$ were calculated for different values of ΔK and corresponding da/dN given by the Paris equation. For K_c equal to $K_{Ic} = 61.5\ MPa\sqrt{m}$ and R = 0, the relation between $\{[(1 - R)\,K_c - \Delta K]\,da/dN\}$ and ΔK is as shown in Figure 6.5. When plotted on logarithmic scales, the curve is seen to be straight for values of ΔK up to about 30 $MPa\sqrt{m}$. Assuming that the curve in Figure 6.5 will remain a straight line

when R takes values other than zero, Eq. (6-21) can be fitted to the straight line portion of the curve. This yields values of α and m equal to 1.69×10^{-10} and 2.78, respectively.

Using Forman's model for crack growth, the fatigue life expended to propagate the part-through crack to critical size or to the back surface of the plate can be expressed as

$$N_P = \int_{c_i}^{c_f} \frac{(1 - R)\, K_c - \Delta K_P}{\alpha\, (\Delta K_P)^m}\, dc \qquad (6\text{-}22)$$

where c_i is the initial crack size and c_f the final part-through crack size corresponding to the the critical crack size given by Eq. (6-17) or to the pipe wall thickness, whichever is least. The range of stress intensity factor, ΔK_P, is given by Eq. (6-12) for a drill pipe modeled by a uniformly loaded flat plate.

The fatigue life expended to propagate a through-thickness crack to critical size is expressed as

$$N_T = \int_{a_i}^{a_f} \frac{(1 - R)\, K_c - \Delta K_T}{\alpha\, (\Delta K_T)^m}\, da \qquad (6\text{-}23)$$

where the range of stress intensity factor for a through thickness crack, ΔK_T, is given by Eq. (6-16). If the critical crack size is smaller than the initial crack size obtained from Eq. (6-18), then unstable fracture takes place at the instant the part-through crack becomes a through-thickness crack. The total fatigue life is obtained by summing N_P given by Eq. (6-21) and N_T given by Eq. (6-22).

The effect of mean stress on fatigue life in air has also been investigated experimentally on small samples of different materials. As a result of those investigations, expressions have been proposed to predict the change in fatigue strength as a result of a change in mean stress. Some of those empirical expressions are presented by Fuchs and Stephens (1980) as follows:

Modified Goodman equation $$\frac{S_a}{S_f} + \frac{S_m}{S_U} = 1 \qquad (6\text{-}24)$$

Gerber equation $$\frac{S_a}{S_f} + \left(\frac{S_m}{S_U}\right)^2 = 1 \qquad (6\text{-}25)$$

Soderberg equation $$\frac{S_a}{S_f} + \frac{S_m}{S_Y} = 1 \qquad (6\text{-}26)$$

where S_a is the alternating stress equal to half of the stress range, S_r. S_f is the fully reversed fatigue strength, S_m is the mean stress, and S_U and S_Y are the tensile strength and the yield strength of the material, respectively.

Equations (6-24) to (6-26) give a prediction of the fatigue strength (stress amplitude for a fixed number of cycles to failure) as a function of the mean stress. In contrast, the experimental program presented in Chapter 4 resulted in prediction of fatigue life in number of loading cycles as a function of the mean stress. In order to obtain the change in fatigue life at a fixed stress amplitude as a result of a change of mean stress from equations (6-24) to (6-26), the following transformations were implemented.

The S-N curve obtained in the experimental program and given by Eq.(5-2) is used as a reference fatigue curve from which a reference fatigue life, N_{ref}, is obtained for the reference stress range, S_{ref}, at which the mean stress effect is investigated. It can be recalled that Eq. (5-2) applies for a mean stress of 125 MPa. The fully reversed fatigue strength, S_f, can be obtained from transformation of equations (6-24) to (6-26) in the following forms:

For the Goodman line, $$S_f = \frac{S_a}{1 - \frac{S_m}{S_U}} \qquad (6\text{-}27)$$

for the Gerber line, $$S_f = \frac{S_a}{1 - \left(\frac{S_m}{S_U}\right)^2} \qquad (6\text{-}28)$$

and for the Soderberg line, $$S_f = \frac{S_a}{1 - \frac{S_m}{S_Y}} \qquad (6\text{-}27)$$

Since the experimental S-N curve described by Eq. (5-2) is used as a reference curve, the mean stress S_m in equations (6-27) to (6-29) is taken as 125 MPa. The stress amplitude, S_a, is set to 145 MPa in order to compare the predicted effect of mean stress with the results obtained in the experimental program presented in Chapter 4. It can be recalled that the effect of mean stress was investigated experimentally at a stress range of 290 MPa, which corresponds to a stress amplitude of 145 MPa.

Once the fully reversed fatigue strength has been obtained for the stress amplitude under investigation, the reduced stress amplitudes at the reference fatigue life, N_{ref}, can be obtained for various values of mean stress. For example, referring to Figure 6.6, the reduced stress amplitude S_{r1} is obtained for a mean stress of S_{m1}. Assuming that S-N curves for different mean stresses are parallel, the S-N curve for mean stress S_{m1} can easily be obtained from which the reduced fatigue life N_1 at the reference stress range can be obtained as (refer to Figure 6.6)

$$\log N_1 = \log N_{ref} - b (\log S_{ref} - \log S_{r1}) \qquad (6\text{-}30)$$

where N_{ref} and S_{ref} are the reference fatigue life and the corresponding reference stress range obtained from Eq. (5-2). The constant b is the slope of the regression line presented in Eq. (5-2) and S_{r1} is the reduced stress range (equal to twice the stress amplitude determined from Eq. (6-24), Eq. (6-25), or Eq. (6-26)).

The procedure outlined above was used to calculate the fatigue life at various mean stress values ranging from 0 to 250 MPa. The resulting curves are presented in Figure 6.7, where the square of the mean stress is plotted against the logarithm of the fatigue life. Figure 6.7 also presents curves derived using the Forman model presented above. Two different initial crack sizes, c_i,were used in the Forman model, namely 0.795 mm, used by Kral et al. (1984), and 12.5 percent of the wall thickness, which corresponds to the crack size above which a drill pipe would be rejected during inspection. The test results presented in Chapter 4 and the mean regression line for the test results are also shown in Figure 6.7 for comparison. In general, all the models are more conservative at low values of mean stress. The Forman model is seen to be the most conservative model, although this may be partly due to the fact that appropriate values of crack growth rate constants, α and m, were not available. By comparing the slope of the various prediction models presented in Figure 6.6, it can be seen that the Gerber equation is the one that predicts the smallest sensitivity of the fatigue life to the mean stress.

6.2.5 Analytical Work of Raju and Newman (1984)

Raju and Newman (1984) presented stress intensity factors for a wide range of nearly semi-elliptical surface cracks in circular pipes subjected to either tension or bending loads. A three-dimensional finite element analysis was used to calculate the Mode I stress intensity factor for a part-through thickness crack geometry as shown in Figure 6.8.

The stress intensity factor K_P at the end of the minor axis of a part-through crack in a pipe subjected to bending was given as (Raju and Newman, 1984)

$$K_P = S_b \sqrt{\pi \frac{c}{Q}}\, F \tag{6-31}$$

where S_b is the bending stress calculated at the outer surface of the pipe without the crack being present, c is the crack depth as shown in Figure 6.8, and Q is the shape factor for an ellipse, given as (Raju and Newman, 1984)

$$Q = 1 + 1.464\left(\frac{c}{a}\right)^{1.65} \tag{6-32}$$

The boundary correction factor, F, was calculated for various combinations of parameters (c/t, c/a, R/t) and was presented in tabular form. Examination of tabulated F values from Raju and Newman indicated that an almost linear relation exists between the ratio of crack depth to wall thickness and the boundary correction factor. A linear relationship was also found to exist between the crack aspect ratio, c/a, and the boundary correction factor. Although the relation between R/t, ratio of pipe inner radius to wall thickness, and F was found to be non-linear, linear interpolation was used to obtain the boundary correction factor for a value of R/t = 5, representative of a 114 mm diameter drill pipe. The linear interpolation was performed between R/t = 4 and R/t = 10, for which values of boundary correction factors were given. The error introduced by interpolating linearly is believed to be small since the change in F value as R/t increases from 4 to 10 is only about 4.0 percent of its value.

For a value of c/a of 0.5, and R/t of 5.0, the boundary correction factor can be closely approximated by

$$F = 1.032 + 0.158\left(\frac{c}{t}\right) \tag{6-33}$$

This equation is needed to update the value of the boundary correction factor as c, the crack depth, increases in fatigue life calculation. For constant amplitude stress cycling, the range of stress intensity factor for a part-through crack is obtained by rewriting Eq. (6-31) as

$$\Delta K_P = S_r \sqrt{\pi \frac{c}{Q}} F \qquad (6\text{-}34)$$

where the stress range, S_r, has been substituted for the bending stress.

The fatigue life expended to grow a part-through crack through the pipe wall can be estimated by using either the Paris model, given by Eq. (6-11), or by the Forman model, given by Eq. (6-21). After the crack has reached the back surface it is assumed that the crack instantaneously becomes a through-thickness crack. Since no solution for the stress intensity factor for a through-thickness crack in a pipe was found in the literature, the fatigue life expended in propagating a through-thickness crack was approximated by the flat plate model proposed by Kral et al. (1984) with ΔK_T given by Eq. (6-16). This assumption is believed to result in only small error since it was found that the fatigue life remaining after the surface crack has become a through-thickness represents less than 5.0 percent of the total fatigue life for the cases investigated herein.

Table 6.2 presents the predicted fatigue life for the test specimens tested in air using the models presented above. Four different models were used to predict the fatigue life of the test specimens in air. Model 1 consisted of the flat plate model presented by Kral et al. (1984) in conjunction with Paris crack growth law. Model 2 consisted of the flat plate model used in conjunction with Forman's crack growth law. The circular pipe with a surface flaw model developed by Raju and Newman (1984) was used with Paris crack growth law in Model 3 and with Forman's crack growth law in Model 4. The ratio of measured to predicted fatigue life was calculated for every predicted value. The ratio varied from a minimum of 0.3 to a maximum of 58. The average of the ratio of measured to predicted fatigue life was 9.4, 9.8, 6.6, and 6.6 for Model 1, 2, 3, and 4, respectively. It can be seen that both Paris model and Forman model err by about the same amount on the average. Since the models used here were not developed to predict the fatigue life at stress ranges approaching the endurance limit, it is to be expected that the ratio of measured to predicted fatigue life will be large for the specimens which experienced a fatigue life in excess of 10 million cycles of loading. Figure 6.9 shows a comparison of the same four models with the mean regression line obtained from the test specimens tested at a mean stress of 125 MPa. It can be observed from the figure that the circular pipe model gives

better prediction of the fatigue life than the flat plate model. It can also be observed that the predicted fatigue life using Forman's crack growth law is less than the predicted values based on Paris crack growth law. This is the case for both the flat plate and circular pipe model. All four models used in this study yield predicted fatigue lives lower than the mean values obtained in the test program. A line located at two standard deviations from the mean regression line is also shown in Figure 6.9. All four fracture mechanics models lie within two standard deviations from the mean.

There are several sources of error which may account for the difference between the measured fatigue life and the predicted life using fracture mechanics models. The crack propagation rate constants, A and n for Paris model and α and m for the Forman model, were not specifically applicable to Grade E drill pipe steel. Instead, values of crack propagation rate constants for an AISI 4140 quenched and tempered steel were used for the predictions. Another important source of error is the portion of the total fatigue life spent to initiate a fatigue crack. Classical fracture mechanics approach predicts only the part of the fatigue life expended in propagating an existing crack. The part of the fatigue life spent to initiate the fatigue crack cannot be estimated using fracture mechanics although, for structures with geometries free of strong stress concentrators, the part of the fatigue life spent at initiating a fatigue crack can be significant. This factor is believed to contribute to the discrepancy between predicted and experimental values as well as to the large scatter observed in the test results. For test specimens where a crack might have existed prior to testing, a significant difference between predicted and measured fatigue life can also be introduced by varying the assumed value of initial crack size. Finally, as mentioned previously, when a test specimen is tested at a stress range close to its endurance limit, the fatigue life increases considerably for only a small decrease in stress range. This behaviour near the endurance limit was not considered in the fracture mechanics models used for the predictions.

6.3 Fatigue of Drill Pipe in Corrosive Environment

6.3.1 Experimental Work of Helbig and Vogt (1987)

Helbig and Vogt (1987) investigated the effect of heat treatment on Grades D, E, and S-135 drill pipe. Fatigue tests were performed on full-size sections of drill pipe body in corrosive environment. The test specimens were tested in rotating bending under four-point loading, thus creating a constant moment region. The corrosive fluid, circulated inside the test specimen, consisted of either tap water or a 20 percent NaCl solution. A

total of 38 full-size specimens were tested in tap water and 11 full-size specimens were tested in a 20 percent NaCl solution. All the tests presented by Helbig and Vogt were performed under zero mean stress.

Regression analysis performed on the test results obtained from the Helbig and Vogt tests in tap water gives the following fatigue life equation (see Appendix F for listing of test data and details of the regression analysis)

$$\log N = 11.24 - 2.28 \log S_r \tag{6-35}$$

where N and S_r are the fatigue life in cycles and the stress range in MPa, respectively. The coefficient of determination was calculated to be 0.618 and the standard error of the estimate is 0.292.

In order to compare the regression line obtained in the test program presented in Chapter 4 with the regression line given by Eq. (6-35), the regression line obtained for the combined effect of stress range and mean stress, Eq. (5-31), is used with the mean stress set to zero. The fatigue life of the test specimens used in the test program presented in Chapter 4 can be expressed as

$$\log N = 11.43 - 2.31 \log Sr \tag{6-36}$$

The standard error of the estimate for Eq. (6-36) is assumed to be the same as for the model of Eq. (5-31) from which Eq.(6-36) is obtained. Eq. (6-36) is presented in Figure 6.10, along with the test data obtained in tap water by Helbig and Vogt and the mean regression line given by Eq. (6-35).

Equations (6-35) and (6-36) can be compared using the analysis of covariance method outlined in section 6.2.1. The homogeneity of the variance about the lines of Eq. (6-35) and Eq.(6-36) is tested using the F test. The calculated F ratio given by Eq. (6-3) is 7.08 while the tabulated F value for a 5.0 percent level of significance is 2.23. Therefore, it can be concluded that the standard error of the estimate obtained from Helbig and Vogt data obtained in tap water is significantly different from the test data obtained in the investigation presented herein. The test data presented by Helbig and Vogt and the test data presented in Chapter 4 do not belong to the same population. However, from Figure 6.10, it can be seen that the regression lines for both sets of data are similar, and it can be shown that, statistically, they are not significantly different.

Regression analysis of the test data obtained by Helbig and Vogt in a 20 percent NaCl solution yields the following fatigue life equation

$$\log N = 11.20 - 2.26 \log S_r \tag{6-37}$$

The coefficient of determination was calculated to be 0.896 and the standard error of the estimate is 0.230. Comparison of Eq. (6-37) with Eq. (6-36) results in a calculated F ratio of 4.42. The tabulated F ratio for a 5 percent level of significance is 2.59. Therefore, the scatter for the test data obtained by Helbig and Vogt in a 20 percent NaCl solution is significantly larger than the scatter observed in the test data presented in Chapter 4. Again, comparing the mean regression line for Helbig and Vogt data with the mean regression line for the test data obtained in the test program presented herein, shows that both lines are similar (see Figure 6.11). However, because the standard error of the estimate for both sets of test data are different, the test data of Helbig and Vogt cannot be pooled with the test data presented in Chapter 4. The difference between the test results presented by Helbig and Vogt and the results of the investigation reported herein can be attributed to the differences between the conditions used in the two test programs. Helbig and Vogt investigated drill pipes of different grades. Although no significant difference was detected between the different grades investigated, it may have caused a greater scatter in the test results. The test frequency used by Helbig and Vogt was 100 rpm compared to 60 rpm used in the investigation reported herein. The corrosive environment used in the latter investigation was different from the environments used by Helbig and Vogt and, in addition, the corrosive environment in Helbig and Vogt's test program was acting on the inner surface of the test specimens.

6.3.2 Experimental Work of Joosten et al. (1985)

Joosten et al. (1985) tested 0.9 m lengths of 89 mm diameter grade G-105 drill pipe loaded in three-point bending. Tests were carried out in a potassium chloride - seawater solution maintained at 38° C. The test frequency was not reported. Since the tests were performed under cyclic bending, the mean stress may have varied with the stress range. The mean stress for each test was not reported. Regression analysis of the test data presented by Joosten et al. results in the following expression for the fatigue life (see Appendix F for listing of the test data presented by Joosten el al.)

$$\log N = 10.21 - 2.14 \log S_r \tag{6-38}$$

The standard error of the estimate was calculated to be 0.208 for the nine test results reported by Joosten et al. (1985).

The results presented by Joosten et al. are compared with the results presented in this investigation using equation (5-18), obtained at a mean stress of 125 MPa and stress ranges varying from 290 MPa to 90 MPa. An analysis of covariance is performed to compare the regression line presented in Eq. (6-37) with the regression line of Eq. (5-18). The homogeneity of the variance about the lines of Eq. (6-37) and Eq.(5-18) is tested using the F test. The calculated F ratio given by Eq. (6-3) is 2.99 while the tabulated F value for a 5.0 percent level of significance is 3.79. Therefore it can be concluded that the standard error of the estimate from Joosten's data and from the data obtained in this test program are independent estimates of the same population standard error of the estimate, that is to say, the test data presented herein and the test data presented by Joosten et al. belong to the same population. Using Eq. (6-5) the standard error of the pooled data becomes 0.170

The t test is used to check whether the slope of Eq. (6-38) is equal to the slope of Eq. (5-18). The calculated t value using Eq. (6-6) is 0.77. For a level of significance of 5.0 percent and a number of degrees of freedom of 15, the tabulated t value is 2.13. The two slopes are therefore a common estimate of the true slope of the regression line for the population. The final check in comparing the two regression lines is to check the significance of the difference between the line intercepts. The value of t calculated from Eq. (6-9) is 8.56 and the tabulated t value for a 5.0 percent level of significance and number of degrees of freedom of 15 is 2.13. This indicates that there is a significant difference between the two regression line intercepts. The fatigue lives obtained from the specimens tested by Joosten et al. are significantly lower than the fatigue lives measured in the present investigation. This can be observed in the plot of stress range versus fatigue life shown in Figure 6.12. This discrepancy between the two test programs may be explained by the different grades of steel used and also by the different corrosive environments employed. Adequate consideration of the effect of mean stress could not be taken into account since the mean stress was not reported in the work of Joosten et al. In addition, it is likely that the test frequency was different for the two test programs.

6.4 Evaluation of Present Fatigue Design Guidelines

6.4.1 Effect of Stress Range and Mean Stress on Fatigue Life

The present guidelines for fatigue design of drill pipe (American Petroleum Institute, 1988) have evolved from work presented by Lubinski (1961) and Hansford and Lubinski (1964, 1966). Their analytical work made use of the experimental fatigue data presented earlier by Bachman (1951). A lower bound curve on the test data presented by Bachman was used for the prediction of fatigue life (Lubinski, 1961). The experiments presented by Bachman were satisfactory for their intended use, namely testing of tool joint welds. However, they were neither performed in a corrosive environment nor under axial tension, two factors considered important in the fatigue life. The S-N curve used by Lubinski (1961) and later by Hansford and Lubinski (1964, 1966) for their analytical work in a non-corrosive environment took the following form

$$\log N = 17.13 - 4.56 \log S_r \tag{6-38}$$

where N is the fatigue life expressed in loading cycles and S_r is the stress range in MPa. The endurance limit was set at 248 MPa for drill pipe operating in a non-corrosive environment (Lubinski, 1961).

A modified Goodman diagram was used to account for the effect of the mean stress (Lubinski, 1961). The standard Goodman diagram, expressed by Eq. (6-24), takes the form of a straight line when the stress range is plotted against the mean stress. In the modified version of the Goodman diagram, Lubinski (1961) assumed a reduction of the stress range at a low mean stress in order to make allowance for the presence of slip marks on the drill pipe body. This reduction corresponds to approximately 18 percent of the stress range under zero mean stress used in the standard Goodman diagram. The fatigue curve, corresponding to a lower bound of the test results presented by Bachman (1951), therefore is lowered by 18 percent to account for the detrimental effect of slip marks on the surface of the drill pipe. In addition, a cut-off on the mean stress was assumed at 460 MPa, where the fatigue strength was assumed to be 11 percent larger than the fatigue strength predicted from the Goodman diagram (see Figure 6.13). A quadratic curve was used to interpolate between the point at zero mean stress and the point at a mean stress of 460 MPa. Figure 6.13 shows a graphical representation of the Goodman diagram and the modified interaction diagram proposed by Lubinski (1961). A tensile strength of 690 MPa

was used in the analytical work presented by Lubinski (1961). Therefore, the nonlinear portion of their interaction equation, at the endurance limit, can be expressed as

$$S_r = 249 - 0.156\,S_m - 3.072\text{x}10^{-4}\,S_m^2 \qquad (6\text{-}39)$$

where S_r and S_m are the stress range and the mean stress, respectively, expressed in MPa.

The curves presented in Figure 6.13 represent the effect of mean stress on the endurance limit for Grade E drill pipe. For stress range levels above the endurance limit the standard Goodman diagram was used (Hansford and Lubinski, 1964). The Goodman interaction equation illustrated in Figure 6.13 can be expressed as

$$S_f = S_a\left(\frac{S_u}{S_u - S_m}\right) \qquad (6\text{-}40)$$

where S_a is the stress range acting with the mean stress S_m, S_f is an equivalent fully reversed fatigue stress range (i.e. stress range under zero mean stress which yields the same fatigue life as the stress range S_a acting with the mean stress S_m), and S_u is the tensile strength of the material. The term in brackets is the correction factor presented by Hansford and Lubinski (1964). The reduced fatigue life is obtained by using the equivalent fully reversed stress range, given by Eq. (6-40), into the fatigue life eqation (6-38).

Fatigue curves for different mean stress levels can be obtained by using Eq.(6-40). Figure 6.14 presents a comparison of the fatigue test results presented in Chapter 4 with S-N curves obtained using Eq. (6-40) and Eq. (6-38). Three different S-N curves are presented, namely, one for a mean stress of 250 MPa , one for a mean stress of 125 MPa, and one for the fully reversed bending condition, for which the mean stress is zero. Of the 20 test results, obtained at a mean stress of 125 MPa in a non-corrosive environment, eight are found to lie below the S-N curve used by Lubinski (1961) for a mean stress of 125 MPa. This indicates that, despite the fact that the fatigue curve used by Lubinski represents a lower bound to fatigue test results presented by Bachman (1951) and a further reduction of 18 percent to account for the detrimental effect of slip marks, the curve used by Lubinski (1961) is unconservative when compared to the test data obtained more recently.

A comparison of the effect of mean stress on fatigue life observed in the test program reported herein with the work of Lubinski is presented in Figure 6.15. The tests were carried out at a fixed stress range of 290 MPa. The curve derived from Lubinski's work is shown along with the test results from Chapter 4. Comparing the mean regression

line of the test results with the curve used by Lubinski, it is seen that the rate of change of fatigue life with a change in mean stress is underestimated by the curve used for the present design guidelines. The test results show a greater effect of the mean stress than accounted for in the work of Lubinski. In addition, a line drawn at two standard errors below the mean regression line is seen to lie to the left of curve used by Lubinski, indicating that the latter is unconservative for pipes used in a non-corrosive environment.

When drilling is carried out in a corrosive environment, the fatigue curve obtained from tests performed in a non-corrosive environment cannot be used. In order to obtain a fatigue curve that would be applicable to a severe corrosive environment, Lubinski (1961) simply lowered the fatigue curve applicable to the non-corrosive environment by 40 percent throughout. As a consequence, the endurance limit observed in a non-corrosive environment was also retained, although 40 percent lower, for a corrosive environment. It was recognized at that time (Lubinski, 1961) that this method of obtaining a fatigue curve for a corrosive environment could be very conservative at high stress ranges, where failure occurs at an early life, and unconservative at low stress ranges, where failure occurs at stress range levels below the resulting endurance limit. Decreasing the fatigue stress in Eq. (6-38) by 40 percent results in the following expression for the fatigue life in a corrosive environment,

$$\log N = 16.12 - 4.56 \log S_r \qquad (6\text{-}41)$$

The endurance limit used by Lubinski becomes 150 MPa in a severe corrosive environment.

The effect of mean stress on the fatigue life in a corrosive environment was assumed by Lubinski to be the same as its effect in a non-corrosive environment. Therefore, the Goodman diagram expressed by Eq. (6-40) was also used for fatigue life prediction in a corrosive environment. Fatigue curves for three different mean stress levels, namely, 250 MPa, 125 MPa, and 0 MPa, are presented in Figure 6.16 with test results obtained in the work presented herein at a mean stress level of 125 MPa. As can be seen from Figure 6.16, the fatigue curve used by Lubinski is very conservative at high values of stress range. However, at lower stress ranges, some of the data points lie below the fatigue curve corresponding to a mean stress of 125 MPa. Although this effect was expected when the work of Lubinski was carried out, no provision was made to account for it.

The effect of mean stress on the fatigue life in a corrosive environment is presented in Figure 6.17 for two different stress range levels. The curves derived from the work of Lubinski (1961) are shown along with the test results from the work presented in Chapter 4. Comparing the slope of the mean regression lines of the test data with the slope of the lines from Lubinski's work, it is seen that the slope of the latter is similar to the slope of the regression lines obtained from the present work. This indicates the same degree of sensitivity of the fatigue life to the mean stress in a corrosive environment. However, as was observed in Figure 6.16, the predicted fatigue life from Lubinski's work is seen to be more conservative at higher stress ranges. Lubinski's curve is in better agreement with the test results at a stress range of 130 MPa than it is at a stress range of 290 MPa, where a large discrepancy is observed between the work presented by Lubinski and the work presented herein.

6.4.2 Stresses in a Drill Pipe Located in a Dogleg

When a drill pipe is deformed to fit into a dogleg and subjected to tensile load, bending stresses are induced in the drill pipe. Because of the presence of those bending stresses, the drill pipe will undergo stress cycling as it rotates in the dogleg. In order to determine the stress range under which a drill pipe operates when it rotates in a dogleg, a section of drill pipe must be analyzed. The stresses in the drill pipe result from the bending of the drill pipe as it deforms to fit in a dogleg and the axial tension which is produced by the weight of drill pipe below the dogleg. As tension increases, the middle portion of a pipe between two tool joints partially straightens and moves toward the wall of the hole, thereby causing more bending near the tool joint. At higher tensions, the middle portion of the drill pipe may come in contact with the wall of the hole. From this point, the bending stresses are not expected to increase as rapidly with increasing tension. The method used by Lubinski to obtain the bending stresses in a drill pipe under axial tension in a dogleg will be described below. This is followed by the analysis proposed by the writer.

6.4.2.1 Work of Lubinski (1961)

In order to evaluate the magnitude of the bending stresses in a drill pipe subjected to an axial load, Lubinski (1961) considered a length of drill pipe loaded axially in a curved configuration. The configuration of the dogleg was assumed to be an arc of a circle. This dogleg geometry was referred to as a gradual dogleg. To simulate the bending stress concentration which occurs near a tool joint, the end rotation of the section of drill pipe at

the tool joint was fully restrained. Considering equilibrium of a uniform section of drill pipe, the following expression was obtained by Lubinski (1961):

$$c_o = c_d \frac{KL}{\tanh KL} \tag{6-42}$$

where c_o is the curvature of the drill pipe body adjacent to the support (near the tool joint), c_d is the curvature of the dogleg, L is half the length of the drill pipe, and K is given by

$$K = \sqrt{\frac{T}{E\,I}} \tag{6-43}$$

where T is the tension force in the drill pipe, E is the modulus of elasticity of the pipe material, and I is the moment of inertia of the cross-section of the drill pipe body. It can be observed from Eq. (6-42) that, as the tension force goes to zero, the curvature of the drill pipe becomes equal to the curvature of the hole. Once the curvature of the drill pipe, c_o, has been evaluated for a given dogleg curvature, c_d, and axial load, T, the bending stress in the drill pipe body is obtained from (Lubinski, 1961):

$$\sigma_b = \frac{c_o E D}{2} \tag{6-44}$$

where σ_b is the bending stress resulting from the curvature, c_o, of a drill pipe of diameter D. In his work, Lubinski did not consider the effect of contact between the drill pipe body and the wall of the borehole as the axial load is increased. This should lead to an over-estimation of the bending stresses in the drill pipe body.

Equation (6-42) represents a first order analysis for the effect of the tension force on drill pipe curvature. Since the application of a tension force on the drill pipe tends to straighten the pipe, the moment induced at the critical section near the tool joint will be overestimated if the initial eccentricity of the axial load is used to calculate the moment induced at the tool joint. A decrease in eccentricity (corresponding to the deflection at the middle portion of the drill pipe with respect to the tool joint) would reduce the calculated moment near the tool joint.

6.4.2.2 Finite Element Method

Because of the shortcomings identified in the analysis presented by Lubinski, a more general analysis, using the finite element method, was performed on a section of drill pipe. The effect of increased stiffness in the upset and tool joint area, of drill pipe contact

with the wall of the hole, and the non-linear behaviour resulting from second order effects in the curved pipe under tension were considered in the analysis.

The finite element analysis of a drill pipe in a dogleg was performed in order to determine the maximum bending moment induced in a drill pipe as a function of axial load and dogleg severity. The analysis was performed on two lengths of drill pipe located in a gradual dogleg. The configuration of the dogleg was assumed to be a circular arc and the wall of the borehole was assumed to be rigid. The assumed dogleg configuration is the same as that used by Lubinski to simulate a gradual dogleg. Although any dogleg configuration can be used in the analysis, since the actual configuration can vary significantly from one situation to another, it is hard to justify the use of a more complex configuration that the simple one used herein. Furthermore, as the drill pipe rotates with the tool joints in contact with the wall of the borehole any abrupt change in configuration would be removed by wearing down the wall of the borehole. The assumption of a rigid borehole surface was made to simplify the borehole-to-drill pipe interaction. This is believed to simulate adequately the case where the drill pipe is rotating in a cemented casing.

The analysis assumes that the tool joints of the drill pipe are all in contact with the same side of the borehole, as shown in Figure 6.18 (a). This would be the case for a drill pipe under axial tension. However, as the axial load decreases, or as the hole curvature (expressed as dogleg severity) increases, the drill pipe may be in contact with opposite sides of the borehole, as depicted schematically in Figure 6.18 (b). For the condition illustrated in Figure 6.18 (a), the curvature of the drill pipe is the same as the curvature of the borehole. However, for the condition depicted in Figure 6.18 (b), the curvature of the drill pipe is not the same as the curvature of the borehole, but, instead, the curvature of the drill pipe is dependent on both the borehole curvature and the borehole size. For the analysis presented herein the pipe is assumed to be in contact with the same side of the borehole. The validity of this assumption will be checked from the results of the analysis.

A nonlinear three-dimensional beam element, implemented in program NISA (Stegmüller et al., 1983), was used for the analysis of a drill pipe in a dogleg. A nonlinear element was used in order to take into account the effect of the tension in the drill pipe on the bending stresses. The program implements an updated Lagrangian formulation. Tension and bending moment terms were included in the geometric stiffness. When tension is applied to a drill pipe, the middle portion of the drill pipe between the tool joints will partially straighten and move toward the wall of the bore hole, thus creating more

bending in the drill pipe near the tool joint. This behaviour was recognized by Lubinski (1961) in his early work and it was also obeserved in a recent finite element investigation performed by Zeren (1986). This phenomenon is depicted in Figure 6.19. The non-linear element allows for updating of the configuration of the drill pipe as it is loaded. As a result, unlike the results of a first order analysis, in the analysis described herein the final configuration of the drill pipe on which an axial load is applied is the equilibrium configuration. The finite element model is shown in Figure 6.20. The model consists of four different sizes of element. The drill pipe itself is modelled by body elements, upset elements, and tool joint elements. Contact of the borehole at the tool joints is modeled by using stiff elements, pinned at both extremities, of length equal to the radius of the dogleg. The stiff elements are pinned at the center of rotation and allow displacement of the tool joints along the surface of the borehole only as deflections take place under axial loading.

The drill pipe reference configuration is taken as the condition where only residual stresses are acting. This corresponds to the straight line configuration of the unloaded drill pipe. At the reference configuration, the stiff radial elements are not of equal length, as shown by Figure 6.20. The curved configuration of the drill pipe is obtained by applying a load at the tool joint (node 10 in Figure 6.20) equal to,

$$P = k_s \, \delta \tag{6-49}$$

where k_s is the axial stiffness of a stiff radial member and δ is the deflection at the middle tool joint of the model required for the pipe to fit in the borehole. Once the desired configuration of the drill pipe has been reached, an axial load of 1000 kN, corresponding to the maximum axial load on a drill pipe accounted for in the present design guidelines (American Petroleum Institute, 1988), was applied gradually in discrete load steps. A standard Newton-Raphson iteration procedure was used at every load step. To accelerate convergence the loads were applied incrementally. The load factor versus time step curves for loading a drill pipe are presented in Figure 6.21. The radial loads required to deform the drill pipe to fit in the dogleg were applied in ten equal load steps, whereas the axial load, decomposed into an horizontal component T_h and a vertical component T_v, was applied into ten unequal load steps. The load steps corresponded to 5, 10, 15, 20, 30, 40, 50, 60, 80, and 100 percent of the full axial load. The resultant of T_h and T_v is the axial load applied in a direction tangential to the wall of the dogleg. The equilibrium configuration was obtained at each loading step and the internal forces at the nodal points were calculated.

The analysis showed that as the tension on the drill pipe is increased the body of the drill pipe straightens until it comes in contact with the wall of the borehole. In order to prevent deflection of the drill pipe body beyond the position where contact between the drill pipe and the wall of the hole takes place, the equilibrium configuration of the drill pipe was examined at every load step and, if a nodal point had displaced enough to make contact with the wall of the hole, the analysis was repeated with a stiff radial member attached to the node that had made contact with the hole. The first stage of loading then consisted in applying forces at the nodes attached to a rigid radial bar in order to deform the bars to the position corresponding to contact between the drill pipe and the wall of the borehole at the supported nodal points. The axial load was then applied on the deformed drill pipe. The results of the analysis on the modified structure were then combined with the results of the previous analyses, performed on a drill pipe with a lesser amount of node point supports. This was done in order to obtain the load-response curve up to the load level at which contact between the drill pipe and the borehole would take place at another location corresponding to the location of a nodal point. For a 10° / 30 m dogleg, it was found that only one point on each length of drill pipe had to be supported (nodes 5 and 15 in Figure 6.20) from a load step of 50 kN up to 800 kN. Additional supports at nodes 4 and 16 had to be provided after load step of 800 kN. No contact at all between the drill pipe and the wall of the hole was detected for a dogleg severity of 5° / 30 m. The assumption made earlier with respect to contact between tool joints and the same side of the borehole was found to be valid for all the load steps except for the condition of a drill pipe under no axial load. No adjustment was made to account for the different curvature in the pipe that would be obtained if contact was made with alternate sides of the borehole.

6.4.2.3 Comparison of Analysis of Lubinski with Finite Element Method

From the finite element analysis of two lengths of drill pipe in a dogleg, the effect of axial load on the bending moment adjacent to the pipe upset was determined. The bending moments identified in the following are those obtained near the middle tool joint in the model shown in Figure 6.20. Although the bending moment in the upset and tool joint was found to be slightly larger than that in the drill pipe body, the larger cross-section at those locations means that the resulting bending stresses are smaller than they will be in the pipe body.

The calculated moment in the drill pipe body adjacent to the upset is plotted in Figure 6.22 for values of axial tension varying from 0 to 1000 kN. The analysis was performed for two different dogleg severities, namely, a dogleg severity of 5° / 30 m (5 degrees per 30 m of hole) and a dogleg severity of 10° / 30 m. It was found that for a dogleg severity of 5° / 30 m no contact between the drill pipe and the wall of the hole takes place for axial loading of up to 1000 kN. However, for a dogleg severity of 10° / 30 m, it was found that contact between the drill pipe and the wall of the borehole takes place under even a small axial load, as shown in Figure 6.22.

Figure 6.22 also shows the relation between the moment in a drill pipe and the axial load calculated from the analysis presented by Lubinski (1961). Under small axial load, the analysis presented by Lubinski underestimates the moment in the drill pipe. This smaller moment is due to the assumed curvature of the pipe body between tool joints under no axial load. However, for reasons explained earlier, as the axial load increases, the moment predicted from the work of Lubinski overestimates the value of the bending moment. From both analyses, it is evident that the axial load significantly increases the bending moment in the drill pipe body near the tool joint. The second order moment created by the tension force was found to be more than twice the primary bending moment (moment created by deforming the drill pipe in the dogleg without the presence of an axial load). From the analysis performed using finite element method, it can be seen that the rate of increase of the bending moment with increasing tension force is decreased after contact occurs between the drill pipe and the wall of the hole.

6.4.3 Cumulative Fatigue Damage

When a fatigue test is run on a drill pipe, uniform load cycles are applied to the specimen until the cumulative effect of all the cycles eventually produces failure (unless the stress range is below the endurance limit). When the load cycles are not applied uniformly but in an irregular manner, a condition which likely prevails in the field as a drill pipe rotates through doglegs of different severities, the cumulative effect of these events may also lead to fatigue failure. Fatigue effects of loading events other than uniform cycles are referred to as cumulative damage.

Numerous methods for the prediction of fatigue life under non-uniform cycles have been proposed (Osgood, 1982; Führing and Seeger, 1984). In general, theories of cumulative fatigue damage are either linear or non-linear. Linear methods assume that the

damage rate of each cycle is independent of the load history and depends only on the stress range, mean stress, and geometry of the structure. In contrast, non-linear models account for load interactions and the assumptions of linear elastic fracture mechanics are ignored. Although non-linear models are more realistic, such models are generally semi-empirical in nature and, consequently, those laws can be used with confidence only for those cases in which the parameters were applicable. Furthermore, since non-linear models account for loading sequence, a good knowledge of the loading spectrum applicable to the problem at hand is imperative if the model is to yield satisfactory results.

The simplest rule based on concepts of fatigue damage is the one of Palmgren and Miner (Fuchs and Stephens, 1980). In spite of the tendency of the Palmgren-Miner law to sometimes overestimate life (Osgood, 1982) and its inability to account for the loading sequence, it is still used extensively, mostly for its simplicity, but also because more sophisticated rules have yet to be shown to be generally applicable to all types of service loading. Based on the Palmgren-Miner law, the fatigue damage sustained under one cycle of loading can be expressed as

$$\text{Fatigue damage} = \frac{1}{N} \tag{6-50}$$

where N is the fatigue life under uniform load cycling. Fatigue failure is predicted to take place when the total damage sustained represents 100 percent of the fatigue life.

The Palmgren-Miner law was used by Hansford and Lubinski (1964) in their work on cumulative fatigue of drill pipe and it is also used in the present work. In order to predict the percentage of the total fatigue life expended when a drill pipe is rotating in a dogleg, the stress range and mean stress, calculated using the method outlined in the previous section, need to be used in conjunction with the S-N curve applicable for the mean stress applied on the drill pipe. The curves used by Hansford and Lubinski (1964) were the same as the curves proposed by Lubinski (1961) and presented in Figure 6.14 and Figure 6.16 for a non-corrosive and a corrosive environment, respectively.

In the work presented herein, the design fatigue curve will be taken as the curve corresponding to 2.0 standard deviations below the mean regression line fitted through the test results. This corresponds to a probability of survival of approximately 95 percent. The design curve for fatigue in air can be obtained from Eq. (5-16) as

$$\log N = 13.8 - 3.46 \log S_r - 1.67 \times 10^{-5} (S_m)^2 \tag{6-51}$$

while the design curve for drill pipes operating in a corrosive environment can be obtained from Eq. (5-32) as

$$\log N = 11.21 - 2.31 \log S_r - 2.67 \times 10^{-6} \log S_r (S_m)^2 \qquad (6\text{-}52)$$

Once the fatigue life at a stress range and mean stress has been evaluated from test results, the percent fatigue life expended can be evaluated from the Palmgren-Miner law for a number of stress cycles at calculated stress conditions. In order to derive the present cumulative fatigue guidelines (API, 1988) Hansford and Lubinski assumed a rotary speed of 100 rpm and a drilling rate of 3 m/hr, which means that a total of 20 000 cycles of loading is put on a drill pipe as 10 m of hole is drilled. Those same assumptions with respect to drilling conditions have been retained here so that the cumulative fatigue curves derived using the method presented herein can be compared directly with the existing guidelines. However, when corrosion fatigue is considered, since the fatigue life is dependent on the speed of testing, the rotary speed used for cumulative fatigue calculations was 60 rpm, the speed used for the experimental work presented in Chapter 4. Assuming that the rate of drilling is directly proportional to the rotary speed, a rate of drilling of 1.8 m/hr was used in the calculation. Since this also results in 20 000 cycles of loading while drilling a 10 m section of hole, direct comparison can be made between present guidelines (API, 1988) and the cumulative damage predicted from this work.

Using the procedure outlined in this chapter, cumulative fatigue curves were obtained for drilling in air and also drilling in a corrosive environment. Figure 6.23 presents cumulative fatigue curves for drilling in a non-corrosive environment, while Figure 6.24 is applicable to a corrosive environment. In both figures, curves are presented for dogleg severities of 5° / 30 m and 10° / 30 m. The curves corresponding to present design guidelines (American Petroleum Institute, 1988) are also shown for comparison.

Figure 6.23 shows that the present design guidelines for drilling in a non-corrosive environment are an unconservative predictor for the drill pipes tested in the test program presented herein. It can be seen, however, that for a dogleg severity of 10° / 30 m the two design curves presented in Figure 6.23 are closer together than the curves shown for a dogleg severity of 5° / 30 m. This difference observed between the two different dogleg severities is due to the fact that contact between the drill pipe and wall of the borehole was neglected in the analysis presented by Lubinski (1961). This led to more conservative

prediction of stresses in the drill pipe, which compensated for the less conservative S-N curves used to predict the fatigue life.

In contrast, Figure 6.24 indicates that the present cumulative fatigue design curves for corrosive environment are more conservative than the cumulative fatigue predictions resulting from the work of the author. Again, however, the API curves are seen to give an unconservative estimate of the fatigue damage at low axial load. This is probably due to the lower pipe bending moment predicted at low axial load by Lubinski.

Figure 6.25 shows a comparison of predicted cumulative damage in air and in a corrosive environment. The figure, which is based on the work presented herein, indicates that the fatigue damage predicted for a non-corrosive environment is greater than that predicted for a corrosive environment. In other words, for the same probability of survival the predicted fatigue life in a non-corrosive environment is less than it is in a corrosive environment. This paradoxical result arises from the fact that a very large scatter was observed for the test results obtained in air, whereas the scatter for the results obtained in the corrosive environment was relatively small. It is logical that the same probability of survival be used for these two cases, and the design curve in air was therefore established at two standard deviations from the mean in each case. The consequence is that the design curve for drill pipe in a non-corrosive environment actually lies below the design curve for drill pipe in a corrosive environment. If the mean fatigue life curves had been used directly, the result would have been as expected: the cumulative damage for a pipe in a non-corrosive environment would be less than that for pipe in a corrosive environment.

Table 6.1

Spreadsheet Calculation of Fatigue Life in Air
(after the work of Kral et al. (1984))

			Part-Through Crack			Through- Thickness Crack		
Stress Range	Mean Stress	Maximum Stress	Q Eq. (6-13)	c_{cr} Eq. (6-17)	N_p Eq. (6-11)	a_{cr} Eq. (6-18)	N_T Eq. (6-15)	N_f Eq. (6-10)
(1)	(2)	(3)	(4)	(5)	(6)	(7)	(8)	(9)
150	125	200	1.268	30.415	1570976	29.314	77144	1648120
160	125	205	1.267	28.939	1280443	27.968	57439	1337882
170	125	210	1.267	27.568	1056614	26.710	42834	1099448
180	125	215	1.266	26.291	881501	25.531	31881	913382
190	125	220	1.266	25.100	742619	24.425	23573	766192
200	125	225	1.265	23.988	631117	23.387	17212	648329
210	125	230	1.265	22.947	540608	22.413	12300	552908
220	125	235	1.264	21.972	466407	21.496	8484	474891
230	125	240	1.264	21.058	405023	20.632	5500	410523
240	125	245	1.263	20.198	353821	19.819	3160	356981
250	125	250	1.263	19.390	310790	19.051	1318	312108
260	125	255	1.262	18.629	274374	18.327	0	274374
270	125	260	1.262	17.912	243356	17.642	0	243356
280	125	265	1.261	17.234	216781	16.994	0	216781
290	125	270	1.260	16.594	193885	16.381	0	193885
300	125	275	1.260	15.989	174058	15.800	0	174058
310	125	280	1.259	15.415	156806	15.248	0	156806
320	125	285	1.259	14.872	141728	14.725	0	141728
330	125	290	1.258	14.356	128493	14.228	0	128493
340	125	295	1.257	13.867	116832	13.755	0	116832
350	125	300	1.257	13.401	106518	13.305	0	106518

Constants for spreadsheet calculations

c/a = 0.5; A= 1.16E-09; n = 3.16; K_{Ic} = 61.5; c_i = 0.795 mm;

a_i = 18.4 mm; σ_Y = 620 MPa; t = 9.2 mm; w = 330.2 mm;

Pipe O.D. = 114 mm

Table 6.2

Comparison Of Test Results With Fracture Mechanics Models

		Predicted Fatigue Life (Measured/Predicted)			
		Flat Plate Model		Circular Pipe Model	
Test Specimen	Measured Life	Paris Model	Forman Model	Paris Model	Forman Model
RBT4-B	472 600	168 200 (2.8)	138 100 (3.4)	245 300 (1.9)	210 000 (2.3)
RBT5-B	1 181 500	250 200 (4.7)	215 00 (5.5)	362 100 (3.3)	318 600 (3.7)
RB1	10 000 000+	213 900 (47)	448 700 (22)	297 500 (34)	619 300 (16)
RB1-B	10 000 000+	314 300 (32)	261 400 (38)	453 600 (22)	384 700 (26)
RB2	468 500	192 200 (2.4)	173 500 (2.7)	278 900 (1.7)	259 000 (1.8)
RB2-B	189 800	121 300 (1.6)	116 600 (1.6)	176 800 (1.1)	176 900 (1.1)
RB3	882 800	192 200 (4.6)	172 400 (5.1)	278 900 (3.2)	257 600 (3.4)
RB3-B	1 876 000	250 200 (7.5)	216 300 (8.2)	362 100 (5.2)	320 500 (5.3)
RB6	1 389 900	221 300 (6.3)	463 800 (3.0)	307 700 (4.5)	639 500 (2.2)
RB7	10 000 000+	186 000 (54)	167 700 (60)	269 900 (37)	250 800 (40)
RB7-B	508 500	233 000 (2.2)	201 400 (2.5)	337 500 (1.5)	299 300 (1.7)
RB8	4 771 100	214 000 (22)	448 700 (11)	297 500 (16)	619 300 (7.7)
RB9-B	259 900	121 300 (2.1)	116 600 (2.2)	176 800 (2.0)	176 900 (1.5)

Table 6.2 (Cont'd)

Test Specimen	Measured Life	Predicted Fatigue Life (Measured/Predicted)			
		Flat Plate Model		Circular Pipe Model	
		Paris Model	Forman Model	Paris Model	Forman Model
RB13-B	568 800	309 800 (1.8)	257 000 (2.2)	447 400 (1.3)	37860000 (1.5)
RB14	511 200	115 600 (4.4)	111 100 (4.6)	168 700 (3.0)	169 000 (3.0)
RB14-B	300 400	140 300 (2.1)	130 900 (2.3)	204 300 (1.5)	197 800 (1.5)
RB15	262 800	178 700 (1.5)	80 300 (3.3)	278 200 (0.9)	134 800 (2.0)
RB16	82 100	174 100 (0.5)	77 900 (1.1)	271 700 (0.3)	131 200 (0.6)
RB18	352 900	168 900 (2.1)	77 300 (4.6)	264 800 (1.3)	125 900 (2.8)
RB18-B	461 600	305 800 (1.5)	254 300 (1.8)	441 700 (1.0)	374 800 (1.2)
RB19-B	586 000	645 700 (0.9)	459 400 (1.3)	921 300 (0.6)	665 300 (0.9)
RB20-B	1 237 500	471 200 (2.6)	354 300 (3.5)	676 200 (1.8)	517 200 (2.4)
RB21-B	982 000	910 000 (1.1)	595 600 (1.6)	1 293 200 (0.8)	857 100 (1.1)
RB22-B	10 000 000+	890 100 (11)	570 900 (18)	1 267 300 (7.9)	823 800 (12)
RB22-BR	1 451 800	632 600 (2.3)	441 200 (3.3)	904 300 (1.6)	640 700 (2.3)
RB23-B	10 000 000+	960 100 (10)	616 000 (16)	1 364 100 (7.3)	886 100 (11)
RB23-B1R	10 000 000+	645 000 (16)	456 200 (22)	920 700 (11)	661 000 (15)

Table 6.2 (Cont'd)

		Predicted Fatigue Life (Measured/Predicted)			
		Flat Plate Model		Circular Pipe Model	
Test Specimen	Measured Life	Paris Model	Forman Model	Paris Model	Forman Model
RB23-B2R	10 000 000+	472 300 (21)	359 100 (28)	677 000 (15)	523 700 (19)
RB23-B3R	1 289 500	310 200 (4.2)	258 700 (5.0)	447 700 (2.9)	380 800 (3.4)
Average (Measured/Predicted)		9.4	9.8	6.6	6.6

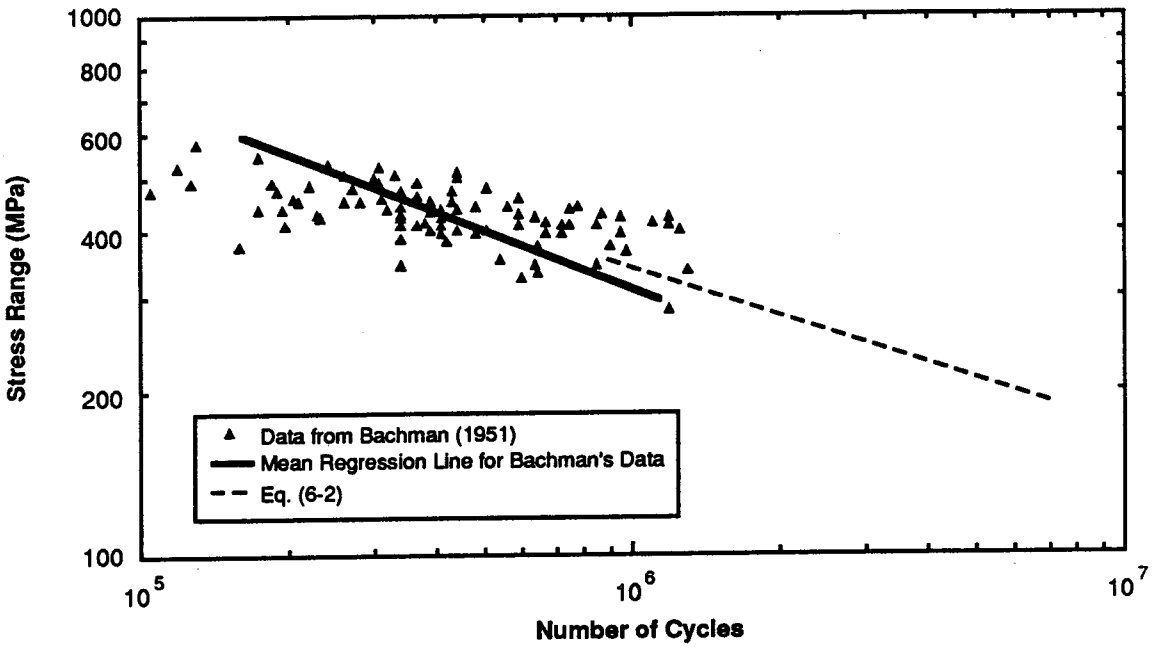

Figure 6.1 Comparison With Bachman's Test Data

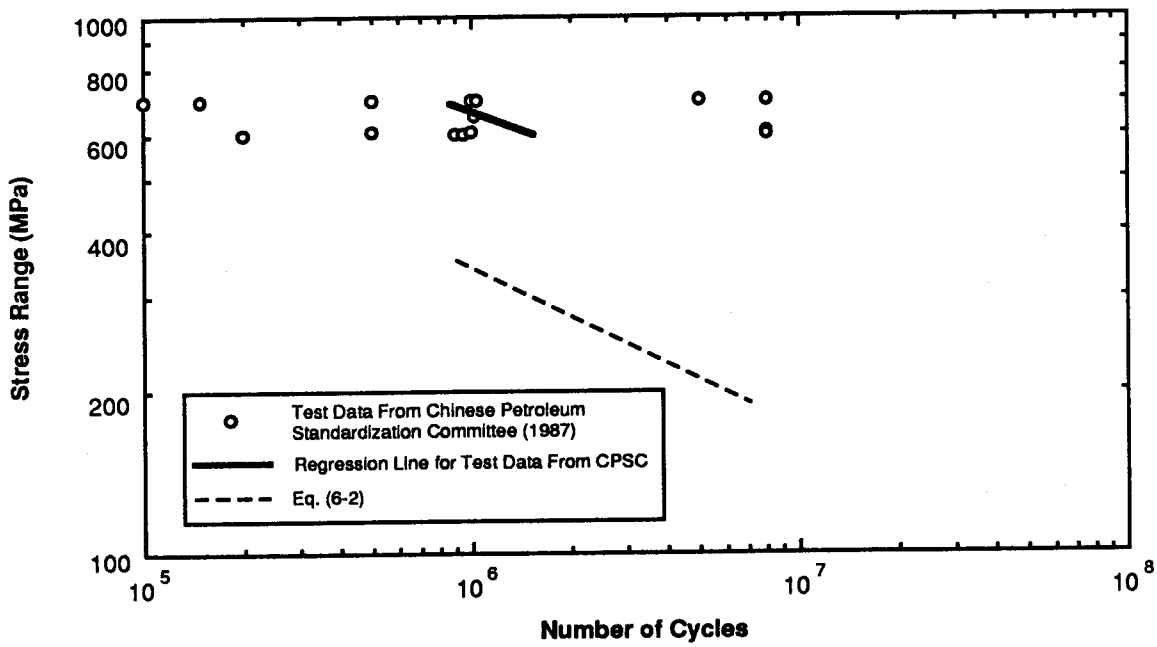

Figure 6.2 Comparison With Chinese Petroleum Standardization Committee Test Data

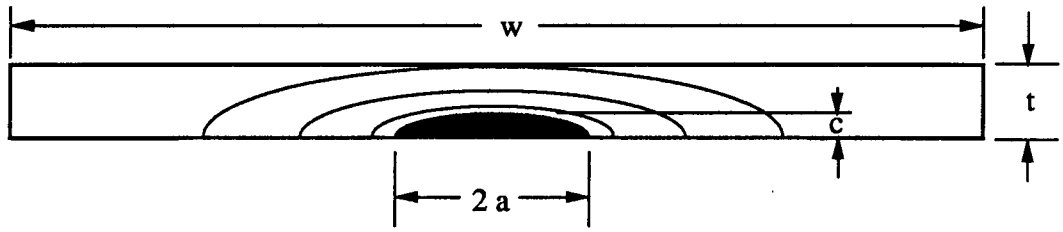

(a) Part-Through Thickness Crack

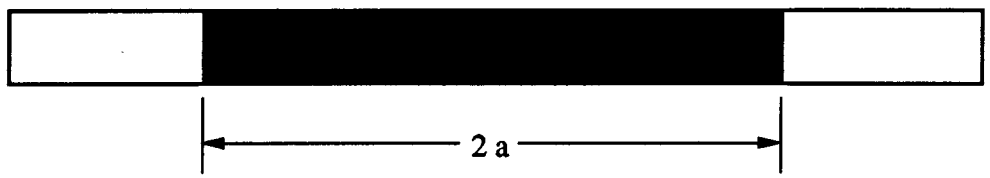

(b) Through-Thickness Crack

Figure 6.3 Fatigue Crack Geometry in Flat Plate

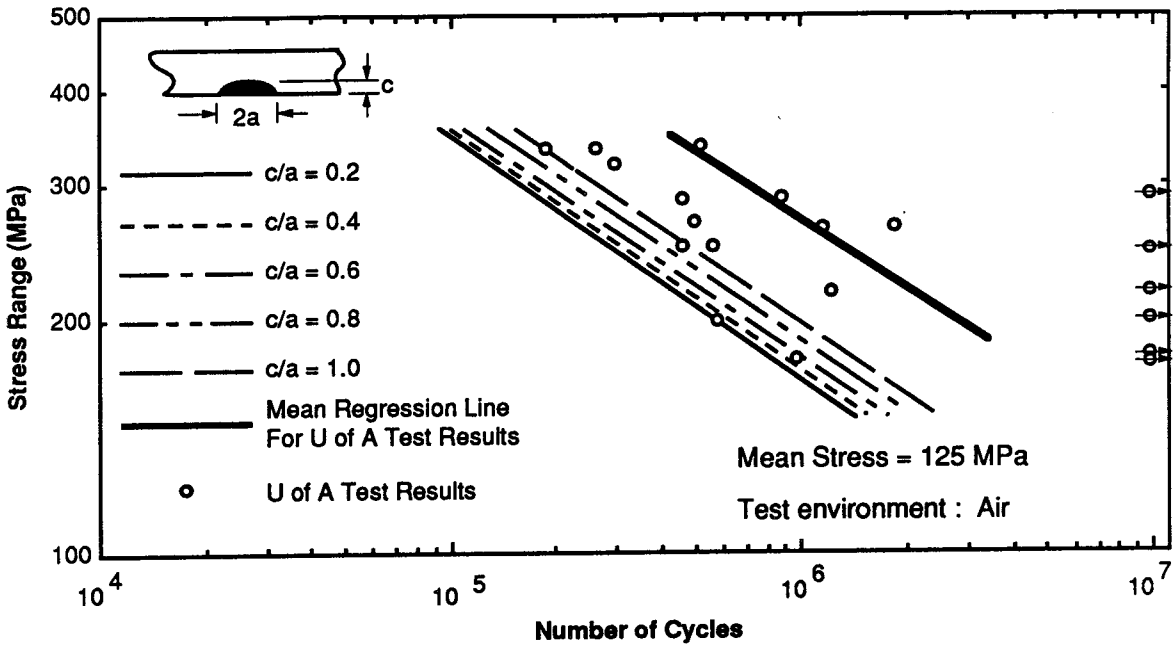

Figure 6.4 Effect of Crack Aspect Ratio on Fatigue Life of Drill Pipe

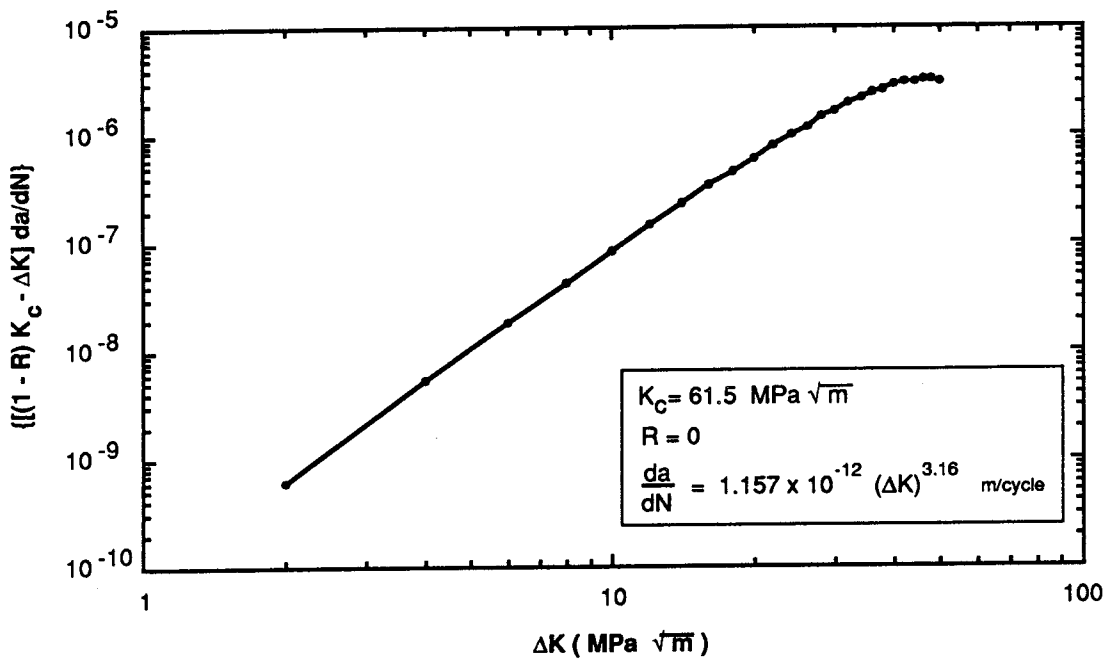

Figure 6.5 Plot of $\{[(1-R)\,K_c - \Delta K]\,da/dN\}$ Versus ΔK for Calibration of Forman's Model

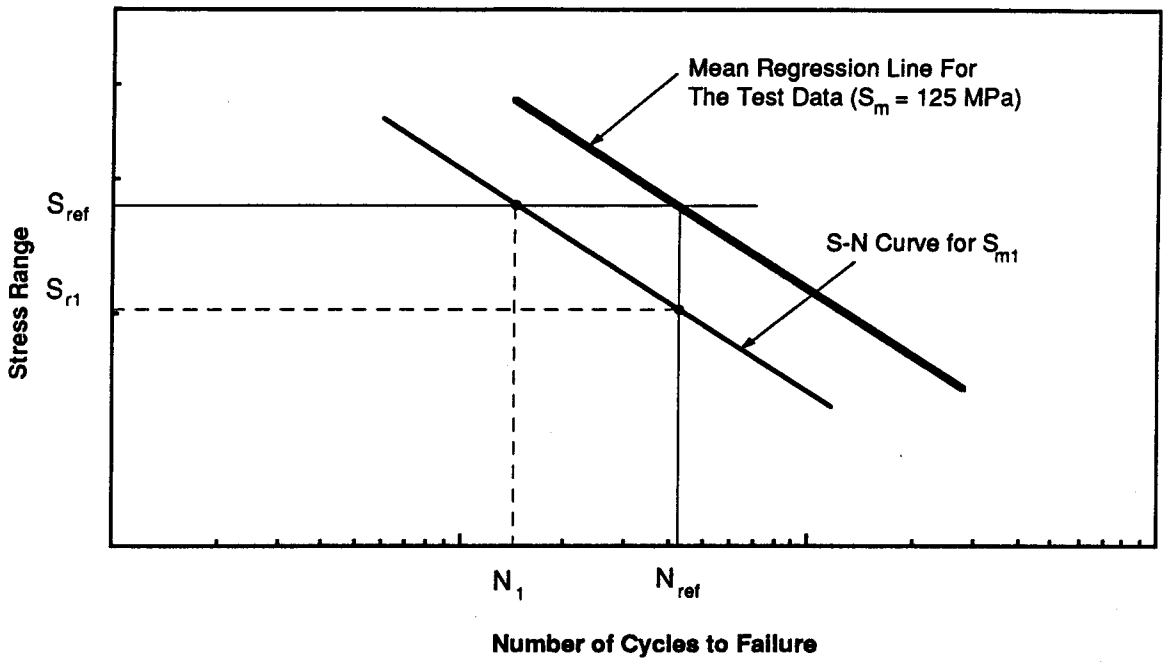

Figure 6.6 Calculation of Reduced Fatigue Life due to Mean Stress

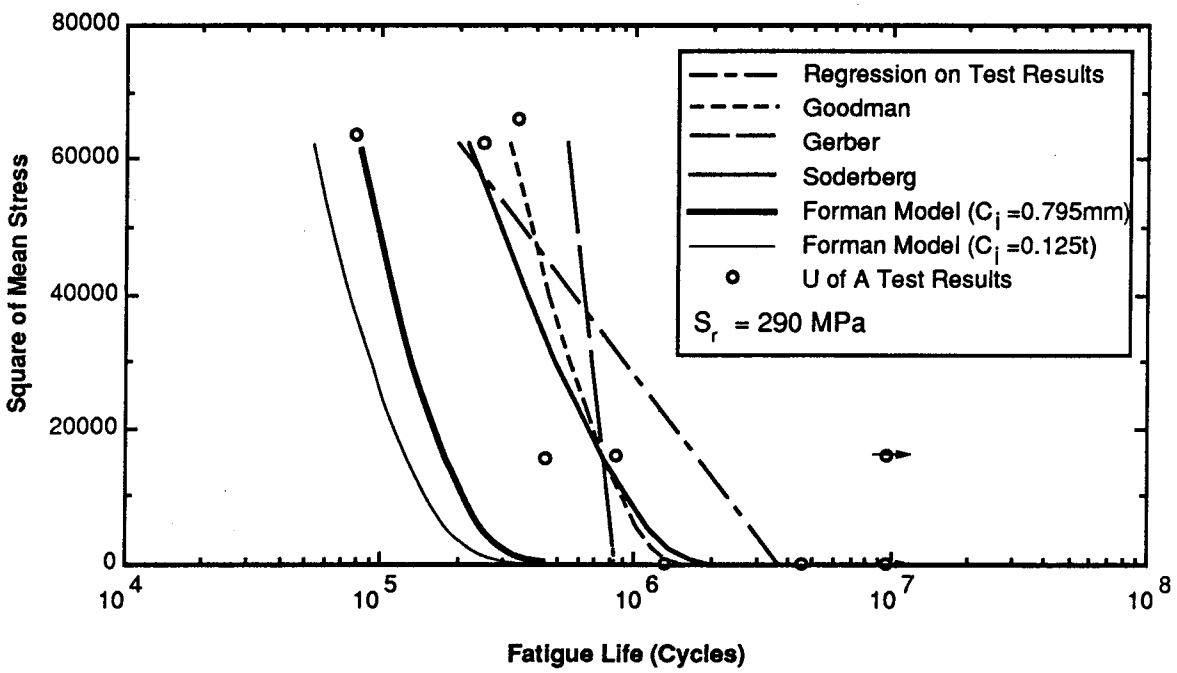

Figure 6.7 Effect of Mean Stress on Fatigue Life in Air

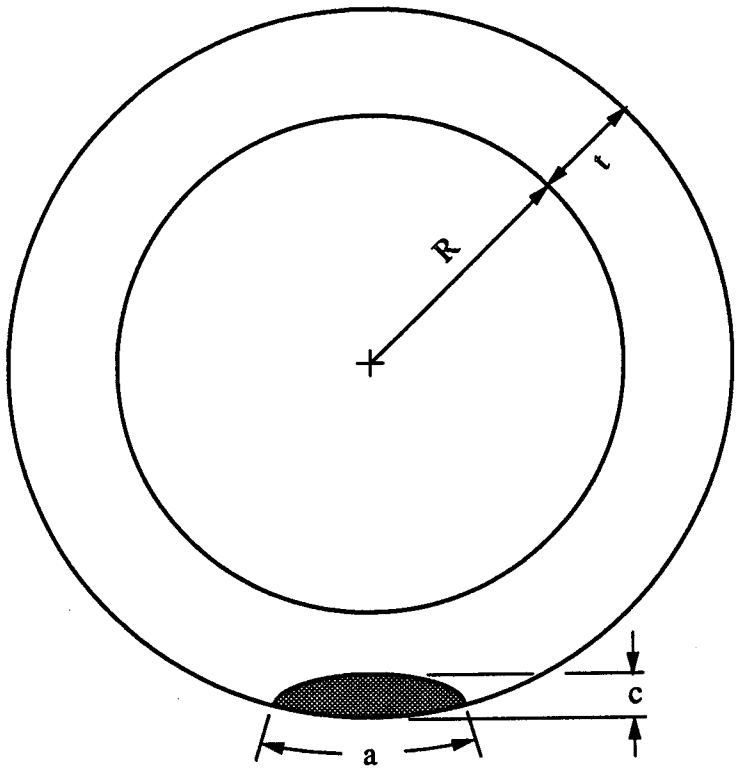

Figure 6.8 Crack Geometry in a Circular Pipe Used by Raju and Newman (1984)

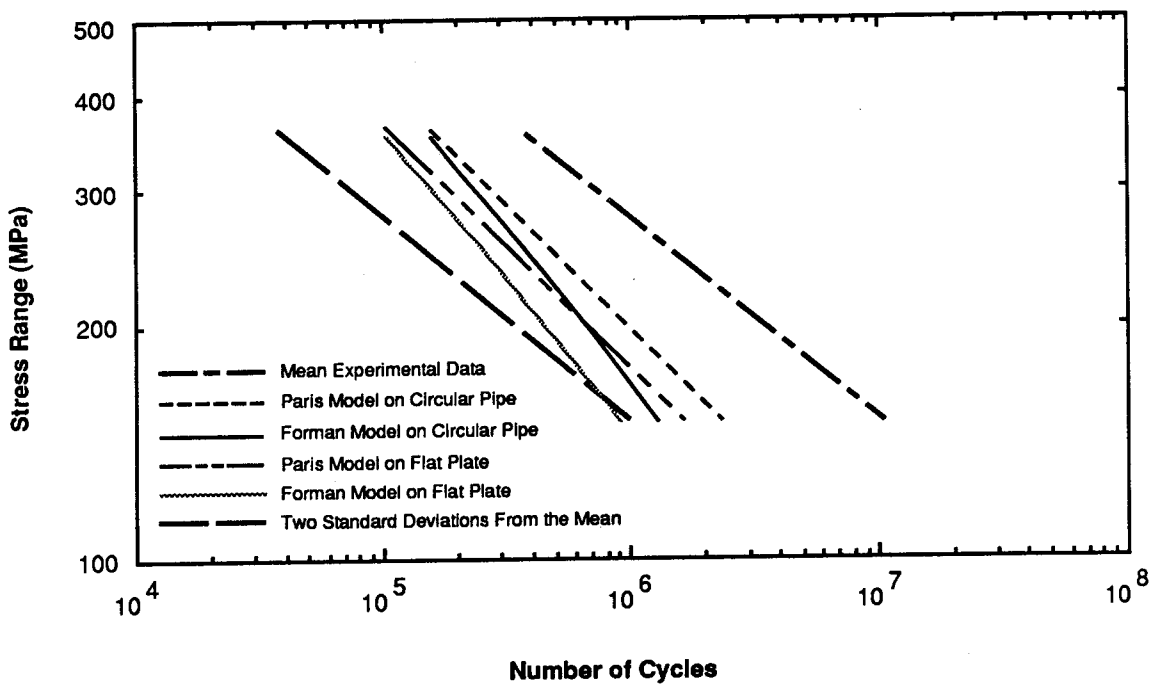

Figure 6.9 Comparison of Mean Test Results With Fracture Mechanics Models

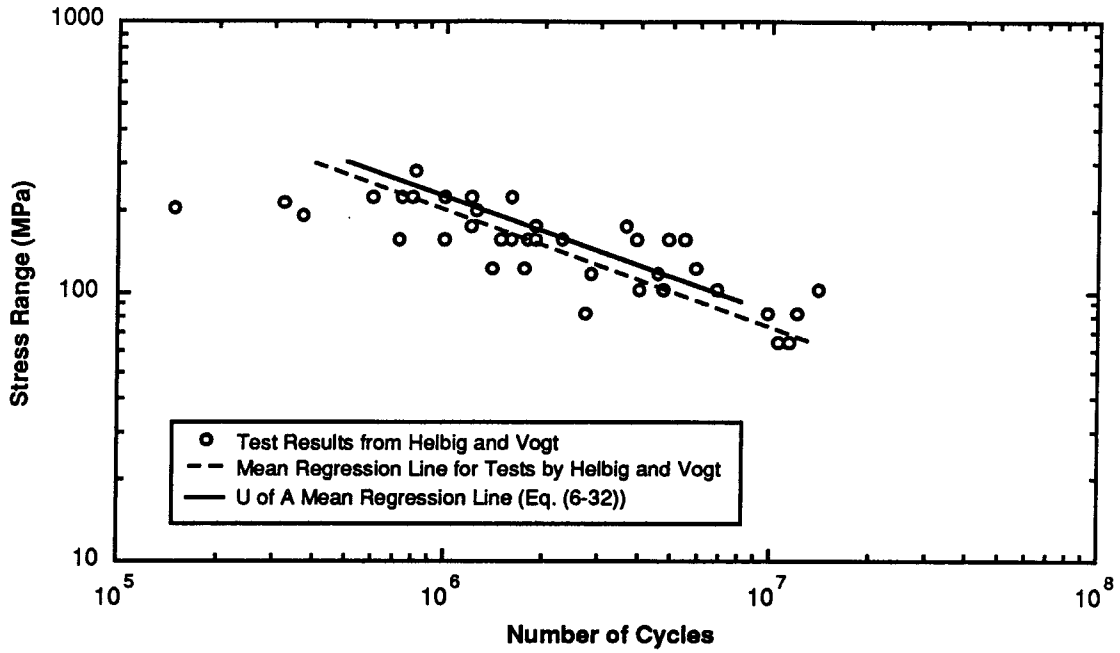

Figure 6.10 Comparison With Test Data Presented by Helbig and Vogt (1984) in Tap Water

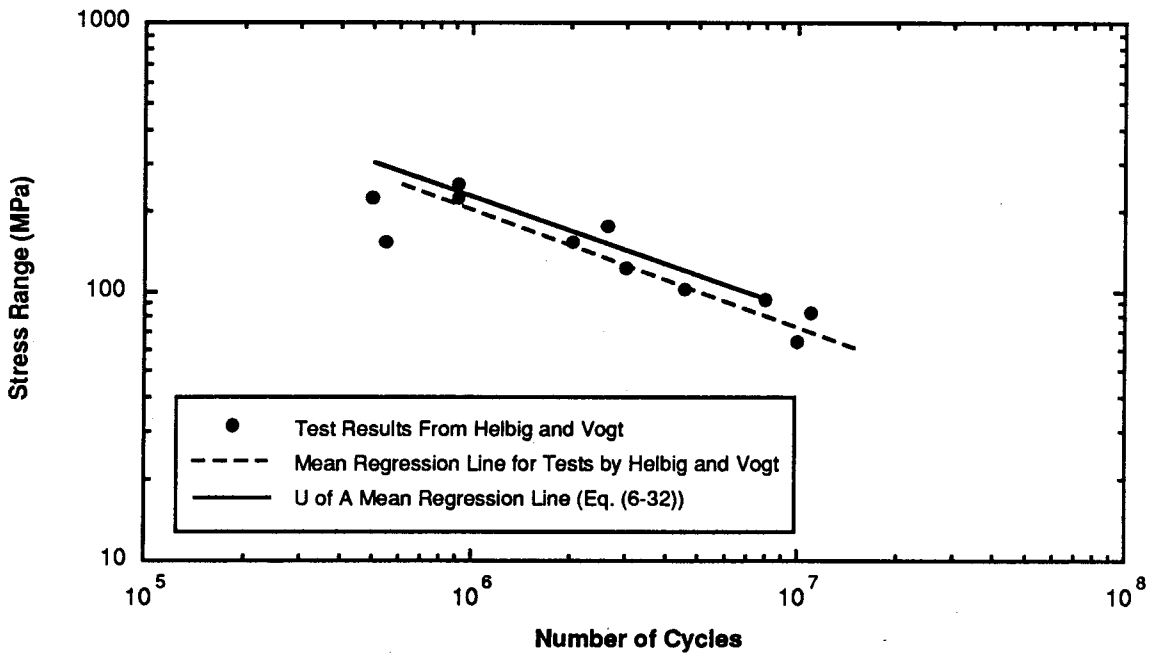

Figure 6.11 Comparison With Test Data Presented by Helbig and Vogt (1984) in 20% NaCl Solution

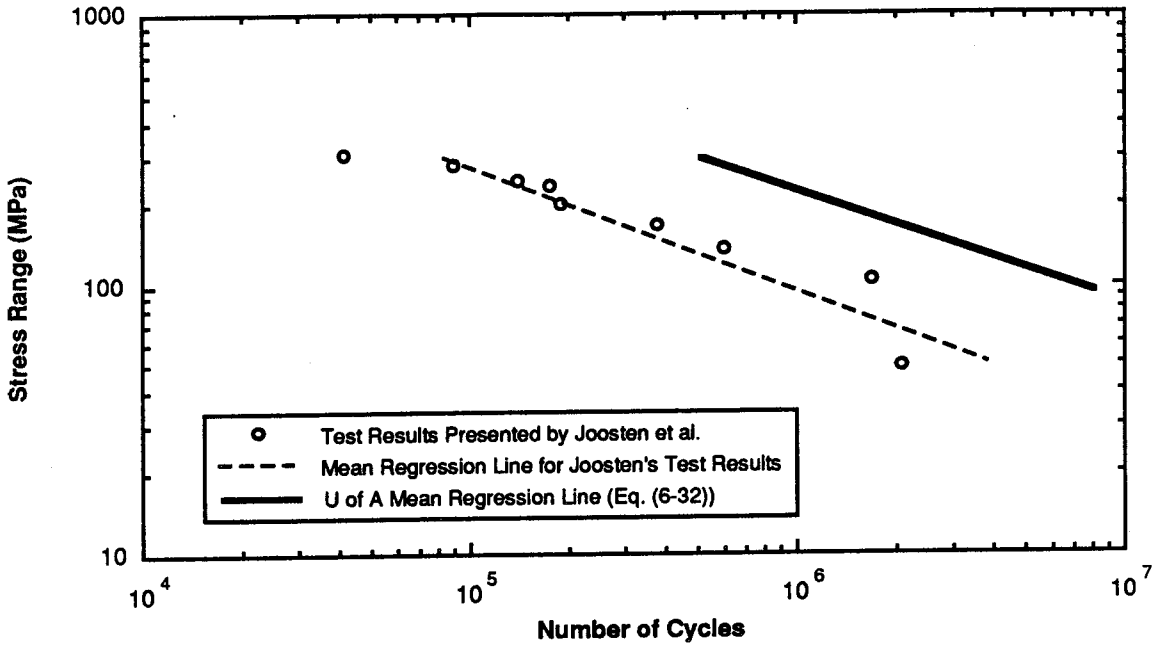

Figure 6.12 Comparison With Test Data Presented by Joosten et al. (1985)

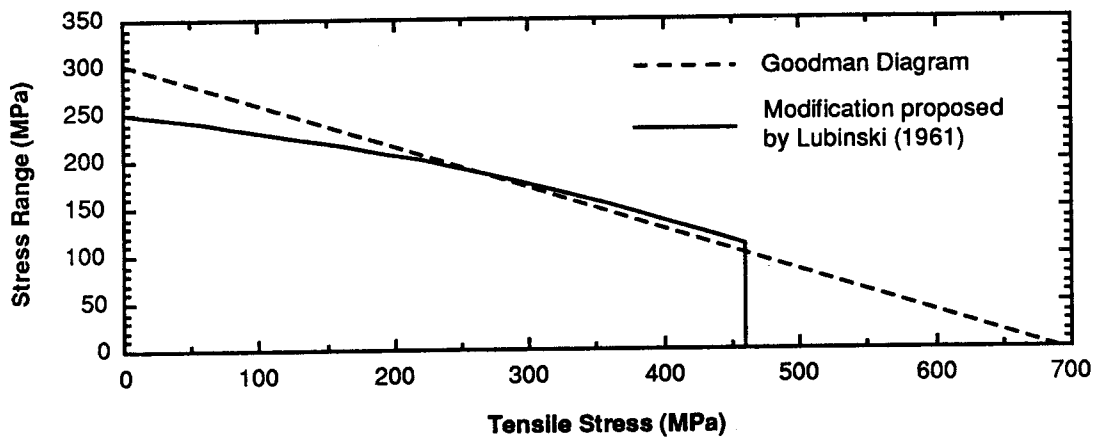

Figure 6.13 Effect of Mean Stress on Endurance Limit of Grade E Drill Pipe

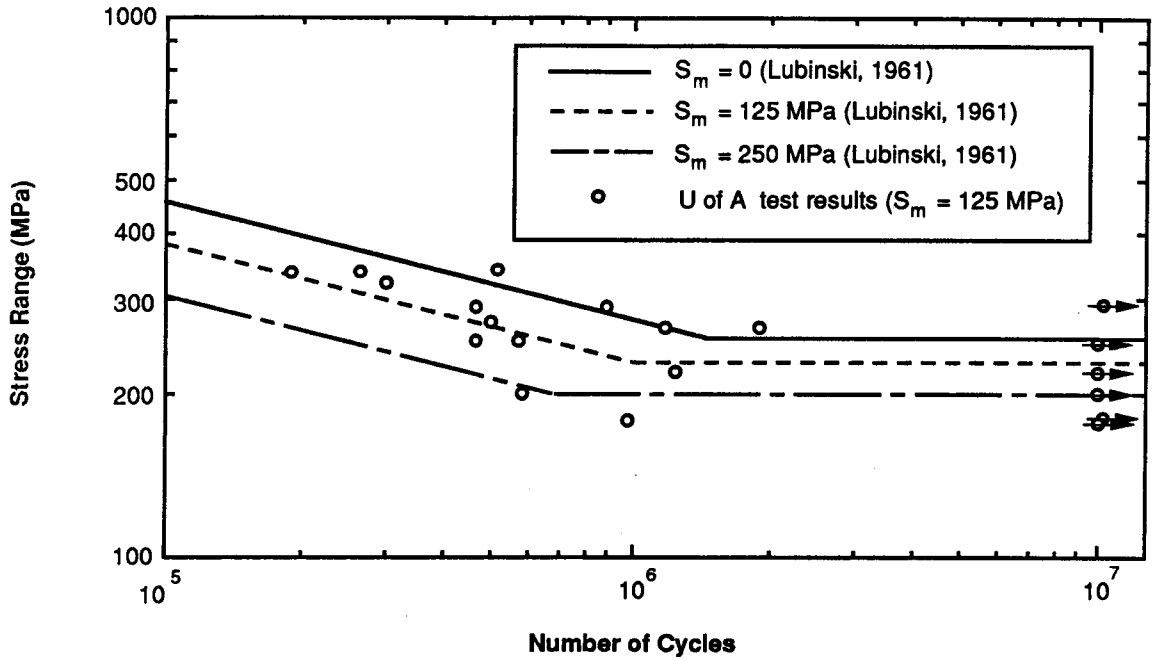

Figure 6.14 Effect of Mean Stress on S-N Curve in Non-Corrosive Environment

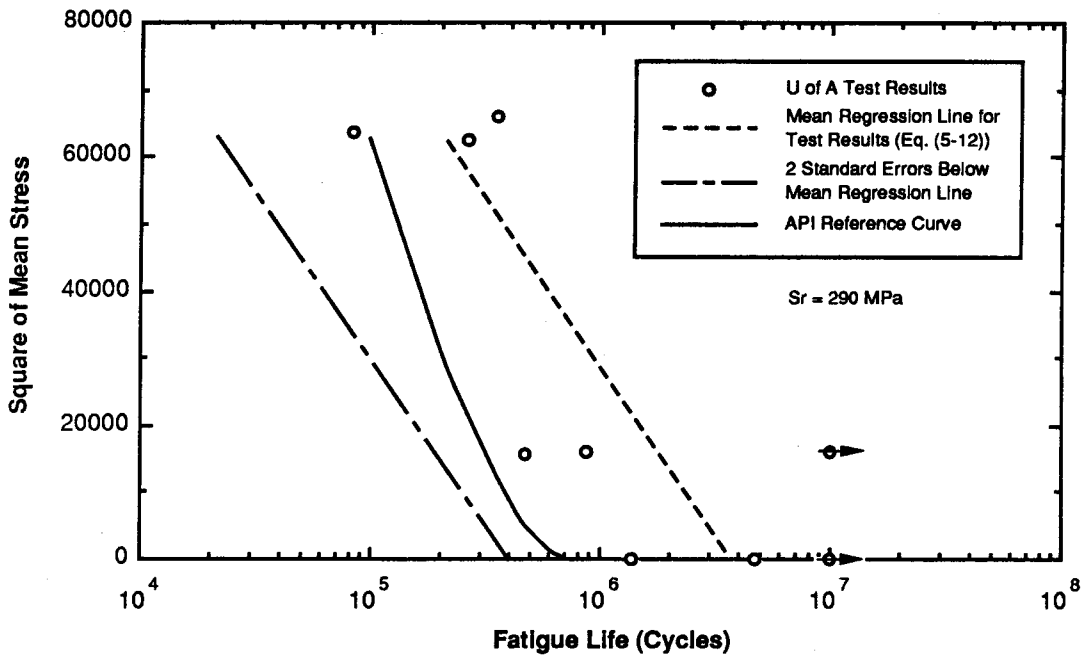

Figure 6.15 Comparison of Test Results Obtained in Air With the Work of Lubinski (1961)

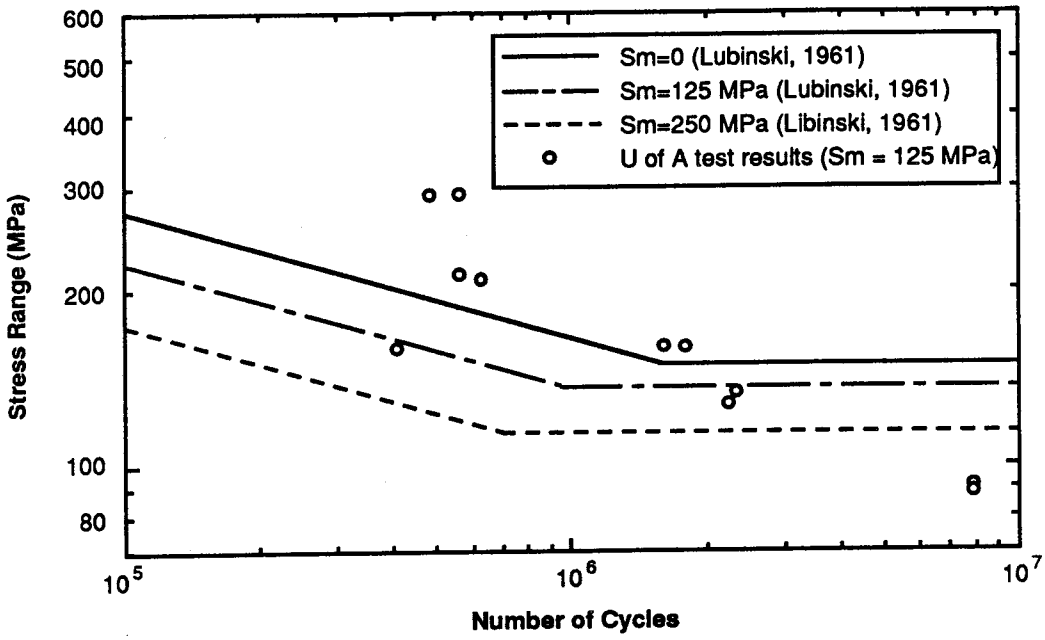

Figure 6.16 Effect of Mean Stress on S-N Curve in Corrosive Environment

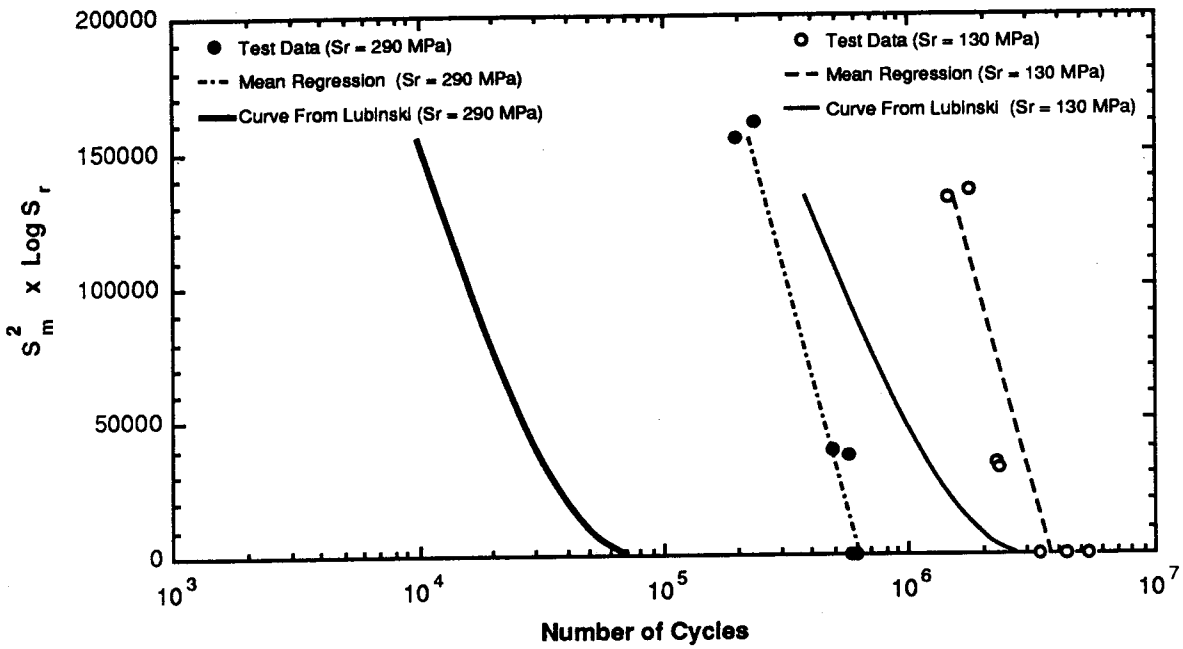

Figure 6.17 Comparison of Test Results Obtained in NaCl Solution with the Work of Lubinski (1961)

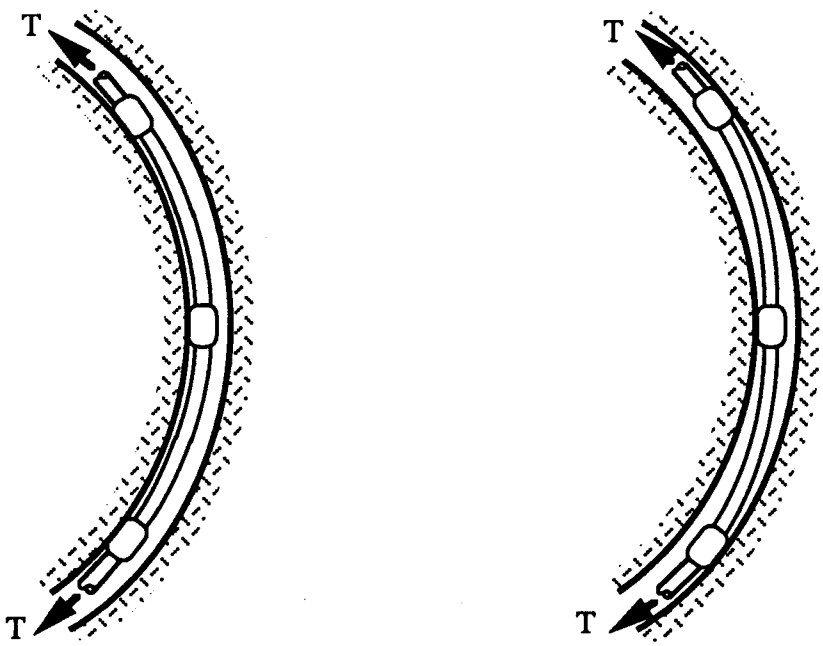

(a) Tool joints in contact with the same side of the borehole

(b) Tool joints in contact with opposite sides of the borehole

Figure 6.18 Bending of a Drill Pipe in a Dogleg

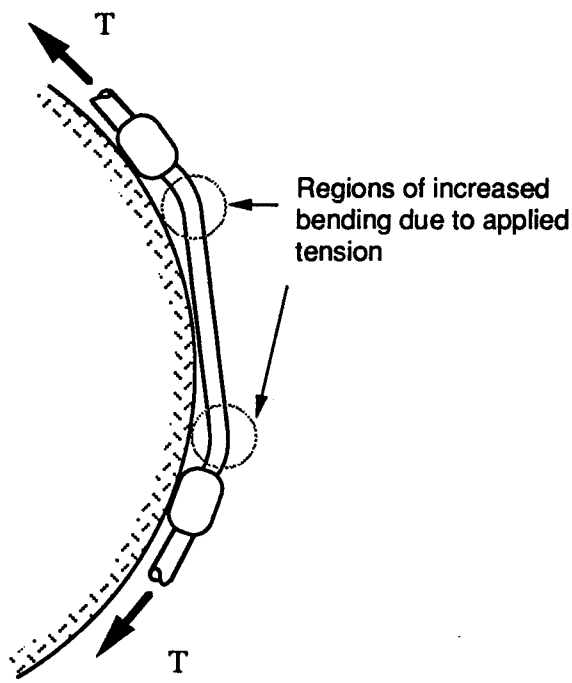

Figure 6.19 Effect of Tension on Drill Pipe Bending

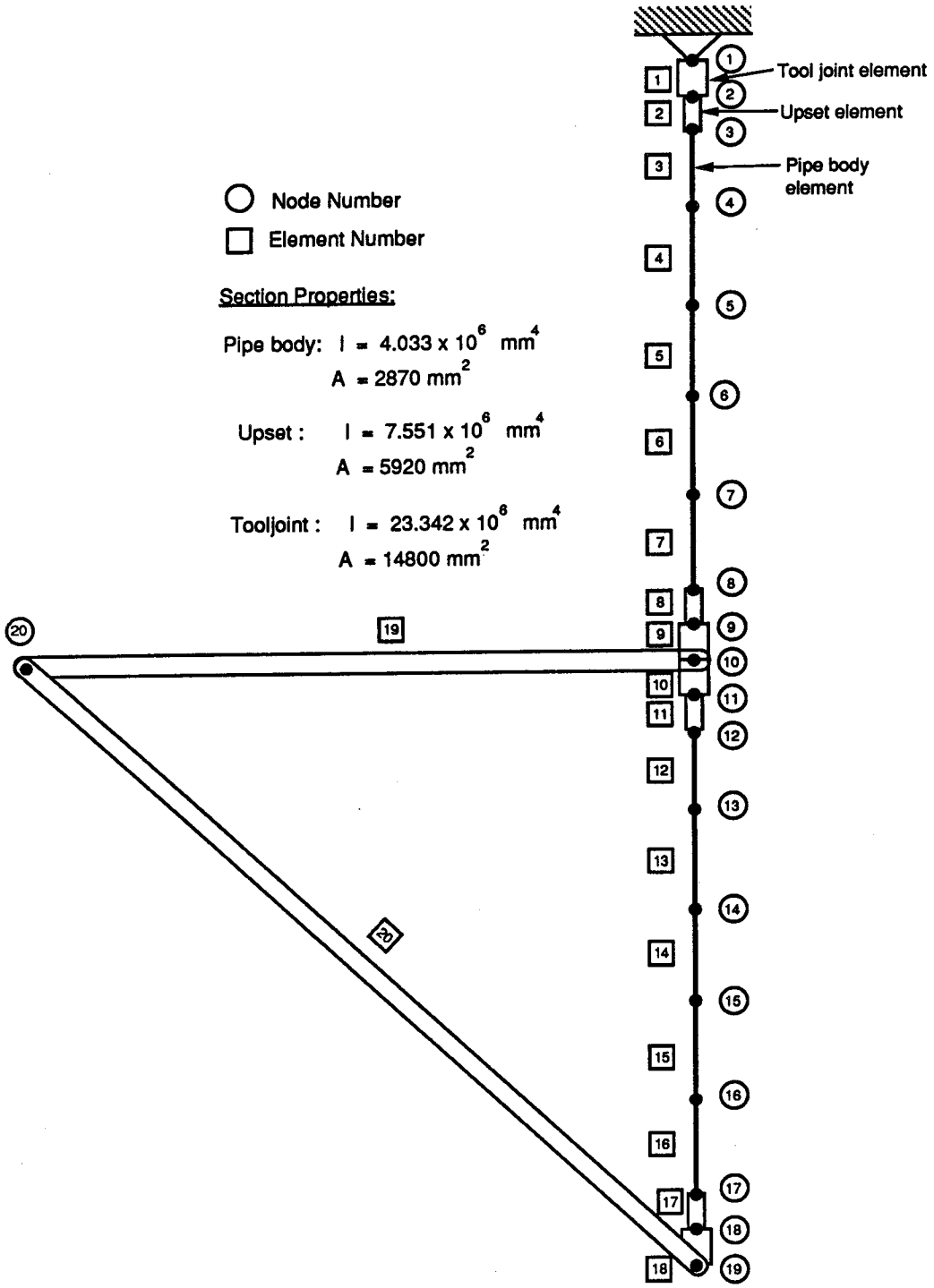

Figure 6.20 Finite Element Model of Drill Pipe in a Dogleg

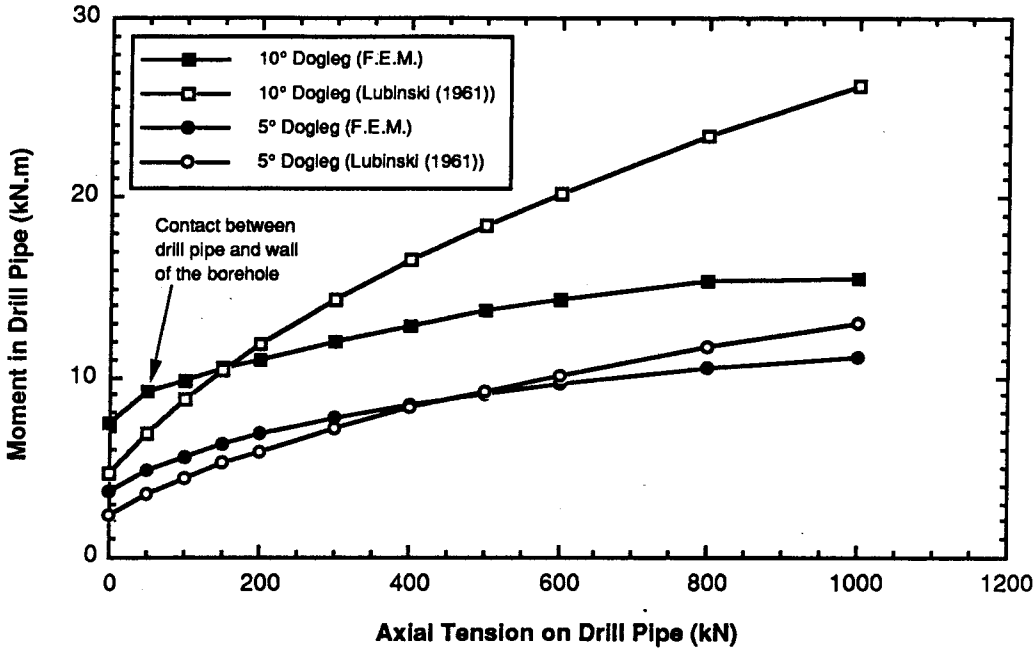

Figure 6.22 Effect of Axial Load on Maximum Bending Moment Induced in a Drill Pipe

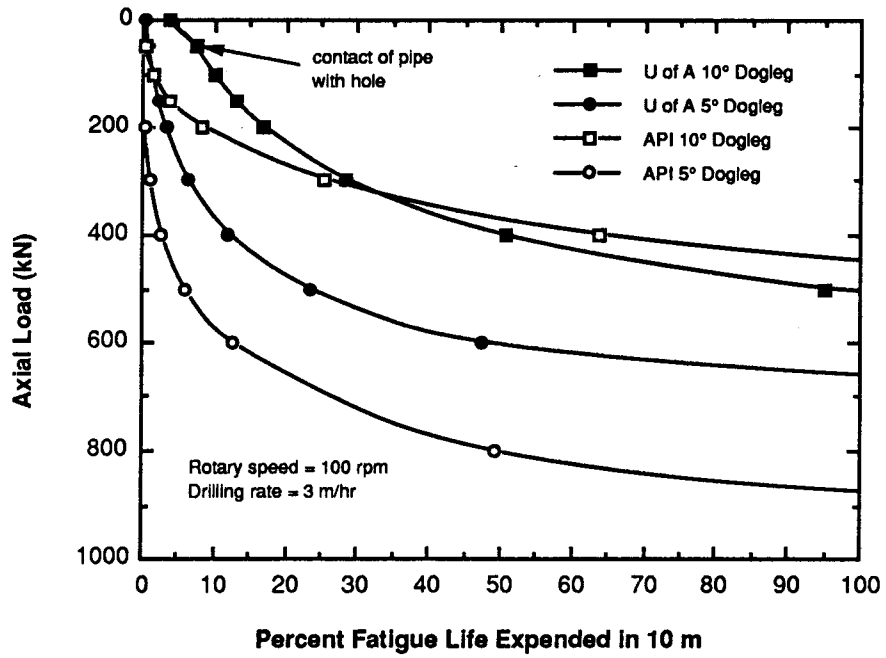

Figure 6.23 Predicted Fatigue Damage of Drill Pipe in Gradual Dogleg - Non-corrosive Environment

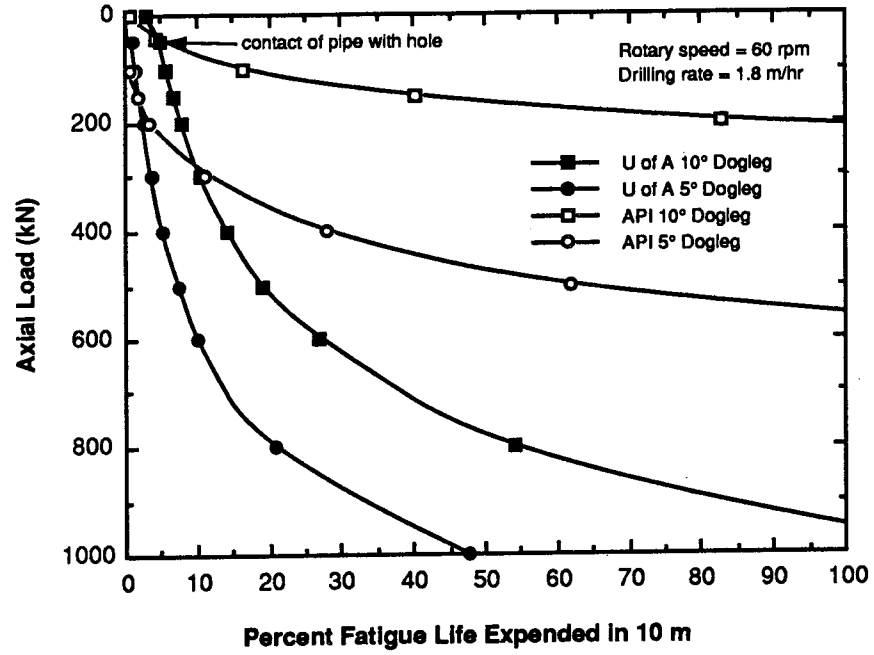

Figure 6.24 Predicted Fatigue Damage of Drill Pipe in Gradual Dogleg - Corrosive Environment

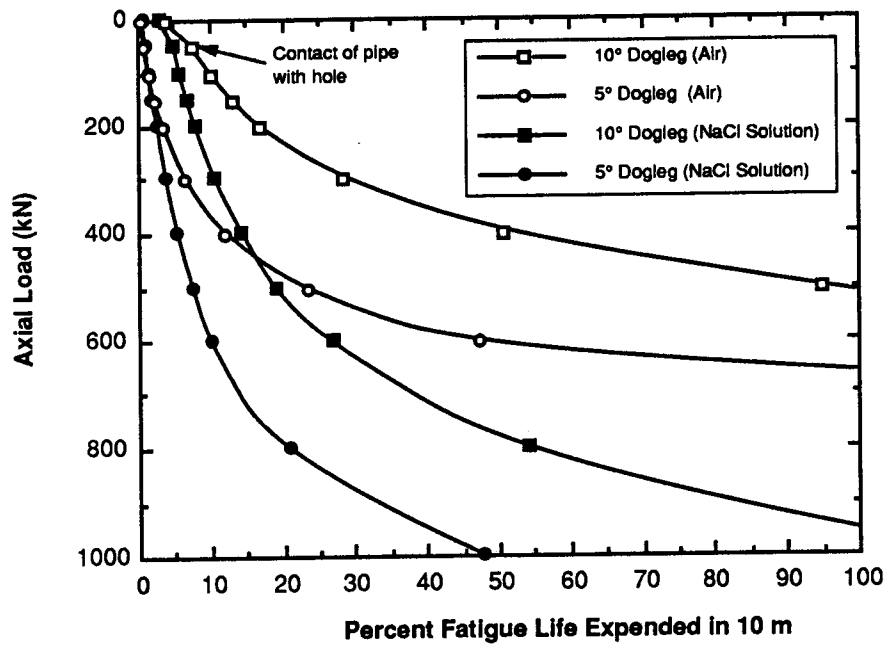

Figure 6.25 Predicted Cumulative Damage in Air or in NaCl Solution

Chapter 7

Summary, Conclusions and Recommendations

7.1 Summary

As shown in the literature review, fatigue of drill pipe has been a major concern of the drilling industry almost since the first time lengths of drill pipe were joined together to make up the drill string. Fatigue of drill pipe is still a major concern today, and, indeed, the number of failures in the field seems to have increased in the past decade.

The oil industry has guidelines for the fatigue life evaluation of drill pipe. These guidelines are based on the test results of full-size drill pipes that were presented in the literature in the early 1950's. All the test data published in the open literature were obtained from drill pipes tested in rotating bending without an axial load. However, in the existing fatigue guidelines, the presence of the axial load is considered to be an important factor. Furthermore, the existing guidelines for drilling in a corrosive environment were simply derived from test data obtained in air. Therefore, a review of the existing fatigue design guidelines (API, 1988) for drill pipe is timely.

The literature review indicated that to date no one has investigated the effect of mean stress on full-size drill pipe in a non-corrosive environment and in a corrosive environment. A research program was therefore initiated to study the effect of stress range, mean stress, and corrosion on fatigue strength of drill pipe. It was considered to be important to use full-size drill pipes for the test program. A preliminary test program was conducted to demonstrate that the type of failure observed in the field could be obtained in the laboratory. The test specimens used in the preliminary test program consisted of Grade E, 89 mm O.D., 19.8 kg/m drill pipe with external upset and Grade E, 114 mm O.D., 24.7 kg/m drill pipe with internal-external upset. The preliminary tests were conducted in cyclic tension and cyclic bending. The tests showed that failure of drill pipe occurs in the drill pipe body. These observations are consistent with the failures observed in the field.

A set-up was devised that permitted drill pipe to be tested in rotating bending, under an axial preload, and with or without corrosion present. Grade E, 114 mm O.D., 24.7 kg/m drill pipes with an internal-external upset were used for the main test program. A total of 29 specimens were tested in air and 21 specimens were tested in a corrosive

environment. Some of the test specimens incorporated a tooljoint, upset region, and pipe body, while others contained only the drill pipe body.

Failure surfaces were examined in order to determine the origin of fatigue failures and to obtain a qualitative estimation of the crack propagation rate. In addition, since the presence of residual stresses affects the mean stress, extensive measurements of residual stresses were made on the surface of drill pipe. Measurements were made using both the method of sectioning and X-ray diffraction.

The finite element method of stress analysis was used to investigate the effect of upset geometry on concentration of stresses in the drill pipe body. Stress concentration was investigated both under an applied axial force and under bending. The test results obtained in the investigation presented herein were compared with the work of other researchers and the prediction of fatigue life made using a fracture mechanics approach. Finally, an assessment of the existing fatigue guidelines was made using the test data obtained in the present research program.

7.2 Conclusions

The effect of stress range and mean stress on the fatigue life of drill pipe were both found to be significant. The effect of stress range and mean stress in air can be described by the relationship

$$\log N = 14.8 - 3.46 \log S_r - 1.65\times10^{-5} (S_m)^2 \qquad (5\text{-}15)$$

The effect of stress range and mean stress in a corrosive environment of 3.5 percent NaCl solution can be described by

$$\log N = 11.43 - 2.31 \log S_r - 2.67\times10^{-6} S_m^2 \log S_r \qquad (5\text{-}31)$$

where N is the fatigue life in cycles, S_m is the mean stress in MPa, and S_r is the stress range in MPa. Eq. (5-31) was developed for a rotational frequency of 1.0 Hz.

Grinding of the surface of a drill pipe during the inspection process is detrimental to the fatigue life of the drill pipe. Of 29 specimens tested in air, 13 failed due to a fatigue crack developing at grinding marks. Of 20 specimens tested in a corrosive environment, 11 failed due to cracks developing at grinding marks. Fractographic examinations showed evidence of a notch effect at the grinding marks made on the surface. In addition, residual

stress measurements using X-ray diffraction showed that beneficial compressive surface stresses are removed by grinding.

Other origins of fatigue cracks observed in the test program are surface pits, surface notches created by pipe handling during and after manufacturing, and surface inclusions. Although not frequent, the presence of surface slag inclusions and notches created by steel stenciling was found to be the most detrimental to the fatigue life of drill pipe. One drill pipe with a surface slag inclusion showed only 27 percent of the average fatigue life of two other specimens tested at the same stress level. The drill pipe with steel stencil markings, tested in a corrosive environment, showed only 25 percent of the average fatigue life of two other specimens tested at the same stress level and in the same environment. (Stencil markings punched into the pipe surface are prohibited by API specification 5D).

Examination of the fracture surfaces indicated that once a fatigue crack has propagated through the wall thickness and has become a through-thickness crack, the rate of propagation of the crack increases. This observation was also substantiated by fracture mechanics analysis which showed that more than 95 percent of the total fatigue life was expended in propagating a part-through crack through the pipe wall thickness.

The effect of upset geometry was found to be minimal when an external upset was compared with an internal-external upset alternative. The stress concentration factor calculated for the external upset geometry was 1.19 for axial tension and 1.13 for pure bending. Corresponding values for the internal-external upset were 1.17 and 1.10. Consequently, the superior performance of 98 mm O.D. drill pipe (which has an external upset) claimed by some drilling contractors cannot be attributed to the upset geometry. The better fatigue performance observed in the smaller diameter drill pipe can be attributed to the diameter of the pipe itself. For a given dogleg severity, the stress range experienced by a drill pipe as it rotates in the dogleg is smaller in smaller diameter drill pipes.

When the test results obtained in the research program presented herein were compared to the early test results presented by Bachman (1951), it was evident that a significant change in the fatigue properties of drill pipe has occurred since the early tests were published. Comparison with more recent tests by other investigators also showed that the test results obtained herein differ significantly from test results by others. This can be explained by the different conditions (stress and environment) used in different test programs.

A critical evaluation of the existing guidelines for drilling in a non-corrosive showed that they overestimate the fatigue life of drill pipe. The existing guidelines consistently predict less fatigue damage than predicted as a result of the present investigation. The converse was found to be true for a corrosive environment. In this case, the existing guidelines were found to be unconservative only at low axial loads. This can be explained partly by the assumption made by Lubinski (1961) that a fatigue endurance limit exists in a corrosive environment, and also partly result from the simplifications made by Lubinski in his stress analysis of a drill pipe in a dogleg.

7.3 Recommendations

The recommendations made in this section can be divided into two parts: general recommendations which are aimed at improving the present situation in the field and recommendations for future research.

7.3.1 General Recommendations

Both the fractographic examination conducted on failed test specimens and a fracture mechanics analysis indicate that a fatigue crack propagates rapidly once it has become a through-thickness crack. The fraction of the total fatigue life remaining after the crack has become a through-thickness crack is very small (in the order of 1 to 3 percent of the total fatigue life). It is recommended, therefore, that a drill pipe be replaced as soon as a washout has been detected since a twistoff is likely to occur shortly after the washout is detected.

Drilling is performed in the presence of drilling mud, which is likely to be more corrosive than air. Since guidelines for non-corrosive environment are based on tests conducted in air, it is very unlikely that the fatigue life prediction based on those tests is applicable to a practical field situation. Tests conducted by Helbig and Vogt (1987) have shown that running drill pipes in tap water is as damaging as running pipes in a saline solution. Because drilling mud provides a corrosive environment that is probably not less corrosive than tap water, it is recommended that in any drilling environment the assumption be made that the environment is corrosive. A cumulative damage curve for a corrosive environment should be used to evaluate the fatigue damage sustained by a drill pipe. The use of the API recommended dogleg severity, below which no fatigue damage is sustained by the drill pipe(API, 1988), should be discontinued. The limits of dogleg severity presently recommended are based on the assumption that an endurance limit exists in a

corrosive environment. Control for fatigue should be done through cumulative damage calculations, rather than through control of dogleg severity. The damage sustained by a drill pipe can be evaluated by identifying each pipe in a drill string and keeping track of its position in the string. Using the borehole directional surveys, the cumulative damage of every drill pipe in a drill string can be evaluated. Any drill pipe which has accumulated a certain percentage of its total fatigue life (the value of the cumulative fatigue life required before a drill pipe is removed from the drill string depends of the amount of risk the contractor is willing to take) should be inspected for cracks. A management scheme to monitor fatigue damage in this way would be initially expensive for a given drilling contractor, but the cost would probably be small compared with typical failure experience.

It was found that the internal-external upset geometry does not give rise to greater stress concentration than does the external upset geometry. Since damage to the internal protective coating has been identified in the internal upset region on field failed specimens, it is recommended that external upset drill pipes, which are flush inside, be used whenever they are available. The flush inside geometry is less susceptible to damage by tools run down into the drill pipe.

Since drill pipes of smaller diameter experience smaller bending stresses than do larger diameter drill pipes in doglegs of the same severity, whenever practicable smaller diameter drill pipes can be used in order to minimize the risks of fatigue failure.

Grinding of the surface of the drill pipe, as done during the inspection process, was found to be detrimental to the fatigue life of the drill pipe. Grinding should therefore be kept to a minimum during the inspection process, especially near the upset region where bending stresses are maximum due to secondary effects of the axial tension. A stress relieve heat treatment of the drill pipe after the inspection stage would be preferable since it would reduce the high tensile residual stresses sometimes introduced by grinding.

7.3.2 Recommendations for Future Research

The work presented herein leaves many questions with respect to fatigue of drill pipe still unanswered. Consequently, there is a need for more research into several areas pertaining to fatigue of drill pipe.

1. Since drilling is usually performed in a corrosive environment, future research in that area should concentrate on fatigue in a corrosive environment. All the tests performed in the present investigation to determine the effect of a corrosive

environment on fatigue life were performed in a 3.5 percent NaCl solution. Since our present understanding of the corrosion fatigue problem does not enable us to predict the behaviour of drill pipes in other environments from the results obtained in a sodium chloride solution, different environments should be investigated experimentally. Other environments that are encountered in the field are those containing CO_2 and H_2S. Hydrogen sulfide is considered to be one of the most detrimental environments to high strength steel.

2. All the tests were conducted on one size and a single grade of drill pipe. Although the size of drill pipe is not believed to significantly influence the fatigue resistance, the grade of steel could be a significant factor on fatigue of drill pipe in various environments. Therefore, different grades of drill pipe should be investigated in different environments.

3. The effect of mean stress in a corrosive environment was found to be dependent on the level of stress range. The expressions proposed for the effect of mean stress (equations (5-27) and (5-29)) are based on tests performed at only two different stress range levels. More tests, at various mean stress levels and at a stress range level different from the levels already investigated, should be conducted to verify the interaction of stress range and mean stress. A minimum of six more tests (duplicate tests at three different mean stress levels (0, 125 MPa, and 250 MPa) and at a stress range of 210 MPa) are recommended.

4. The effect of testing frequency on the fatigue life in a corrosive environment is known to be influential. The sensitivity of the fatigue life to testing frequency should be investigated within a range covering the frequencies used in the field. A range of frequency from 1.0 Hz to 2.5 Hz should cover all the conditions encountered in the field. This parameter was investigated by Helbig and Vogt (1987) on small coupons. Testing frequencies of 1.7 Hz and 17 Hz were used for the investigation. It is recommended that testing frequency should be investigated using full-size drill pipes and within a more narrow range of testing frequencies

5. All the drill pipes tested in the test program presented herein were new drill pipes with a surface free from field related damage. When drill pipes are put into use in the field, the use of slips sometimes produces notches on the pipe

body in the critical region (the region where bending stresses are maximum when the pipe is subjected to axial tension in a crooked hole). Many times in the past such slip marks have been associated with fatigue failures (Grant and Texter, 1941; Vingoe, 1972). The effect of slip marks, or other surface notches, should be investigated in order to determine the decrease in fatigue life that can be expected from those notches.

6. In predicting the cumulative fatigue damage, it was assumed that the Palmgren-Miner rule applies equally to corrosive and non-corrosive environment. Because of the complex interaction that exists between stresses and the environment, it is likely that this simple rule does not apply in a corrosive environment. The problem of cumulative damage should therefore be investigated for a corrosive environment.

7. The interaction between cyclic bending, cyclic axial tension, and cyclic torsion was neglected in the present investigation. Field conditions, however, are likely to encounter a combination of cyclic bending, axial loading, and torsion. Having only one kind of cyclic loading is the exception rather than the rule. The problem of cyclic load combinations should therefore be investigated.

8. In order to come up with more realistic predictions of field performance, more field data on loading of drill pipe need to be obtained in order to derive a load spectrum that would be representative of field loading conditions. Such a load spectrum would be used in future test programs.

9. The fracture mechanics approach was found to give inadequate predictions of the test results. Part of the reason for the observed discrepancy between predicted and measured fatigue lives is the unavailability of fracture toughness data and fatigue crack growth curves for grade E drill pipe steel. Crack growth studies and fracture toughness measurements should be conducted on drill pipe steel having the same microstructure and texture as the pipes used by the industry. It is believed that the grain elongation observed in the direction of the pipe axis in these tests is also influential on the toughness of the material and should be considered in fracture toughness studies. The fracture toughness and crack growth studies should be performed in various environments.

10. The problem of drill string dynamics was not addressed in this research program. However, it must be recognized that vibration of the drill pipe has the potential of introducing many cycles of loading within a short time. This number of cycles can significantly exceed the number of cycles predicted in the work presented in Chapter 6. More research on drill string dynamics is needed in order to estimate more realistically the number and the magnitude of loading cycles to which a drill pipe is subjected.

List of References

Aarrestad, T.V., H.A. Tϕnnesen, and Å. Kyllingstad (1986). **Drillstring Vibrations: Comparison Between Theory and Experiments on a Full-Scale Research Drilling Rig.** Paper SPE 14760 presented at the 1986 IADC/SPE Drilling Conference, Dallas, Feb. 10-12.

Adams, N.J. and T. Charrier (1985). **Drilling Engineering, A Complete Well Planning Approach.** PennWell Publishing Company, Tulsa, Oklahoma.

American Petroleum Institute (1988). **Specification for Drill Pipe.** API Specification 5D, first edition, Washington, DC., March 15.

American Petroleum Institute (1989). **Recommended Practice for Drillstem Design and Operating Limits.** API Recommended Practice Bulletin RP7G, 13th Edition, Washington, DC., April 1.

American Petroleum Institute Mid-Continent District Study Committee on Straight-Hole Drilling (1963). **Determination of Maximum Possible Dog Legs From Field Data.** Drilling and Production Practice, American Petroleum Institute, New York, N.Y., pp. 106-111.

American Society for Testing and Materials (1989). Standard Test Methods and Definitions for Mechanical Testing of Steel Products. ASTM A370-88a, Volume 01.03

Anon. (1990). **Drill string failures are scrutinized.** Drilling Contractor, Vol. 46, No. 12, p. 55-57.

Azar, J.J. (1979). **How O_2 and Chlorides Affect Drill Pipe Fatigue.** Petroleum Engineer, Vol. 51, No. 3, pp. 72-78.

Azar, J.J. and J.L. Lummus (1976). **Mud pH vs Corrosion Performance.** Petroleum Engineer, Vol. 48, No. 11, pp. 86-90.

Bachman, W.S. (1951). **Fatigue Testing and Development of Drill Pipe to Tool Joint Connections.** World Oil, Vol. 132, No. 1, pp. 104-116.

Bailey, J.J. and Finnie, I. (1960). **An Analytical Study of Drill-String Vibration.** Journal of Engineering for Industry, Transactions, ASME, Series B, Vol. 82, No. 2, pp. 122-128.

Baldy, M.F. (1961). **Sulfide Stress Cracking of Steels for API Grade N-80 Tubular Products.** Corrosion, Vol. 17, p. 509t-513t.

Best, B. (1983). **Casing Wear Caused by Tool Joint Hardfacing.** Society of Petroleum Engineers of AIME, SPE No. 11992.

Boice, E.G. and R.S. Dalrymple (1963). **The Design and Performance Characteristics of Aluminum Drill Pipe.** Journal of Petroleum Technology, Vol. 15, No. 12, pp. 1285-1291.

Boniszewski, T. and J. Moreton (1967). **Effect of Microvoids and Manganese Sulfide Inclusions in Steel on Hydrogen Evolution and Embrittlement.** British Welding Journal, Vol. 14, p.321.

Box, G.E.P., W.G. Hunter, and J.S. Hunter (1978). **Statistics for Experimenters: An Introduction to Design, Data Analysis, and Model Building.** John Wiley & Sons, New York.

Broek, D. (1986). **Elementary Engineering Fracture Mechanics.** 4th Edition, Martinus Hijhoff Publishers, Boston.

Broek, D. (1989). **The Practical Use of Fracture Mechanics.** Kluwer Academic Publishers, Boston.

Brown, B.F. (1977). **Solution Chemistry Within Cracks in Steels.** Stress Corrosion Cracking and Hydrogen Embrittlement of Iron Base Alloys. NACE-5 International Conference Series, Staehle, Hochmann, McCright, and Slater, Editors, pp. 747-750.

Buscemi, C.D., L.J. Klein, and G.B. Kohut (1988). **Criterion Proposed to Reduce Drill Pipe Failures.** Oil and Gas Journal, Vol. 86, No. 41, pp. 64-68.

Bush, H.E., R. Barbee, and J.P. Simpson (1966). **Current Techniques for Combating Drill-Pipe Corrosion.** Drilling and Production Practice, American Petroleum Institute, New York, N.Y., pp. 59-69.

Carter, C.S. and M.V. Hyatt (1977). **Review of Stress Corrosion Cracking of Low Alloy Steels with Yield Strengths Below 150 ksi.** Stress Corrosion Cracking and Hydrogen Embrittlement of Iron Base Alloys. NACE-5 International Conference Series, Staehle, Hochmann, McCright, and Slater, Editors, pp. 524-600.

Casner, J.A. (1961). **Care and Handling of High-Strength Tubular Goods.** Drilling and Production Practice, American Petroleum Institute, New York, N.Y., pp. 169-176.

Chinese Petroleum Standardization Committee (1987). **Drill Pipe Life Could be Drastically Increased.** Drilling Contractor, Vol. 43, No. 5, p.33.

Chin, W.C. (1988). **Why Drill Strings Fail At The Neutral Point.** Petroleum Engineer International, Vol. 60, No. 7, pp. 62-67.

Committee E-9 on Fatigue (1963). **A Guide for Fatigue Testing and the Statistical Analysis of Fatigue Data.** ASTM Special Technical Publication No. 91-A, Second Edition, American Society for Testing and Materials, Philadelphia, .

Cunningham, R.A. (1968). **Analysis of Downhole Measurements of Drill String Forces and Motions.** Journal of Engineering for Industry, Transactions, ASME, Series B, Vol. 90, No. 2, pp. 208-216.

Dale, B.A. (1988a). **An Experimental Investigation of Fatigue Crack Growth in Drillstring Tubulars.** SPE Drilling Engineering, Vol. 3, No. 4, pp. 356-362.

Dale, B.A. (1988b). **Inspection Interval Guidelines to Reduce Drillstring Failures.** Paper SPE 17207, 1988 IADC/SPE Drilling Conference, Dallas, Texas, Feb. 28 - March 2.

Dareing, D.W. (1982). **Drill Collar Length Is a Major Factor in Vibration Control.** Paper SPE 11228, SPE 1982 Fall Meeting, New Orleans, LA., Sept. 26-29.

Dareing, D.W. (1983). **Rotary Speed, Drill Collars Control Drillstring Bounce.** Oil and Gas Journal, Vol. 81, No. 23, pp. 63-68.

Dareing, D.W. (1984). **Drillstring Vibrations Create Crooked Holes.** Oil and Gas Journal, Vol. 82, No. 2, pp. 83-86.

Dareing, D.W. and Livesay, B.J. (1968). **Longitudinal and Angular Drill String Vibrations With Damping.** Journal of Engineering for Industry, Transactions, ASME, Series B, Vol.90, No. 4, pp. 1-9.

Darken, L.S. and R.P. Smith (1949). **Behavior of Hydrogen in Steel During and After Immersion in Acid.** Corrosion, Vol. 5, p.1-16.

Dawson, R., Y.Q. Lin, and P.D. Spanos (1987). **Drill String Stick-Slip Oscillations.** Proceedings of the 1987 Spring Conference of the Society of Experimental Mechanics, Houston, June 14-19.

Deily, F.H., D.W. Dareing, G.H. Paff, J.E. Ortloff, and R.D. Lynn (1968). **Downhole Measurements of Drill String Forces and Motions.** Journal of Engineering for Industry, Transactions, ASME, Series B, Vol. 90, No. 2, pp. 217-225.

Desvignes, M., B. Gentil, and L. Castex, (1987). **Fatigue Progressing of Shot Peened Steel.** Residual Stresses in Science and Technology, Vol. 1, Macherauch and Hauk, Editors, DGM Informationsgesellschaft mbH, Germany, pp. 441-448.

Dieter, G.E. (1986). **Mechanical Metallurgy.** McGraw-Hill, New York.

Finnie, I. and J.J. Bailey (1960). **An Experimental Study of Drill-String Vibration.** Journal of Engineering for Industry, Transactions, ASME, Series B, Vol. 82, No. 2, pp.129-135.

Fisher, J.W., K.H. Frank, M.A. Hirt, and B.M. McNamee (1970). **Effect of Weldments on the Fatigue Strength of Steel Beams.** National Cooperative Highway Research Program Report 102, Highway Research Board, Washington D.C.

Flavenot, J.F. (1987). **Effect of Grinding Conditions on Fatigue Behaviour of 42CD4 Grade Steel: Fatigue Strength Estimation Incorporating Residual Stresses Using Different Fatigue Criteria.** Residual Stresses in Science and Technology, E. Macherauch and V. Hauk, Editors, Volume 2, Informationsgesellshaft-Verlag, pp. 735-742.

Fletcher, H.W. (1935). **Drill Stem.** Drilling and Production Practice, American Petroleum Institute, New York, N.Y., pp. 150-161.

Fontana, M.G. (1986). **Corrosion Engineering.** McGraw-Hill, New York.

Fontana, M.G. and R.W. Staehle (1967). **Fundamentals of Corrosion of High Strength Steels.** Seventh World Petroleum Congress, Mexico, D.F., March 2-8, pp. 183-200.

Frazer, J.P. and R.S. Treseder (1952). **Cracking of High Strength Steels in Hydrogen Sulfide Solution.** Corrosion, Vol. 8, p. 342-350.

Fuchs, H.O., and R.I. Stephens (1980). **Metal Fatigue in Engineering.** John Wiley & Sons, New York.

Führing, H. and T. Seeger (1984). **Fatigue Crack Growth Under Variable Amplitude Loading.** Subcritical Crack Growth Due to Fatigue, Stress Corrosion and Creep, L. H. Larsson, editor, Elsevier Applied Science, New York.

Gensmer, R. P. (1986). **A Contractor's View of Drill Pipe Life.** Paper SPE 14790, 1986 IADC/SPE Drilling Conference, Dallas, Texas, Feb. 10-12.

Gensmer, R.P. (1988). **Field Correlation Between Internal Taper Length and Tube Failures in 4.5 in. 16.60E, IEU Drill Pipe.** Paper SPE 17205, 1988 IADC/SPE Drilling Conference, Dallas, Texas, Feb. 28 - March 2.

Gooch, A.E. (1977). **Casing Wear Minimized by Tool Joint Hard Facing.** Transactions of the 1977 IADC Drilling Technology Conference, New Orleans, Louisiana, March 16-18.

Graham, H.W. (1935). **The Development of Rotary Drill Pipe.** Drilling and Production Practice, American Petroleum Institute, New York, N.Y., pp. 162-177.

Grant, R.S. and H.G. Texter (1941). **Causes and Prevention of Drill Pipe and Tool-joint Troubles.** Drilling and Production Practice, American Petroleum Institute, New York, N.Y., pp. 9-48.

Halsey, G.W., Å. Kyllingstad, T.V. Aarrestad, and D. Lysne (1986). **Drillstring Torsional Vibrations: Comparison Between Theory and Experiment on a Full-Scale Research Drilling Rig.** Paper SPE 15564, 1986 SPE Annual Technical Conference and Exhibition, New Orleans, LA., October 5-8.

Hampton, S. (1987). **A Contractor's History of Drill String Failures in the Anadarko Basin.** Paper SPE 16072, 1987 SPE/IADC Drilling Conference, New Orleans, Louisiana, March 15-18.

Hansford, J.E. and A. Lubinski (1964). **Effects of Drilling Vessel Pitch or Roll on Kelly and Drill Pipe Fatigue.** Journal of Petroleum Technology, Vol. 16, No. 1, pp. 77-86.

Hansford, J.E. and A. Lubinski (1966). **Cumulative Fatigue Damage of Drill Pipe in Doglegs.** Journal of Petroleum Technology, Vol. 18, No. 3, pp. 359-363.

Harnett, D.L. (1982). **Statistical Methods.** Third edition, Addison-Wesley, Don Mills, Ontario.

Hauk, V., P. Höller, and E. Macherauch (1987). **Measuring Techniques of Residual Stresses - Present Situation and Future Aims.** Residual Stresses in Science and Technology, Vol. 1, Macherauch and Hauk, Editors, DGM Informationsgesellschaft mbH, Germany, pp. 231-242.

Helbig, R and G.H. Vogt (1987). **Reversed Bending Fatigue Strength of Drill Strings Subject to the Attack of Drilling Fluids.** Oil and Gas European Magazine, International Edition of Erdöl Erdgas Kohle, No. 2, pp. 16-20.

Hertzberg, R.W. (1989). **Deformation and Fracture Mechanics of Engineering Materials.** Third edition, John Wiley and Sons, New York.

Holbert, D. (1985). **Conventional Tubulars Can Cut Cost of Drilling in Horizontal Holes.** Oil and Gas Journal, Vol. 83, No. 23, pp. 68-73.

Hudgins, C.M., R.L. McGlasson, P. Mehdizadeh, and W.M. Rosborough (1966). **Hydrogen Sulfide Cracking of Carbon and Alloy Steels.** Corrosion, Vol. 22, p.238.

Jackson, L.R., H.M. Banta, and R.C. McMaster (1947). **Battelle Reports on Field Survey.** The Drilling Contractor, Vol. 3, No. 4, pp. 11-16.

Jaske, C.E., J.H. Payer and V.S. Balint (1981). **Corrosion Fatigue of Metals in Marine Environments.** Springer-Verlag, New York.

Joosten, M.W., J. Shute, and R.A. Ferguson (1985). **New Study Shows How to Predict Accumulated Drill Pipe Fatigue.** World Oil, Vol. 201, No. 5, pp. 65-70.

Karpenko, G.V. and I.I. Vasilenko (1977). **Stress Corrosion Cracking of Steels.** Freund Publishing House, Tel-Aviv, Israel.

Kennedy, J.B. and A.M. Neville (1976). **Basic Statistical Methods for Engineers and Scientists.** Second Edition, Harper and Row, New York.

Kihara, H., M. Watanabe, K. Horikawa, and M. Inagaki (1967). **Studies on the Sulfide Corrosion Cracking of High Strength Steels Caused by H_2S.** Proceedings of Seventh World Petroleum Congress, Elsevier Publishing Co.

Kondo, Y. (1989). **Prediction of Fatigue Crack Initiation Life Based on Pit Growth.** Corrosion, Vol. 45, No. 1, pp. 7-11.

Kral, E., P.K. Sengupta, L. Newlin, and S.S. Quan (1984a). **Drillpipe Fracture, Pt. 1.** Fracture Mechanics Estimates Drillpipe Fatigue. Oil and Gas Journal, Vol. 82, No. 32, pp. 50-55.

Kral, E., P.K. Sengupta, L. Newlin, and S.S. Quan (1984b). **Drillpipe Fracture, Pt. 2.** Fracture Mechanics Concept Offers Models to Help Calculate Fatigue Life in Drill Pipe. Oil and Gas Journal, Vol. 82, No. 33, pp. 115-121.

Kyllingstad, Å. and G.W. Halsey (1988). **A Study of Slip/Stick Motion of the Bit.** SPE Drilling Engineering, Vol. 3, No. 4, pp. 369-373.

Laird, C. and D.J. Duquette (1973). **Mechanisms of Fatigue Crack Nucleation.** Corrosion Fatigue: Chemistry, Mechanics and Microstructure. NACE-2, International Conference Series, Devereux, McEvily and Staehle, Editors, pp. 88-117.

Little, R.E. and E.H. Jebe (1975). **Statistical Design of Fatigue Experiments.** Applied Science Publishers Ltd., Essex, England.

Low, J.R. Jr. (1959). **Fracture.** John Wiley and Sons, New York.

Lubinski, A. (1961). **Maximum Permissible Dog-Legs in Rotary Boreholes.** Journal of Petroleum Technology, Vol. 13, No. 2, pp. 175-194.

Maddox, S.J. (1975). **The Effect of Mean Stress on Fatigue Crack Propagation: A Literature Review.** International Journal of Fracture. Vol. 11, No.3, pp. 389-408.

Macherauch, E. and K.H. Kloos (1987). **Origin, Measurement, and Evaluation of Residual Stresses.** Residual Stresses in Science and Technology, Vol. 1, Macherauch and Hauk, Editors, DGM Informationsgesellschaft mbH, Germany, pp. 3-26.

Marion, T.L. (1987). **IADC Tackles Drill Pipe Failures.** Drilling Contractor, Vol. 42, No. 1, pp. 25-26.

Miller, C.E. and H.M. Rollins (1968). **Evaluation of a Vibration Damping Tool and of Drill Stem Torque Requirements From Data Recorded by an Instrumented Drill Stem Member.** Journal of Engineering for Industry, Transactions, ASME, Series B, Vol. 90, No. 2, pp. 226-230.

Millheim, K.K. and M.C. Apostal (1981). **The Effect of Bottomhole Assembly Dynamics on the Trajectory of a Bit.** Journal of Petroleum Technology, December, pp. 2323-2338.

Millheim, K., S. Jordan, and C. Ritter (1978). **Bottom-hole Assembly Analysed by the Finite Element Method.** Journal of Petroleum Technology, Vol. 30, No. 2, pp. 265-274.

Mitchell, R.F. and M.B. Allen (1985). **Lateral Vibration: The Key to BHA Failure Analysis.** World Oil, Vol. 200, No. 4, pp. 101-106.

Moore, M.G., and W.P. Evans (1958). **Mathematical Correction for Stress in Removed Layers in X-Ray Diffraction Residual Stress Analysis.** SAE Transactions, Vol. 66, pp. 340-345.

Moritis, Guntis (1990). **Horizontal Drilling Scores More Successes.** Oil and Gas Journal, Vol. 88, No. 9, pp. 53-64.

NACE Committee T1G (1954). **Sulfide Corrosion Cracking of Oil Production Equipment.** Corrosion, Vol. 10, p.413-419.

NACE Committee 1-G (1952). **Field Experience With Cracking of High Strength Steels in Sour Gas and Oil Wells.** Corrosion, Vol. 8, p.351-354.

NACE Standard MR-01-75 (1984 Editorial Revision). **Sulfide Stress Cracking Resistance Metallic Materials for Oil Field Equipment.** Approved January 1984, National Association of Corrosion Engineers, Houston, Texas.

Nicholson, R.W. (1974). **Simple Procedure Can Help Reduce Drill Pipe Damage.** World Oil, Vol. 178, No. 6, pp.73-77.

Noyan, I.C. and J.B. Cohen (1987). **Residual Stress Measurement by Diffraction and Interpretation.** Springer-Verlag, New York.

Osgood, C. C. (1982). **Fatigue Design.** Second edition, Pergamon Press, New York.

Paslay, P.R. and D.B. Bogy (1963). **Drill String Vibrations Due to Intermittent Contact of Bit Teeth.** Journal of Engineering for Industry, Transactions, ASME, Series B, Vol. 85, No. 2, pp. 187-194.

Patton, C.C. (1974). **Corrosion Fatigue Causes Bulk of Drill-String Failures.** Oil and Gas Journal, Vol. 72, No. 30, p. 163-168.

Phelps, E.H. (1967). **Stress Corrosion Behavior of High Yield-Strength Steels.** 7th World Petroleum Congress, Mexico, D.F. April 2-8, pp. 201-209.

Raju, I.S. and J.C. Newman (1984). **Stress-Intensity Factors for Circumferential Surface Cracks in Pipes and Rods under Tension and Bending Loads.** Fracture Mechanics: Seventeenth Volume, ASTM STP 905, J.H. Underwood et al. Editors, American Society for Testing and Materials, Philadelphia, pp. 789-805.

Raseev, von D. and V. Ulmann (1983). **Untersuchungen zur Dauerfestigkeit von Bohrstangen und Gestängeverbindern.** (Studies on the Fatigue of Drill Pipes and Tool Joints). Erdoel Erdgas, Vol. 99, No. 12, pp. 396-402.

Reemsnyder, H.S. (1969). **Procurement and Analysis of Structural Fatigue Data.** Journal of the Structural Division, Proceedings ASCE, No. 95, ST7, pp. 1533-1551.

Rollins, H.M. (1966). **What We Know About Drill-Pipe Fatigue Failure.** The Oil and Gas Journal, Vol. 64, No. 16, pp. 98-107.

Roth, M., and J. Bernasconi, (1987). **Residual Stress Distribution in Shot Peened Plates - Analysis of Experimental Data.** Residual Stresses in Science and Technology, Vol. 1, Macherauch and Hauk, Editors, DGM Informationsgesellschaft mbH, Germany, pp. 427-440.

Scholtes, B. (1987). **Residual Stresses Introduced by Machining.** Advances in Surface Treatments, Technology - Applications - Effects. A. Niku-Lari, editor, Volume 4, Pergamon Press, Toronto, pp. 59-71.

Shryne, R. and J.E. Smith (1986). **New Tool Joint Improves High-Angle Drilling.** Petroleum Engineer International, September, pp. 44-46.

Shutts, W.C. (1934). **Recent Developments in Joint Designs of Tubular Goods.** Drilling and Production Practice, American Petroleum Institute, New York, N.Y., pp. 132-139.

Smith, T. (1978). **Tool Joint - Drill Pipe Welding Techniques.** Paper SPE 7100P, Offshore South East Asia Conference, Society of Petroleum Engineers Session, February 21-24.

Snape, E. (1967). **Sulfide Stress Corrosion of Some Medium and Low Alloys Steels.** Corrosion, Vol. 23, p.154-172.

Snape, E. (1968). **Role of Composition and Microstructure in Sulfide Cracking of Steel.** Corrosion, Vol. 24, p.261-282.

Speidel, M.O. (1977). **Corrosion Fatigue in Fe-Ni-Cr Alloys.** Stress Corrosion Cracking and Hydrogen Embrittlement of Iron Base Alloys. NACE-5 International Conference Series, Staehle, Hochmann, McCright, and Slater, Editors, pp. 1071-1094.

Speller, F.N. (1935). **Corrosion Fatigue of Drill Pipe.** Drilling and Production Practice, American Petroleum Institute, New York, N.Y., pp. 239-247.

Stanley, R. (1987). **Streamline Magnetic Inspection of OCTGs.** Drilling. Vol. 48, No. 1, pp. 10-13.

Stegmüller, H., L. Hafner, E. Ramm, and J.M. Sattele (1983). **Theoretische grundlagen sum FE-programm system NISA 80.** Mitteilung Nr. 1, Institut für Baustatik de Universität Stuttgart, Germany.

Suhr, R.W. (1986). **The Effect of Surface Finish on High Cycle Fatigue of a Low Alloy Steel: The Behaviour of Short Fatigue Cracks.** EGF Publication 1, K.J. Miller and E.R. de los Rios, Editors, Mechanical Engineering Publications, London, pp. 69-86.

Szklarz, K.E. (1990). **Fracture Toughness Criteria for High-Strength Drillpipe.** Paper No. 19964, 1990 IADC/SPE Drilling Conference, Houston, Texas, February 27 - March 2.

Tebedge, N., G.A. Alpsten, and L. Tall (1971). **Measurement of Residual Stresses - A Study of Methods.** Fritz Engineering Laboratory Report No. 337.8, Lehigh University, Bethlehem, Pa.

Thompson, A.W. and H.G. Texter (1948). **Field Test on Rejected Drill Pipe.** Drilling and Production Practice, pp. 87-104.

Treseder, R.S. and T.M. Swanson (1968). **Factors in Sulfide Corrosion of High Strength Steels.** Corrosion, Vol. 24, p. 31-37.

True, M.E. (1975). **Optimum Means of Protecting Casing and Drill Pipe Tool Joints Against Wear.** Journal of Petroleum Technology, Vol. 27, No. 2, pp. 246-252.

Tsukano, Y., S. Nishi, H. Miyoshi, and Y. Sogo (1988). **Appropriate Design of Drillpipe Internal Upset Geometry Focusing on Fatigue Property.** Proceedings of the IADC/SPE Drilling Conference, Dallas, Texas, 2/28/88 - 3/2/88, pp. 255-262.

Tumuluru, M. (1987). **Toughness Study of Drillpipes by the Use of Instrumented Impact Tests.** SPE Drilling Engineering, Vol. 2, No. 3, pp. 275-282.

Tuttle, R.N. and R.D. Kane, Editors (1981). **H_2S Corrosion in Oil and Gas Production ~ A Compilation Of Classic Papers.** National Association of Corrosion Engineers, Houston, Texas.

Vingoe, R.L. (1972). **Corrosion Fatigue and Bending Still Plague Drill Strings.** Oil and Gas Journal, Vol. 70, No. 15, pp. 108-111.

Warren, T. (1977). **The Effect of Hole Curvature on Drill Pipe While Drilling Inside an Open Hole.** Paper SPE 6780, SPE of AIME Conference, Colo., Oct. 9-12.

Warren, D. and G.W. Beckman (1957). **Sulfide Corrosion Cracking of High Strength Bolting Material.** Corrosion. Vol. 13, p. 631t-646t.

Williamson, J.S. and Bolton, J.B. (1983). **A User's Guide to Drill String Hardfacing.** Petroleum Engineer International, Vol. 55, No. 9, pp. 54-64.

Wolf, S.F., M. Zaksenhouse, and A. Arian (1985). **Field Measurements of Downhole Drilling Vibrations.** Paper SPE 14330, 60th Annual Technical Conference and Exhibition of the Society of Petroleum Engineers, Las Vegas, Nev., Sept. 22-25.

Zeren, F. (1986). **Fatigue Limits Analyzed for Drill Pipe in a Dogleg.** Oil and Gas Journal, Vol. 84, No. 38, pp. 31-35.

Appendix A

Test Specimens Dimensions

Test Specimens Dimensions

Prior to testing, dimensions of the test specimens were measured. The measured dimensions are presented in Table A.1. Test specimens DST1, BT1, and BT2 were 89 mm O.D., 19.8 kg/m, EU drill pipes. All the other test specimens were 114 mm O.D., 24.7 kg/m, IEU drill pipes. The first column of Table A.1 presents the specimen designation corresponding to the drill pipe from which they were obtained. Dimensions are referred to the section of the drill pipe containing the box or the pin. As shown in the figure attached to the table, dimension A is the box or pin length. Dimension B is the threaded length of the pipe section, C is the distance from the face of the box or pin to the end of the external upset. D1, D2, and D3 are the external diameter of the box or pin, the upset, and pipe body, respectively. E is the distance from the face of the box or pin to the inertia or flash weld between the pipe upset and the tool joint. F is the distance from the face of the box or pin to the start of the internal upset runout. Finally, t is the wall thickness of the pipe body.

Table A.1

Specimens Dimensions (see sketch on page 275)

Specimen	Section	A	B	C	D1	D2	D3	E	F	t
DST1	Box	**		468.0	120.9	97.1	87.9		N.A.	9.50
				467.6	120.7	97.4	89.0			9.50
							88.9			9.55
										9.55
DST1	Pin	203.0		370.0	121.0	96.8	89.2		N.A.	9.45
		203.4		369.5	120.8	96.0	89.9			9.55
							89.4			9.55
										9.60
BT1	Box	**		470.0	120.7	96.4	88.5		N.A.	9.45
				469.2	120.4	96.2	89.2			9.45
							89.0			9.45
										9.45
BT1	Pin	203.0		372.1	121.1	96.6	88.1		N.A.	9.25
		202.6		371.4	120.8	96.3	89.0			9.45
							88.7			9.20
										9.45
BT2	Box	**		483.4	120.9	97.2	88.9		N.A.	9.52
				481.6	120.7	96.8	89.0			9.47
							88.7			9.32
										9.45
BT2	Pin	201.9		368.0	121.0	97.9	87.8		N.A.	9.52
		201.7		369.0	121.4	97.6	88.3			9.55
							88.5			9.37
										9.32
BT3	Box	**		402.0	157.4	117.6	114.6		490	8.81
				403.0	157.2	117.9	114.8		485	8.53
							114.2			8.89
										8.76

Table A.1

Specimens Dimensions (cont'd)

Specimen	Section	A	B	C	D1	D2	D3	E	F	t
BT3	Pin	180.0	112.4	291.0	158.9	117.7	114.1		498	9.10
		180.4	112.9	290.6	159.4	118.2	114.6		490	8.60
							114.3			8.00
										8.94
BT4	Box	**		413.0	159.1	117.1	114.7		486	8.51
				412.6	158.7	117.8	114.9		478	8.69
							114.5			8.53
										8.15
BT4	Pin	180.1	114.0	292.0	159.1	116.7	114.7		481	8.15
		180.3	114.3	291.5	158.6	116.3	114.7		475	9.07
							114.6			8.69
										8.61
BT5	Box			415.0	158.0	116.5	114.5		495	8.33
				414.3	157.6	116.5	114.5		489	8.36
							114.3			8.54
										8.78
BT5	Pin	180.1	115.4	293.1	160.0	117.1	114.4		480	8.35
		179.8	115.2	292.6	159.7	116.9	114.5		485	8.10
							114.9			8.17
										8.24
BT6	Box	**		415.0	158.0	116.5	114.5		492	8.33
				414.6	157.9	116.1	114.5		498	8.54
							114.3			8.90
										8.77
BT6	Pin	179.8	113.5	293.3	158.5	116.0	114.5		475	8.55
		180.2	113.7	294.2	158.4	116.7	114.4		479	8.78
							114.4			8.72
										8.48

Table A.1

Specimens Dimensions (cont'd)

Specimen	Section	A	B	C	D1	D2	D3	E	F	t
BT7	Box	**		404.4	158.5	116.8	114.6		492	8.67
				405.5	158.7	116.8	114.6		495	8.43
							114.5			8.38
										8.66
BT7	Pin	179.4	113.9	290.9	159.1	116.8	114.6		485	8.46
		179.2	114.5	292.0	158.9	116.6	114.5		480	8.47
							114.4			8.53
										8.64
BT8	Box	**		414.0	159.0	117.0	114.3		476	8.69
				413.5	159.1	116.8	114.3		478	8.31
							114.3			8.33
										8.61
BT8	Pin	179.6	114.0	292.0	159.3	116.9	115.0		480	8.81
		179.4	113.9	291.3	159.2	116.7	114.9		484	8.51
							115.1			8.15
										8.36
RB1	Box	260.0		452.0	159.6	119.0	114.2	327	482	8.33
		260.0		452.4	159.4	119.7	114.4	323	474	8.70
							114.5			8.65
										9.50
RB1	Pin	180.7	112.8	350.1	159.4	119.0	114.4	338	486	8.15
		180.4	112.8	348.2	159.1	119.6	114.4	340	488	8.76
							114.0			8.14
										8.85
RB2	Box	256.3		433.4	159.5	118.8	114.35	360	497	8.33
		255.8		430.4	159.5	118.8	114.55	325	498	8.42
							115.35			8.89
										8.79

Table A.1

Specimens Dimensions (cont'd)

Specimen	Section	A	B	C	D1	D2	D3	E	F	t
RB2	Pin	182.2	113.3	332.1	159.0	119.6	114.90	339	500	8.61
		182.2	112.9	322.0	159.0	120.0	114.65	340	503	8.84
							114.8			8.45
										8.59
RB3	Box	258.8		431.3	159.3	119.2	114.7	337	490	8.45
		258.5		426.9	159.2	119.2	114.85	335	482	8.24
							114.90			8.81
										8.95
RB3	Pin	183.3	112.0	331.1	159.5	119.1	114.35	339	499	8.57
		183.7	112.4	332.0	159.2	119.0	114.95	343	503	9.00
							115.15			9.28
										9.11
RB4	Box	256.4		429.5	159.3	119.2	114.25	334	472	8.92
		256.3		429.8	159.1	119.2	114.35	335	468	8.66
							114.90			8.99
										8.92
RB4	Pin	184.4	112.0	334.2	158.7	118.8	114.3	337	473	8.62
		181.0	112.0	333.8	158.7	119.1	114.45	337	471	9.02
							114.55			8.89
										8.66
RB5	Box	254.4		430.9	159.3	118.7	114.45	325	463	8.33
		254.6		433.5	159.2	118.9	114.25	330	460	8.89
							114.25			8.86
										8.64
RB5	Pin	180.9	113.6	330.4	159.6	119.4	114.25	333	474	8.64
		181.0	113.4	328.9	159.4	119.8	114.60	331	467	9.32
							114.30			9.00
										9.09

Table A.1

Specimens Dimensions (cont'd)

Specimen	Section	A	B	C	D1	D2	D3	E	F	t
RB6	Box	258.4		415.0	159.6	119.5	113.85	328	447	8.27
		257.4		412.2	159.9	119.6	114.25	335	445	8.08
							114.45			8.22
										8.69
RB6	Pin	173.4	113.2	305.4	159.3	119.5	114.00	328	445	8.08
		174.4	113.2	304.0	159.3	119.6	114.40	330	447	7.81
							114.45			8.59
										8.38
RB7	Box	257.2		435.1	159.4	119.3	114.35	325	467	8.17
		257.2		434.6	159.3	119.1	114.15	322	470	8.70
							114.10			8.36
										9.18
RB7	Pin	182.5	113.0	337.5	159.1	119.2	115.0	336	472	9.26
		181.6	114.0	335.2	159.1	119.8	114.8	337	482	9.35
							114.9			8.93
										8.38
RB8	Box	255.0		436.8	159.5	119.2	114.7	330	475	8.55
		254.3		430.2	159.6	119.1	114.8	320	470	7.64
							114.9			8.14
										8.65
RB8	Pin	183.6	110.0	336.4	159.4	119.3	114.7	337	482	8.05
		183.7	110.0	325.6	159.4	119.8	115.0	338	485	8.51
							115.0			8.31
										8.71
RB9	Box	257.5		436.8	159.3	119.0	115.0	330	480	8.94
		257.3		431.7	159.2	119.3	114.9	332	485	8.23
							114.4			8.15
										9.02

Table A.1

Specimens Dimensions (cont'd)

Specimen	Section	A	B	C	D1	D2	D3	E	F	t
RB9	Pin	181.4	114.0	333.9	159.5	119.6	114.6	335	480	9.14
		181.3	112.0	337.4	159.4	119.4	114.8	335	482	8.72
							114.9			8.43
										8.38
RB10	Box	259.5		453.1	159.6	119.9	114.2	328	463	8.74
		259.7		449.3	159.5	118.6	114.4	327	459	8.86
							114.3			8.79
										8.15
RB10	Pin	177.8	111.6	332.8	159.6	119.9	114.7	335	462	7.59
		177.5	111.5	336.2	159.4	119.0	114.2	336	462	8.91
							114.5			8.64
										8.89
RB11	Box	259.8		460.8	159.1	119.3	114.6	325	498	8.38
		259.8		463.3	158.9	118.8	114.5	327	499	9.78
							114.0			8.66
										7.90
RB11	Pin	181.2	112.9	364.2	159.0	119.3	114.8	345	495	8.61
		181.1	112.9	367.4	158.9	119.2	114.3	346	500	8.74
							114.4			8.00
										7.67
RB12	Box	258.2		444.4	159.2	119.1	114.6	328	492	9.47
		258.1		444.5	159.1	118.8	114.0	329	498	8.18
							114.1			8.36
										8.69
RB12	Pin	180.6	113.7	348.4	159.2	119.7	114.4	343	498	9.68
		180.9	113.7	350.0	159.2	119.2	114.6	343	490	9.17
							114.6			8.69
										8.13

Table A.1

Specimens Dimensions (cont'd)

Specimen	Section	A	B	C	D1	D2	D3	E	F	t
RB14	Box	257.0		407.9	159.5	119.3	114.5	338	453	7.26
		256.4		408.5	159.5	119.2	114.4	340	452	8.13
							114.5			8.08
										7.75
RB14	Pin	184.1	112.3	313.2	159.0	119.2	114.3	374	456	8.33
		183.8	112.3	308.3	159.1	118.9	114.6	375	455	7.98
							144.2			8.43
										6.86
RB15	Box	258.1		458.7	159.4	119.2	114.5	344	467	7.70
		257.4		461.4	159.3	119.0	115.0	342	463	8.43
							115.2			8.10
										8.31
RB15	Pin	181.2	113.6	356.8	159.0	120.1	114.5	331	333	8.15
		180.3	113.2	355.6	159.1	119.4	115.0	333	475	8.33
							114.9			8.33
										8.23
RB16	Box	255.6		429.1	159.1	118.9	114.6	333	436	8.28
		256.2		430.0	159.2	119.0	114.7	334	440	8.41
							114.6			8.66
										8.28
RB16	Pin	183.7	112.8	331.5	159.1	119.1	114.8	340	462	8.05
		183.8	112.6	340.9	159.2	118.9	114.9	340	461	8.64
							114.8			8.79
										8.08
RB17	Box	257.9		449.6	159.1	119.6	114.4	328	463	7.92
		257.1		449.2	159.1	119.1	114.2	329	471	8.05
							114.8			8.74
										8.10

Table A.1

Specimens Dimensions (cont'd)

Specimen	Section	A	B	C	D1	D2	D3	E	F	t
RB17	Pin	182.5	113.1	351.6	159.3	119.7	114.5	339	478	8.15
		182.7	113.0	351.6	159.3	119.5	114.5	340	475	8.26
							114.4			8.74
										8.53
RB18	Box	256.9		450.4	159.2	119.2	114.5	334	461	9.17
		257.3		447.1	159.1	118.8	114.5	339	459	8.66
							113.4			8.76
										8.67
RB18	Pin	183.0	112.3	351.2	159.6	119.4	114.6	372	470	9.27
		183.3	112.3	354.8	159.7	119	114.1	373	469	8.56
							113.8			8.97
										8.71
RB19	Pin	184.2	113.3	330.9	159.9	118.6	114.3	345	441	8.69
		184.8	113.2	326.5	159.9	118.8	114.3	348	441	8.61
							114.3			8.66
										8.36
RB19	Box	265.0		420.0	159.4	118.6	114.3	368	435	8.61
		265.2		420.0	159.2	118.4	114.7	370	436	8.61
							114.5			9.04
										8.66
RB20	Pin	181.6	112.8	313.8	159.5	118.9	114.6	365	442	8.79
		181.3	113.4	314.0	159.5	118.9	114.7	369	440	8.84
							114.5			8.43
										8.76
RB20	Box	255.0		430.0	159.5	118.8	114.6	330	395	9.09
		259.3		425.0	159.4	119.4	114.3	335	410	9.17
							114.5			8.20
										9.14

Table A.1

Specimens Dimensions (cont'd)

Specimen	Section	A	B	C	D1	D2	D3	E	F	t
RB21	Pin	183.3	113.3	315.0	159.3	119.0	114.5	340	441	8.56
		183.5	113.1	305.0	159.2	119.4	114.5	345	440	8.59
							115.5			8.99
										8.74
RB21	Box	260.0		423.0	159.9	119.0	114.4	368	430	9.02
		259.5		416.5	159.8	118.5	114.3	365	435	8.36
							114.2			8.53
										8.99
RB22	Pin	182.6	115.0	323.5	159.4	119.4	114.3	340	451	8.86
		182.3	114.5	315.0	159.6	119.1	114.10	342	457	9.55
							114.20			8.64
										9.09
RB22	Box	260.0		420.0	159.5	118.6	114.3	370	430	9.26
		260.5		420.0	159.3	118.4	114.4	367	440	9.35
							114.3			8.93
										8.38
RB23	Pin	183.6	113.4	317.2	159.3	119.1	114.4	342	440	8.55
		183.7	113.7	316.5	159.4	119.0	114.7	350	438	8.36
							114.5			8.66
										8.64
RB23	Box	265.0		420.0	160.0	118.8	114.3	368	435	8.36
		265.0		420.0	159.6	119.7	114.1	364	436	8.84
							114.5			8.43
										8.10
RB24	Pin	174.4	112.2	285.0	158.2	118.3	114.2	365	435	9.02
		174.6	112.2	296.0	158.4	118.9	114.1	354	440	8.36
							114.2			8.84
										8.94

Table A.1

Specimens Dimensions (cont'd)

Specimen	Section	A	B	C	D1	D2	D3	E	F	t
RB24	Box	255.0		395.0	159.4	118.5	114.3	325	445	8.64
		256.2		395.0	159.4	118.6	114.4	350	441	8.28
							115.3			8.26
										8.56
RB25	Pin	182.4	113.3	327.8	159.6	118.8	114.2	339	430	8.76
		182.6	112.8	323.5	159.4	120.0	114.3	346	431	9.27
							114.4			8.94
										8.69
RB25	Box	265.0		420.0	159.0	118.7	114.1	360	430	8.69
		264.3		424.3	159.2	119.2	113.9	365	420	9.25
							114.0			8.64
										8.64
RB26	Pin	182.6	112.5	313.5	159.5	118.6	114.5	370	435	8.66
		182.9	112.1	316.0	159.2	118.4	114.5	376	446	8.97
							115.6			8.69
										8.59
RB26	Box	255.0		420.0	159.2	118.4	114.4	360	443	8.74
		255.0		420.0	159.1	118.4	114.4	366	450	8.69
							114.5			8.69
										8.61
RB27	Pin	176.2	113.8	319.3	159.4	119.6	115.2	325	475	8.43
		176.2	113.9	324.0	159.4	119.9	114.8	329	471	8.59
							115.0			7.80
										7.92
RB27	Box	255.0		420.0	159.5	119.2	115.1	325	460	7.95
		254.6		425.0	159.2	119.4	115.3	330	475	7.92
							113.9			8.36
										8.53

Table A.1

Specimens Dimensions (cont'd)

Specimen	Section	A	B	C	D1	D2	D3	E	F	t
RB28	Pin	183.8	112.8	328.4	159.8	119.7	114.4	340	490	8.51
		184.0	112.6	330.6	159.7	119.6	114.4	337	500	8.46
							113.7			8.59
										8.53
RB28	Box	255.0		435.2	159.3	118.6	115.0	320	482	8.18
		256.0		430.1	159.5	118.7	115.1	327	490	9.19
							115.2			8.99
										7.98

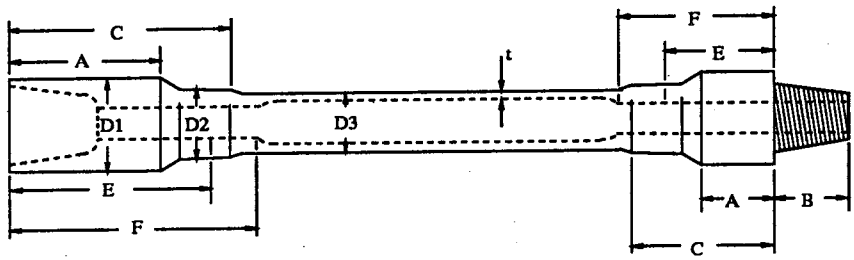

* * Box length could not be measured because of the presence of hardsurfacing.

Appendix B

Pin Attachment for Cyclic Tension Specimen

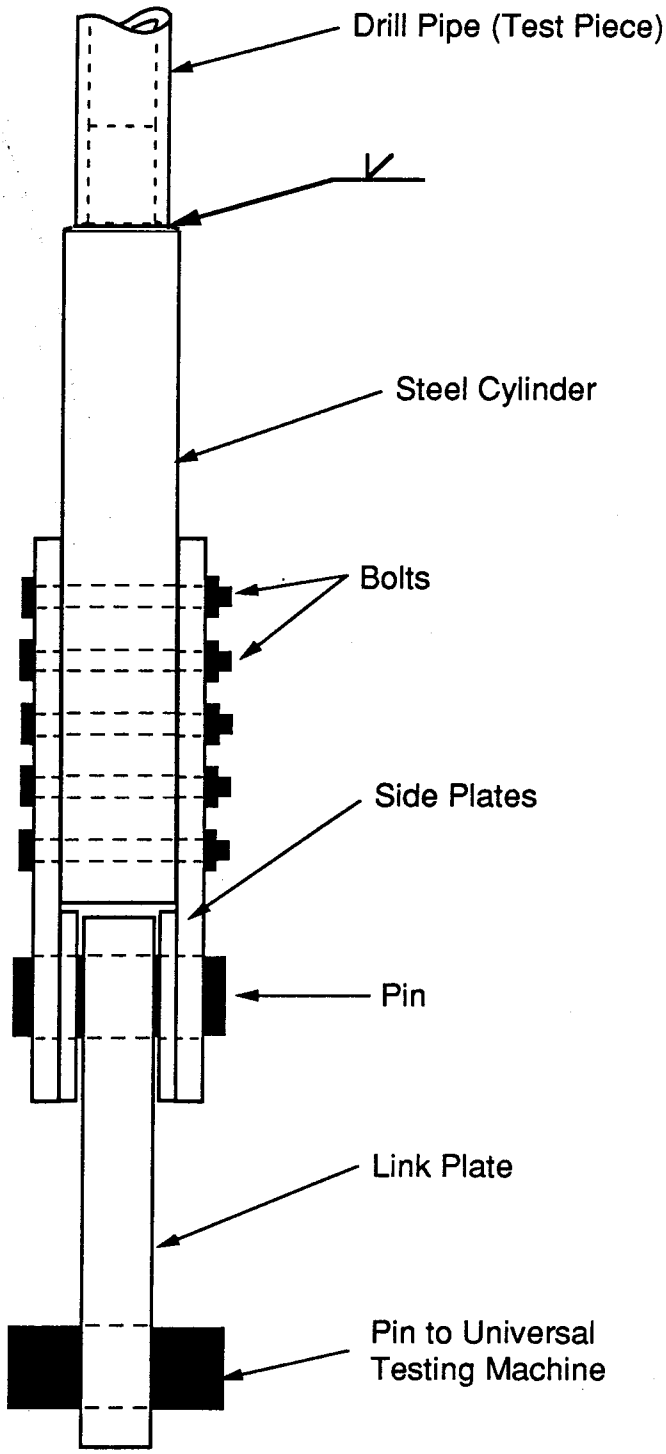

Figure B.1 Pin Connection Detail For Cyclic Tension Test

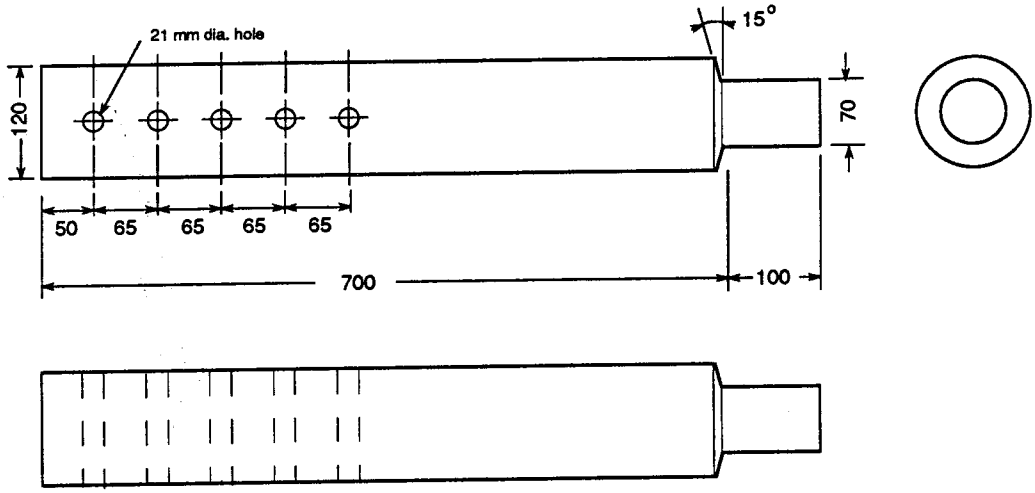

Note: Steel is AISI 4130 grade

Figure B.2 Solid Cylindrical End Piece

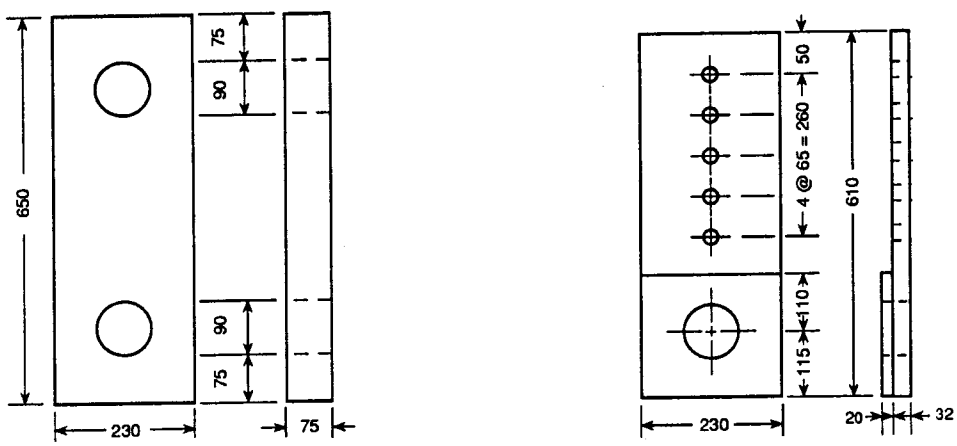

Link Plate

Side Plate

Figure B.3 Load Transfer Plates Dimensions

Appendix C

Hardware for Prestressing of Drill Pipes

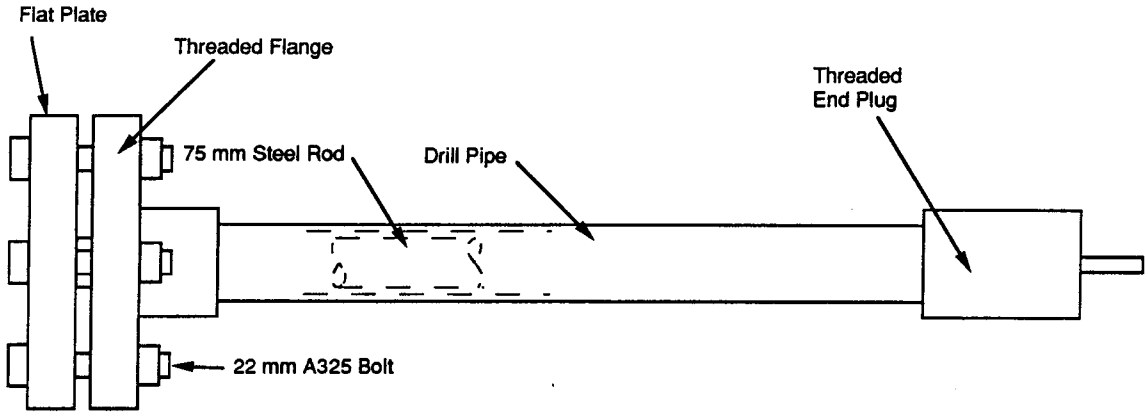

Figure C.1 Prestressing Arrangement

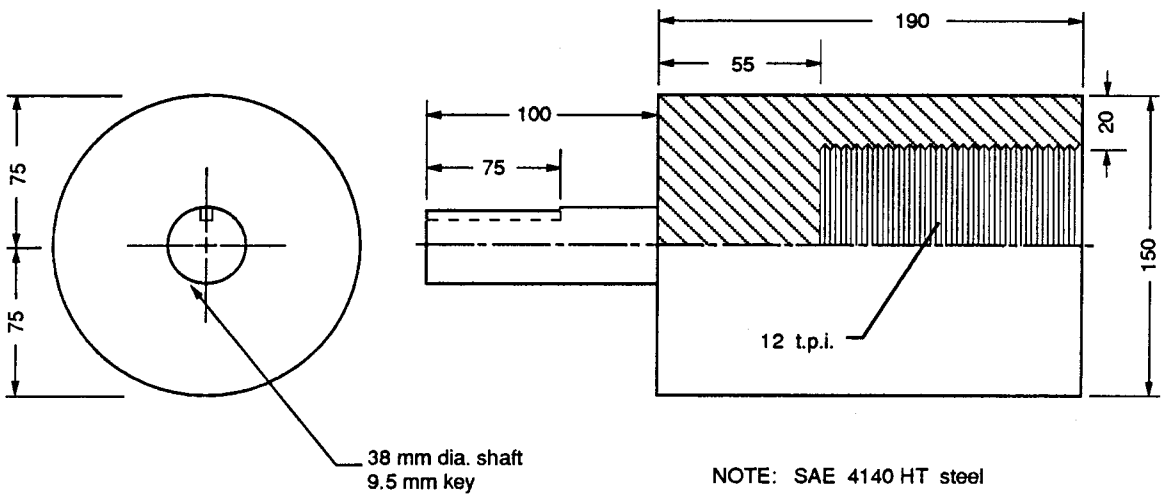

Figure C.2 Threaded End Plug

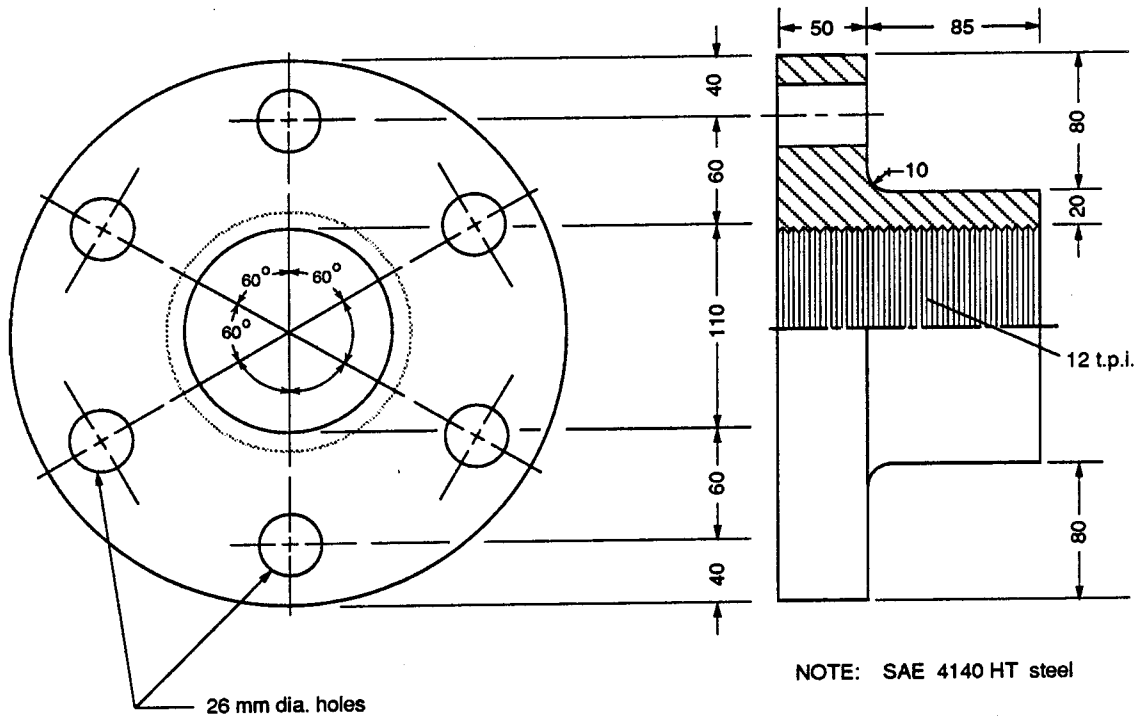

Figure C.3 Threaded Flange

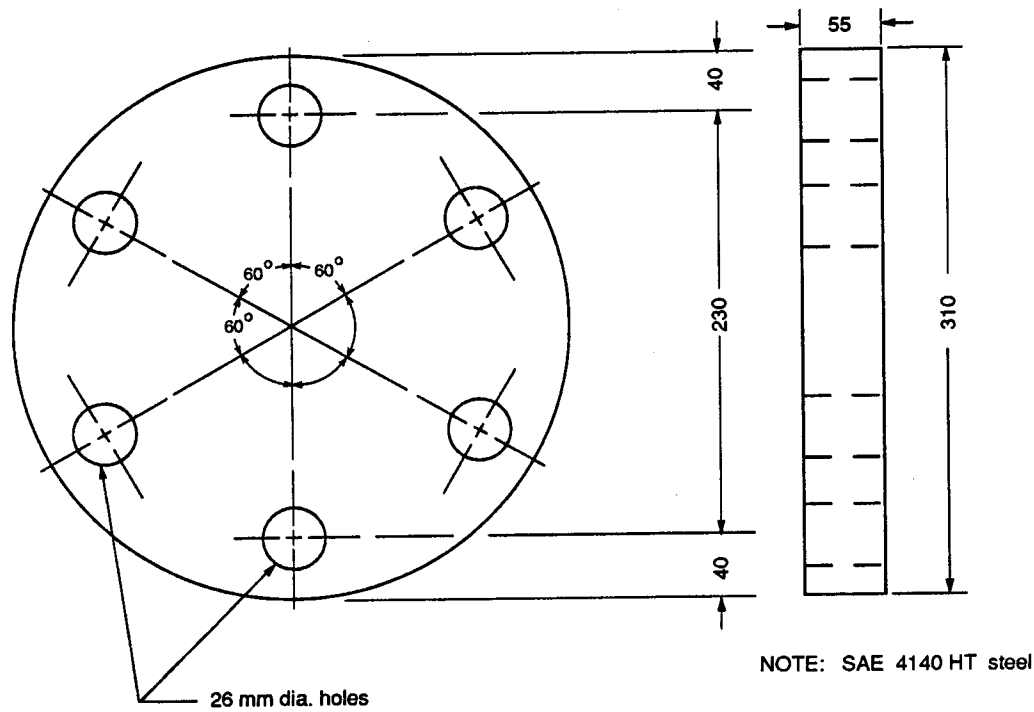

Figure C.4 Flat Plate

Appendix D

Finite Element Analysis of Drill Pipe Upset

Finite Element Analysis of Drill Pipe Upset

Motivation for the following analysis came from field observations that 89 mm O.D. drill pipe with external upset geometry experiences failures significantly less frequently than does 114 mm O.D. drill pipe with an internal-external upset. The stress concentration in the upset area was investigated to determine if this could explain the difference in performance observed in the two different pipes. Both uniaxial tension and bending cases were investigated using the finite element method.

Three different upset geometries were investigated, namely: internal upset (IU), external upset (EU), and internal-external upset (IEU). The upset geometries specified by the American Petroleum Institute (API Spec. 5A, 1987) were investigated. Figure D.1 shows the specified geometry parameters for the three types of upset used by the industry. Table D.1 lists API specified upset dimensions used in the finite element analysis.

Drill Pipe Under Uniaxial Tension

As a first analysis, the load on a pipe was assumed to be uniaxial tension creating a uniform stress of 100 MPa in the drill pipe body. Rectangular and triangular axisymmetric elements with two translational degrees of freedom at each node were selected to model the different upset geometries. The element was obtained from the finite element package SAP IV.

A general coarse mesh, as shown in figures D.2, D.3, and D.4 for an internal upset, an external upset, and internal-external upset, respectively, is used to analyze the stress distribution using an axisymmetric element. The shaded portion of the mesh in Figure D.2 was refined as shown in Figure D.5 to get a better estimate of the peak stress in the region of stress concentration. Nodal displacements at the boundary of the shaded portion of the coarse mesh were used as boundary conditions for the fine mesh. The boundary nodes (Figure D.5), where displacements are specified, are nodes common to both the coarse and fine mesh. Nodes on the boundary of the fine mesh which are not coincident nodes in the coarse mesh are left free to move. The coarse meshes for the external upset and the internal-external upset were not refined in the region of stress concentration for reasons explained below.

Because only a short portion of the drill pipe was modeled and the tool joint was not included in the analyzed section, an investigation of boundary conditions on the

modeled section was needed. Two extreme cases were modeled. The first case is the condition where the tool joint offers negligible restraint to the radial displacement of the upset near the tool joint. For this case, the radial degrees of freedom were released at both extremities of the modeled section and the longitudinal displacements at the far right nodes were fully restrained to maintain equilibrium (see Figure D.6 (a)). Nodal loads were applied at the left boundary to create a uniform stress of 100 MPa in the drill pipe body. The second case was meant to simulate restraining action in the radial direction that might result from a very stiff tool joint. The radial degrees of freedom were fully restrained at the nodes closest to the tool joint (see Figure D.6(b)).

Stress contour lines were drawn using the results of the finite element analysis. The element centroidal stress in the longitudinal direction, σ_x, was used to generate the stress contour lines. Comparison of Figure D.7 with Figure D.8 shows that the stiffness of the tool joint has a negligible effect on the stress distribution in the upset runout. In both cases, a stress concentration factor (SCF), defined as the ratio of maximum stress to the stress in the body of the drill pipe, is equal to 1.17.

The longitudinal stress distribution in the refined mesh of Figure D.5 is presented in Figure D.9. The stress concentration factor obtained using the fine mesh is 1.21, which is only 3.4 percent larger than the stress concentration factor obtained using the coarse mesh. Considering that only a small change in stress concentration factor was obtained by refining the mesh in the stress concentration region, the coarse mesh was not refined for the other two upset geometries.

The longitudinal stress distribution in the upset region for an external upset configuration was presented in Figure 5.3. Stress concentration occurs in the pipe body near the upset runout. The calculated stress concentration factor based on the coarse mesh is 1.15. If the stress concentration factor is increased by 3.5 percent to account for the inaccuracy of the coarse mesh, the stress concentration factor becomes 1.19.

Figure 5.3 also showed the stress distribution in an internal-external upset region. Stress concentration also occurs in the pipe body near the upset runout. The stress concentration factor calculated from the coarse mesh is 1.13. With an increase of 3.5 percent to account for the inaccuracy of the coarse mesh, the stress concentration factor becomes 1.17.

Drill Pipe Under Bending

Analysis of a drill pipe upset region under bending was performed using a general three-dimensional, eight-node, isoparametric element with three translational degrees of freedom per node. As was the case for the axisymmetric element of the previous section, the general three-dimensional element is available from the finite element software SAP IV.

The finite element mesh for the internal upset, external upset, and internal-external upset are shown in figures D.10, D.11, and D.12, respectively. Because symmetry is present about the vertical longitudinal plane, only one half of the pipe was modeled. Tangential degrees of freedom were fully restrained along the longitudinal boundary. A stress distribution corresponding to a state of pure bending was applied in the body section of the drill pipe in the form of discrete loads applied at the boundary nodes, as shown in Figure D.13. In order to determine the load to apply at each node, the stress distribution was integrated over the tributary area of the node. Displacements corresponding to each of the three degrees of freedom were prevented at the nodes on the boundary opposite to the loaded end (see Figure D.13).

Longitudinal centroidal stresses in the top section of the drill pipe were plotted in the form of stress contour lines. Longitudinal stresses for the internal upset, external upset, and internal-external upset drill pipe were presented in Figure 5.4

Table D.1
Drill Pipe Upset Dimensions Used in Finite Element Analysis

Upset Type	D (mm)	d (mm)	D_{ou} (mm)	d_{ou} (mm)	m_{eu} (mm)	L_{eu} (mm)	m_{iu} (mm)	L_{iu} (mm)
IU	114.6	100.0	114.6	85.0	---	---	49.0	50.0
EU	114.4	97.2	127.0	97.2	38.1	61.9	---	---
IEU	114.4	97.2	118.2	80.2	30.0	40.0	50.0	60.0

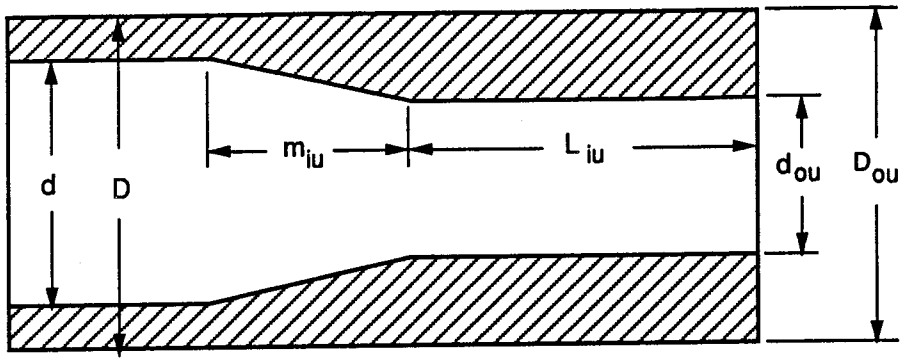

Internal Upset

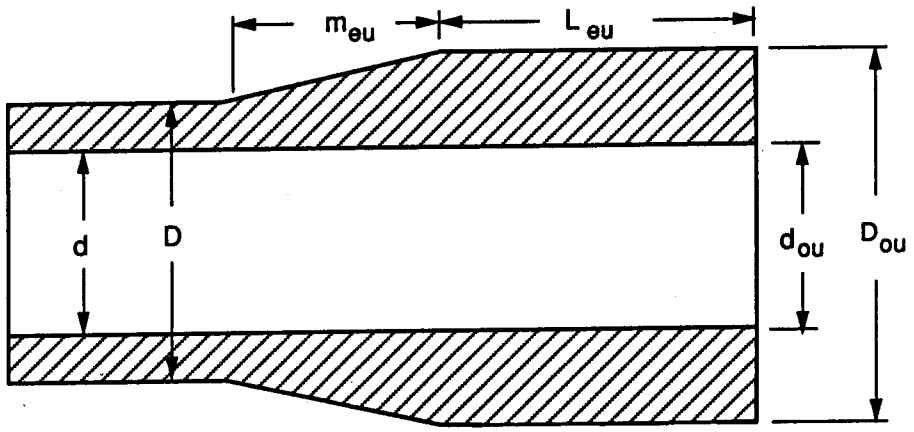

External Upset

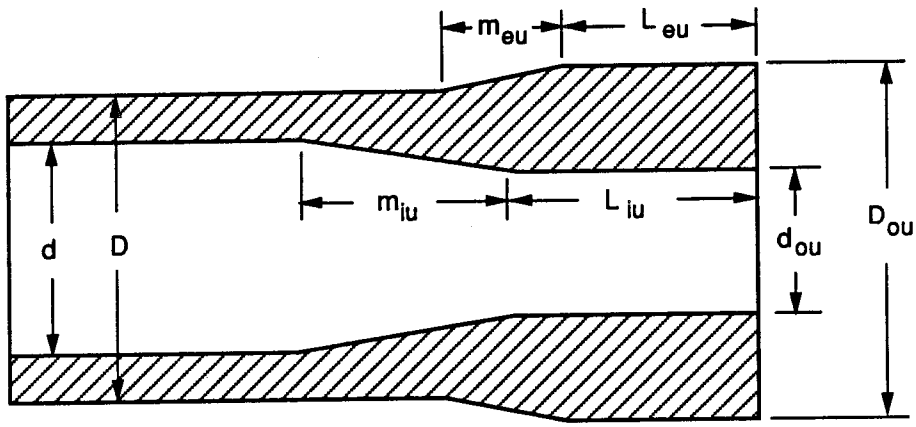

Internal-External Upset

Figure D.1 API Recommended Drill Pipe Upsets for Weld-On Tool Joints

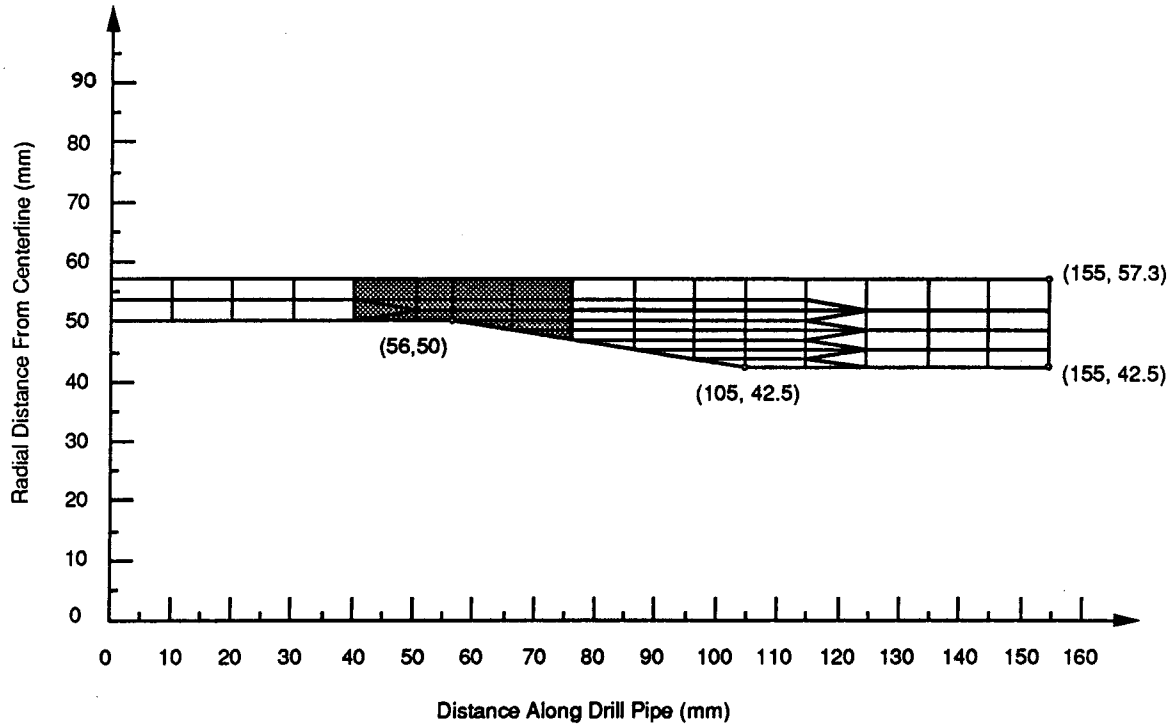

Figure D.2 Finite Element Mesh for Internal Upset Geometry

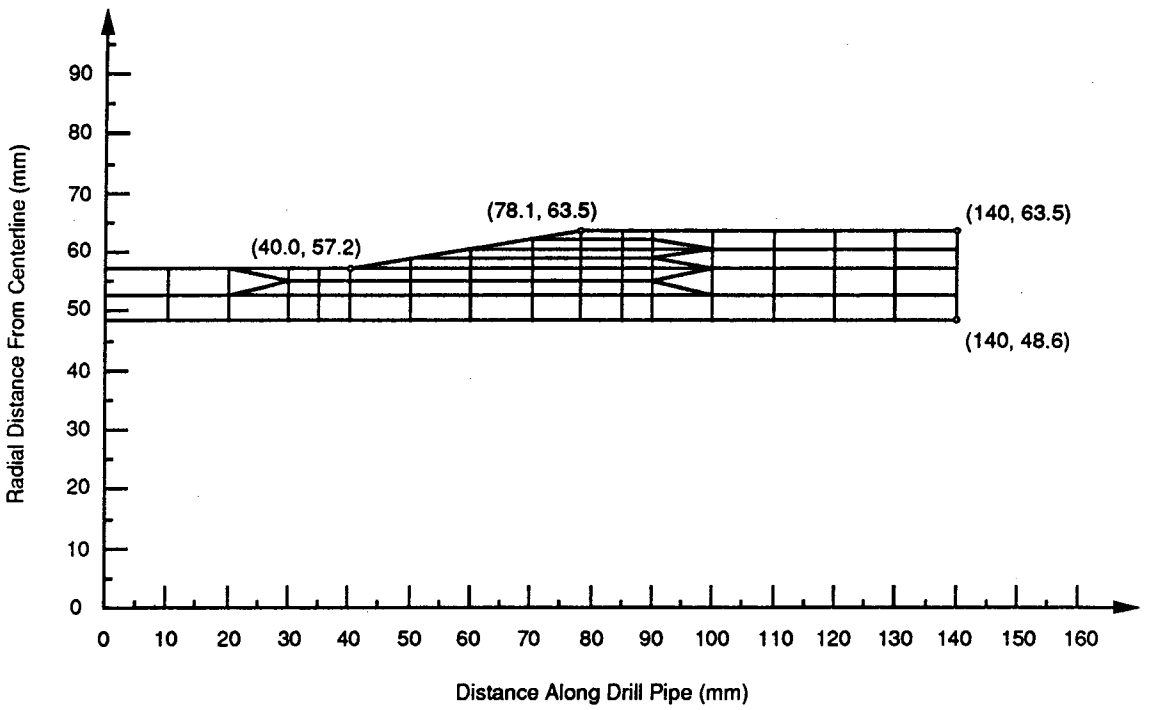

Figure D.3 Finite Element Mesh for External Upset Geometry

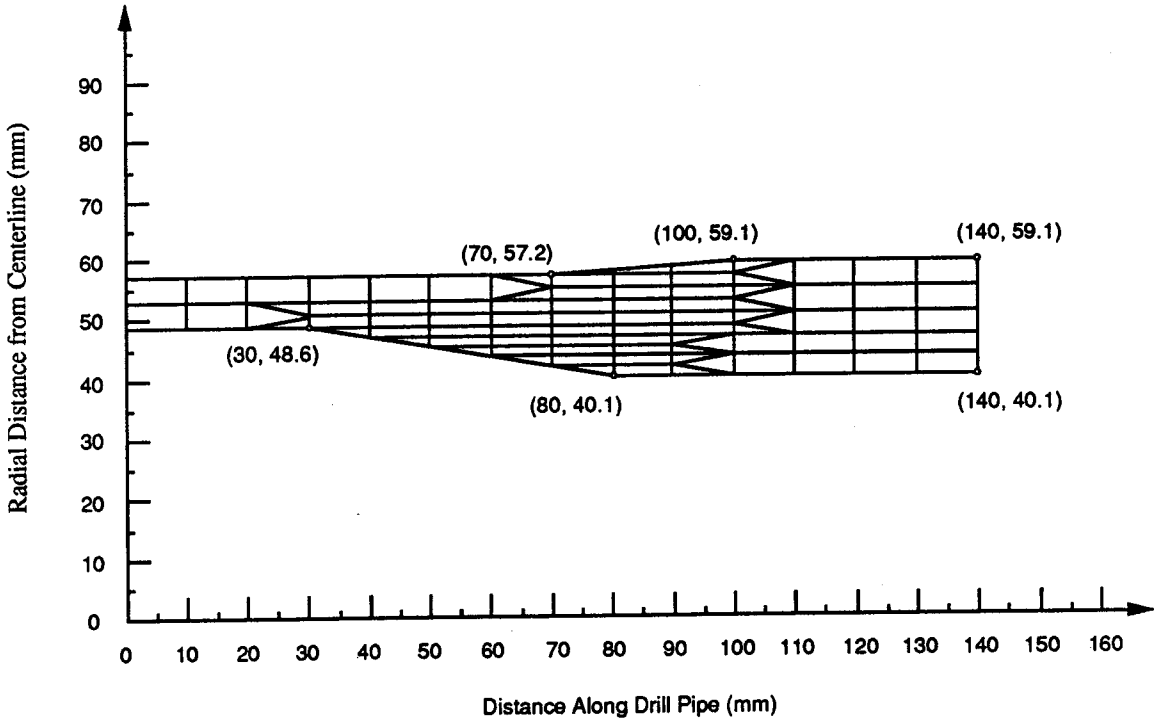

Figure D.4 Finite Element Mesh for Internal-External Upset Geometry

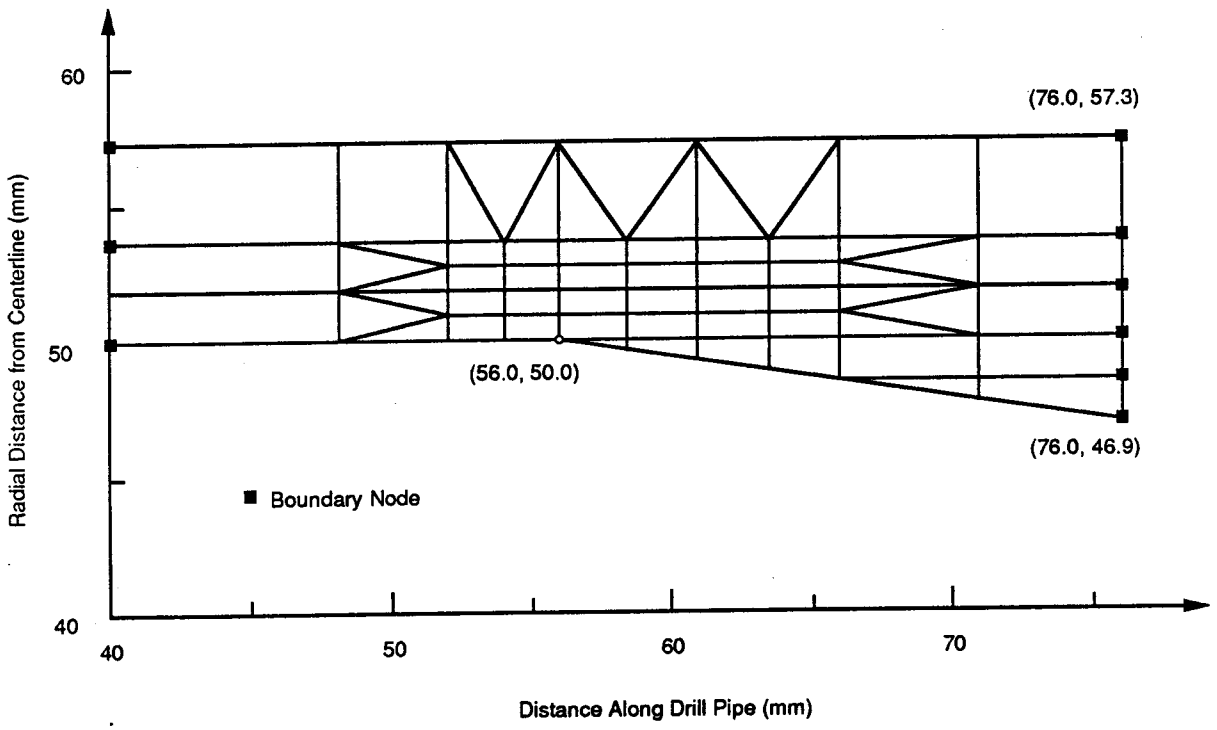

Figure D.5 Refined Mesh for Internal Upset Geometry

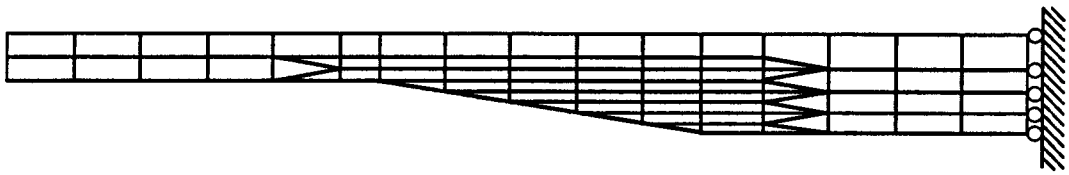

(a) Free radial displacement near tool joint

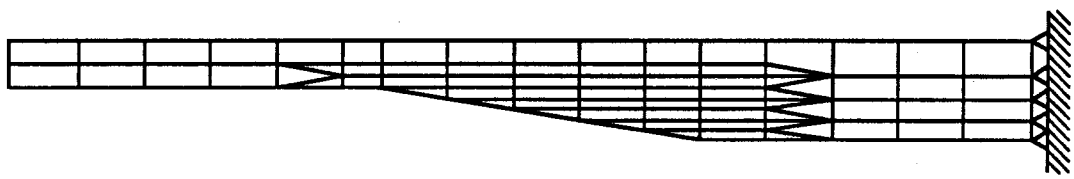

(b) Fully restrained radial displacement near tool joint

Figure D.6 Displacement Boundary Conditions for Drill Pipe Upset

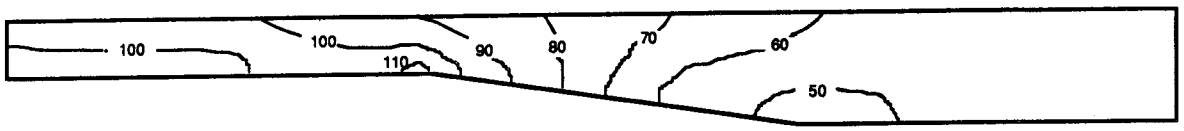

Figure D.7 Stress Distribution in Internal Upset Neglecting the Restraining Action of the Tool Joint (SCF = 1.17)

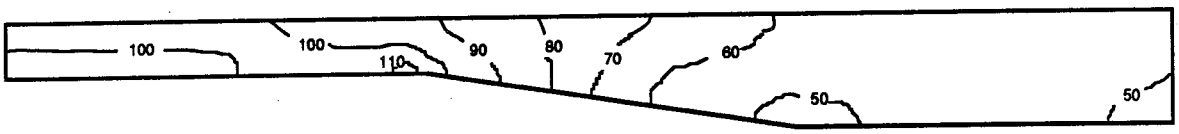

Figure D.8 Stress Distribution in Internal Upset With Simulated Effect of a Stiff Tool Joint (SCF = 1.17)

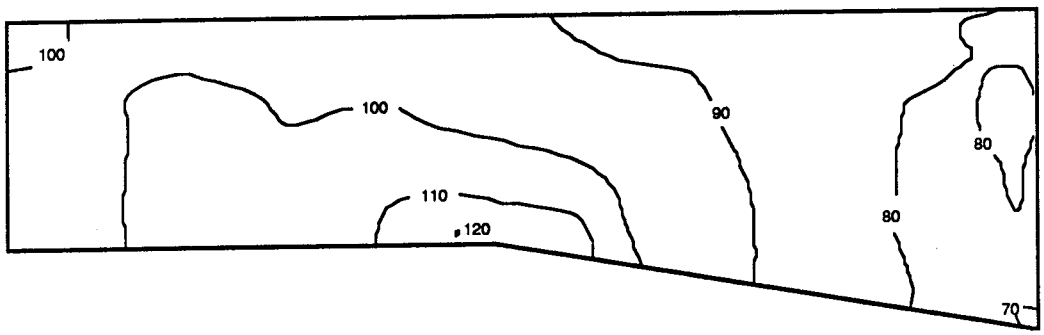

Figure D.9 Stress Distribution in Internal Upset From Fine Mesh (SCF = 1.21)

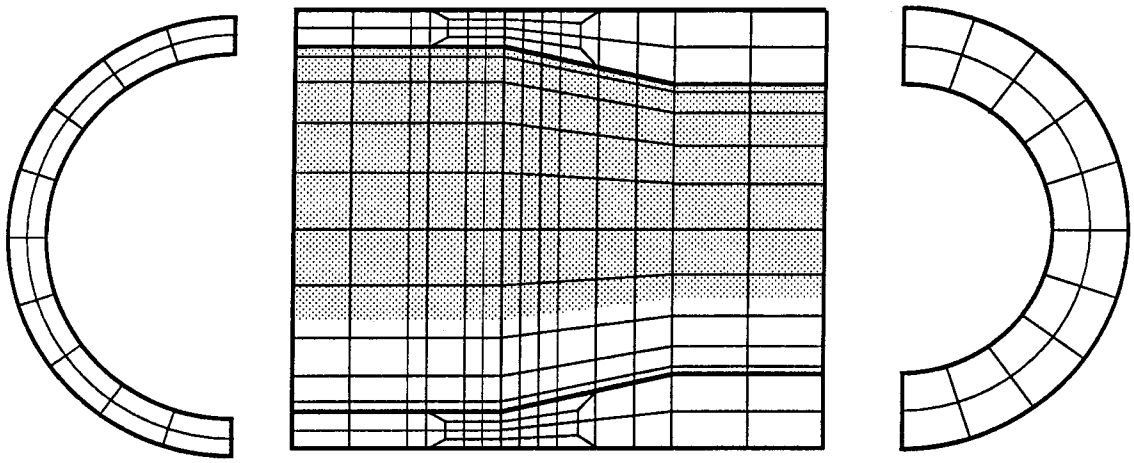

Figure D.10 Finite Element Mesh for Internal Upset Under Bending

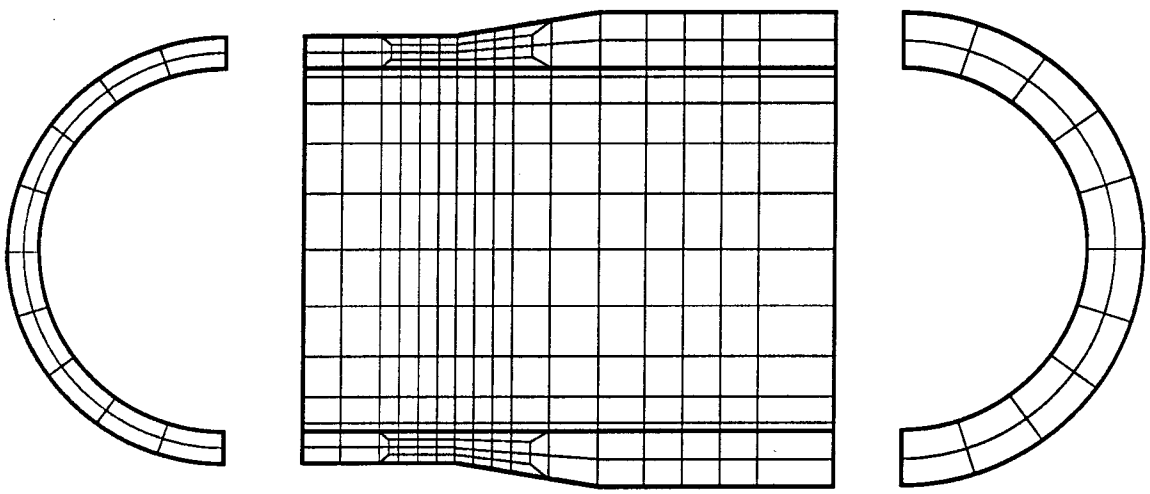

Figure D.11 Finite Element Mesh for External Upset Under Bending

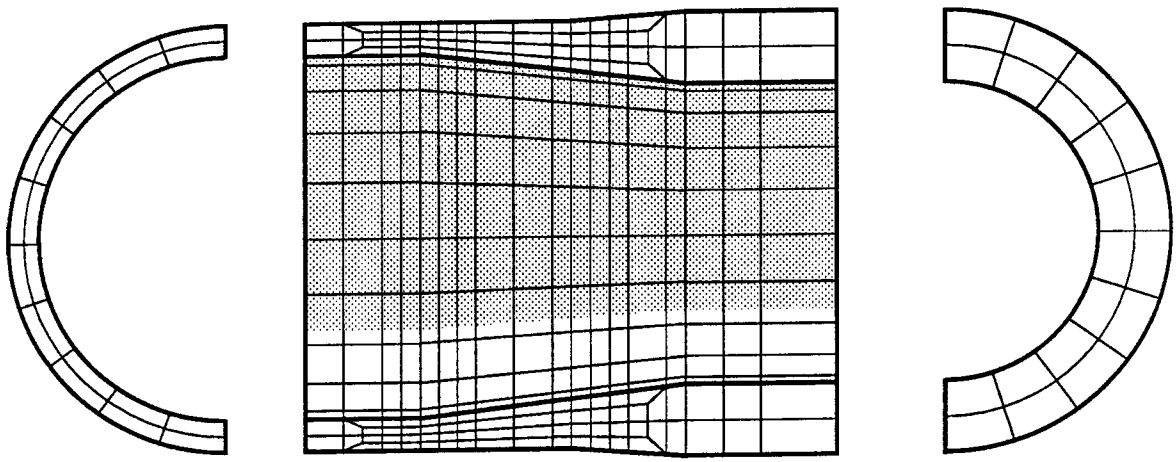

Figure D.12 Finite Element Mesh for Internal-External Upset Under Bending

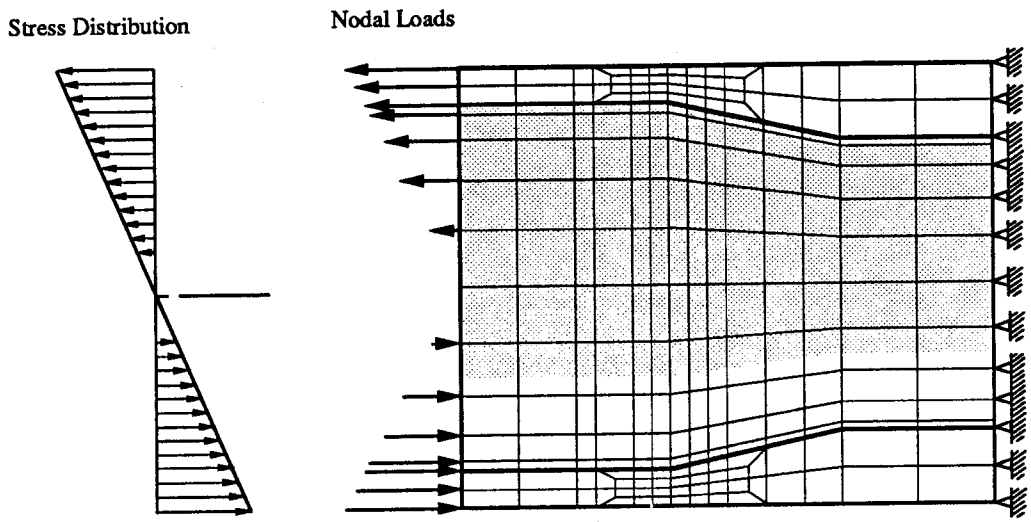

Figure D.13 Load and Displacement Boundary Conditions for Drill Pipe Upset

Appendix E

Effect of Radial Bearing Pressure on the State of Stress in a Drill Pipe

Effect of Radial Pressure on the State of Stress in a Drill Pipe

When bearings are pressure fitted on a drill pipe test specimen, radial pressure is exerted on the pipe body. Radial, longitudinal, and tangential stresses are induced in the drill pipe body under and in the vicinity of the bearing as a result of this radial pressure. The following examination will explore the magnitude of the longitudinal stresses created in the drill pipe body as a result of pressure fitting the bearings on a test specimen.

A section of pipe body 320 mm long was modeled using a quadrilateral axisymmetric element with two degrees of freedom at each node. The length of pipe section was selected so that the radial displacements at its extremitites were negligible although the nodes at the extremities of the pipe section were free to move in the radial direction. In addition, since the test specimens were free to contract or expand when the bearings were mounted, the extremities of the modeled section were left free to expand or contract. The length of the contact surface was 140 mm and the radial pressure was assumed to be uniformly distributed over the bearing surface. The radial pressure was applied as discrete loads at the nodal points over the surface covered by the bearing (see Figure E.1 (a)). Although the pipe was free to expand or contract along its length, the longitudinal displacements under the bearing are partially restrained. This restraint results from the friction between the pipe surface and the rubber pad. In the case where no slip takes place, the longitudinal displacement under the bearing will be controlled by the stiffness of the rubber pad. In order to model this longitudinal restraint, discrete longitudinal springs were attached to the nodal points located immediately under the bearing as depicted in Figure E.1 (b). The investigation presented herein was conducted for a uniform radial pressure of 100 MPa. A finer mesh, shown in Figure E.2, was used in order to obtain a better representation of the longitudinal stress distribution through the wall thickness.

The effect of rubber pad stiffness on the stress distribution in the pipe wall was investigated using the coarse mesh of Figure E.1. For values of spring stiffness from 0 to 10 kN/mm no significant change in the stress state in the pipe body was observed.

Using the fine mesh of Figure E.2, it was found that longitudinal stresses vary linearly through the wall thickness. Figure E.3 shows the stress distribution through the wall thickness plotted from element centroidal stresses. Surface stresses were calculated by extrapolation. Contour lines of longitudinal stresses are presented in Figure E.4 (a).

Maximum calculated stresses were 166 MPa on both the inner and outer surfaces of the drill pipe, as illustrated in Figure E.4 (b). It can be observed from the distribution of surface stresses presented in Figure E.4 (b) that the outer surface of the pipe is in compression under a major portion of the bearing surface. A small tension (about 10 percent of the applied radial pressure) is observed at the centerline of the bearing, while higher tension of 166 MPa is observed outside the bearing area. Stresses on the inner surface of the pipe were found to be of the same magnitude but of opposite sign to those on the outer surface.

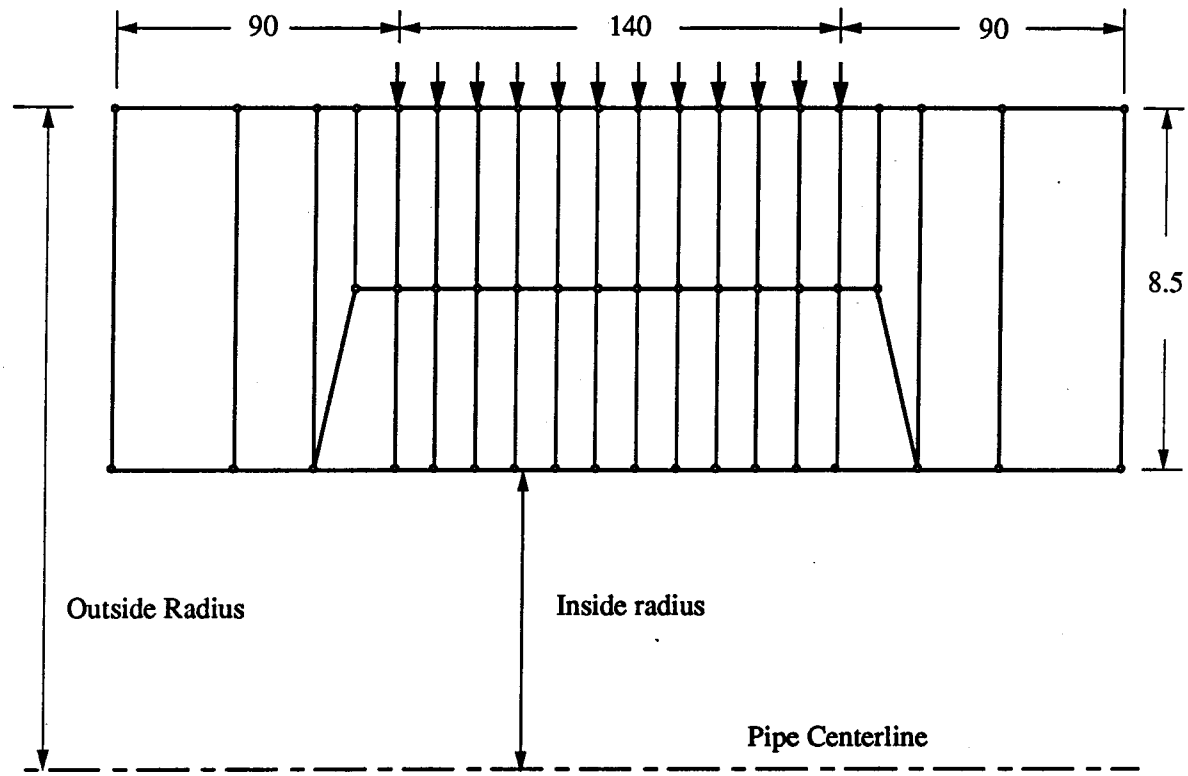

(a) Nodal Loads on Coarse Mesh

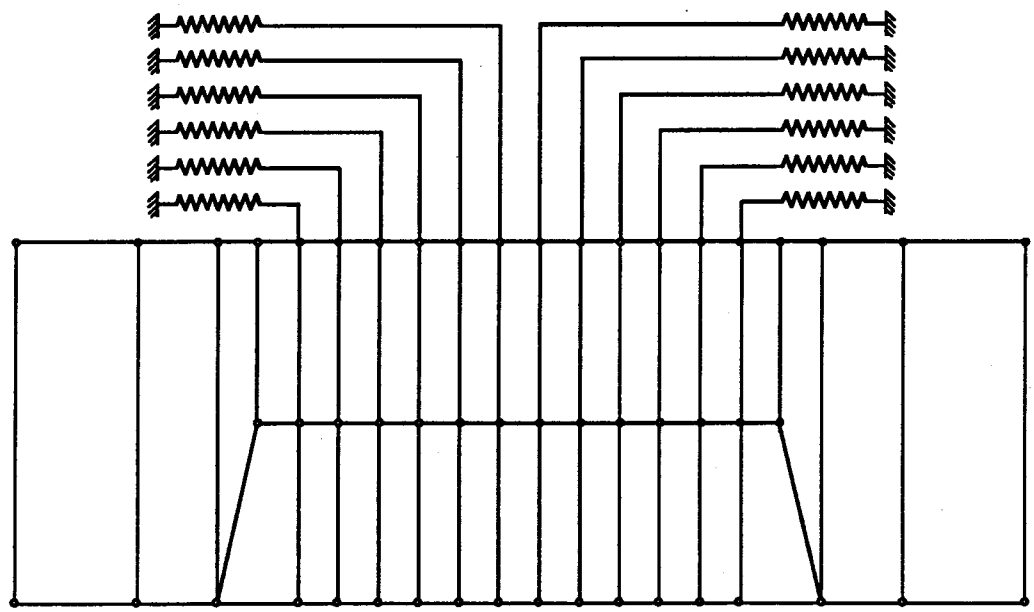

(b) Displacement Boundary Conditions

Figure E.1 Coarse Mesh With Load and Displacement Boundary Conditions

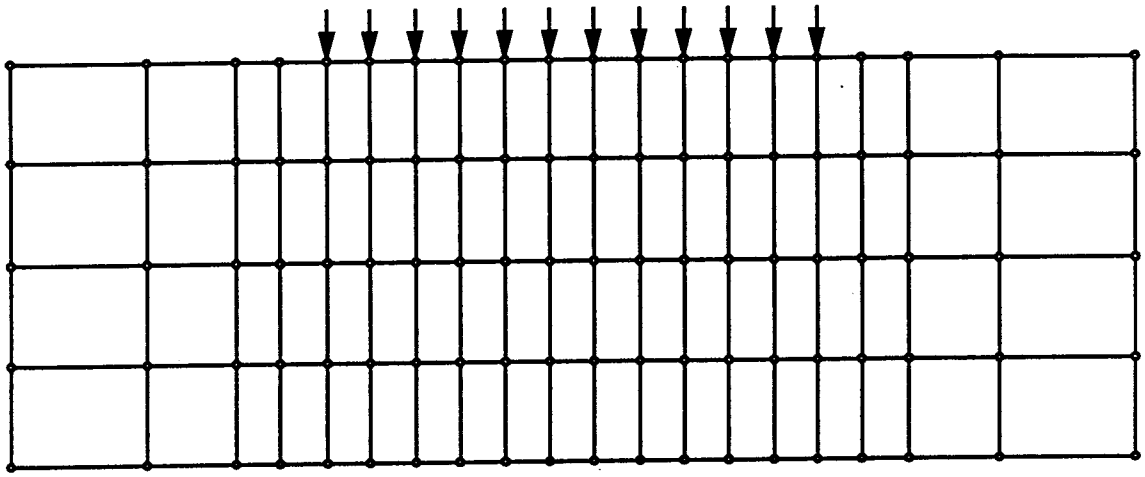

Figure E.2 Fine Mesh of Drill Pipe Body in Bearing Area

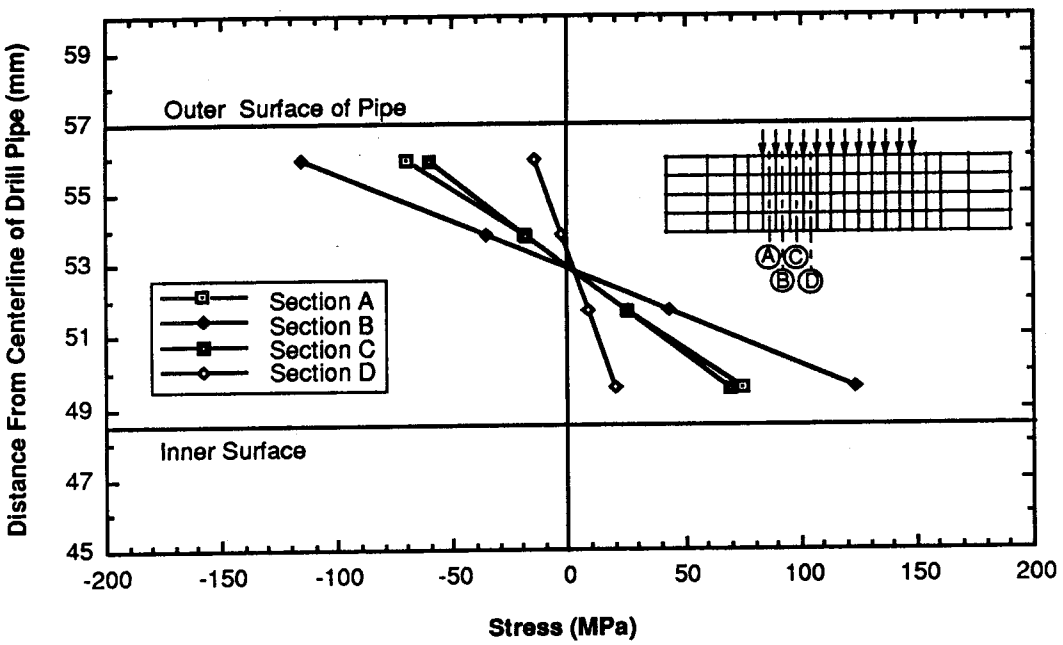

Figure E.3 Stress Distribution Through Pipe Wall Thickness Resulting From Uniform Bearing Pressure

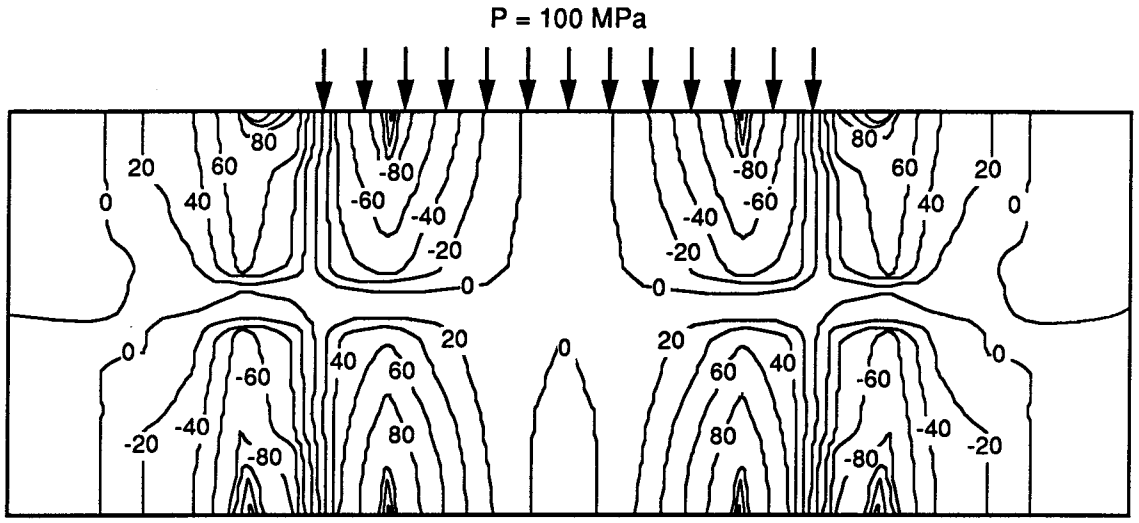

(a) Longitudinal Stress Distribution in Drill Pipe Wall Due to Uniform Radial Pressure

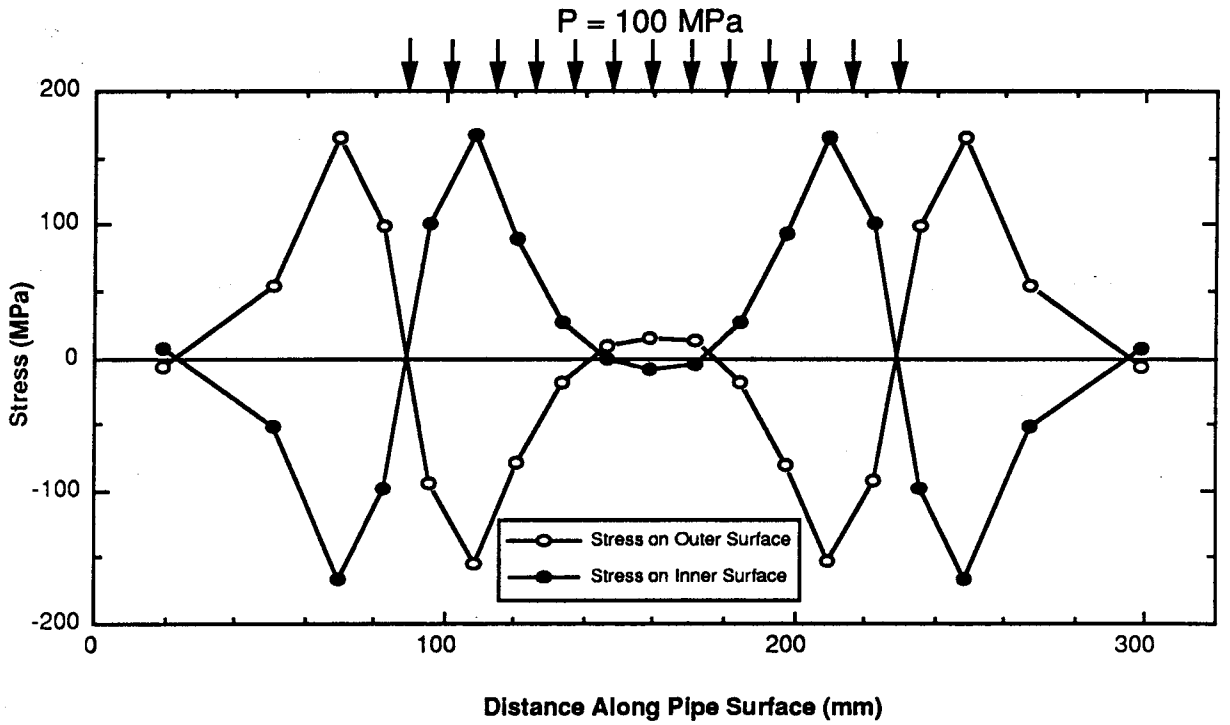

(b) Stress Distribution Along Pipe Surfaces

Figure E.4 Axial Stresses in Drill Pipe Wall Induced By Bearing Pressure

Appendix F

Statistical Analysis of Test Data

Statistical Analysis of Test Data

Statistical analysis of the test data was performed in order to find the relation between the fatigue life of drill pipe and a parameter that took different values during the experimental investigation. The regression analysis provides a description of the fatigue life, assumed to be the dependent variable, on the basis of one or more other variables, called independent variables. The independent variables investigated were the stress range and mean stress. Regression analysis was performed on the test data using the method of least squares.

This appendix serves as a supplement to Chapters 5 and 6. It presents the data used to obtain the regression models presented in Chapters 5 and 6. Tables F.1 to F.7 present the test data obtained in the test program outlined in Chapters 3 and 4. For reasons explained in Chapter 5, some data points obtained during the experimental investigation were not used for the regression analysis. Tables F.8 to F.12 present test data obtained by other investigators. Those data are presented here for easy reference.

The model obtained from the regression analysis can be described as

$$y = a + bx \tag{F-1}$$

where x is the independent variable and y is the dependent variable. The constants a and b are the y-intercept and the slope of the line, respectively. Using the method of least squares, the slope b of the best fit line is obtained from (Harnett, 1982)

$$b = \frac{n\sum_{i=1}^{n} x_i\, y_i \;-\; \sum_{i=1}^{n} x_i \sum_{i=1}^{n} y_i}{n\sum_{i=1}^{n} x_i^{2} \;-\; \left(\sum_{i=1}^{n} x_i\right)^{2}} \tag{F-2}$$

where, n is the number of data points, x_i is the ith value of the independent variable, and y_i is the ith measured value of the dependent variable. The values for the sums used in Eq. (F-2) are tabulated in the tables presented in this appendix. The value of a can be obtained from

$$a = \bar{y} - b\bar{x} \tag{F-3}$$

where $\bar{y}$ is the mean of y and $\bar{x}$ is the mean of x.

The goodness of fit of the regression model is measured using the correlation coefficient, r, given by (Kennedy and Neville, 1976)

$$r = \left(\frac{\sum_{i=1}^{n}(y_i - \bar{y})^2 - \sum_{i=1}^{n}(y_i - \hat{y}_i)^2}{\sum_{i=1}^{n}(y_i - \bar{y})^2} \right)^{\frac{1}{2}} \qquad \text{(F-4)}$$

where $\hat{y}_i$ is the predicted value of y. An r^2 value of zero indicates that y is not linearly predicted in any useful way by x, and an r^2 value of unity indicates that y is linearly predicted perfectly by x, so that the residual of each y is zero.

Multiple Linear Regression

Analysis of the test data indicated that the fatigue life of drill pipe depends both on the stress range and on the mean stress. The relation between the dependent variable and the independent variables can be expressed as

$$y = a + b_1 x_1 + b_2 x_2 \qquad \text{(F-5)}$$

where y is the logarithm of the fatigue life, x_1 is some transformation of the stress range, x_2 is some transformation of the mean stress, and a, b_1, and b_2 are regression coefficients. Using the method of least squares, b_1 and b_2 are given by (Kennedy and Neville, 1976)

$$b_1 = e_{11} \Sigma X_1 Y + e_{12} \Sigma X_2 Y \qquad \text{(F-6)}$$

$$b_2 = e_{21} \Sigma X_1 Y + e_{22} \Sigma X_2 Y \qquad \text{(F-7)}$$

where

$$Y = y - \bar{y} \qquad \text{(F-8)}$$

$$X_1 = x_1 - \bar{x}_1 \qquad \text{(F-9)}$$

$$X_2 = x_2 - \bar{x}_2 \qquad \text{(F-10)}$$

$$e_{11} = \frac{\Sigma X_2^2}{\Sigma X_1^2 \Sigma X_2^2 - (\Sigma X_1 X_2)^2} \qquad \text{(F-11)}$$

$$e_{22} = \frac{\Sigma X_1^2}{\Sigma X_1^2 \ \Sigma X_2^2 - (\Sigma X_1 X_2)^2} \tag{F-12}$$

$$e_{12} = e_{21} = \frac{-\Sigma X_1 X_2}{\Sigma X_1^2 \ \Sigma X_2^2 - (\Sigma X_1 X_2)^2} \tag{F-13}$$

In a manner similar to that used for the linear regression model, the constant a can be found from

$$a = \bar{y} - b_1 \bar{x}_1 - b_2 \bar{x}_2 \tag{F-14}$$

The goodness of fit of the multiple linear regression model is measured using the correlation coefficient given by Eq. (F-4). To obtain the standard deviation of each partial regression coefficient, the residual variance of the dependent variable is first calculated from (Kennedy and Neville, 1976)

$$s_{y|x}^2 = \frac{\Sigma Y^2 - b_1 \Sigma YX_1 - b_2 \Sigma YX_2}{n - 3} \tag{F-15}$$

where the terms in the equation have been defined above. The standard deviation of the partial regression corfficients can be estimated from (Kennedy and Neville, 1976)

$$s_{b_1} = s_{y|x} \sqrt{e_{11}} \tag{F-16}$$

$$s_{b_2} = s_{y|x} \sqrt{e_{22}} \tag{F-17}$$

The significance of the regression coefficients can be tested using the t test where the t value is obtained from

$$t = \frac{b_i}{s_{b_i}} \tag{F-18}$$

where i takes a value of 1 or 2. The number of degrees of freedom is n-3, since three constraints were used in obtaining the regression equation, i.e., in determining a, b_1, and b_2.

Analysis of Variance

The significance of the main effects (stress range and mean stress) and the interaction between the main effects has been investigated by other researchers using the technique known as analysis of variance (Fisher et al., 1970). The model investigated herein takes the following form:

$$\log N = a + b_1 \log S_r + b_2 (S_m)^2 \qquad \text{(F-19)}$$

where a, b_1, and b_2 are regression coefficient, log N, the logarithm of the fatigue life, is the response variable, and log S_r and $(S_m)^2$ are the main effects. A complete factorial is used to investigate the significance of the main effects and their interaction. A complete factorial, which consists of 13 tests, was obtained during the experimental program in a corrosive environment, with stress range values of 130 MPa and 290 MPa and mean stress values of 0, 125, and 250 MPa. Table F.13 summarizes the analysis of variance performed on the complete factorial. Column 1 lists the sources of variation in the regression model. These are the two main effects, the interaction between the two main effects, and the error. The interaction refers to the combined effect of the two main factors and assesses whether the response variable, as measured for one of the factors, changes at different levels of the other factor. The error term is a measure of the variation caused by experimental error and is obtained from the replicate tests performed at each stress combination. The degrees of freedom associated with the sources of variation are presented in Column 2 of Table F.13. Details for calculation of the sum of squares for the various sources (Column 3) can be found elsewhere (Box et al., 1978). The mean squares presented in Column 4 are obtained by dividing the sum of squares by the corresponding number of degrees of freedom. The F value presented in Column 5 is the ratio of the mean square for a source of variation to the mean square for the error, that is, the mean square for each of the first three sources in Column 5 is divided by 0.0043. A comparison of the calculated F values with the tabulated F values listed in Column 6 shows that stress range and mean stress are both significant parameters. The interaction of stress range and mean stress is seen to be insignificant at the confidence level of 95 percent.

It should be noted that conclusions obtained from the analysis of variance presented above apply to the range of values investigated for the stress range and for the mean stress. The calculations involved in the analysis of variance do not take into account the range of values of the main effects, but only the value of the response variable (log N). Therefore, the results obtained indicate that a change in stress range from 130 MPa to 290 MPa has a significant effect on the fatigue life. Similarly, a change of mean stress from 0 to 250 MPa has a marked effect on the fatigue life. The conclusions drawn from an analysis of variance are strongly dependent on the range of values of each parameter (mean stress and stress range) investigated in the test program. This is an obvious drawback of the analysis of variance presented above and, therefore, the results of the analysis should be interpreted with caution.

Table F.1

Regression Analysis for the Effect of Stress Range in Air
(Mean Stress = 125 MPa)

Stress Range Sr	N	Log Sr (x)	Log N (y)	x^2	x y	y^2	(x-meanx)^2	Predicted yp	Residual^2
267	1181500	2.427	6.072	5.89	14.73	36.87	0.0007	6.0386	0.0011
249	10000000	2.396	7.000	5.74	16.77	49.00	0.0000	6.1584	0.7083
290	468500	2.462	5.671	6.06	13.96	32.16	0.0038	5.8969	0.0511
335	189800	2.525	5.278	6.38	13.33	27.86	0.0155	5.6493	0.1377
290	882800	2.462	5.946	6.06	14.64	35.35	0.0038	5.8969	0.0024
267	1876000	2.427	6.273	5.89	15.22	39.35	0.0007	6.0386	0.0550
293	10107400	2.467	7.005	6.09	17.28	49.06	0.0044	5.8792	1.2666
273	508500	2.436	5.706	5.93	13.90	32.56	0.0013	6.0005	0.0866
335	259900	2.525	5.415	6.38	13.67	29.32	0.0155	5.6493	0.0550
250	568800	2.398	5.755	5.75	13.80	33.12	0.0000	6.1515	0.1573
340	511200	2.531	5.709	6.41	14.45	32.59	0.0172	5.6239	0.0072
320	300400	2.505	5.478	6.28	13.72	30.01	0.0110	5.7279	0.0626
251	461600	2.400	5.664	5.76	13.59	32.08	0.0000	6.1447	0.2308
200	586000	2.301	5.768	5.29	13.27	33.27	0.0099	6.5344	0.5875
220	1237500	2.342	6.093	5.49	14.27	37.12	0.0034	6.3709	0.0775
181	10158000	2.258	7.007	5.10	15.82	49.10	0.0204	6.7057	0.0907
177	10000000	2.248	7.000	5.05	15.74	49.00	0.0233	6.7440	0.0655
180	982000	2.255	5.992	5.09	13.51	35.91	0.0211	6.7152	0.5228
200	10000000	2.301	7.000	5.29	16.11	49.00	0.0099	6.5344	0.2168
220	10000000	2.342	7.000	5.49	16.40	49.00	0.0034	6.3709	0.3958
Mean		2.400	6.142						
Sum		48.009	122.831	115.41	294.20	761.73	0.16514	122.83115	4.77835

a = 15.625 b = -3.951 r^2 = 0.350 Se = 0.515

Table F.2

Regression Analysis for the Effect of Mean Stress in Air
(Stress range = 290 MPa)

Mean Stress Sm	N	Sm^2 (x)	Log N (y)	x^2	x y	y^2	(x-meanx)^2	Predicted yp	Residual^2
125	468500	15625	5.671	2.44E+08	88605	32.16	1.21E+08	6.2564	0.3430
126	882800	15876	5.946	2.52E+08	94397	35.35	1.15E+08	6.2513	0.0933
126	10107400	15876	7.005	2.52E+08	111206	49.06	1.15E+08	6.2513	0.5675
0	10066800	0	7.003	0.00E+00	0	49.04	7.08E+08	6.5695	0.1879
0	1389900	0	6.143	0.00E+00	0	37.74	7.08E+08	6.5695	0.1819
0	4771100	0	6.679	0.00E+00	0	44.60	7.08E+08	6.5695	0.0119
250	262800	62500	5.420	3.91E+09	338727	29.37	1.29E+09	5.3171	0.0105
252	82100	63504	4.914	4.03E+09	312080	24.15	1.36E+09	5.2969	0.1464
257	352900	66049	5.548	4.36E+09	366417	30.78	1.56E+09	5.2459	0.0910
Mean		26603.33	6.036						
Sum		239430	54.327	1.30E+10	1311431	332.26	6.68E+09	54.32733	1.63336

a = 6.56945
b = -2E-05
r^2 = 0.62

Se = 0.48305

Table F.3

Multiple Linear Regression Analysis on Fatigue Tests in Air

Sr (MPa)	Sm (MPa)	N (cycles)	Log Sr x1	Sm^2 x2	Log N y	X1 = x1-Mean(x1)	X2 =x2-Mean(x2)	Y =y-Mean(y)	Y X1	Y X2	X1^2	X2^2	X1 X2	Predicted y	Residual ^2
267	126	1181500	2.427	15876	6.072	0.009	-3608	-0.01	0.000	34	0.000	1.30E+07	-33	6.110	0.001
302	144	472600	2.480	20736	5.674	0.063	1252	-0.41	-0.026	-510	0.004	1.57E+06	78	5.844	0.029
249	124	10000000	2.396	15376	7.000	-0.021	-4108	0.92	-0.019	-3771	0.000	1.69E+07	87	6.223	0.604
290	125	468500	2.462	15625	5.671	0.045	-3859	-0.41	-0.019	1587	0.002	1.49E+07	-174	5.990	0.102
335	125	189800	2.525	15625	5.278	0.108	-3859	-0.80	-0.087	3101	0.012	1.49E+07	-416	5.772	0.244
290	126	882800	2.462	15876	5.946	0.045	-3608	-0.14	-0.006	491	0.002	1.30E+07	-163	5.985	0.002
267	125	1876000	2.427	15625	6.273	0.009	-3859	0.19	0.002	-738	0.000	1.49E+07	-35	6.114	0.025
293	126	10107400	2.467	15876	7.005	0.050	-3608	0.92	0.046	-3329	0.002	1.30E+07	-179	5.970	1.071
273	127	508500	2.436	16129	5.706	0.019	-3355	-0.38	-0.007	1260	0.000	1.13E+07	-63	6.072	0.134
335	125	259900	2.525	15625	5.415	0.108	-3859	-0.67	-0.072	2574	0.012	1.49E+07	-416	5.772	0.128
250	125	568800	2.398	15625	5.755	-0.019	-3859	-0.33	0.006	1262	0.000	1.49E+07	75	6.213	0.210
340	126	511200	2.531	15876	5.709	0.114	-3608	-0.37	-0.043	1347	0.013	1.30E+07	-412	5.746	0.001
320	127	300400	2.505	16129	5.478	0.088	-3355	-0.60	-0.053	2027	0.008	1.13E+07	-295	5.833	0.126
251	125	461600	2.400	15625	5.664	-0.018	-3859	-0.42	0.007	1612	0.000	1.49E+07	68	6.207	0.294
200	123	586000	2.301	15129	5.768	-0.116	-4355	-0.31	0.037	1368	0.014	1.90E+07	507	6.557	0.623
220	126	1237500	2.342	15876	6.093	-0.075	-3608	0.01	-0.001	-38	0.006	1.30E+07	270	6.401	0.095
181	127	10158000	2.258	16129	7.007	-0.160	-3355	0.92	-0.148	-3103	0.025	1.13E+07	536	6.691	0.100
177	124	10000000	2.248	15376	7.000	-0.169	-4108	0.92	-0.155	-3771	0.029	1.69E+07	696	6.737	0.069
180	123	982000	2.255	15129	5.992	-0.162	-4355	-0.09	0.015	391	0.026	1.90E+07	706	6.715	0.523
200	124	10000000	2.301	15376	7.000	-0.116	-4108	0.92	-0.107	-3771	0.014	1.69E+07	478	6.553	0.200
220	124	10000000	2.342	15376	7.000	-0.075	-4108	0.92	-0.069	-3771	0.006	1.69E+07	308	6.409	0.349
290	0	10066800	2.462	0	7.003	0.045	-19484	0.92	0.042	-17944	0.002	3.80E+08	-878	6.248	0.570
287	0	1389900	2.458	0	6.143	0.041	-19484	0.06	0.002	-1190	0.002	3.80E+08	-790	6.264	0.015
290	0	4771100	2.462	0	6.679	0.045	-19484	0.60	0.027	-11626	0.002	3.80E+08	-878	6.248	0.186
290	250	262800	2.462	62500	5.420	0.045	43016	-0.66	-0.030	-28489	0.002	1.85E+09	1938	5.215	0.042
292	252	82100	2.465	63504	4.914	0.048	44020	-1.17	-0.056	-51397	0.002	1.94E+09	2115	5.188	0.075
294	257	352900	2.468	66049	5.548	0.051	46565	-0.53	-0.027	-24878	0.003	2.17E+09	2375	5.135	0.170
		Mean	2.417	19484	6.082										
		Sum				0.000	0	0.00	-0.740	-141275	0.187	7.39E+09	5506	164.212	5.987

e11= 5.45543
e22= 1.38E-10
e12= -4.06E-06

a= 14.78
b1= -3.47
b2= -1.65E-05

r^2 = 0.45

Se^2= 0.249454
Se= 0.499453

Table F.4

Regression Analysis for the Effect of Stress Range in NaCl Solution
(Mean Stress = 125 MPa)

Stress Range Sr	N	Log Sr (x)	Log N (y)	x^2	x y	y^2	(x-meanx)^2	Predicted yp	Residual^2
288	565300	2.459	5.752	6.05	14.15	33.09	0.0492	5.6106	0.0201
291	486600	2.464	5.687	6.07	14.01	32.34	0.0512	5.6003	0.0075
126	2240800	2.100	6.350	4.41	13.34	40.33	0.0188	6.4325	0.0067
132	2345200	2.121	6.370	4.50	13.51	40.58	0.0137	6.3863	0.0003
90	7899000	1.954	6.898	3.82	13.48	47.58	0.0803	6.7671	0.0170
158	1605700	2.199	6.206	4.83	13.64	38.51	0.0015	6.2075	0.0000
158	1792500	2.199	6.253	4.83	13.75	39.11	0.0015	6.2075	0.0021
209	627800	2.320	5.798	5.38	13.45	33.61	0.0068	5.9294	0.0173
210	564200	2.322	5.751	5.39	13.36	33.08	0.0072	5.9247	0.0300
Mean		2.238	6.118						
Sum		20.138	55.066	45.29	122.69	338.23	0.23023	55.06598	0.10108

a = 11.24081
b = -2.289254
r^2 = 0.923

Se = 0.1202

Table F.5

Regression Analysis for the Effect of Mean Stress in NaCl Solution
(Stress range = 130 MPa)

Mean Stress Sm	N	Sm^2 (x)	Log N (y)	x^2	x y	y^2	(x-meanx)^2	Predicted yp	Residual^2
252	1783200	63504	6.251	4.03E+09	396976	39.08	1.68E+09	6.1754	0.0057
250	1455600	62500	6.163	3.91E+09	385190	37.98	1.60E+09	6.1817	0.0003
123	2345200	15129	6.370	2.29E+08	96374	40.58	5.38E+07	6.4798	0.0120
127	2240800	16129	6.350	2.60E+08	102426	40.33	4.02E+07	6.4735	0.0151
0	4356200	0	6.639	0.00E+00	0	44.08	5.05E+08	6.5750	0.0041
0	3383200	0	6.529	0.00E+00	0	42.63	5.05E+08	6.5750	0.0021
0	5395700	0	6.732	0.00E+00	0	45.32	5.05E+08	6.5750	0.0247
Mean	22466	6.434							
Sum	157262	45.035	8.43E+09	980966	290.00	4.89E+09	45.03531	0.06413	

a = 6.57496
b = -6.29E-06
r^2 = 0.75

Se = 0.11325

Table F.6

Regression Analysis for the Effect of Mean Stress in NaCl Solution
(Stress range = 290 MPa)

Mean Stress Sm	N	Sm^2 (x)	Log N (y)	x^2	x y	y^2	(x-meanx)^2	Predicted yp	Residual^2
250	196400	62500	5.293	3.91E+09	330821	28.02	1.31E+09	5.3490	0.0031
255	234600	65025	5.370	4.23E+09	349206	28.84	1.50E+09	5.3309	0.0016
122	565300	14884	5.752	2.22E+08	85617	33.09	1.31E+08	5.6912	0.0037
125	486600	15625	5.687	2.44E+08	88862	32.34	1.15E+08	5.6859	0.0000
0	578500	0	5.762	0.00E+00	0	33.20	6.94E+08	5.7982	0.0013
0	613900	0	5.788	0.00E+00	0	33.50	6.94E+08	5.7982	0.0001
Mean		26339	5.609						
Sum		158034	33.653	8.60E+09	854506	189.00	4.44E+09	33.65332	0.00980

a = 5.79816
b = -7.19E-06
r^2 = 0.96

Se = 0.04949

Table F.7

Multiple Linear Regression Analysis on Fatigue Tests in NaCl Solution

Sr (MPa)	Sm (MPa)	N (cycles)	Log Sr x1	Sm^2 * LogSr x2	Log N y	X1 = x1-Mean(x1)	X2 =x2-Mean(x2)	Y =y-Mean(y)	Y X1	Y X2	X1^2	X2^2	X1 X2	Predicted y	Residual ^2
296	250	196400	2.471	154456	5.293	0.218	104842	-0.80	-0.173	-83396	0.047	1.10E+10	22813	5.306	0.000
290	255	234600	2.462	160117	5.370	0.209	110504	-0.72	-0.150	-79370	0.044	1.22E+10	23062	5.311	0.003
288	122	565300	2.459	36606	5.752	0.206	-13008	-0.34	-0.069	4375	0.042	1.69E+08	-2676	5.648	0.011
291	125	486600	2.464	38498	5.687	0.210	-11116	-0.40	-0.084	4462	0.044	1.24E+08	-2336	5.632	0.003
288	0	578500	2.459	0	5.762	0.206	-49614	-0.33	-0.067	16188	0.042	2.46E+09	-10205	5.746	0.000
290	0	613900	2.462	0	5.788	0.209	-49614	-0.30	-0.063	14908	0.044	2.46E+09	-10354	5.739	0.002
158	125	1792500	2.199	34354	6.253	-0.055	-15260	0.16	-0.009	-2516	0.003	2.33E+08	840	6.257	0.000
90	125	7899000	1.954	30535	6.898	-0.299	-19079	0.81	-0.242	-15435	0.090	3.64E+08	5713	6.832	0.004
132	252	1783200	2.121	134665	6.251	-0.133	85051	0.16	-0.022	13830	0.018	7.23E+09	-11323	6.169	0.007
130	250	1455600	2.114	132121	6.163	-0.140	82508	0.07	-0.010	6143	0.020	6.81E+09	-11531	6.191	0.001
132	123	2345200	2.121	32082	6.370	-0.133	-17532	0.28	-0.037	-4937	0.018	3.07E+08	2334	6.443	0.005
126	127	2240800	2.100	33877	6.350	-0.153	-15737	0.26	-0.040	-4120	0.024	2.48E+08	2413	6.485	0.018
210	123	564200	2.322	35133	5.751	0.069	-14481	-0.34	-0.023	4882	0.005	2.10E+08	-992	5.969	0.047
209	125	627800	2.320	36252	5.798	0.066	-13362	-0.29	-0.019	3885	0.004	1.79E+08	-888	5.971	0.030
158	125	1605700	2.199	34354	6.206	-0.055	-15260	0.12	-0.006	-1787	0.003	2.33E+08	840	6.257	0.003
130	0	4356200	2.114	0	6.639	-0.140	-49614	0.55	-0.077	-27313	0.020	2.46E+09	6934	6.544	0.009
129	0	3383200	2.111	0	6.529	-0.143	-49614	0.44	-0.063	-21867	0.020	2.46E+09	7100	6.552	0.001
130	0	5395700	2.114	0	6.732	-0.140	-49614	0.64	-0.090	-31925	0.020	2.46E+09	6934	6.544	0.035
		Mean	2.254	49614	6.089										
		Sum				0.000	0	0.00	-1.246	-203991	0.506	5.16E+10	28677	109.595	0.180

e11= 2.03999
e22= 2.00E-11
e12= -1.13E-06

a= 11.42926
b1= -2.31100
b2= -2.6680E-06

r^2 = 0.95

Se^2= 0.012013
Se= 0.109605

Table F.8

Test Data From Bachman (1951)

Stress Range Sr	N	log Sr (x)	Log N (y)	x^2	x y	y^2	(x-meanx)^2	Predicted yp	Residual^2
576.422	130000	2.76074	5.11394	7.62E+00	14.118	26.152	0.017	5.252	0.019
524.02	120000	2.71935	5.07918	7.39E+00	13.812	25.798	0.008	5.368	0.084
468.86	105000	2.67104	5.02119	7.13E+00	13.412	25.212	0.002	5.504	0.233
489.546	127000	2.68979	5.10380	7.23E+00	13.728	26.049	0.004	5.451	0.121
372.33	160000	2.57093	5.20412	6.61E+00	13.379	27.083	0.004	5.784	0.337
434.386	175000	2.63788	5.24304	6.96E+00	13.830	27.489	0.000	5.597	0.125
544.706	175000	2.73616	5.24304	7.49E+00	14.346	27.489	0.011	5.321	0.006
489.546	185000	2.68979	5.26717	7.23E+00	14.168	27.743	0.004	5.451	0.034
468.86	190000	2.67104	5.27875	7.13E+00	14.100	27.865	0.002	5.504	0.051
434.386	195000	2.63788	5.29003	6.96E+00	13.954	27.984	0.000	5.597	0.094
406.806	198000	2.60939	5.29667	6.81E+00	13.821	28.055	0.000	5.677	0.144
455.07	205000	2.65808	5.31175	7.07E+00	14.119	28.215	0.001	5.540	0.052
452.312	210000	2.65544	5.32222	7.05E+00	14.133	28.326	0.001	5.548	0.051
482.65	220000	2.68363	5.34242	7.20E+00	14.337	28.541	0.003	5.469	0.016
482.65	220000	2.68363	5.34242	7.20E+00	14.337	28.541	0.003	5.469	0.016
427.49	230000	2.63093	5.36173	6.92E+00	14.106	28.748	0.000	5.616	0.065
419.216	231000	2.62244	5.36361	6.88E+00	14.066	28.768	0.000	5.640	0.076
529.536	240000	2.72390	5.38021	7.42E+00	14.655	28.947	0.009	5.356	0.001
448.176	260000	2.65145	5.41497	7.03E+00	14.358	29.322	0.000	5.559	0.021
503.336	260000	2.70186	5.41497	7.30E+00	14.630	29.322	0.005	5.417	0.000
475.756	270000	2.67738	5.43136	7.17E+00	14.542	29.500	0.002	5.486	0.003
448.176	280000	2.65145	5.44716	7.03E+00	14.443	29.672	0.000	5.559	0.012
496.44	300000	2.69587	5.47712	7.27E+00	14.766	29.999	0.004	5.434	0.002
489.546	305000	2.68979	5.48430	7.23E+00	14.752	30.078	0.004	5.451	0.001
524.02	305000	2.71935	5.48430	7.39E+00	14.914	30.078	0.008	5.368	0.013
455.07	310000	2.65808	5.49136	7.07E+00	14.596	30.155	0.001	5.540	0.002
434.386	320000	2.63788	5.50515	6.96E+00	14.522	30.307	0.000	5.597	0.008

Table F.8 (cont'd)

Stress Range Sr	N	log Sr (x)	Log N (y)	x^2	x y	y^2	(x-meanx)^2	Predicted yp	Residual^2
503.336	330000	2.70186	5.51851	7.30E+00	14.910	30.454	0.005	5.417	0.010
468.86	340000	2.67104	5.53148	7.13E+00	14.775	30.597	0.002	5.504	0.001
427.49	340000	2.63093	5.53148	6.92E+00	14.553	30.597	0.000	5.616	0.007
441.28	340000	2.64471	5.53148	6.99E+00	14.629	30.597	0.000	5.578	0.002
420.596	340000	2.62387	5.53148	6.88E+00	14.514	30.597	0.000	5.636	0.011
406.806	340000	2.60939	5.53148	6.81E+00	14.434	30.597	0.000	5.677	0.021
386.12	340000	2.58672	5.53148	6.69E+00	14.308	30.597	0.002	5.740	0.043
344.75	340000	2.53750	5.53148	6.44E+00	14.036	30.597	0.009	5.878	0.120
406.806	365000	2.60939	5.56229	6.81E+00	14.514	30.939	0.000	5.677	0.013
461.966	365000	2.66461	5.56229	7.10E+00	14.821	30.939	0.001	5.522	0.002
489.546	365000	2.68979	5.56229	7.23E+00	14.961	30.939	0.004	5.451	0.012
448.176	390000	2.65145	5.59106	7.03E+00	14.824	31.260	0.000	5.559	0.001
433.006	390000	2.63649	5.59106	6.95E+00	14.741	31.260	0.000	5.601	0.000
399.91	390000	2.60196	5.59106	6.77E+00	14.548	31.260	0.001	5.697	0.011
413.7	380000	2.61669	5.57978	6.85E+00	14.601	31.134	0.000	5.656	0.006
393.016	410000	2.59441	5.61278	6.73E+00	14.562	31.503	0.001	5.718	0.011
406.806	410000	2.60939	5.61278	6.81E+00	14.646	31.503	0.000	5.677	0.004
420.596	410000	2.62387	5.61278	6.88E+00	14.727	31.503	0.000	5.636	0.001
434.386	410000	2.63788	5.61278	6.96E+00	14.806	31.503	0.000	5.597	0.000
379.226	420000	2.57890	5.62325	6.65E+00	14.502	31.621	0.003	5.762	0.019
468.86	430000	2.67104	5.63347	7.13E+00	15.047	31.736	0.002	5.504	0.017
448.176	430000	2.65145	5.63347	7.03E+00	14.937	31.736	0.000	5.559	0.006
399.91	440000	2.60196	5.64345	6.77E+00	14.684	31.849	0.001	5.697	0.003
434.386	440000	2.63788	5.64345	6.96E+00	14.887	31.849	0.000	5.597	0.002
496.44	440000	2.69587	5.64345	7.27E+00	15.214	31.849	0.004	5.434	0.044
510.23	440000	2.70777	5.64345	7.33E+00	15.281	31.849	0.006	5.401	0.059
393.016	485000	2.59441	5.68574	6.73E+00	14.751	32.328	0.001	5.718	0.001
441.28	485000	2.64471	5.68574	6.99E+00	15.037	32.328	0.000	5.578	0.012
399.91	510000	2.60196	5.70757	6.77E+00	14.851	32.576	0.001	5.697	0.000

Table F.8 (cont'd)

Stress Range Sr	N	log Sr (x)	Log N (y)	x^2	x y	y^2	(x-meanx)^2	Predicted yp	Residual^2
475.756	510000	2.67738	5.70757	7.17E+00	15.281	32.576	0.002	5.486	0.049
351.646	540000	2.54611	5.73239	6.48E+00	14.595	32.860	0.007	5.854	0.015
441.28	560000	2.64471	5.74819	6.99E+00	15.202	33.042	0.000	5.578	0.029
406.806	590000	2.60939	5.77085	6.81E+00	15.058	33.303	0.000	5.677	0.009
427.49	590000	2.63093	5.77085	6.92E+00	15.183	33.303	0.000	5.616	0.024
455.07	590000	2.65808	5.77085	7.07E+00	15.339	33.303	0.001	5.540	0.053
324.066	600000	2.51063	5.77815	6.30E+00	14.507	33.387	0.014	5.953	0.031
420.596	635000	2.62387	5.80277	6.88E+00	15.226	33.672	0.000	5.636	0.028
344.75	635000	2.53750	5.80277	6.44E+00	14.725	33.672	0.009	5.878	0.006
372.33	645000	2.57093	5.80956	6.61E+00	14.936	33.751	0.004	5.784	0.001
330.96	645000	2.51978	5.80956	6.35E+00	14.639	33.751	0.012	5.928	0.014
393.016	670000	2.59441	5.82607	6.73E+00	15.115	33.943	0.001	5.718	0.012
413.7	670000	2.61669	5.82607	6.85E+00	15.245	33.943	0.000	5.656	0.029
406.806	720000	2.60939	5.85733	6.81E+00	15.284	34.308	0.000	5.677	0.033
393.016	720000	2.59441	5.85733	6.73E+00	15.196	34.308	0.001	5.718	0.019
434.386	750000	2.63788	5.87506	6.96E+00	15.498	34.516	0.000	5.597	0.077
406.806	750000	2.60939	5.87506	6.81E+00	15.330	34.516	0.000	5.677	0.039
441.28	780000	2.64471	5.89209	6.99E+00	15.583	34.717	0.000	5.578	0.099
406.806	850000	2.60939	5.92942	6.81E+00	15.472	35.158	0.000	5.677	0.064
344.75	850000	2.53750	5.92942	6.44E+00	15.046	35.158	0.009	5.878	0.003
427.49	870000	2.63093	5.93952	6.92E+00	15.626	35.278	0.000	5.616	0.105
372.33	900000	2.57093	5.95424	6.61E+00	15.308	35.453	0.004	5.784	0.029
420.596	950000	2.62387	5.97772	6.88E+00	15.685	35.733	0.000	5.636	0.117
393.016	950000	2.59441	5.97772	6.73E+00	15.509	35.733	0.001	5.718	0.067
365.436	980000	2.56281	5.99123	6.57E+00	15.354	35.895	0.005	5.807	0.034
413.7	1100000	2.61669	6.04139	6.85E+00	15.808	36.498	0.000	5.656	0.148
406.806	1200000	2.60939	6.07918	6.81E+00	15.863	36.956	0.000	5.677	0.162
420.596	1200000	2.62387	6.07918	6.88E+00	15.951	36.956	0.000	5.636	0.196
282.696	1200000	2.45132	6.07918	6.01E+00	14.902	36.956	0.032	6.119	0.002

Table F.8 (cont'd)

Stress Range Sr	N	log Sr (x)	Log N (y)	x^2	x y	y^2	(x-meanx)^2	Predicted yp	Residual^2
399.91	1250000	2.60196	6.09691	6.77E+00	15.864	37.172	0.001	5.697	0.160
337.856	1300000	2.52873	6.11394	6.39E+00	15.461	37.380	0.010	5.902	0.045
Mean		2.630586	5.61713						
Sum		228.861	488.69054	6.02E+02	1284.838	2750.738	0.252	488.691	3.723

a = 12.987 b = -2.802 r^2 = 0.35 n = 87

Table F.9

Fatigue Tests by the Chinese Standardization Committee (1987)

Stress Range Sr	N	Log Sr (x)	Log N (y)	x^2	x y	y^2	(x-meanx)^2	Predicted yp	Residual^2
610	500000	2.785	5.699	7.758	15.874	32.478	0.0007	6.182	0.233
610	1000000	2.785	6.000	7.758	16.712	36.000	0.0007	6.182	0.033
650	1020000	2.813	6.009	7.912	16.902	36.103	0.0000	6.063	0.003
610	8000000	2.785	6.903	7.758	19.227	47.653	0.0007	6.182	0.520
600	8020000	2.778	6.904	7.718	19.181	47.668	0.0011	6.213	0.478
700	150000	2.845	5.176	8.095	14.726	26.792	0.0012	5.924	0.559
700	500000	2.845	5.699	8.095	16.214	32.478	0.0012	5.924	0.051
700	1000000	2.845	6.000	8.095	17.071	36.000	0.0012	5.924	0.006
700	8000000	2.845	6.903	8.095	19.640	47.653	0.0012	5.924	0.959
600	200000	2.778	5.301	7.718	14.727	28.101	0.0011	6.213	0.831
600	900000	2.778	5.954	7.718	16.542	35.453	0.0011	6.213	0.067
600	950000	2.778	5.978	7.718	16.607	35.733	0.0011	6.213	0.055
600	8000000	2.778	6.903	7.718	19.178	47.653	0.0011	6.213	0.476
700	100000	2.845	5.000	8.095	14.225	25.000	0.0012	5.924	0.854
700	1030000	2.845	6.013	8.095	17.107	36.154	0.0012	5.924	0.008
700	5000000	2.845	6.699	8.095	19.059	44.876	0.0012	5.924	0.601
Mean		2.811	6.071						
Sum		44.975	97.141	126.4	272.99	595.795	0.0155	97.141	5.734

a = 18.20235 b = -4.31563 r^2 = 0.048 Se = 0.639975197

Table F.10

Helbig and Vogt's Test Results in 20% NaCl Solution

Stress Range Sr	N	Log Sr (x)	Log N (y)	x^2	x y	y^2	(x-meanx)^2	Predicted yp	Residual^2
247	910000	2.392	5.959	5.72	14.25	35.510	0.066	5.797	0.026
224	500000	2.351	5.699	5.53	13.40	32.478	0.047	5.889	0.036
224	910000	2.351	5.959	5.53	14.01	35.510	0.047	5.889	0.005
173	2600000	2.239	6.415	5.01	14.36	41.152	0.011	6.142	0.074
153	550000	2.185	5.740	4.77	12.54	32.952	0.002	6.265	0.275
153	2050000	2.185	6.312	4.77	13.79	39.838	0.002	6.265	0.002
122	3000000	2.088	6.477	4.36	13.52	41.953	0.002	6.484	0.000
102	4500000	2.009	6.653	4.04	13.36	44.265	0.016	6.663	0.000
92	7900000	1.963	6.898	3.85	13.54	47.577	0.030	6.766	0.017
82	11000000	1.912	7.041	3.66	13.46	49.581	0.050	6.882	0.025
65	10000000	1.810	7.000	3.28	12.67	49.000	0.105	7.111	0.012
Mean		2.135	6.378						
Sum		23.485	70.153	50.52	148.92	449.817	0.378	70.153	0.474

a = 11.20374 b = -2.260 r^2 = 0.803 n = 11

Se^2 = 0.053 Se = 0.230

Table F.11

Helbig and Vogt's Test Results in Tap Water

Stress Range Sr	N	Log Sr (x)	Log N (y)	x^2	x y	y^2	(x-meanx)^2	Predicted yp	Residual^2
276	820000	2.441	5.914	5.96	14.44	34.973	0.079	5.683	0.053
224	600000	2.351	5.778	5.53	13.59	33.387	0.036	5.889	0.012
224	740000	2.351	5.869	5.53	13.80	34.448	0.036	5.889	0.000
224	800000	2.351	5.903	5.53	13.88	34.846	0.036	5.889	0.000
224	1000000	2.351	6.000	5.53	14.11	36.000	0.036	5.889	0.012
224	1200000	2.351	6.079	5.53	14.29	36.956	0.036	5.889	0.036
224	1600000	2.351	6.204	5.53	14.59	38.491	0.036	5.889	0.099
209	320000	2.321	5.505	5.38	12.77	30.307	0.026	5.959	0.206
204	150000	2.310	5.176	5.34	11.96	26.792	0.022	5.983	0.651
197	1250000	2.295	6.097	5.27	13.99	37.172	0.018	6.017	0.006
190	370000	2.280	5.568	5.20	12.69	31.005	0.014	6.051	0.233
173	1200000	2.239	6.079	5.01	13.61	36.956	0.006	6.144	0.004
173	1900000	2.239	6.279	5.01	14.06	39.423	0.006	6.144	0.018
173	3600000	2.239	6.556	5.01	14.68	42.985	0.006	6.144	0.170
153	730000	2.185	5.863	4.77	12.81	34.379	0.001	6.267	0.163
153	1000000	2.185	6.000	4.77	13.11	36.000	0.001	6.267	0.072
153	1500000	2.185	6.176	4.77	13.49	38.144	0.001	6.267	0.008
153	1600000	2.185	6.204	4.77	13.56	38.491	0.001	6.267	0.004
153	1800000	2.185	6.255	4.77	13.67	39.128	0.001	6.267	0.000
153	1900000	2.185	6.279	4.77	13.72	39.423	0.001	6.267	0.000
153	2300000	2.185	6.362	4.77	13.90	40.472	0.001	6.267	0.009
153	3900000	2.185	6.591	4.77	14.40	43.442	0.001	6.267	0.105
153	4900000	2.185	6.690	4.77	14.62	44.759	0.001	6.267	0.179
153	5500000	2.185	6.740	4.77	14.73	45.432	0.001	6.267	0.224
122	1400000	2.088	6.146	4.36	12.83	37.775	0.005	6.488	0.117
122	1750000	2.088	6.243	4.36	13.04	38.976	0.005	6.488	0.060
122	5900000	2.088	6.771	4.36	14.14	45.844	0.005	6.488	0.080

Table F.11 (Cont'd)

Stress Range Sr	N	Log Sr (x)	Log N (y)	x^2	x y	y^2	(x-meanx)^2	Predicted yp	Residual^2
116	2800000	2.063	6.447	4.26	13.30	41.566	0.009	6.545	0.010
116	4500000	2.063	6.653	4.26	13.73	44.265	0.009	6.545	0.012
102	4000000	2.009	6.602	4.04	13.26	43.587	0.023	6.668	0.004
102	4700000	2.009	6.672	4.04	13.40	44.517	0.023	6.668	0.000
102	6800000	2.009	6.833	4.04	13.72	46.683	0.023	6.668	0.027
102	14000000	2.009	7.146	4.04	14.35	51.067	0.023	6.668	0.228
82	2700000	1.912	6.431	3.66	12.30	41.362	0.062	6.889	0.209
82	9800000	1.912	6.991	3.66	13.37	48.877	0.062	6.889	0.010
82	12000000	1.912	7.079	3.66	13.53	50.115	0.062	6.889	0.036
65	10500000	1.810	7.021	3.28	12.71	49.297	0.123	7.120	0.010
65	11500000	1.810	7.061	3.28	12.78	49.853	0.123	7.120	0.004
Mean		2.161	6.323						
Sum		82.102	240.266	178.35	516.93	1527.197	0.959	240.266	3.074

a = 11.242 b = -2.277 r^2 = 0.618 Se^2= 0.085

N = 38

Table F.12

Corrosion Fatigue Tests from Conoco (Joosten et al., 1985)
Variable Mean Stress

Stress Range Sr	N	Log Sr (x)	Log N (y)	x^2	x y	y^2	(x-meanx)^2	Predicted yp	Residual^2
303	41000	2.481	4.613	6.16	11.45	21.278	0.066	4.912	0.090
276	90000	2.441	4.954	5.96	12.09	24.545	0.047	4.999	0.002
241	140000	2.382	5.146	5.67	12.26	26.483	0.025	5.125	0.000
234	175000	2.369	5.243	5.61	12.42	27.489	0.021	5.152	0.008
200	190000	2.301	5.279	5.29	12.15	27.865	0.006	5.298	0.000
166	375000	2.220	5.574	4.93	12.37	31.070	0.000	5.470	0.011
134	600000	2.127	5.778	4.52	12.29	33.387	0.010	5.669	0.012
103	1700000	2.013	6.230	4.05	12.54	38.818	0.045	5.913	0.101
49	2100000	1.690	6.322	2.86	10.69	39.970	0.286	6.602	0.078
Mean		2.225	5.460						
Sum		20.025	49.140	45.06	108.26	270.905	0.504		0.303

a = 10.21263 b = -2.13604 r^2 = 0.884 Se = 0.208

Table F.13

Analysis of Variance

(Comparison Between Stress Range and Mean Stress in a Corrosive Environment)

Source (1)	Degrees of Freedom (2)	Sum of Squares (3)	Mean Square (4)	Calculated F-ratio (5)	Tabulated F-ratio * (6)
$\log S_r$	1	1.9896	1.9896	463	5.59
$(S_m)^2$	2	0.4158	0.2079	48.3	4.74
Interaction	2	0.0351	0.0176	4.09	4.74
Error	7	0.0301	0.0043		
Total	12	2.6943			

* $\alpha = 0.05$

RECENT STRUCTURAL ENGINEERING REPORTS

Department of Civil Engineering
University of Alberta

143. Shrinkage and Flexural Tests of Two Full-Scale Composite Trusses by A. Brattland and D.J.L. Kennedy, December 1986.

144. *Combined Flexure and Torsion of I-Shaped Steel Beams* by R.G. Driver and D.J.L. Kennedy, March 1987.

145. *Cyclic and Static Behaviour of Thin Panel Steel Plate Shear Walls* by E.W. Tromposch and G.L. Kulak, April 1987.

146. *Postbuckling Behavior of Thin Steel Cylinders Under Transverse Shear* by V.G. Roman and A.E. Elwi, May 1987.

147. *Incipient Flow in Silos - A Numerical Approach* by R.A. Link and A.E. Elwi, May 1987.

148. *Design of Web-Flange Beam or Girder Splices* by D. Green and G.L. Kulak, May 1987.

149. *Spreadsheet Solution of Elastic Plate Bending Problems* by G.E. Small and S.H. Simmonds, July 1987.

150. *Behaviour of Transversely Loaded Continuous Steel-Concrete Composite Plates* by S.J. Kennedy and J.J. Cheng, July 1987.

151. *Behaviour and Ultimate Strength of Partial Joint Penetration Groove Welds* by D.P. Gagnon and D.J.L. Kennedy, July 1987.

152. *KBES for Design of Reinforced Concrete Columns* by A. Bezzina and S.H. Simmonds, July 1987.

153. *Compressive Behavior of Gusset Plate Connections* by S.Z. Hu and J.J. Cheng, July 1987.

154. *Development of Structural Steel Design Standards* by P.J. Marek and D.J.L. Kennedy, October 1987.

155. *Behaviour of Bolted Joints of Corrugated Steel Plates* by R.W.S. Lee and D.J.L. Kennedy, January 1988.

156. *Masonry Veneer Wall Systems* by W.M. McGinley, J. Warwaruk, J. Longworth and M. Hatzinikolas, January 1988.

157. *Stability of Concrete Plates* by A.O. Aghayere and J.G. MacGregor, February 1988.

158. *The Flexural Creep Behaviour of OSB Stressed Skin Panels* by P.C.K. Wong, L. Bach and J.J. Cheng, April 1988.

159. *Ultimate Strength of Eccentrically Loaded Fillet Welded Connections* by D.F. Lesik and D.J.L. Kennedy, May 1988.

160. *Fatigue Strength of Coped Steel Beams* by M.C.H. Yam and J.J. Cheng, June 1988.

161. *Analysis of Concrete Panels* by B. Massicotte, A.E. Elwi and J.G. MacGregor, July 1988.

162. *Behavior and Design of Reinforced Concrete Ice-Resisting Walls* by R.M. Ellis and J.G. MacGregor, November 1988.

163. *An Analysis of the Performance of Welded Wide Flange Columns* by D.E. Chernenko and D.J.L. Kennedy, December 1988.

164. *Nonlinear Dynamic Analysis of Caisson-Type Offshore Structures* by I.R. Soudy and T.M. Hrudey, March 1989.

165. *NORCO - A Program for Nonlinear Finite Element Analysis of Reinforced Concrete Structures - Users' Manual* by S. Balakrishnan, A.E. Elwi and D.W. Murray, April 1989.

166. *An Eigenvector-Based Strategy for Analysis of Inelastic Structures* by J. Napoleao, Fo., A.E. Elwi and D.W. Murray, May 1990.

167. *Elastic-Plastic and Creep Analysis of Casings for Thermal Wells* by S.P. Wen and D.W. Murray, May, 1990.

168. *Erection Analysis of Cable-Stayed Bridges* by Z. Behin and D.W. Murray, September 1990.

169. *Behavior of Shear Connected Cavity Walls* by P.K. Papinkolas, M. Hatzinikolas and J. Warwaruk, September 1990

170. *Inelastic Transverse Shear Capacity of Large Fabricated Steel Tubes,* by K.H. Obaia, A.E. Elwi and G.L. Kulak, April 1991.

171. *Fatigue of Drill Pipe* by G.Y. Grondin and G.L. Kulak, April 1991.